Doctoral Dissertation

Seismic Strengthening of RC Exterior Beam-Column Joints with Deficient Beam Rebar Anchorage by Wing Walls

SYAFRI WARDI

July 2019

International Program of Maritime and Urban Engineering
Division of Global Architecture
Graduate School of Engineering
Osaka University

Abstract

Recent earthquakes in developing countries have revealed that collapse of RC (reinforced concrete) building structure was often initiated by the brittle failure of beam-column joints, i.e. joint shear failure or anchorage failure of beam longitudinal rebar into exterior joints. The strengthening method to prevent the brittle failure of joints is a very important issue to upgrade the existing buildings in earthquake-prone area. This study focuses on strengthening of exterior RC beam-column joints with deficient anchorage by installing wing walls and verifies the effectiveness experimentally. This dissertation consists of 7 chapters as follows:

Chapter 1 introduces the background, literature review, objectives, and the outline of this thesis.

Chapter 2 describes a field investigation in West Sumatra, Indonesia. This area had experienced significant damage by the 2009 Sumatra earthquake. The investigation was focused on the observation of deficiencies in newly constructed RC buildings. The investigation results showed that substandard materials and deficiencies of seismic detailing, particularly deficient details of beam-column joint, exist in current construction practice in this area. The worst detail observed on beam-column joints was straight anchorage of beam reinforcement to the exterior joint.

Chapter 3 describes the experimental tests on existing exterior beam-column joints with deficient beam rebar anchorage. The experimental tests were focused on typical Bangladeshi buildings with low strength concrete using brick chip aggregate. The deficient anchorage detail combined with poor material specification gives the worst scenario on the vulnerability of existing beam-column joints. Two 0.7-scaled exterior joint specimens were constructed and tested. One of the specimens failed in anchorage failure and showed more brittle failure than

another specimen which failed in shear at the joint. The specimen with anchorage failure was chosen as the benchmark specimen for strengthening with wing walls.

In Chapter 4, a series of pullout tests to evaluate the performance of post-installed anchors in low-strength concrete with brick chip aggregate is described. The results of this test contribute to the design of the details of post-installed anchors to obtain minimum embedment length of anchors to prevent brittle failure of anchors in a strengthened beam-column joint.

Chapter 5 describes an experimental test to verify the effectiveness of strengthening by wing walls to upgrade an exterior joint with deficient anchorage. The proposed strengthening method was applied to one of the tested beam-column joint specimen showing vulnerability to anchorage failure. A design concept considering the length of wing walls to extend the development length of beam rebar was proposed. The strengthened specimen failed in beam yielding mechanism and the anchorage failure of the joint was successfully prevented. An evaluation method to evaluate the deformation capacity of beam due to shortening of the beam span after installation of wing walls was also presented.

In Chapter 6, a pushover analysis was conducted to evaluate the seismic performance of an RC building before and after strengthening by wing walls. The analytical results showed that application of the proposed strengthening method improved the global seismic performance of the building, in term of lateral strength and deformation capacity.

Chapter 7 summarizes the main conclusions of this study and suggestions for future work.

Acknowledgments

I would like to express my deepest gratitude and thanks to my supervisor Prof. Yasushi Sanada for continues support and guidance during my study at Osaka University. Moreover, my sincere thanks go to Prof. Yuji Miyamoto and Prof. Motohide Tada for taking their time to review this thesis.

I am grateful to Japanese Government (MEXT) for the scholarship. The field investigation in this study was supported by JSPS-KAKENHI grant number 16H05650 (headed by Prof. Yasushi Sanada) and the experiments were supported by JICA/JST SATREPS (headed by Prof. Yoshiaki Nakano, the University of Tokyo).

I would also like to thank Dr. Jafril Tanjung of Andalas University, Indonesia and Dr. Maidiawati of Padang Institute of Technology, Indonesia for their support during the field investigation.

Thanks are extended to former and present fellow students of Concrete Structure Laboratory for their support, especially during the experimental works.

Finally, I would like to express my great appreciation to my family for their support and encouragement during my study. I would like to dedicate this thesis to them.

List of Publications

Journal Papers

1. Syafri Wardi, Yasushi Sanada, Michihiro Kita, Jafril Tanjung, and Maidiawati, Common Structural Details and Deficiencies in Indonesian RC Buildings: Preliminary Report on Field Investigation in Padang City, West Sumatera, *International Journal on Advanced Science, Engineering and Information Technology*, Vol. 8, No. 2, pp. 418-425, 2018.04. https://doi.org/10.18517/ijaseit.8.2.4207 [**Chapter 2**]
2. Syafri Wardi, Nandita Saha, Yasushi Sanada, and Susumu Takahashi, Pullout Test of Post-Installed Anchors in Low Strength Concrete with Brick Chips Representing Bangladeshi Concrete, *AIJ Journal of Technology and Design*, Vol. 25, No. 59, pp.199-204, 2019.02. https://doi.org/10.3130/aijt.25.199 [**Chapter 4**]

International Conference Papers

1. Syafri Wardi, Yasushi Sanada, and Susumu Takahashi, Retrofitting by Installing Wing Walls for an Exterior RC Beam-Column Joint with Substandard Straight Anchorage of Beam Longitudinal Rebar, *Proceedings of the 20th Taiwan-Korea-Japan Joint Seminar on Earthquake Engineering for Building Structures*, pp. 45-54, Kyoto, Japan, November, 2018. [**Chapters 3 and 5**]
2. Syafri Wardi, Yasushi Sanada, Michihiro Kita, Jafril Tanjung, and Maidiawati, Investigation on Implementation of Seismic Detailing of Reinforced Concrete Buildings in West Sumatra Indonesia, *Proceedings of the 7th Asia Conference on Earthquake Engineering*, Paper ID ACEE0069, Bangkok, Thailand, November, 2018. [**Chapter 2**]

Table of Contents

List of Figures

List of Tables

Chapter 1
Introduction

1.1 Background

Reinforced concrete (RC) beam-column joints with substandard detailing, which typically contain little/no shear reinforcement and/or insufficient anchorage of beam longitudinal rebar, exist in many buildings designed according to older design codes, such as those before the 1970s in the United States or those that do not comply with current seismic codes in developing countries. Recent earthquakes in developing countries have revealed that severe damage or collapse of RC buildings is often caused by poor performance of the beam-column joints with substandard detailing [1]–[3]. Additionally, such poorly detailed joints still exist in newly constructed buildings in an area affected by a recent earthquake in Indonesia, as observed in a field survey which will be described later in **Chapter 2**. **Figure 1(a)** shows a collapsed building due to joint failure, in which the beam rebar had a straight anchorage into the exterior beam-column joints. **Figure 1(b)** shows that similar poor anchorage detail was also observed on a moderately damaged building due to a recent earthquake. Seismic strengthening of beam-column joints with substandard details is a very urgent issue to prevent building collapse against future earthquakes.

Various strengthening methods have been developed for RC exterior joints without sufficient shear reinforcement, for example, by using steel jacketing [4], by using fiber-reinforced polymer (FRP) materials [5]–[7], by using steel prop [8], or by installing slurry infiltrated fiber concrete blocks using anchors [9]. The effectiveness of these strengthening methods has been verified for improving the shear resistance of exterior joints. However, strengthening methods that are effective for improving beam rebar anchorage in exterior joints are still limited, as described later in **Section 1.2**.

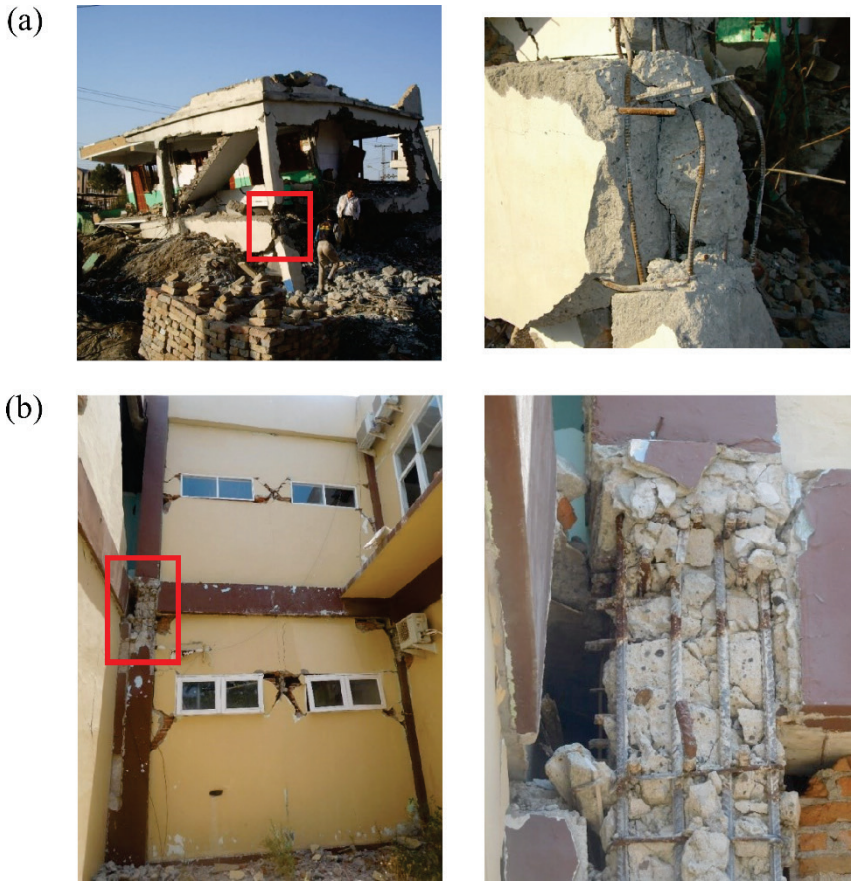

Figure 1.1 Earthquake-damaged RC exterior beam-column joints: (a) 2005 Kashmir earthquake in Pakistan [10] (b) 2018 Lombok earthquake in Indonesia (image by author)

In consideration of the economic situation and technical level of developing countries, a strengthening method has been proposed for substandard RC exterior beam-column joints by installing RC wing walls by Li et al. [11]. The effectiveness of this strengthening method has been validated to upgrade the joints without shear reinforcement. In this study, the strengthening method by installing wing walls is proposed to upgrade joints with substandard anchorage of beam longitudinal rebar.

1.2. Literature Review on Strengthening of Exterior Beam-Column Joint with Deficient Anchorage

Biddah [12] did an attempt to strengthen a beam-column joint with straight anchorage of the beam bottom longitudinal bar by attaching steel plates to the beam sides to replace deficient reinforcement bars, shown in **Figure 1.2**. The dimensions and details of reinforcement of the benchmark specimen with deficient anchorage are shown in **Figure 1.3**. A corrugated steel jacketing system was applied for confining the critical region of the joint and the column. For the joint region, two steel angles fixed with anchor bolts were installed at the beam sides to resist the pullout of the beam bottom longitudinal bars. The proposed systems did not effectively improve the joint response because of the failure of the anchor bolts.

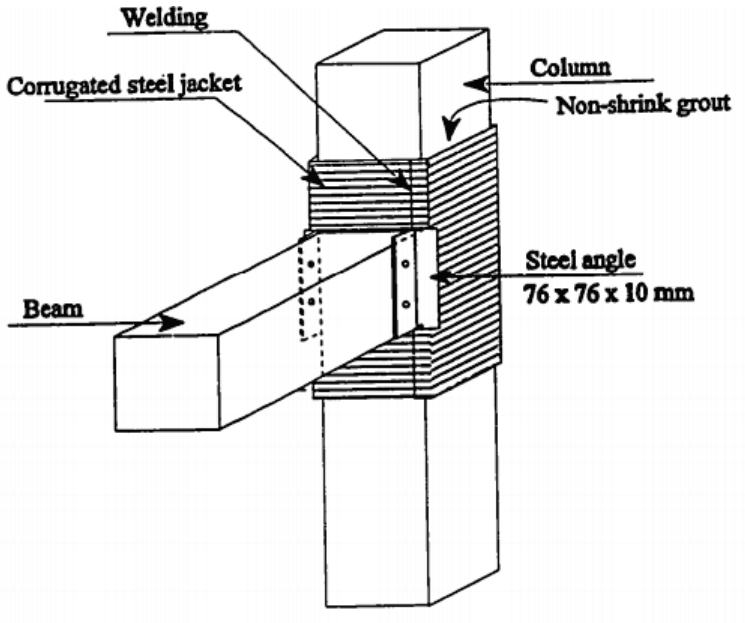

Figure 1.2 Proposed rehabilitation technique of specimen J6 [12]

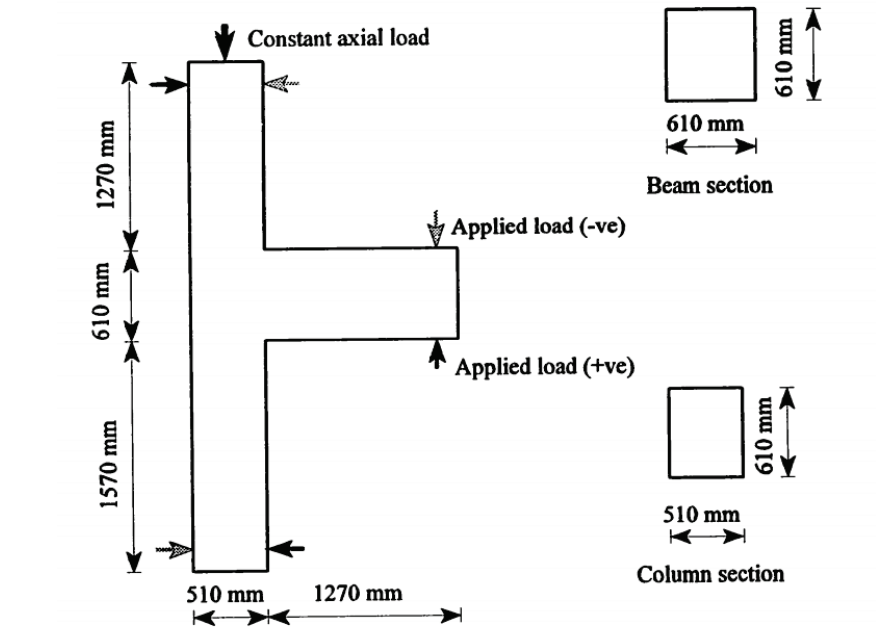

(a)

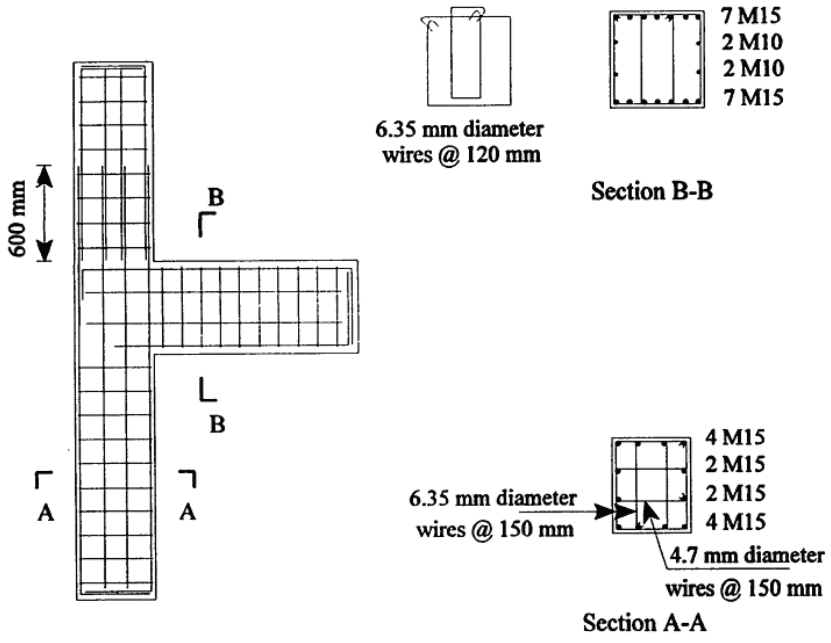

(b)

Figure 1.3 (a) Dimensions of the specimens (b) Details of reinforcement of specimens with deficient anchorage [12]

Ghobarah and El-Amoury [13] proposed strengthening methods for the beam-column joints with straight anchorage of the beam bottom longitudinal bars by using FRP sheets, steel plates, rods, and a welding process. The proposed strengthening method was applied to the anchorage-deficient joint, and the shear-anchorage-deficient joint, as shown in **Figure 1.4(a)** and **Figure 1.5(a)**, respectively. The anchorage-deficient joint was strengthened by using carbon fiber-reinforced polymer (CFRP) sheets which were attached to the beam bottom face and extended along the column face, as shown in **Figure 1.4(b)**. The shear/anchorage-deficient joint was strengthened by external tie-rods welded to the existing beam bottom longitudinal bars for the anchorage strengthening, combined with GFRP wrapping around the joint for the shear strengthening, as shown in **Figure 1.5(b)**.

The proposed strengthening methods were effective to improve the seismic performance of the joints and preventing the pullout of the beam bottom longitudinal bars, as shown in **Figure 1.6** and **Figure 1.7**. The splitting crack at the column face in **Figure 1.6(a)** indicated the slippage of the beam's bottom bars of the benchmark specimen, while the crack at the beam-column face in **Figure 1.6(b)** indicated the beam flexural hinging of the strengthened specimen. **Figure 1.7(a)** shows the failure pattern of the benchmark specimen which failed in shear failure and bond-slip failure of beam's bottom bars and **Figure 1.7(b)** shows the failure pattern of the strengthened specimen, in which both shear and anchorage failure were prevented.

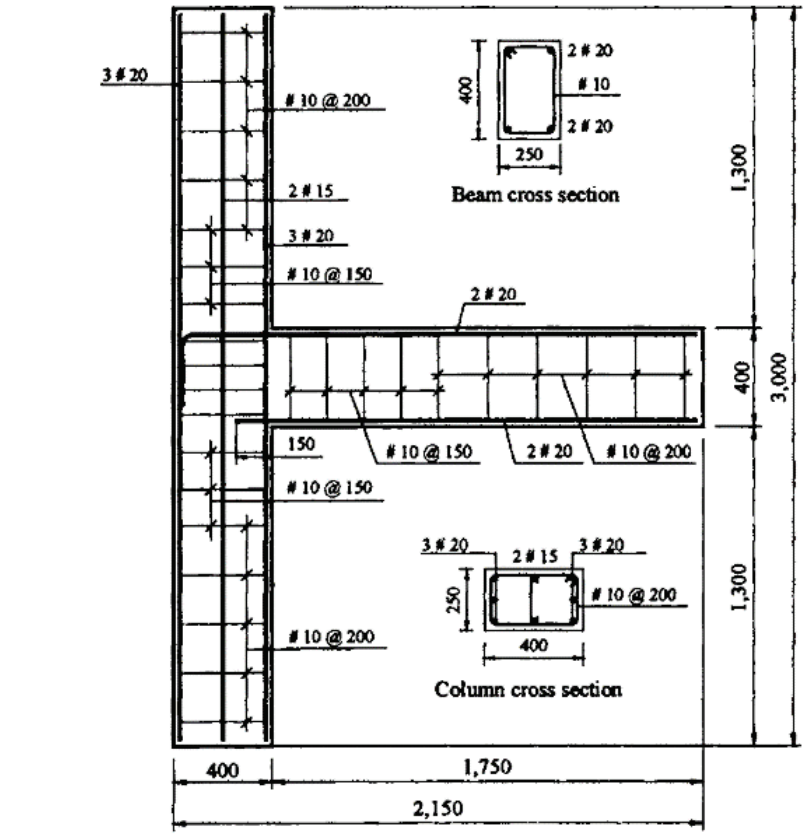

(a)

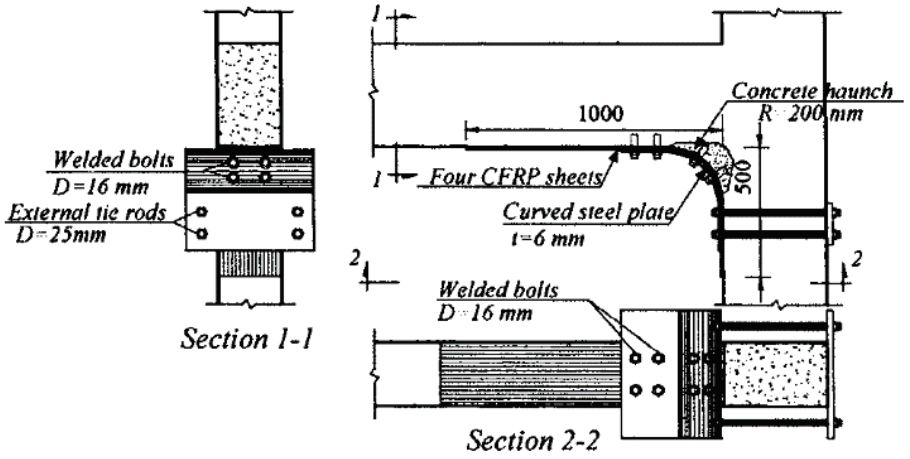

(b)

Figure 1.4 (a) Specimen dimensions and reinforcement details of anchorage-deficient joint

(b) Strengthened joint TB-11 [13]

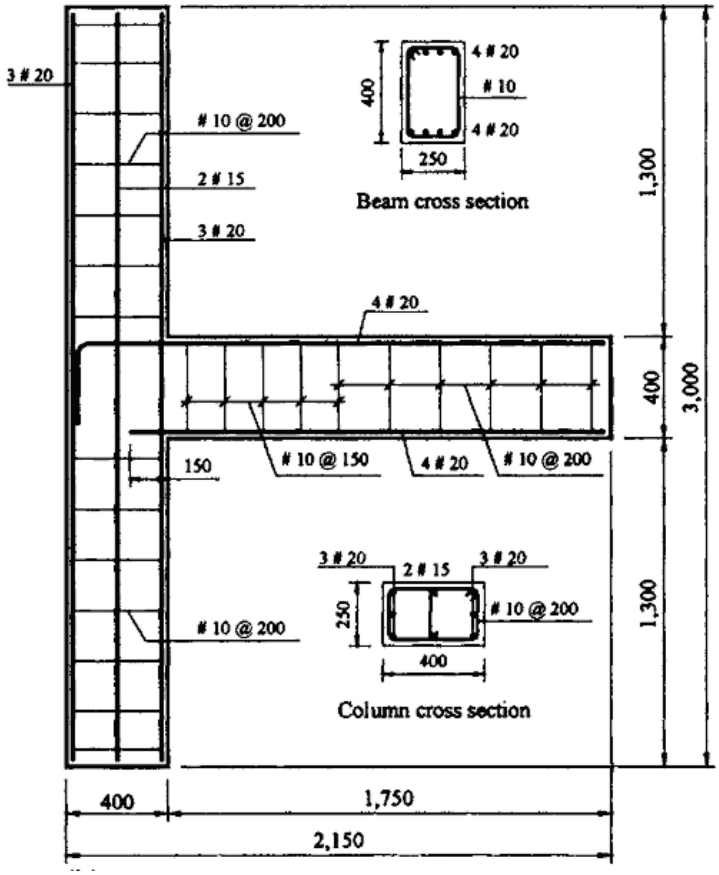

(a)

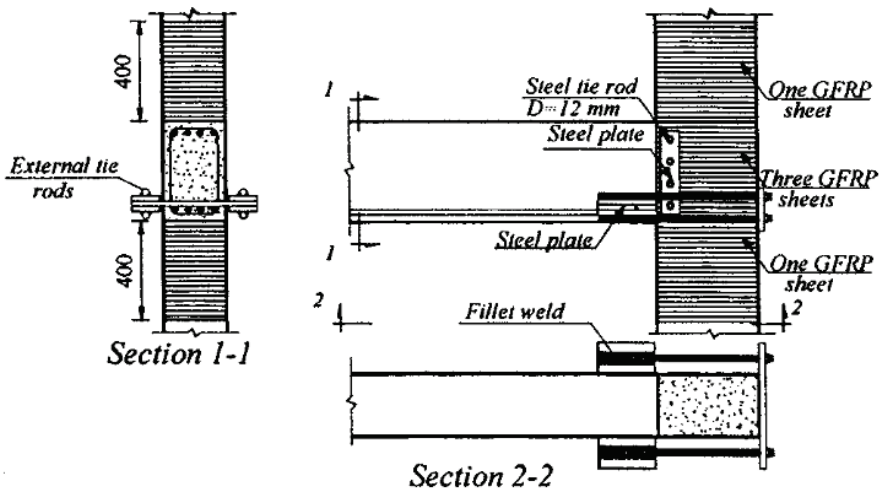

(b)

Figure 1.5 (a) Specimen dimensions and reinforcement details of anchorage-deficient joint

(b) Strengthened joint T-SB7 [13]

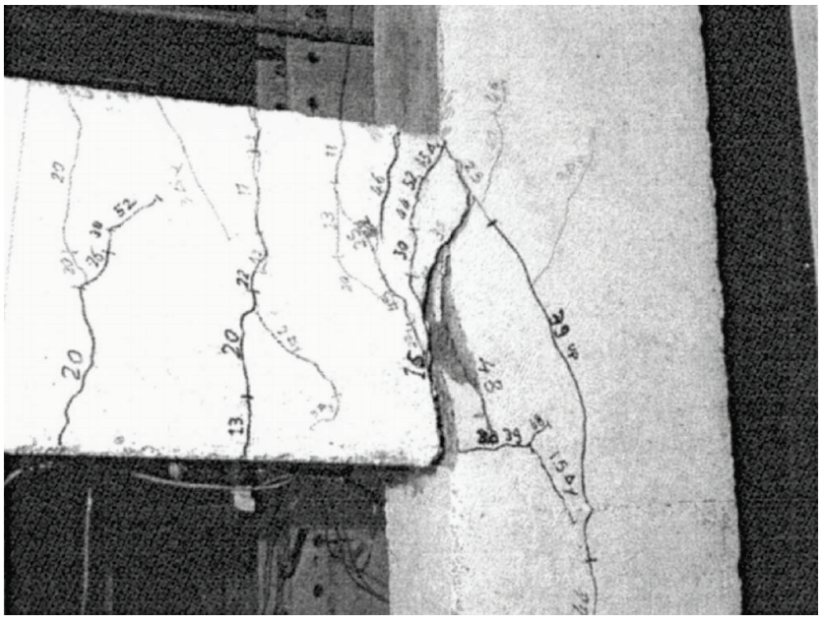

(a)

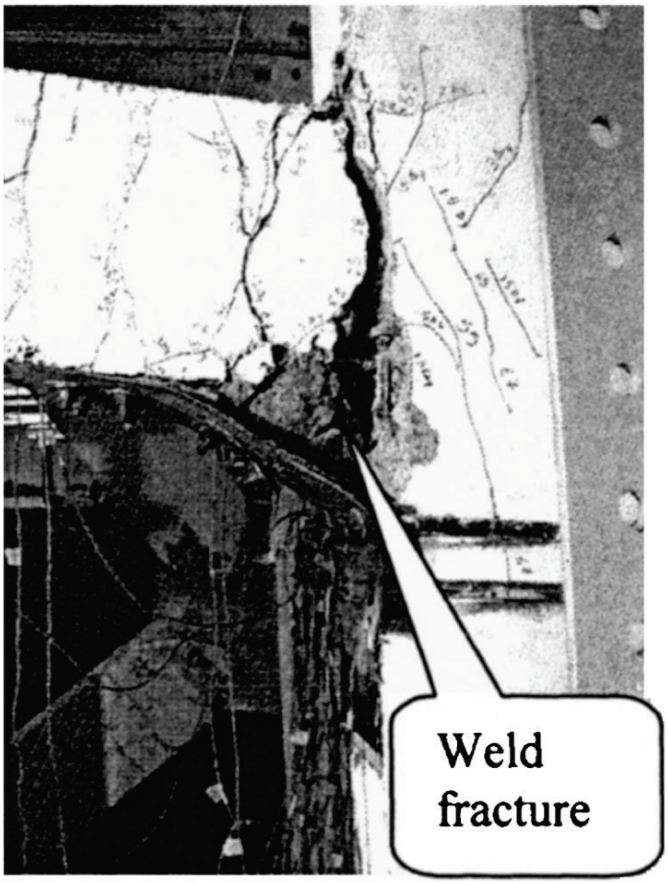

(b)

Figure 1.6 Failure pattern of: (a) Benchmark specimen,
(b) Strengthened specimen TB-11 [13]

(a)

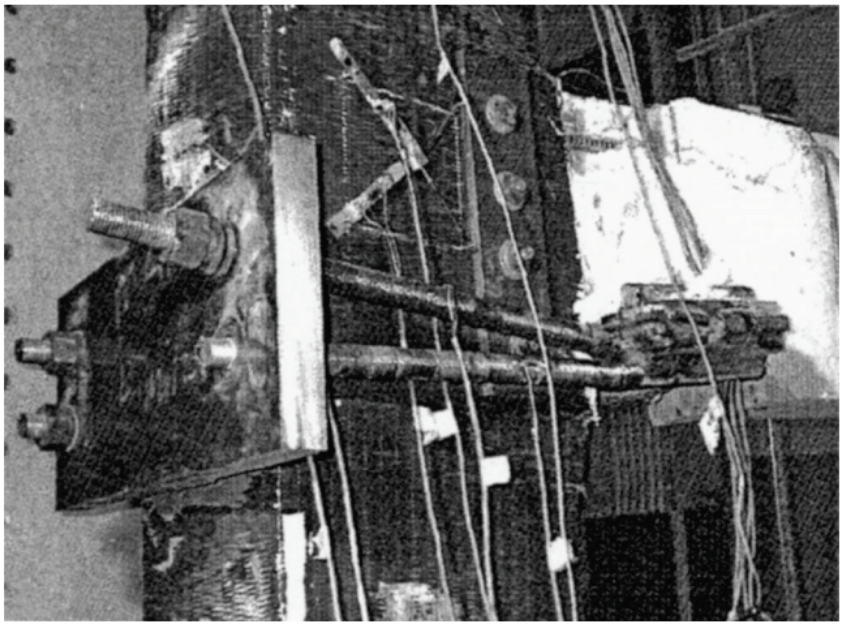

(b)

Figure 1.7 Failure pattern of: (a) Benchmark specimen,

(b) Strengthened specimen T-SB7 [13]

Parvin et al. [14] proposed a strengthening method for the beam-column joints with straight anchorage of the beam bottom longitudinal bars by using CFRP. The reinforcement details and dimensions of the benchmark specimens are shown in **Figure 1.8**. Two CFRP wrapping configurations were proposed, as shown in **Figure 1.9**. The proposed CFRP configurations in the retrofitted specimens successfully delayed the shear failure of joint and slippage failure of beam longitudinal bars from the joint. **Figure 1.10** shows the crack patterns of the benchmark specimen due to shear failure and slippage of the beam bottom longitudinal reinforcements. **Figure 1.11** shows the failure pattern of the strengthened specimens, in which the failure mode was governed by the rupture and the debonding of the CFRP sheets.

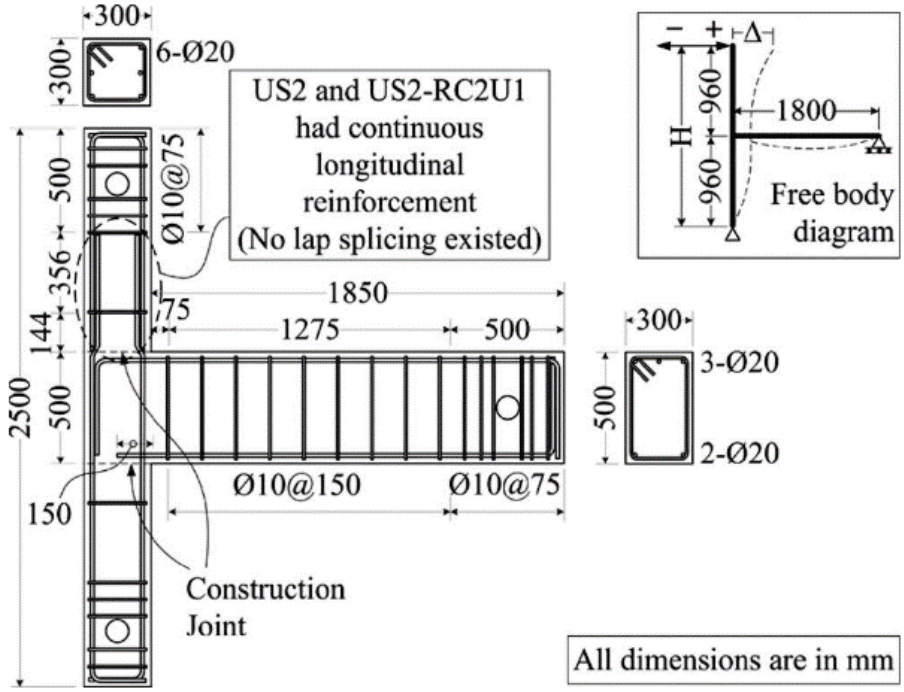

Figure 1.8 Reinforcement details and dimensions [14]

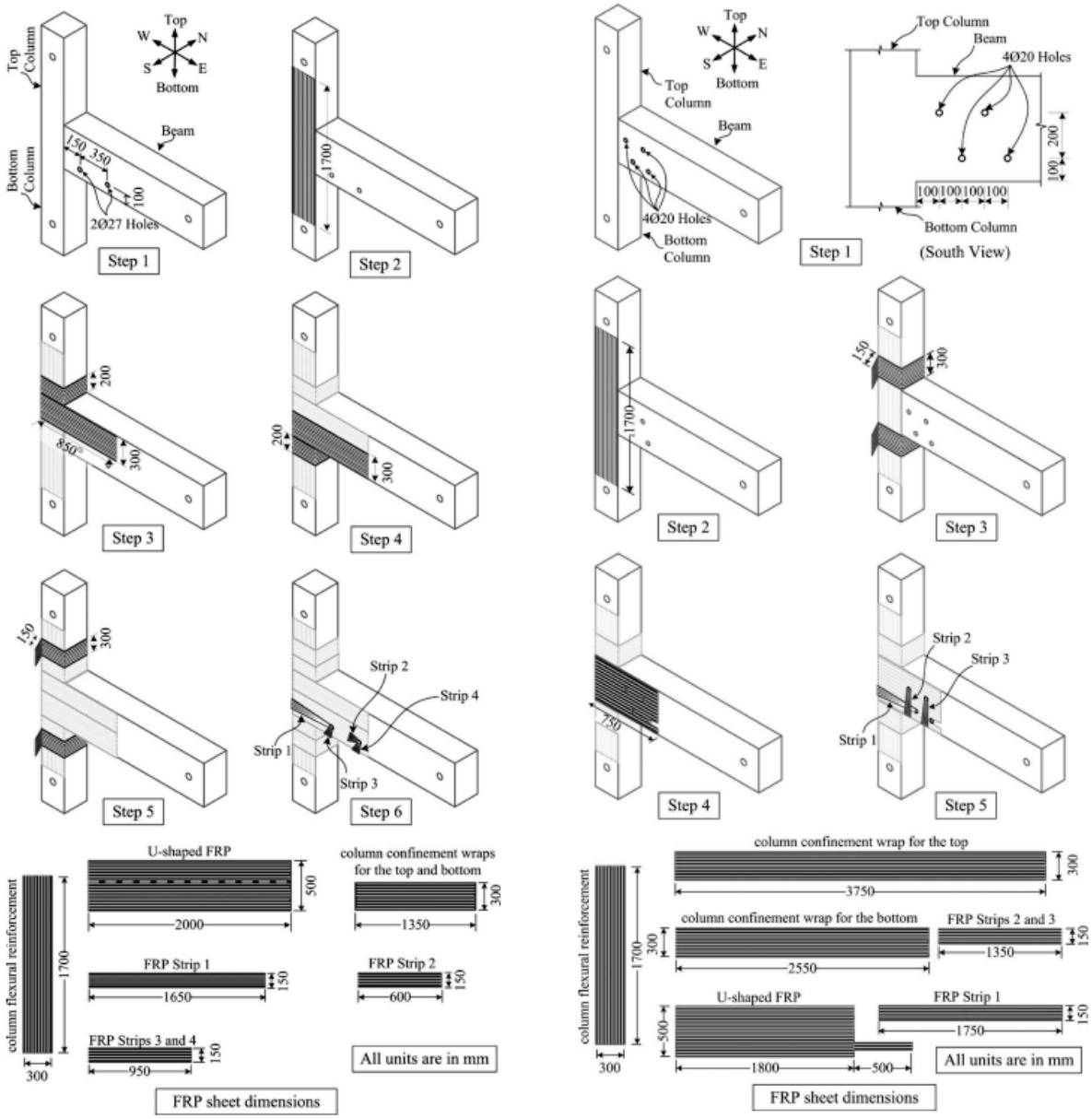

(a) CFRP wrapping configuration RC2U1 (b) CFRP wrapping configuration RC3U3

Figure 1.9 Proposed CFRP wrapping configurations [14]

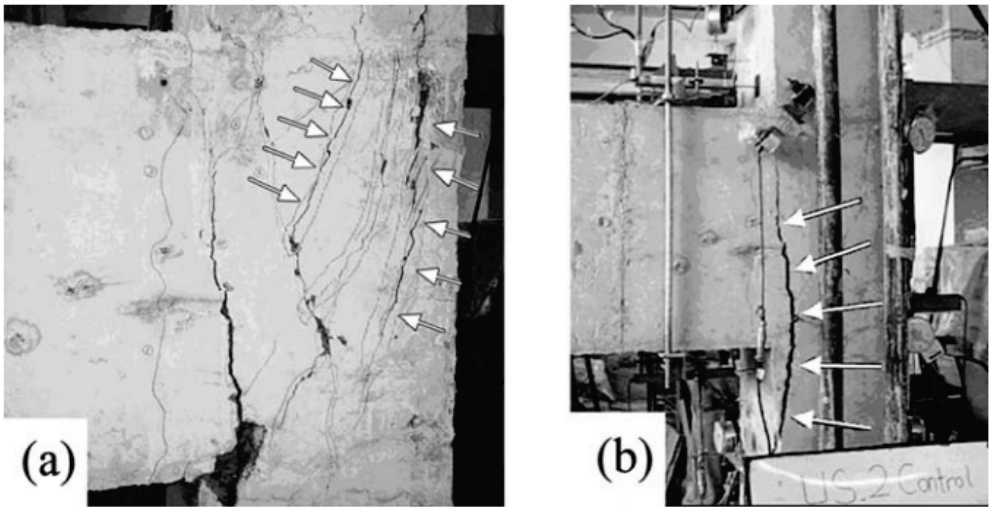

Figure 1.10 Crack pattern of benchmark specimen: (a) the shear failure at the joint; (b) the slippage of the beam bottom longitudinal reinforcements [14]

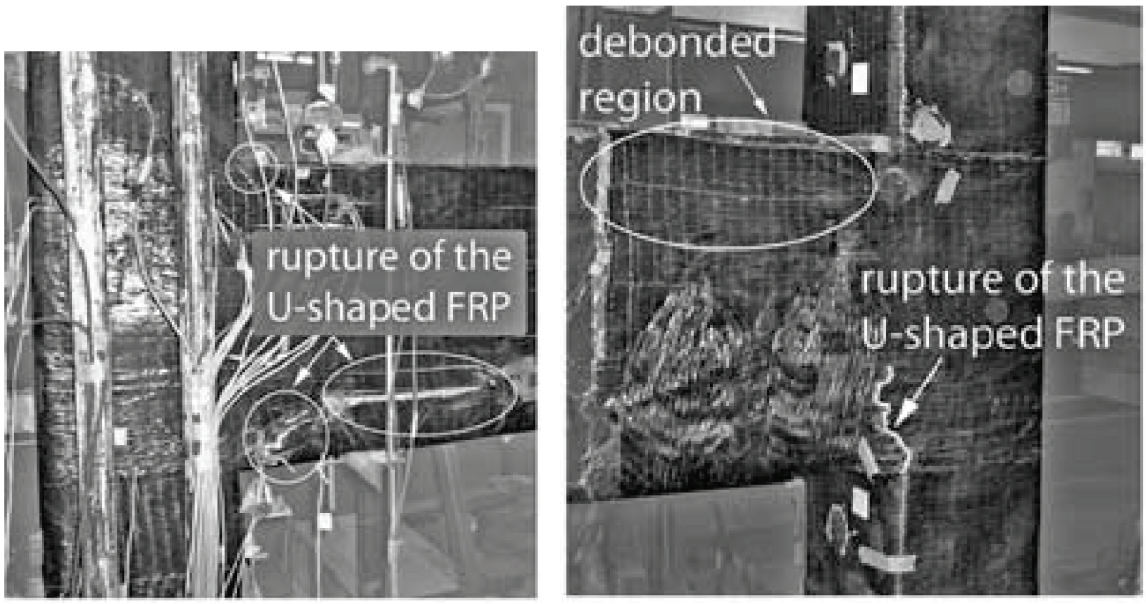

(a) (b)

Figure 1.11 Failure pattern of: (a) strengthened specimen U.S.2-RC2U1, (b) strengthened specimen U.S.3-RC3U1 [14]

Kalogeropoulus et al. [15] proposed a strengthening method for the beam-column joints with straight anchorage of the beam top and bottom longitudinal bars by using extension bars welded to the existing beam rebar and steel plates for the anchorage of the extension bars, combined with the RC jacketing of the columns and the joint region. The details of the benchmark specimen are shown in **Figure 1.12** and the strengthening scheme is shown in **Figure 1.13**. The proposed strengthening method was effective to improve the seismic performance of the joints and to prevent the premature pullout of the beam reinforcing bars from the joint. **Figure 1.14(a)** shows the benchmark specimen which failed due to the pullout failure of the beam longitudinal rebar and **Figure 1.14(b)** shows the failure pattern of the strengthened specimen, in which the damage was shifted to the beam.

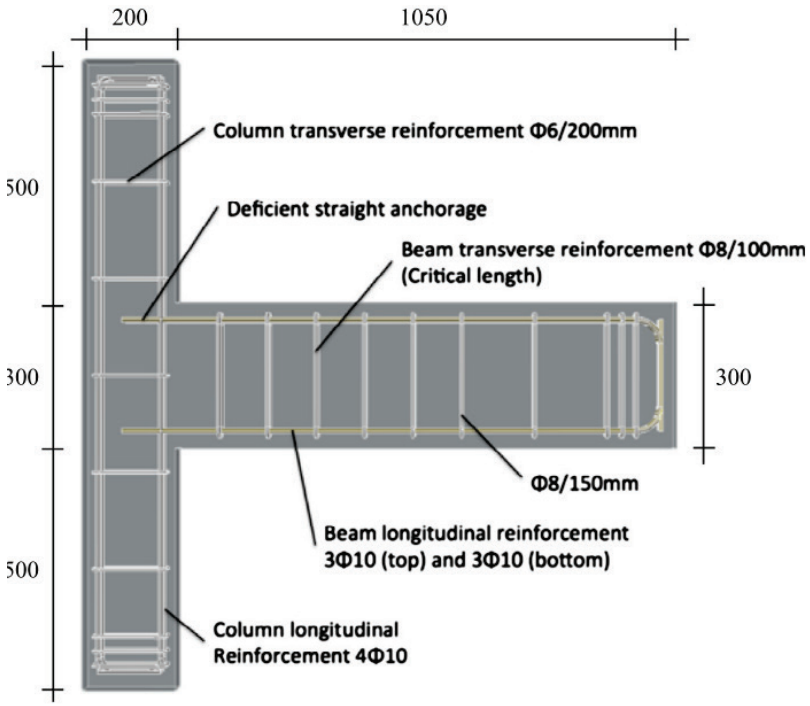

Figure 1.12 Reinforcement details of the benchmark specimen [15]

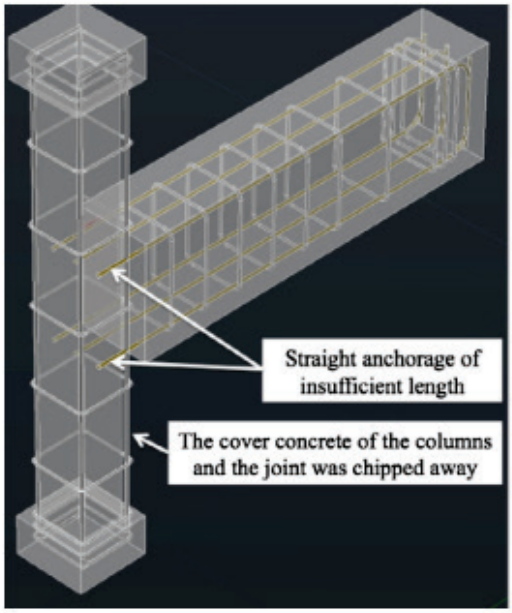

(a) Step 1: The cover concrete of the columns and the joint was chipped away.

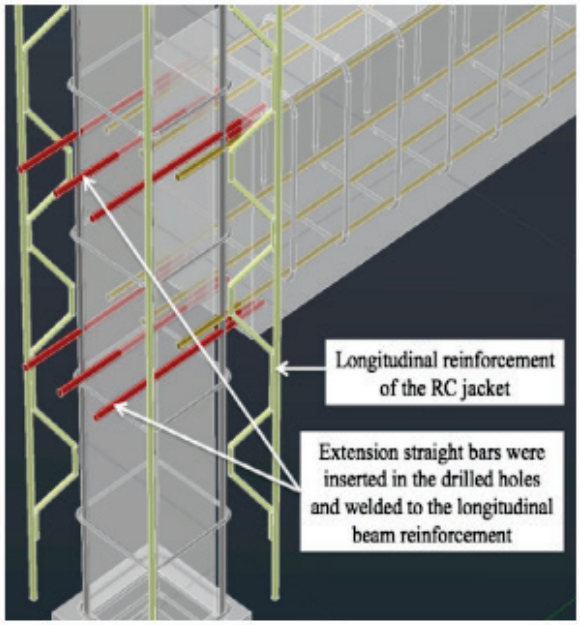

(b) Step 2: Longitudinal reinforcement of the RC jacket. Extention bars were used to extend the beam logitudinal reinforcement.

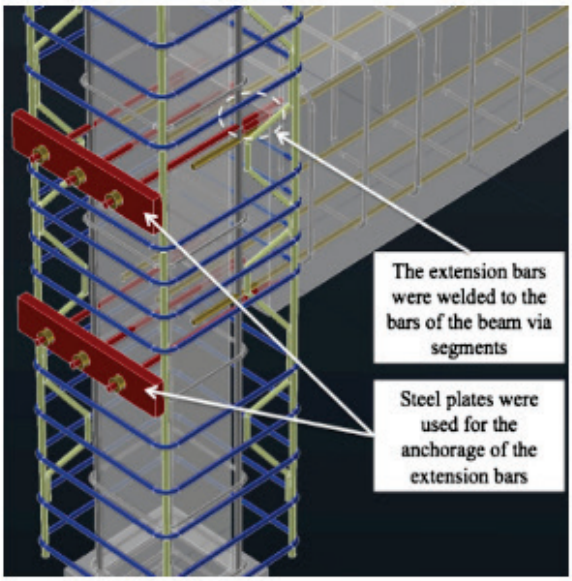

(c) Step 3: Closed ties were used for the transverse reinforcement of the RC jacket, while the anchorage of the beam reinforcement was achieved via steel plates and bolts.

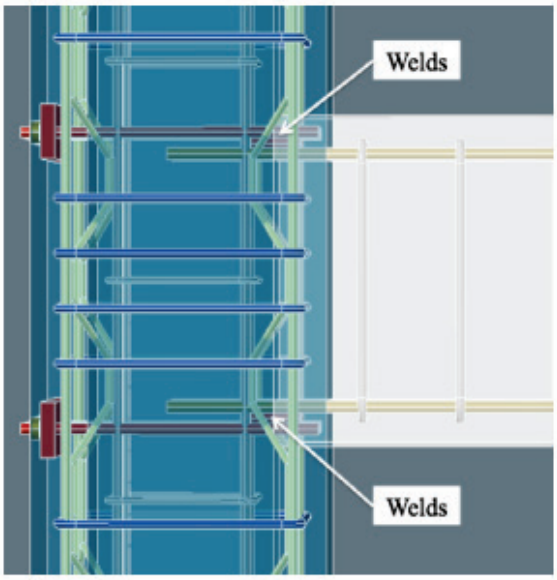

(d) Joint of the retrofitted specimens SK_1 and SL_1 after the implementation of the retrofitting scheme (1).

Figure 1.13 Strengthening scheme [15]

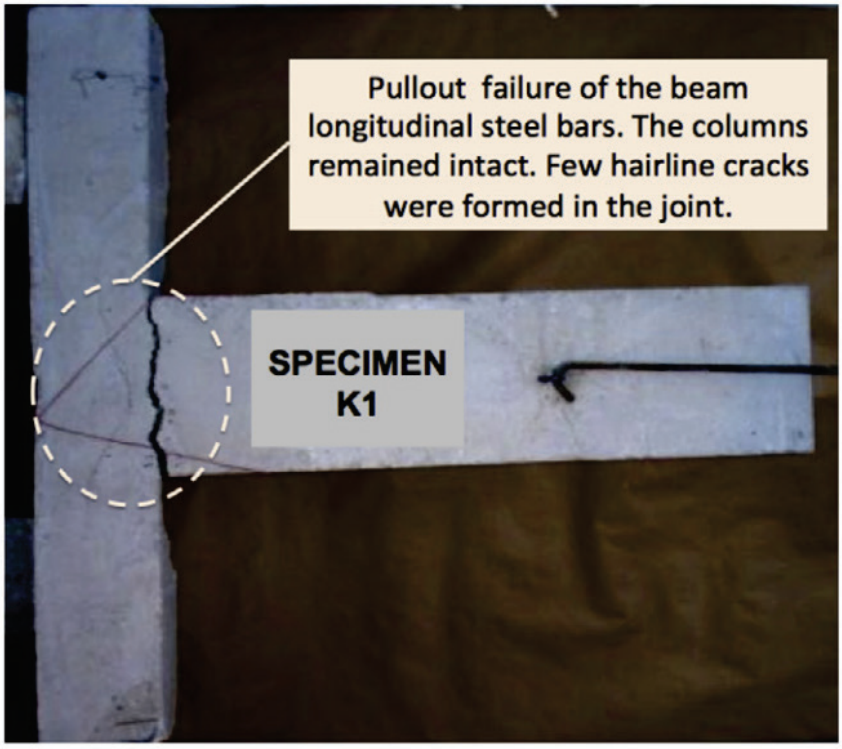

(a)

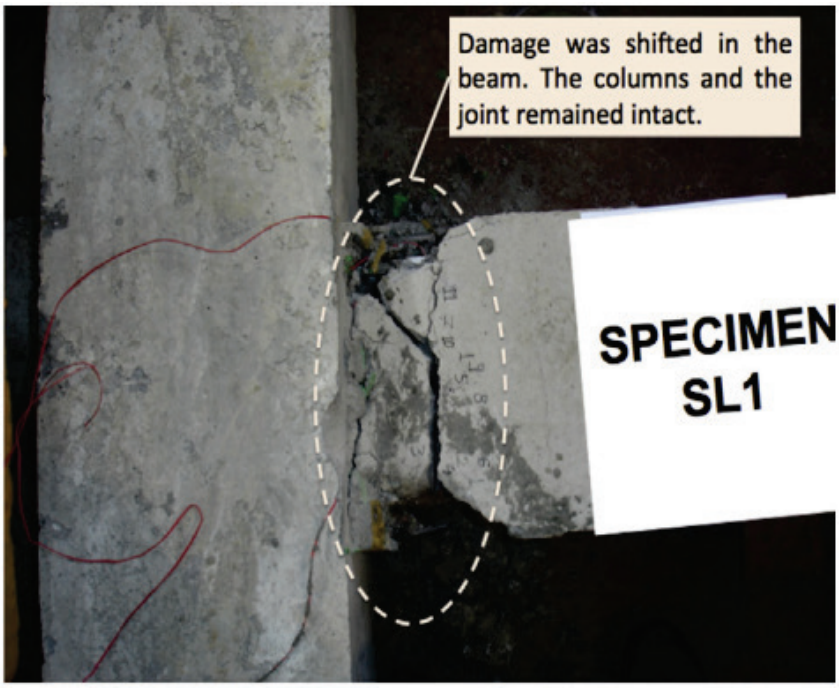

(b)

Figure 1.14 Failure mode of: (a) benchmark specimen (b) strengthened specimen

Some of the strengthening methods explained above were effective in improving the anchorage of the beam rebar by preventing or delaying the pullout of beam longitudinal bars from the joints. However, they are not easily implemented in developing countries because of the need for advanced materials and the complexity of the construction process. In addition, the construction of these strengthening methods may be difficult because of the existence of orthogonal beams and slabs, as well as the needs to remove existing concrete/steel.

1.3. Research Objective

The main objective of this study is to propose a strengthening method by installing wing walls for exterior beam-column joints with deficient anchorage. Experimental tests were conducted to develop the effective strengthening design, even for an extreme case with low-strength concrete. The main goal of the proposed strengthening method is to prevent brittle failure due to anchorage failure of the joints and improving the seismic performance of the building structure. Several stages of research were conducted as follows:

1. Field investigation on seismic detailing of newly constructed RC buildings in West Sumatra, Indonesia.
2. Experimental tests on existing exterior beam-column joints with deficient anchorage representing Bangladeshi buildings with low strength concrete.
3. Pullout tests to investigate the performance of post-installed anchors in low strength concrete.
4. Experimental test on strengthening of an exterior beam-column joint with deficient anchorage by installing wing walls.
5. Application of pushover analysis to evaluate the seismic performance of an RC building strengthened by the proposed method.

1.4. Outline of Thesis

This thesis is presented in seven chapters that are organized as follows. Chapter 1 introduces the background, literature review, and research objective. The outline of the thesis is also described in this chapter.

Chapter 2 reports a field investigation in West Sumatra, Indonesia, which is an area affected by the 2009 Sumatra Earthquake. It was conducted to investigate the deficiencies in newly constructed RC buildings, particularly material specification and detailing of beam-column joint.

Chapter 3 explains the experiment on existing exterior beam-column joints with deficient anchorage representing Bangladeshi buildings. Two RC exterior beam-column joints with substandard details at beam rebar anchorage were tested to identify the potential brittleness of RC buildings in Bangladesh because significantly low concrete strength of 10 N/mm^2 or less has commonly been used historically in that country.

Chapter 4 explains a series of pullout tests on post-installed anchors in low strength concrete with brick chips representing Bangladeshi concrete. The test results contribute to the design of the details of anchors in installing wing walls, particularly to find the minimum embedment length of the anchor for preventing brittle failure of the anchors.

Chapter 5 explains the experiment on strengthening of an exterior beam-column joint by installing wing walls. The strengthening was applied to one of the beam-column joints showing vulnerability to anchorage failure in Chapter 3. A design concept considering the length of wing walls to extend the development length of beam rebar was proposed.

Chapter 6 presents the application of pushover analysis to evaluate the seismic performance of an RC building strengthened by wing walls. The analysis was conducted to

investigate the improvement of strength and deformation capacity of the building after installation of wing walls.

Finally, Chapter 7 summarizes the main findings of this study and further research needs related to strengthening of exterior RC beam-column joints with wing walls.

Chapter 2
Investigation on Seismic Detailing of RC Buildings in West Sumatra Indonesia

2.1. Introduction

On 30 September 2009, an earthquake of magnitude 7.6 struck off the coast of West Sumatra, Indonesia, causing significant damage to many reinforced concrete (RC) buildings. An example of collapsed buildings in Padang, the capital city of West Sumatra is shown in **Figure 2.1**. The collapsed/damaged buildings showing deficiencies indicated that implementation of seismic detailing of RC buildings built prior to 2009 was lacking in Padang city and surrounding areas.

Deficiencies observed on the collapsed/damaged buildings after the 2009 earthquake were similar to those seen in older RC buildings in the United States and developing regions throughout the world, such as use of plain reinforcing bars, insufficient column ties with 90^{o} hooks with minimal overlap, and absence of column stirrups in beam-column joints [3]. The damage due to these kind of deficiencies should be a lesson learned in construction of new buildings in the affected area in West Sumatra. However, the deficiencies of seismic detailing may exist in recently constructed buildings. Therefore, investigation is needed to observe the current condition in the construction practice.

In this study, the first phase investigation was conducted by field investigation, where implementation of seismic detailing in newly constructed multi-story RC buildings in West Sumatra Province was observed. The requirements of the latest Indonesian concrete design code for buildings SNI 2847:2013 [16] related to seismic detailing of RC buildings in high seismic risk area were compared with the actual condition in construction practice in the investigated areas. The provisions of this code were based on the ACI 318-11 [17]. Therefore, the code

requirements are also generally applied to many regions around the world in which their national building code is based on the ACI code.

The second phase investigation was conducted by inviting local construction workers in a series of workshops to observe the rebar work practice. Then, the results from the second phase investigation were compared with those of the first phase investigation to find the relationship of quality of rebar works by the workers with the seismic detailing of RC buildings in real construction.

Figure 2.1 Example of collapsed buildings [3]

2.2. Investigation Methods

2.2.1. Field Investigation

The field investigation was the first phase of this study, which was conducted in five cities in West Sumatra Province: Padang, Bukittinggi, Pariaman, Solok, and Painan. The location of the cities is shown in **Figure 2.2**. Padang city is the capital city of West Sumatra Province. Bukittinggi, Pariaman, Solok, and Painan cities are located north, north-west, east, and south of Padang city, respectively.

The investigation was conducted from September 2016 to March 2018. There are two categories of RC buildings in the investigated areas: (1) RC frame with infill masonry buildings

and (2) confined masonry buildings. The current investigation is focused on RC frame with infill masonry buildings only, thus confined masonry buildings were excluded.

The structural details of the buildings were obtained by visiting the building construction sites. Investigated items on the structural details are listed in **Table 2-1**. The methods to obtain the data were also shown in the table.

Figure 2.2 Administrative map of West Sumatra Province [18]

The results of field investigation were compared with the requirements of Indonesian design codes. Based on the Indonesian seismic design code SNI 1726:2012 [19], the five cities are located in the seismic design category of D. RC frame buildings built in these areas should

be designed as special moment resisting frame (SMRF). RC frame with infill masonry buildings are commonly designed as open moment resisting frame, while masonry infill walls are regarded as non-structural element of which the stiffness and strength are not typically considered in design. Thus, RC frame with infill masonry buildings built in the investigated areas should meet the requirements for concrete SMRF, as regulated in the Indonesian concrete design code SNI 2847:2013 [16].

Table 2-1 List of Investigated Items and Methods

<table>
<tr><th colspan="2">Investigated items</th><th>Methods</th></tr>
<tr><td rowspan="2">A. Material specification</td><td>Compressive strength of concrete</td><td>- Design drawing
- Hammer test[a)]</td></tr>
<tr><td>Type of rebar</td><td rowspan="4">- Design drawing and field inspection[b)]</td></tr>
<tr><td rowspan="4">B. Detailing of column</td><td>Dimensions</td></tr>
<tr><td>Longitudinal reinforcement</td></tr>
<tr><td>Transverse reinforcement</td></tr>
<tr><td>Lap splice</td><td>- Field inspection[c)]</td></tr>
<tr><td rowspan="4">C. Detailing of beam</td><td>Dimensions</td><td rowspan="3">- Design drawing and field inspection[b)]</td></tr>
<tr><td>Longitudinal reinforcement</td></tr>
<tr><td>Transverse reinforcement</td></tr>
<tr><td>Lap splice</td><td rowspan="3">- Field inspection[c)]</td></tr>
<tr><td rowspan="2">D. Detailing of beam-column joint</td><td>Transverse reinforcement in joint</td></tr>
<tr><td>Anchorage of beam reinforcement</td></tr>
</table>

[a)]Hammer test was used to estimate the compressive strength of concrete if it could not be obtained from design drawing.

[b)]Detailing of these items is commonly provided in design drawing. Then, the data were confirmed through field inspection.

[c)]Detailing of these items is not commonly provided clearly in design drawing. The data were obtained by field inspection

This study investigated 100 buildings in the five cities in West Sumatra Province. Number of the investigated buildings in each city is shown in **Figure 2.3**. **Figure 2.4** and **Figure 2.5** show distributions of the number of stories and category of function of the investigated buildings, respectively.

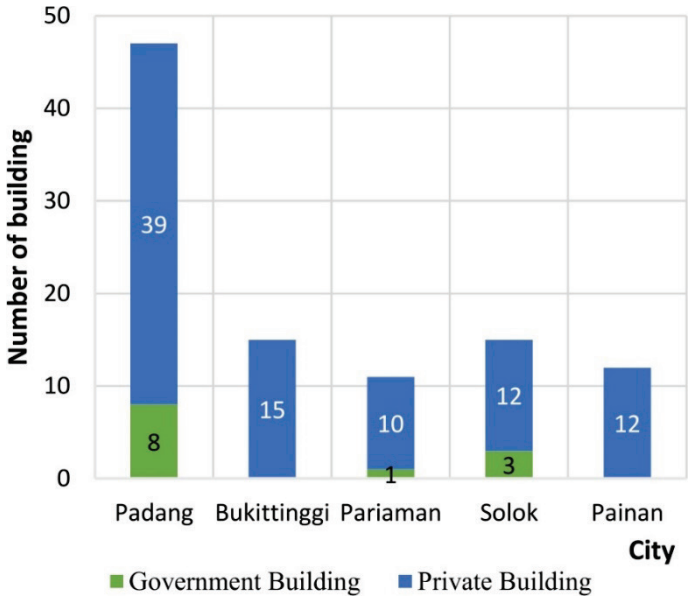

Figure 2.3 Number of investigated buildings in each city

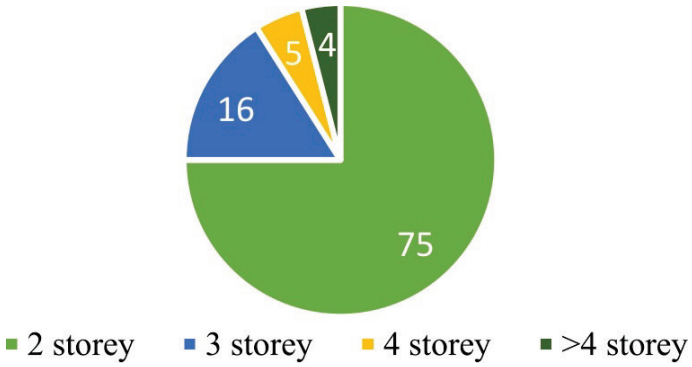

Figure 2.4 Distribution of number of stories of investigated buildings

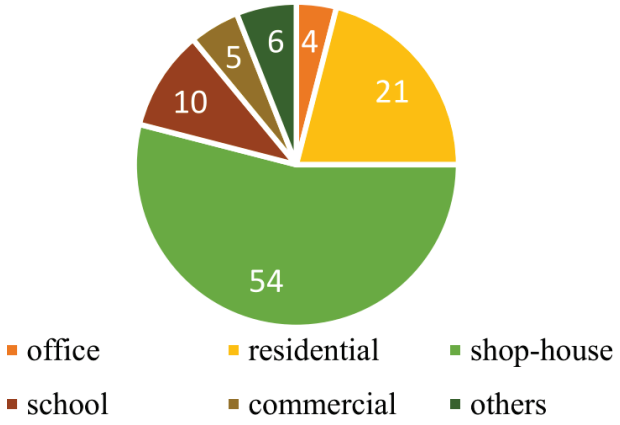

Figure 2.5 Distribution of category of function of investigated buildings

2.2.2. Workshop with Local Construction Workers

In the second phase investigation, local construction workers were invited to a series of workshops. The workers were from the five cities which were focused in the first phase investigation. In every workshop, 18 workers from each city were invited. A total of 90 workers were invited to 5 workshops. In the workshops, the local workers were requested to do rebar work practice using tools and methods that they usually used in real construction. The requested work was rebar fabrication of a full-scale beam-column subassembly, as shown in **Figure 2.6**. The rebar fabrication works consisted of cutting, bending, and assembling of rebar. Evaluation of the works by the workers was done by comparing the result of their works with a given drawing for the practice. Interview was also conducted for several items which could not be observed during the practice.

Figure 2.6 Rebar fabrication by local workers in the workshop

2.3. Investigation Results

In this section, only investigation results on material specification and detailing of beam column-joint are explained. The investigation results for the other items, such as detailing of column and beam, are explained in **Appendix A**.

2.3.1. Material Specification

2.3.1.1. Concrete Material

Indonesian code [16] stipulates that the minimum concrete compressive strength (fc') for RC buildings in high seismic risk area is 20 MPa. In Padang city, more than 80% of the investigated buildings satisfied this requirement, as shown in **Figure 2.7**. However, in other four cities, almost half of the investigated buildings did not meet this requirement because of application of concrete with the standard of K-225 (cubical compressive strength of 225 kg/cm^2) which corresponded to cylindrical compressive strength (fc') of 18 MPa. The concrete material was better in the capital city, Padang, because of the easy availability of ready-mixed concrete.

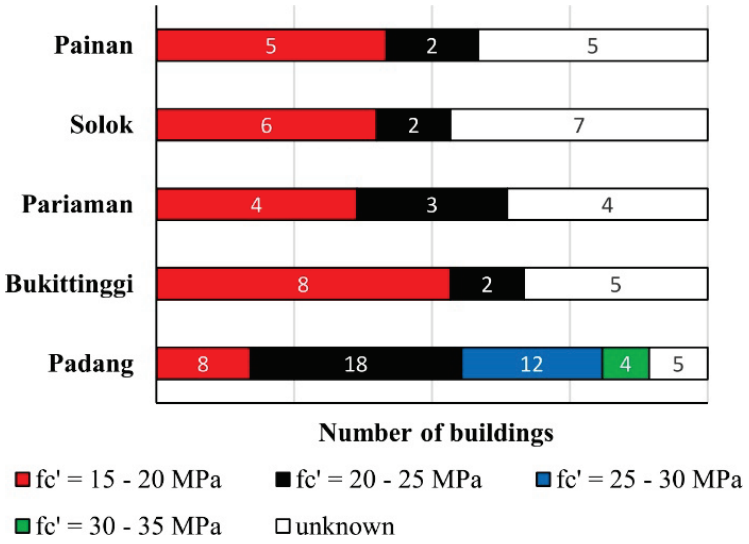

Figure 2.7 Field investigation results on concrete compressive strength

2.3.1.1. Rebar Material

Deformed bar should be used as longitudinal and transverse reinforcement, plain bar is allowed to use only for spiral reinforcement, as regulated in the Indonesian code [16]. More than 70% of the investigated buildings in Padang city were applied deformed bar for longitudinal reinforcement, as shown in **Figure 2.8(a)**. However, in the other four cities, many of the buildings were applied plain bar as longitudinal reinforcement. Focusing on shear reinforcement, most of investigated buildings in all five cities were applied plain bar, as shown in **Figure 2.8(b)**. These results indicated that deformed bar has been widely used only in the capital city, especially for longitudinal reinforcement.

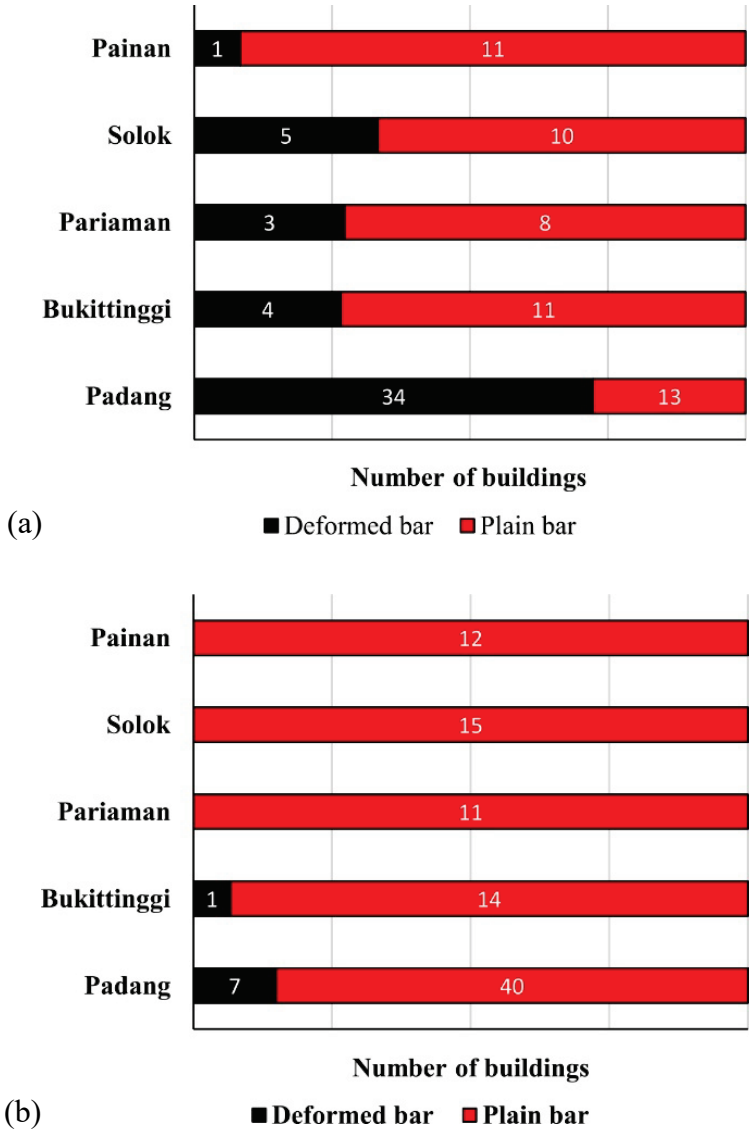

Figure 2.8 Field investigation results on types of rebar used as reinforcement; (a) Longitudinal reinforcement; (b) Transverse reinforcement

2.3.2. Detailing of Beam-Column Joint

2.3.2.1. Transverse Reinforcement in Joint

Referring to the Indonesian code [16], transverse reinforcement should be provided inside beam-column joints. For an exterior joint, amount and spacing of the transverse reinforcement are similar for those on the adjacent column hinge region, as shown in **Figure 2.9**. For an interior joint, if the beam width is at least 3/4 of the column width, the transverse reinforcement can be reduced to 50%, while its spacing shall not exceed 150 mm. **Figure**

2.10(a) and **Figure 2.10(b)** show the field investigation results of hoop details in the exterior and interior beam-column joints, respectively. Most of the observed joints did not satisfy the requirement, because of no hoops or lack of hoops in the joints.

In the rebar works of the workshops with local workers, it was observed that all workers applied the hooks inside the beam-column joint (of the model shown in **Figure 2.6**), which did not agree with the observation results in real buildings from the field investigation. It seemed to be caused by easier works in the practice using the subassembly model. However, in real construction practice, hoops in the exterior and interior joints were not likely to be applied without eliminating difficulties posed by rebar congestion.

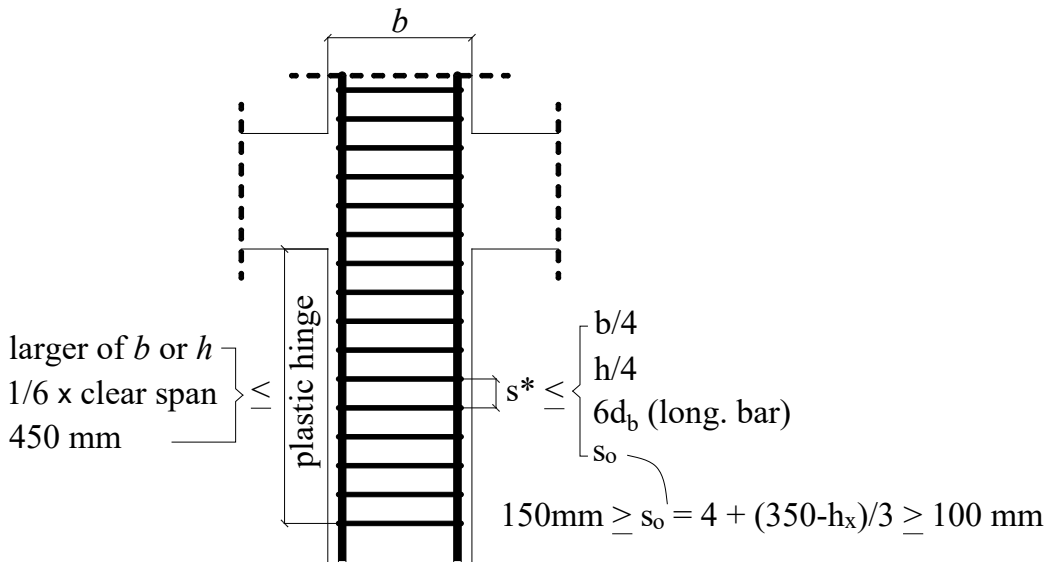

Figure 2.9 Requirements for spacing of transverse reinforcement of column in the plastic hinge and in the beam-column joint

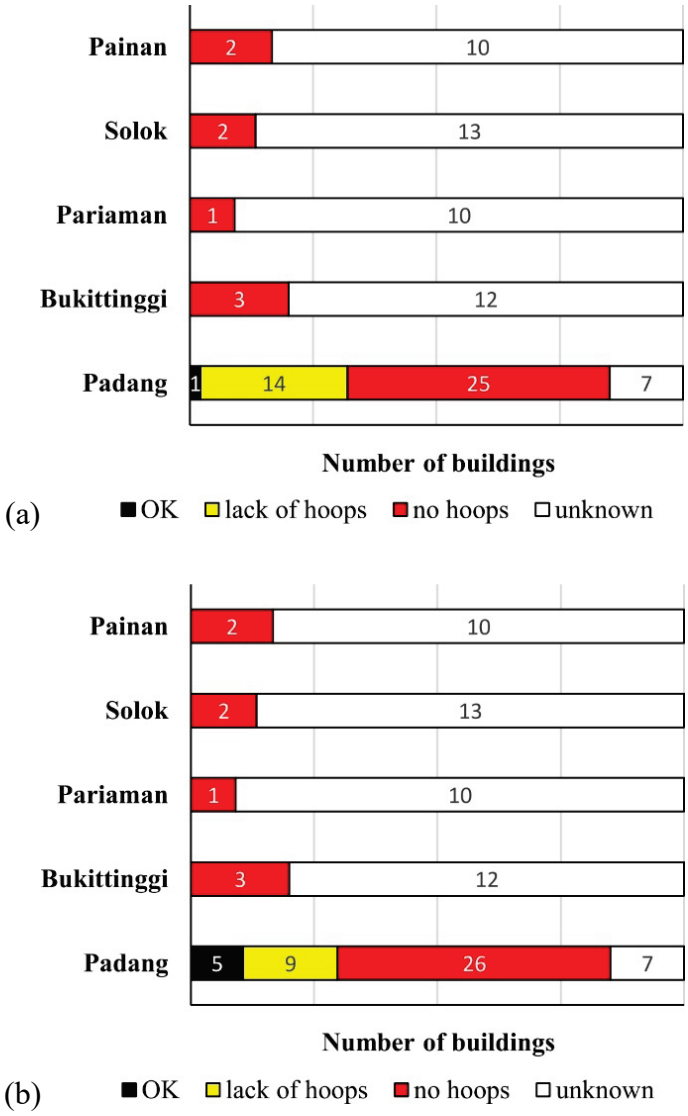

Figure 2.10 Field investigation results on hoops in beam-column joint; (a) Exterior joint; (b) Interior joint

2.3.2.2. Anchorage of Beam Reinforcement

The Indonesian code [16] regarding exterior joints regulates that the longitudinal beam reinforcement in a column shall be extended to the far face of the confined column core and anchored. The length of anchorage (l_{dh}) shall be the largest of 8 bar diameters, 150 mm, and the length required by the following equation:

$$l_{dh} = \frac{f_y d_b}{5.4\sqrt{f_c'}} \qquad (2\text{–}1)$$

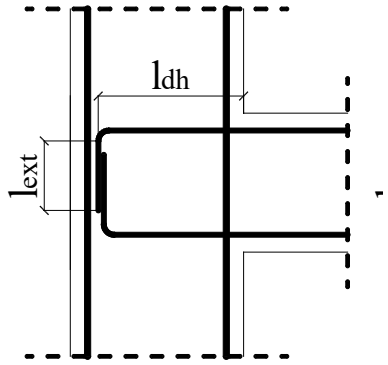

Figure 2.11 Definition of length of anchorage and length of tail extension

Most of the observed joints in the field investigation satisfied the requirement for the length of anchorage, as shown in **Figure 2.12(a)**. The observation of the rebar works in the workshops with local workers showed that all the workers applied the anchorage length to the far face of column, therefore most of the observed joints satisfied the requirement.

Furthermore, the end of rebar shall be bent with a 90^o hook and the length of tail extension (l_{ext}) must not be less than $12d_b$ (diameter of longitudinal bar). However, most of the observed joints in the field investigation did not satisfy the requirement for the length of tail extension, as shown in **Figure 2.12(b)**. In fact, during the rebar works of the workshops with local workers, it was observed that most of the workers applied the length of tail extension less than the requirement, as shown in **Figure 2.13**.

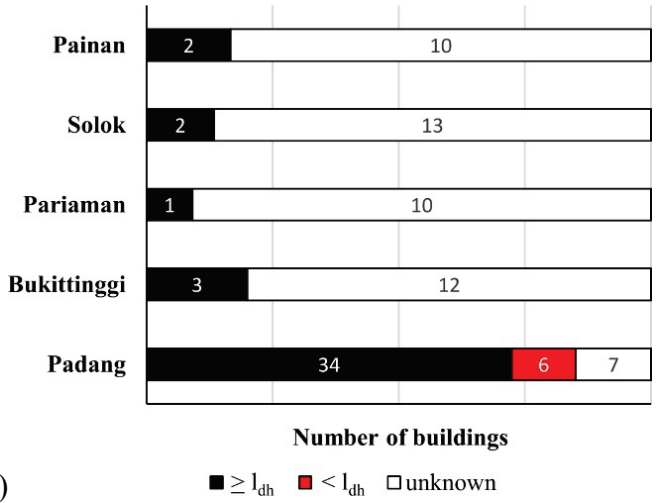

(a)

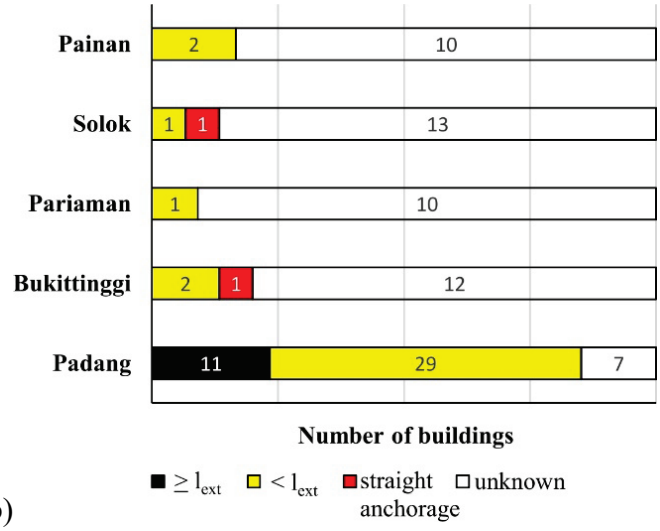

(b)

Figure 2.12 Field investigation results on anchorage of beam reinforcement into exterior joint; (a) Length of anchorage; (b) Length of tail extension

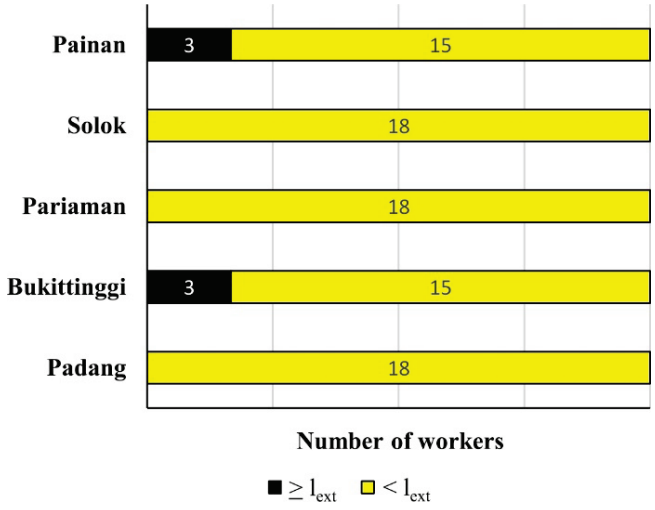

Figure 2.13 Workshop results on anchorage of beam reinforcement into exterior joint; Length of tail extension

Figure 2.14(a) and **Figure 2.14(b)** show typical deficiencies of interior joint and exterior joint without transverse reinforcement, respectively. **Figure 2.14(b)** also shows the worst detail for the anchorage of beam reinforcement to exterior joint in which straight anchorage was applied. The straight anchorage was observed only in case that deformed bar was used as longitudinal reinforcement. The deficient joints had potential shear failure and/or anchorage failure which can lead to building collapse if an earthquake occurs; therefore, a practical strengthening method for the deficient beam-column joints with is a very urgent issue.

(a)

(b)

Figure 2.14 Deficiencies in detailing of beam-column joint; (a) Interior joint; (b) Exterior joint

2.4. Summary

The investigation has been conducted in newly constructed RC buildings in West Sumatra, Indonesia. Major findings are summarized as follows.

1. The application of substandard materials for concrete and reinforcement existed in many buildings in the investigated area.
2. The deficiencies of seismic detailing of beam-column joints, such as lack of hoops inside exterior/interior beam-column joints and deficient anchorage of beam longitudinal reinforcement to exterior beam-column joints, were observed in most of the observed joints.
3. The worst detail of anchorage in exterior beam-column joints was the straight anchorage of beam reinforcement to the exterior joint.
4. A strengthening method for deficient beam-column joints, which is expected to be a practical solution in developing countries, is a very important issue.

Chapter 3
Experiments of Exterior Beam-Column Joints with Deficient Anchorage Representing Bangladeshi Buildings

3.1. Introduction

Bangladesh is a riverine country, most of the surface geology of Bangladesh is dominated by alluvial sediment, and natural stone sources are scarce. As natural stone is in limited availability and hence is expensive, brick chips, which usually produce low-strength concrete, are extensively used as coarse aggregate for RC construction in Bangladesh. Bangladesh is also located in a risky zone for earthquakes because neighboring countries are tectonically active. However, in construction practice, less attention has been given to the seismic resistance of buildings because earthquakes are not frequent in Bangladesh. The latest Bangladeshi National Building Code (BNBC) 2015 [20] has been issued recently with strict requirements for seismic detailing of RC buildings. Many existing buildings do not meet the requirements of the code. The provisions related to the concrete structures in the BNBC 2015 base on the ACI 318-11[17]. Many other countries also base their national building code to the ACI code; therefore, the code requirements (i.e. requirements on anchorage of beam rebar into exterior joints which will be described later in **Section 3.1.1**) also generally apply for many regions around the world.

The seismic detailing of beam-column joints is usually given less attention in construction practice, particularly for details of beam rebar anchorage into exterior joints. **Figure 3.1(a)** shows the typical deficiency of joints with deformed bars and straight anchorages at the end. This deficiency seems to be the worst case observed in buildings built after 1995, when deformed bars were introduced in Bangladesh. **Figure 3.1(b)** shows the other typical details of joints using plain bars with 180° hooks. This case is typical for buildings built before 1995, when all buildings in Bangladesh were constructed using plain bars.

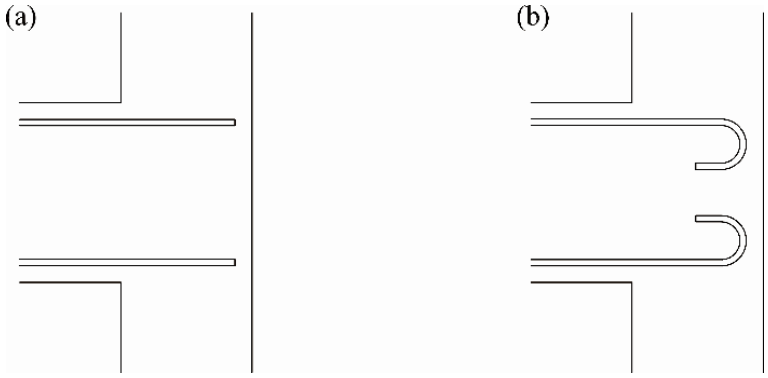

Figure 3.1 Typical details of the anchorage of beam rebar into exterior joints in Bangladesh: (a) after 1995 (b) before 1995

3.1.1. Code Requirements on Anchorage of Beam Rebar into Exterior Joints

The anchorage of beam rebar into exterior joints should be designed to satisfy the requirement of development length for rebar in tension. **Equations (3-1)** to **(3-4)** show the required development length for deformed bar without hooks in tension (l_d) based on the Bangladeshi code [20], which is similar to that of the ACI code [17].

$$l_{d1} = \frac{f_y\,\psi_t\,\psi_e}{2.1\,\lambda\sqrt{f_c'}}\,d_b \qquad \text{for } d_b \le 19 \text{ mm} \tag{3-1}$$

$$l_{d2} = \left(\frac{f_y}{1.1\,\lambda\sqrt{f_c'}}\,\frac{\psi_t\,\psi_e\,\psi_s}{\left(\frac{c_b+K_{tr}}{d_b}\right)}\right)d_b \tag{3-2}$$

$$l_{d3} = 300\ mm \tag{3-3}$$

$$l_d = \max.(l_{d1}, l_{d2}, l_{d3}) \tag{3-4}$$

where f_y is the yield stress of longitudinal reinforcement; ψ_t is a rebar location factor that accounts for the position of rebar in freshly placed concrete (where horizontal reinforcement is placed such that more than 300 mm height of fresh concrete is cast below the development length, use ψ_t = 1.3; for other reinforcement, use ψ_t = 1.0); in this study, ψ_t = 1.0 is used for all beam longitudinal bars; ψ_e = 1.0 for uncoated reinforcement; λ = 1.0 for normal-weight concrete; f_c' is the compressive strength of concrete; d_b is the diameter of the longitudinal reinforcement; ψ_s = 0.8 for bar diameter < 19 mm, c_b is the minimum value between the distance of the bar center to the nearest concrete surface and one-half of the center to center spacing of

the bar; K_{tr} = 0 as a design simplification even if transverse reinforcement is present; and $(c_b + K_{tr})/d_b$ is not taken greater than 2.5.

Equations (3-5) to **(3-8)** show the requirements of the Bangladeshi code [20] or ACI code [17] for the development length of deformed bar with a standard 90° hook or 180° hook in tension (l_{dh}). In the case of plain bar, the Bangladeshi code [20] specifies that the development length should be twice that of deformed bar, as described in **Equation (3-9)**.

$$l_{dh1} = \frac{0.24\,\psi_e\,f_y}{\lambda\sqrt{f_c'}}\,d_b \tag{3-5}$$

$$l_{dh2} = 8d_b \tag{3-6}$$

$$l_{dh3} = 150\,mm \tag{3-7}$$

$$l_{dh} = \text{max.}\,(l_{dh1}, l_{dh2}, l_{dh3}) \tag{3-8}$$

$$l_{dh} = 2\,\times\,\text{max.}(l_{dh1}, l_{dh2}, l_{dh3}) \tag{3-9}$$

3.1.2. Target Building and Exterior Beam-Column Joint

This study focuses on an exterior beam-column joint in an intermediate story of a six-story RC frame building in Dhaka, Bangladesh. This building is an existing building in Dhaka, Bangladesh which was chosen as a model building for this study. The focused joint and reinforcement details of the column and beam are shown in **Figure 3.2**. In this study, low-strength concrete with brick chips was applied to the test specimens described later to represent common RC buildings in Bangladesh. The design strength of the concrete for the specimens was 10 N/mm^2.

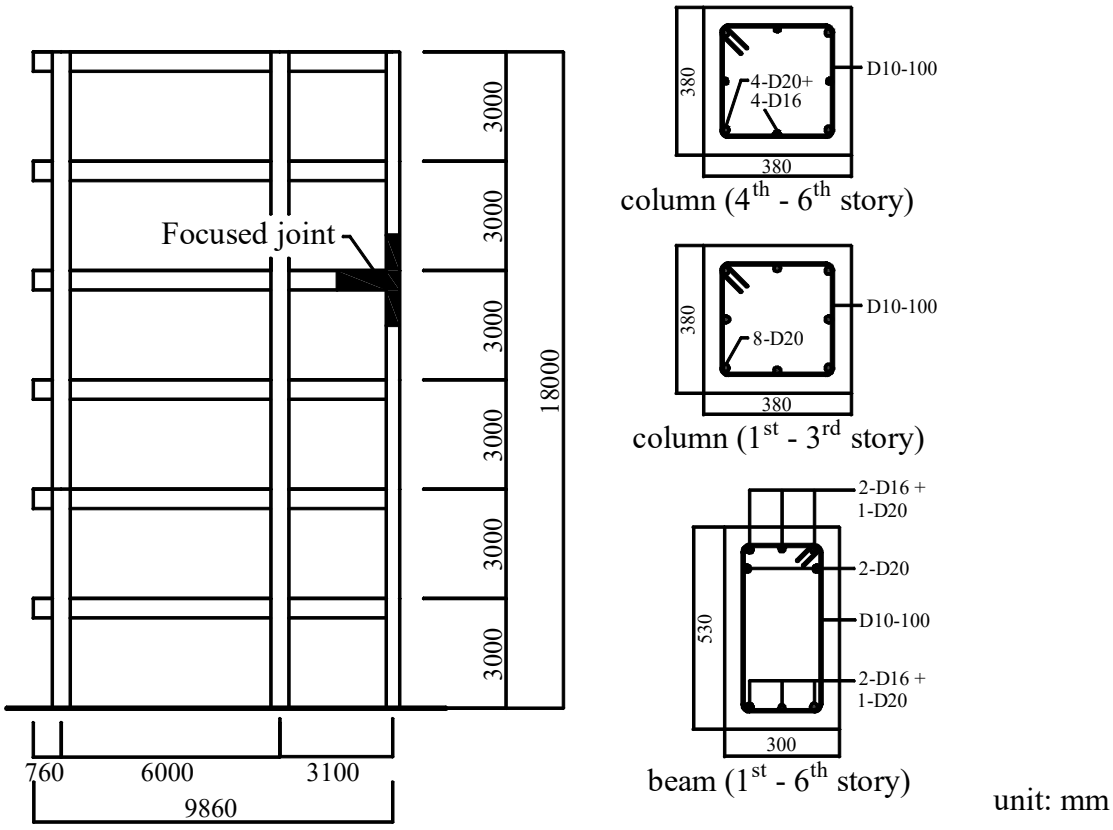

Figure 3.2 The focused joint and reinforcement details of the structural members

3.2. Specimen Details

Two plane-frame specimens were prepared with a 0.7 scale of the exterior joint, as shown in **Figure 3.2**, namely, J1 and J2, representing the typical details shown in **Figure 3.1(a)** and **3.1(b)**, respectively. J1 was a specimen with a deformed bar and a straight anchorage of beam longitudinal bars. J2 was a specimen using a plain bar with standard 180° hook as beam longitudinal bars. These specimens were modeled up to the inflection points of the upper/lower column and beam, where the lengths of pin supports attached to the column ends and beam end were included (refer to **Figure 3.9**).

Figure 3.3 shows the dimensions and reinforcement details of specimen J1. The specimen J1 used a deformed bar with a grade of SD295A (min. specified yield strength 295 MPa) for reinforcement in the column and beam. The existing development length ($_{ex}l_d$) was 235 mm, which was much shorter than the required development length (l_d) of 579 mm, as

calculated by **Equation (3-4)**. Therefore, anchorage failure, bond slip or pullout of the beam longitudinal bars was expected to occur.

Figure 3.4 shows the dimensions and reinforcement details of specimen J2. The same dimensions and details as those of specimen J1 were applied to specimen J2, except for the beam reinforcement details and anchorage of beam rebar to the joint. A plain bar with a grade of SR235 (min. specified yield strength 235 MPa) was used for reinforcement in the beam. Anchorage failure may occur because the existing development length ($_{ex}l_d$) of 235 mm was much shorter than the required development length (l_{dh}) of 464 mm, as calculated by **Equation (3-9)**. The specimens J1 and J2 were designed to yield at nearly equal flexural moment capacity by specified material strengths (values in parentheses in **Table 3-3**).

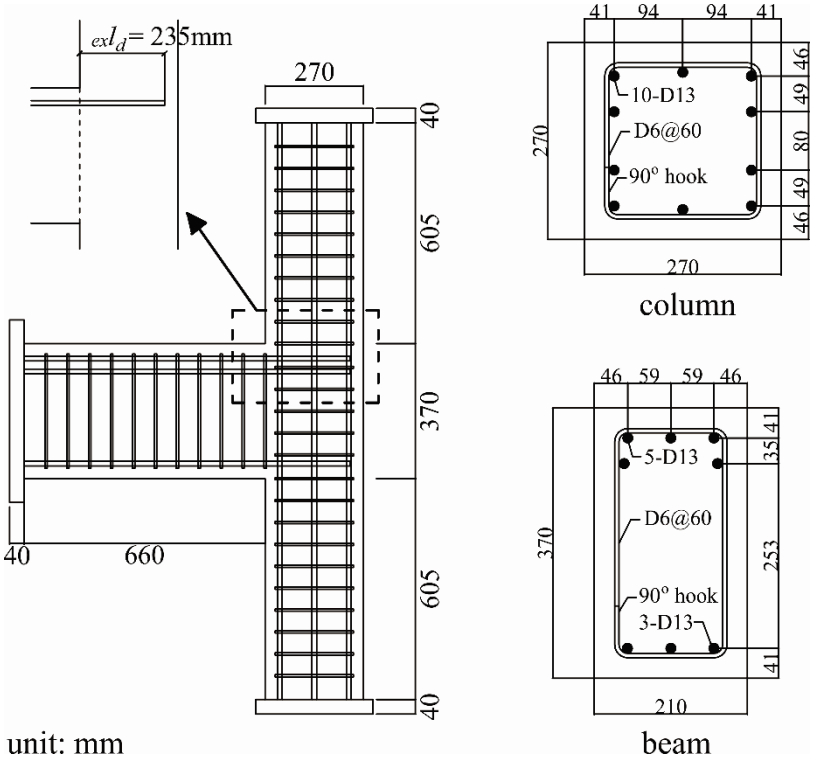

Figure 3.3 Dimensions, reinforcement and anchorage details for specimen J1

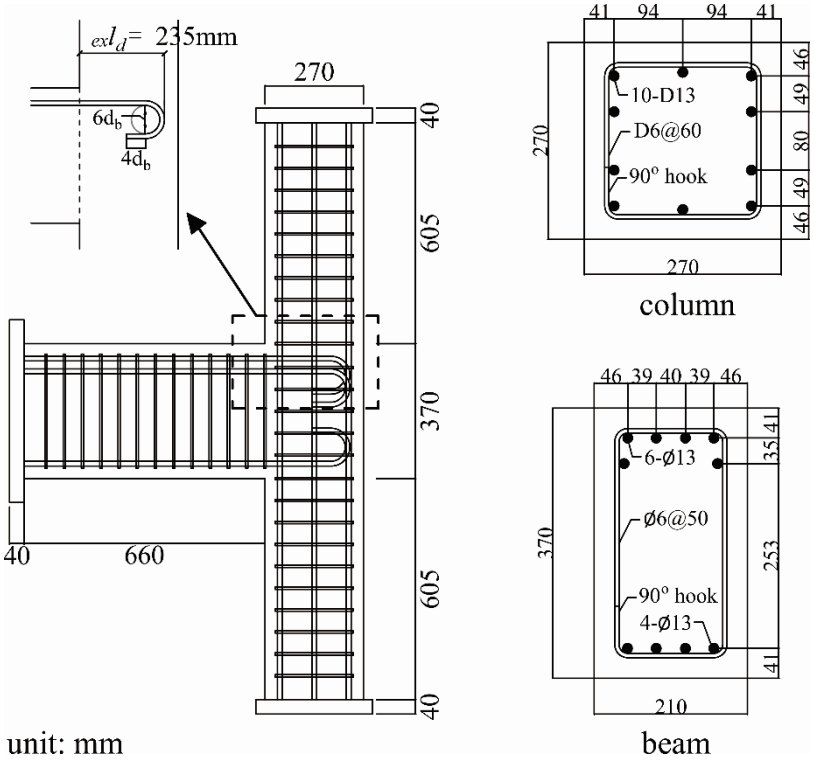

Figure 3.4 Dimensions, reinforcement and anchorage details for specimen J2

The specimens were constructed with low-strength concrete using brick chips as coarse aggregate with a maximum aggregate size of 20 mm. The volumetric ratio of cement:sand:brick chips was 1:2:4 with a water-to-cement ratio of 0.6. This mixture was designed through preliminary material tests [21]. The concrete was mixed on site using a concrete mixer and three batches of concrete mixtures were required to cast each specimen. For each concrete mixture batch, three concrete cylinder samples were prepared for the compressive tests and three concrete cylinder samples were prepared for the splitting tensile tests of concrete. **Table 3-1** gives the average mechanical properties of the concrete from the compressive tests and the split tensile tests of the concrete cylinder. The stress-strain relationship for concrete is shown in **Figure 3.5** and **3.6.** The curves with dashed line in the figures possibly had a problem in strain measurement; therefore, they were neglected in calculating the average Young s modulus.

Table 3-1 Mechanical properties of concrete.

Specimen	Compressive strength (N/mm^2)	Young's modulus (N/mm^2)	Split tensile strength (N/mm^2)
J1	11.0	8,723	0.90
J2	10.3	9,046	0.74

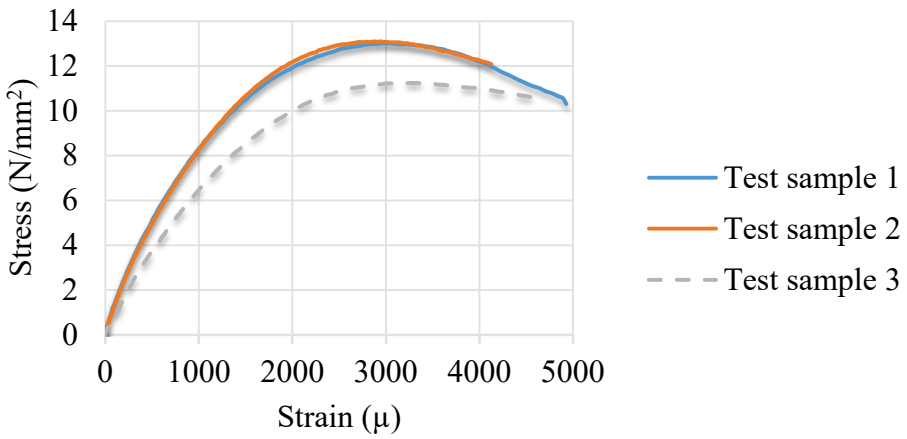

(a)

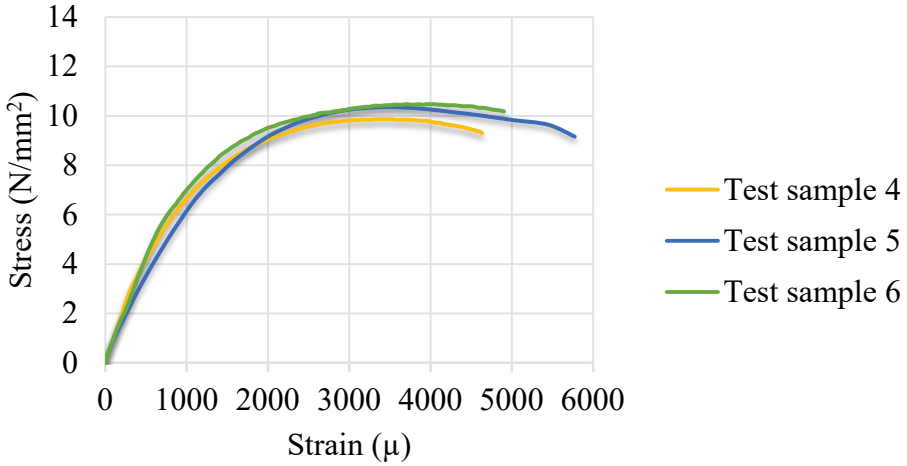

(b)

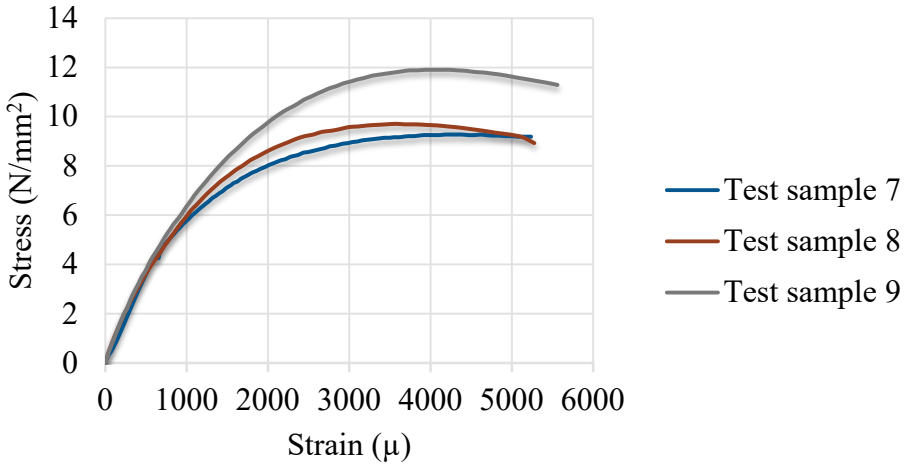

(c)

Figure 3.5 Stress-strain relationship from cylinder tests of concrete for specimen J1: (a) Mixture batch 1, (b) Mixture batch 2, (c) Mixture batch 3

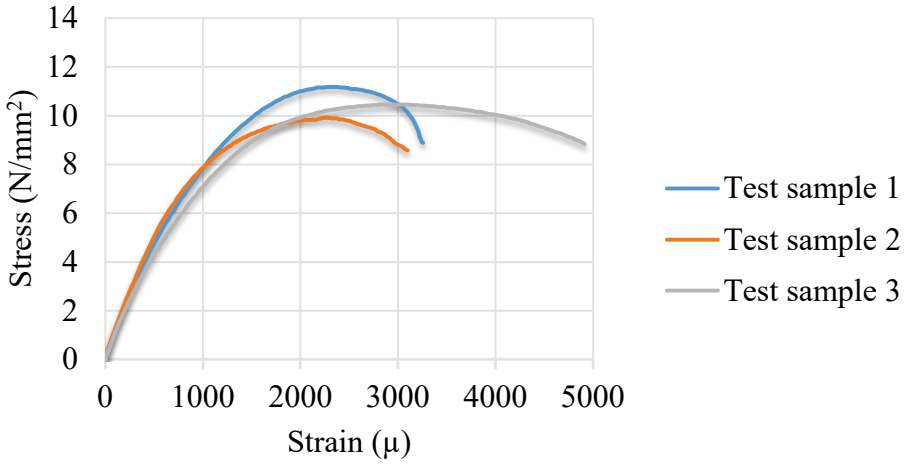

(a)

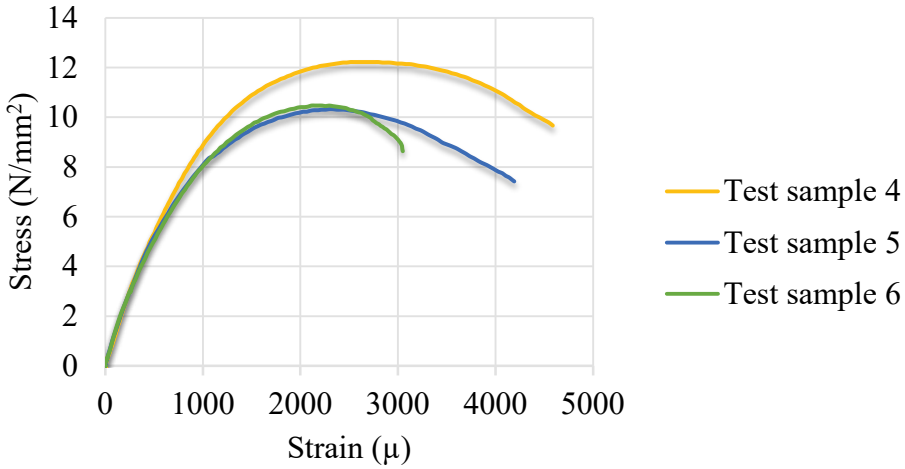

(b)

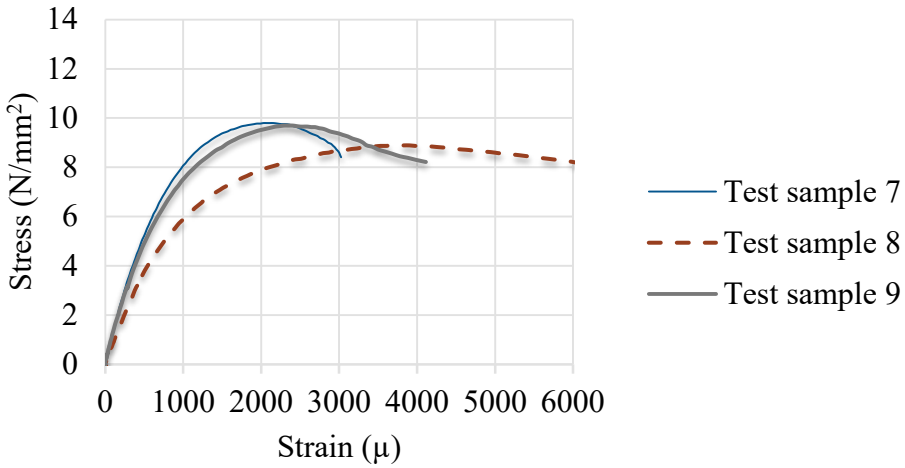

(c)

Figure 3.6 Stress-strain relationship from cylinder tests of concrete for specimen J2: (a) Mixture batch 1, (b) Mixture batch 2, (c) Mixture batch 3

The mechanical properties of reinforcement bars were obtained by the tensile tests. For each type of rebar, three test samples were tested. **Table 3-2** gives the average mechanical properties of the reinforcement bars from the tensile tests and the stress-strain relationships were shown in **Figure 3.7** and **3.8**.

Table 3-2 Mechanical properties of reinforcement.

Type	Grade	Yield stress (N/mm^2)	Tensile strength (N/mm^2)	Young's modulus (N/mm^2)
D13	SD 295A	342	501	174,528
D6	SD 295A	408	547	171,150
Ø13	SR 235	327	456	193,928
Ø6	SR 235	310	393	170,650

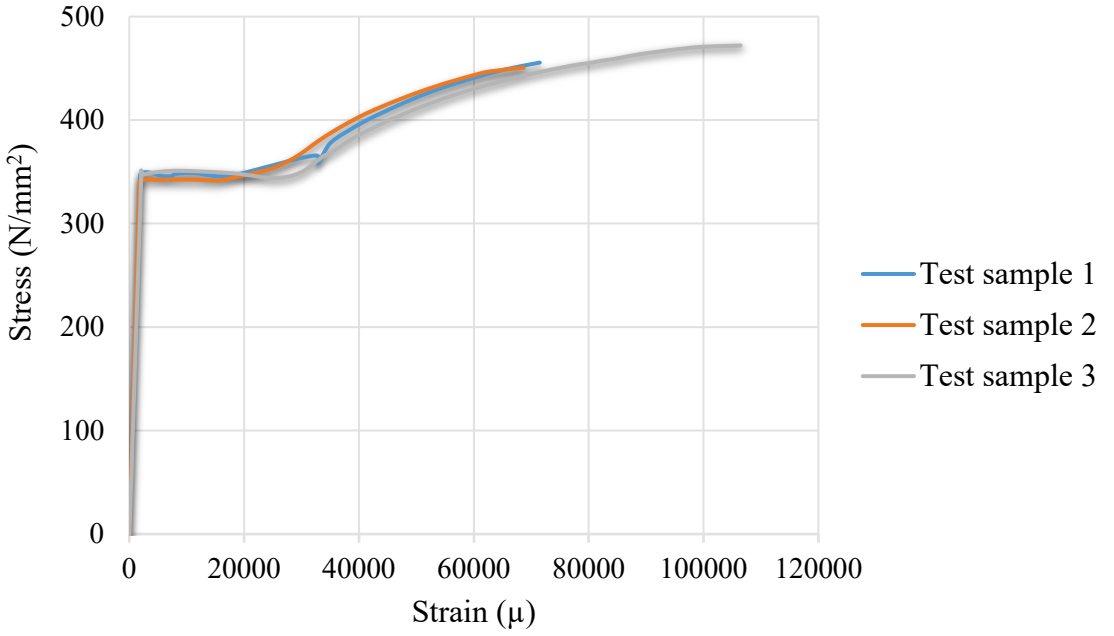

(a)

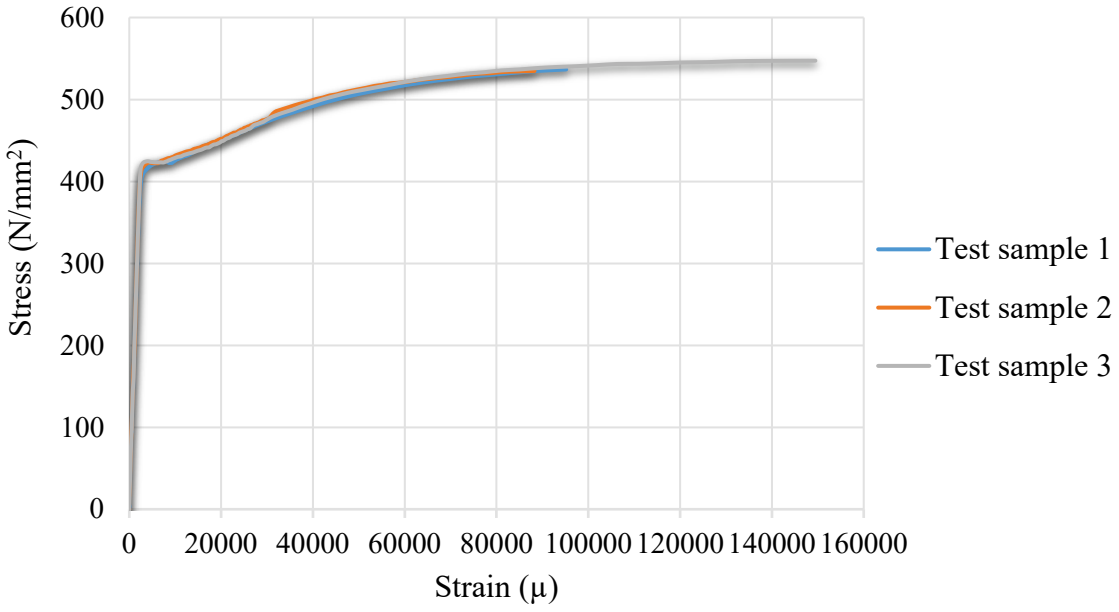

(b)

Figure 3.7 Stress-strain relationship from tensile test of deformed bar: (a) D13, (b) D6

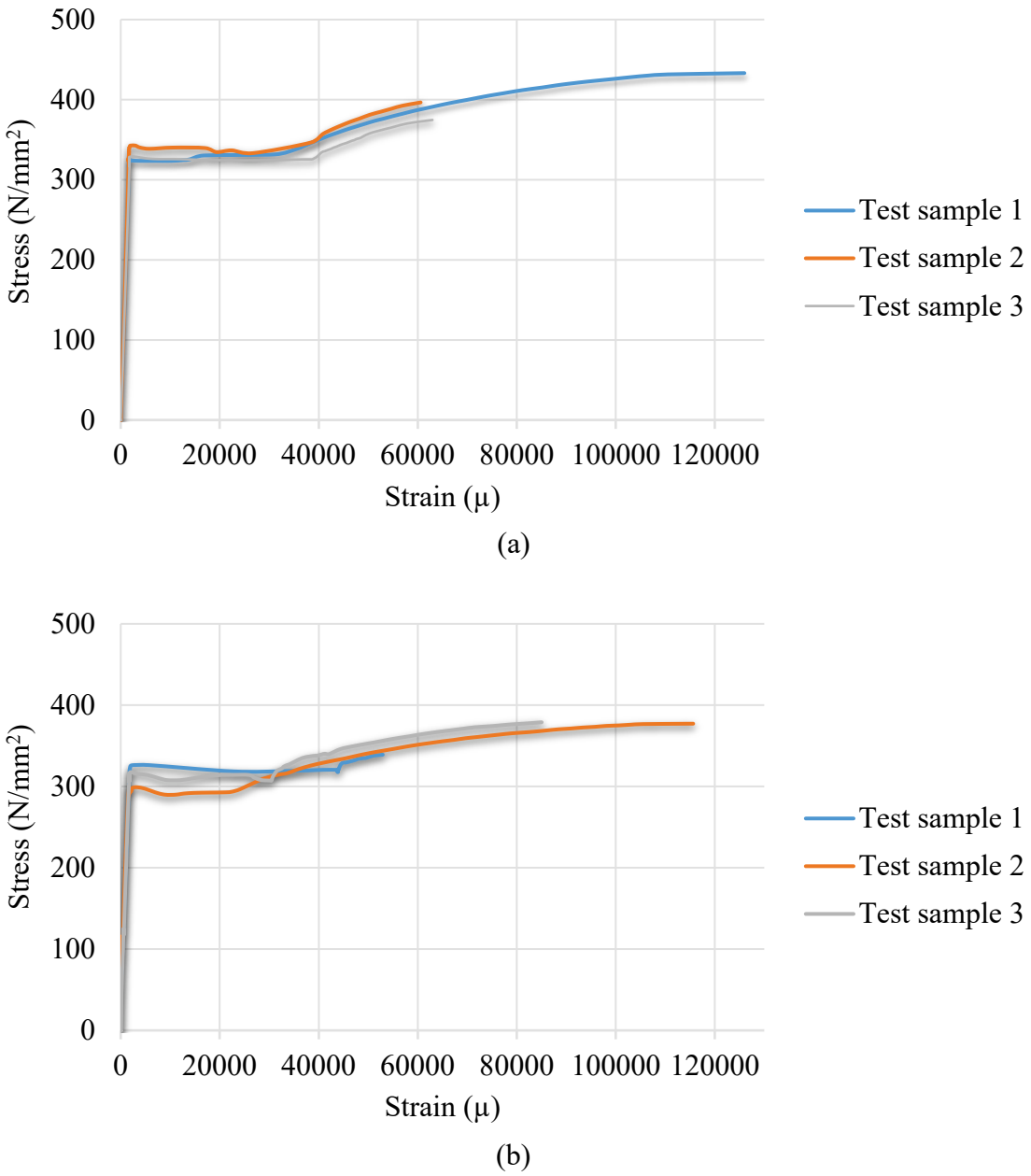

Figure 3.8 Stress-strain relationship from tensile test of plain bar: (a) Ø13, (b) Ø6

3.3. Loading System, Instrumentation, and Loading Program

The test setup is shown in **Figure 3.9**. The upper and lower columns were supported by pin hinges, and the left end of the beam was supported by a roller. To measure the shear force on the beam, a load cell was incorporated into the roller support. The vertical jacks applied a constant axial load with an axial load ratio of 0.10, which represents the axial load on the focused joint in **Figure 3.2**. Horizontal reversed cyclic loading was applied by a horizontal

hydraulic jack controlled by the column drift ratio R=δ/L_c, where δ is the lateral displacement at the column tip. The loading program is shown in **Figure 3.10**. The strain gauge arrangement and the displacement sensor arrangement are shown in **Figure 3.11** and **3.12**, respectively.

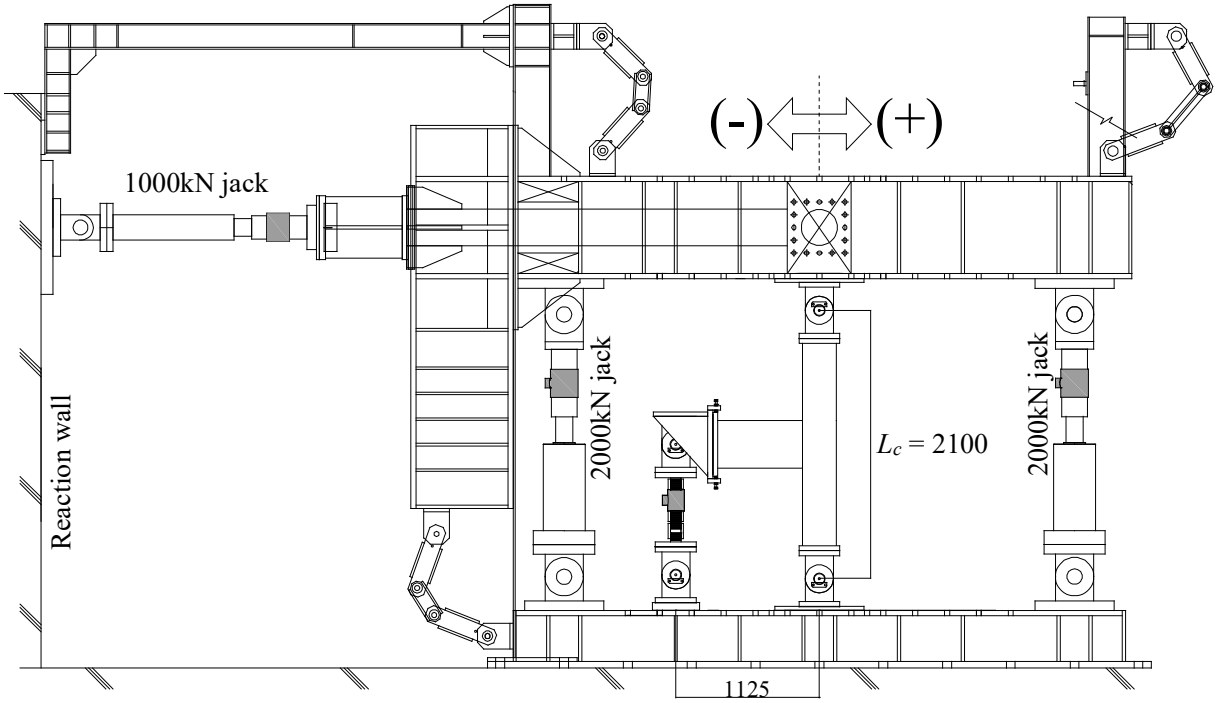

Figure 3.9 Schematic view of the test setup

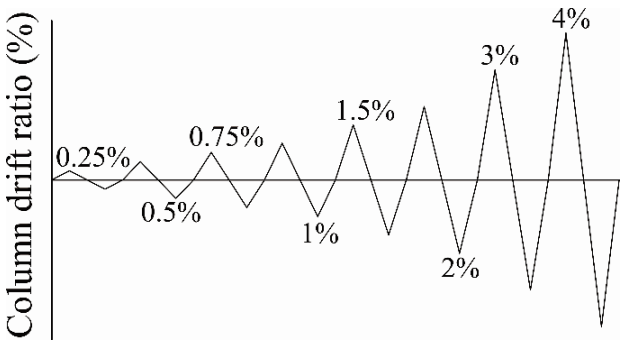

Figure 3.10 Lateral loading history

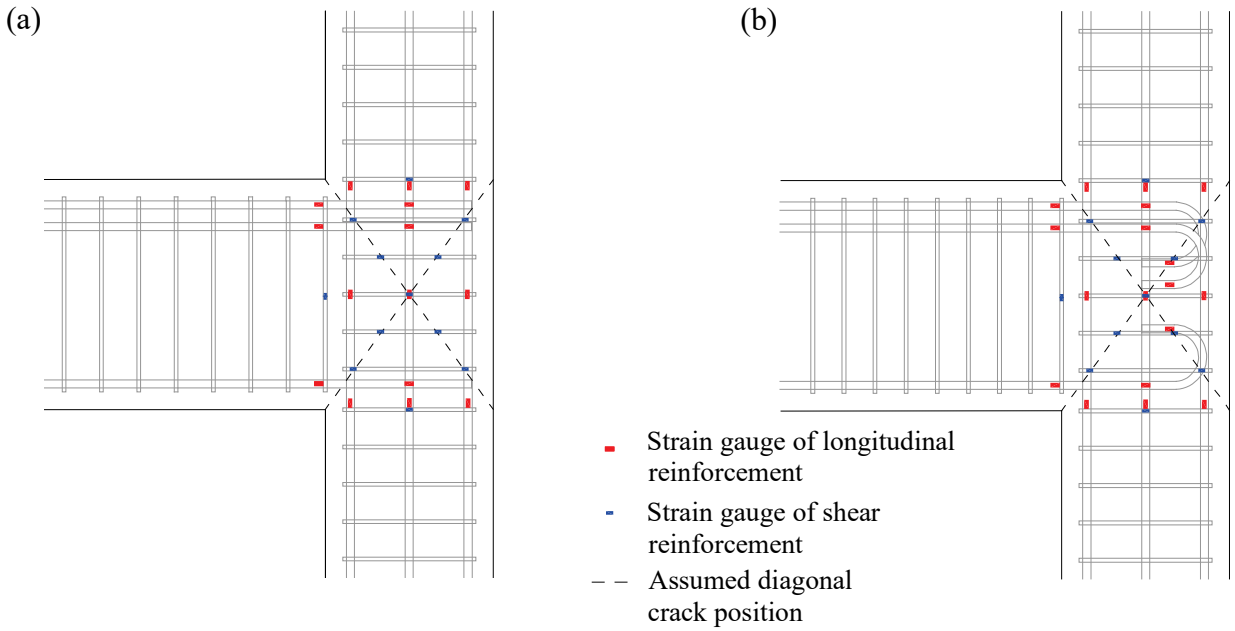

Figure 3.11 Strain gauge arrangements: (a) Specimen J1 (b) Specimen J2

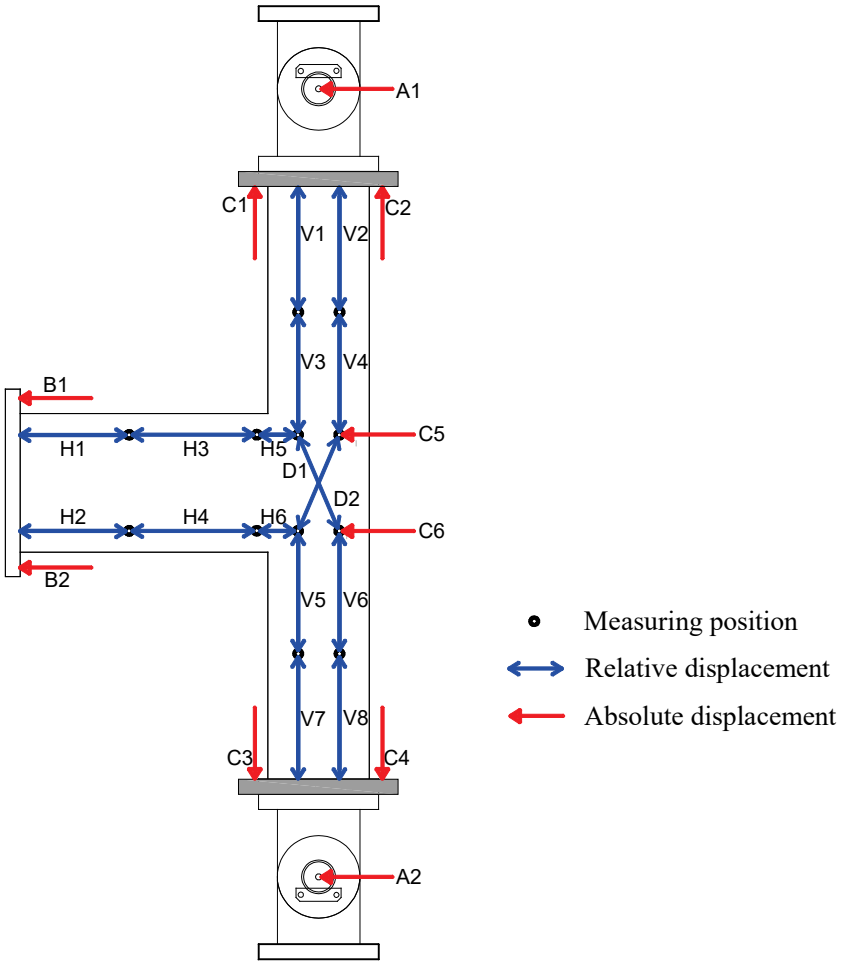

Figure 3.12 Displacement sensor arrangement

3.4. Strength Estimation of the Specimens

The moment diagram of the specimens under seismic loads is shown in **Figure 3.13**, assuming that the inflections are at the midpoint of the columns and beam. The ultimate strength of the frame M_u representing the joint node moment and the failure mode is determined by **Equation (3-10)**.

$$M_u = \text{min. } [\ (\ {}_nM_{cu1} + {}_nM_{cu2}\ ),\ {}_nM_{bu},\ M_{ju}\ ] \qquad (3\text{-}10)$$

where ${}_nM_{cu1}/{}_nM_{cu2}$ is the nodal moment at the joint when the upper/bottom column yields at the critical section, ${}_nM_{bu}$ is the nodal moment at the joint when the beam yields at the critical section, and M_{ju} is the moment capacity of the joint. In this study, the moment capacity of the joint was defined as the nodal moment corresponding to the ultimate shear strength of the joint.

The flexural strength of the beam M_{bu} and the flexural strength of the column M_{cu} were calculated according to the Japanese standards [22] using **Equations (3-11)** and **(3-12)**, respectively. The flexural strength of the column was calculated by considering a variable axial force at the occurrence of the ultimate failure mechanism. The shear strengths of the beam and columns are not discussed here because these shear strengths were greater than their flexural strengths. The conversion of M_{bu} and M_{cu} into the nodal moment of joint ${}_nM_{cu}$ and ${}_nM_{bu}$ is also shown in **Figure 3.13**.

$$M_{bu} = 0.9\ a_t\ \sigma_y\ d \qquad (3\text{-}11)$$

$$M_{cu} = 0.8\ a_t\ \sigma_y\ D_c + 0.5\ N\ D_c\ \left(1 - \frac{N}{b\ D_c\ F_c}\right) \qquad (for\ 0 \le N \le 0.4\ b\ D_c\ F_c) \qquad (3\text{-}12)$$

where a_t is the gross area of tensile longitudinal rebar; $\sigma_y = f_y$; d is the effective depth of the beam; D_c is the full depth of the column; N is the column axial force (positive for compression); b is the column width; and $F_c = f_c'$.

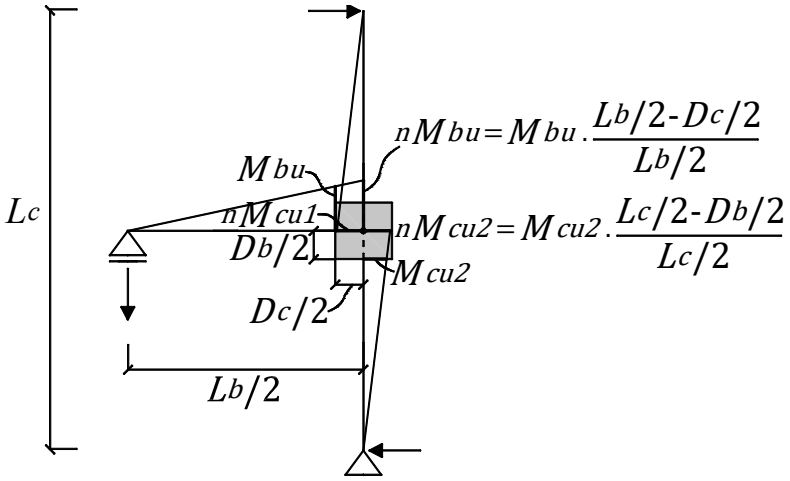

Figure 3.13 Seismic moment diagram of the specimens

The ultimate shear strength of the joint was calculated by **Equation (3-13)** from the Japanese design guidelines [23]. The shear strength of the joint was converted to the joint moment M_{ju} using **Equation (3-15)**, as proposed in a previous study [11].

$$V_{ju} = \kappa \, \phi \, F_j \, b_j \, D_j \tag{3-13}$$

$$b_j = b_b + b_{a1} + b_{ba2} \tag{3-14}$$

$$M_{ju} = \frac{V_{ju}}{\frac{L_b - D_c}{L_b \cdot j} - \frac{1}{L_c}} \tag{3-15}$$

where κ is a joint shape factor (0.7 for an exterior joint); ϕ is a factor accounting for the presence of orthogonal beams (0.85 for a joint without these beams); F_j is the nominal value for calculating the joint shear strength ($F_j = 0.8{F_c}^{0.7}$); b_j is the effective depth of the joint according to **Equation (3-14)**; b_b is the width of the beam, b_{ai} is the smaller of $b_i/2$ and $D_c/4$, b_i is the distance from the side surface of the beam to that of the column; D_j is the effective joint depth, taken to be the horizontal embedding depth of the beam longitudinal bars; T_b is the tensile force of the beam longitudinal rebar; V_c is the column shear force; L_b is the span length of the beam; j is the distance between the compressive/tensile force couple at the beam critical section (i.e., $7/8\ d$); and L_c is the column height

The equivalent joint moment at the ultimate strength of the existing exterior joint specimens, J1 and J2, were calculated and are summarized in **Table 3-3**. In the calculations, the

tested material properties in **Table 3-1** and **Table 3-2** were used. The values in parentheses in the table are based on design values, where the yield stress of the reinforcement was 295 N/mm^2 for rebar SD295A and 235 N/mm^2 for rebar SR235, and the compressive strength of concrete was 10 N/mm^2.

Table 3-3 Equivalent joint moment at the ultimate strength of specimens J1 and J2

Specimen	Loading direction	At column flexural strength $_nM_{cu1} + {}_nM_{cu2}$ (kN·m)	At beam flexural strength $_nM_{bu}$ (kN·m)	At joint shear strength M_{ju} (kN·m)	Expected ultimate strength M_u (kN·m)	Expected failure mode
J1	Positive	99.9 (88.6)	69.8 (60.2)	52.9 (49.5)	52.9 (49.5)	Joint failure
	Negative	90.6 (80.6)	43.7 (37.7)		43.7 (37.7)	Beam yielding
J2	Positive	99.4 (88.6)	80.1 (57.6)	50.6 (49.5)	50.6 (49.5)	Joint failure
	Negative	89.8 (80.3)	55.8 (40.1)		50.6 (40.1)	Joint failure*

*Expected failure mode from the calculated strength based on the tested material properties

3.5. Experimental Results

Figure 3.14 shows the applied joint moment and drift ratio relationships for both specimens. The joint moment is the product of the shear force of the beam measured by the load cell and the distance between the roller center at the end of the beam and column center (refer to **Figure 3.9**).

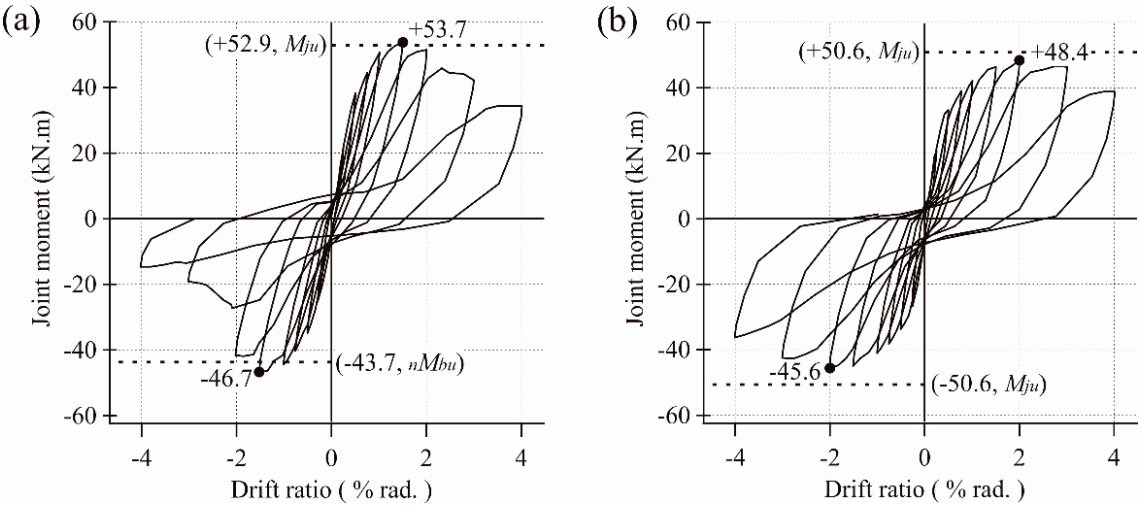

Figure 3.14 Joint moment-drift ratio relationships: (a) Specimen J1 (b) Specimen J2

3.5.1. Failure Process

Specimen J1

During the cycle to R = ± 0.5%, diagonal cracks appeared at the joint panel, as shown in **Figure 3.15(a)**. The bottom beam longitudinal bar at the column face yielded during the cycle to R = - 0.75%. The specimen reached the maximum strength at R = ± 1.5%. Then, the diagonal cracks were extended to the upper column along the external longitudinal bars, indicating joint shear failure in the positive loading direction. Then, a wide vertical crack was observed on the beam-column junction, indicating anchorage failure in the negative loading direction. The decrease in the strength in the negative loading direction was much more significant than that in the positive loading direction, indicating that anchorage failure due to pullout of beam longitudinal bars had more brittle behavior than joint shear failure.

Figure 3.16(a) shows the strain measurement results along the beam bottom longitudinal bar of specimen J1. At a drift ratio of -2%, the anchorage (bond) was lost because there was no obvious difference between the strain values at the middle of the joint and at the column face. The strain gauges malfunctioned after the cycle to R = ± 2%. The strain measurement along the beam top longitudinal bar is not discussed here because anchorage failure was not observed, and the top bars did not yield in the positive loading direction due to the larger amount of the top bar than that of the bottom bar (**Figure 3.3**).

Specimen J2

Diagonal cracks appeared at the joint region during the cycle to R = ± 0.5%, as shown in **Figure 3.15(b)**. The specimen reached the maximum strength at R = ± 2.0%. Then, the diagonal cracks were extended to the upper and bottom columns along the external longitudinal bars, indicating joint shear failure in both the positive and negative loading directions. The

decrease in the strength due to shear failure in specimen J2 was less substantial than that due to anchorage failure in specimen J1.

Figure 3.16(b) shows the strain measurement results along the beam bottom longitudinal bar of specimen J2. The anchorage (bond) was not lost because of the existence of hooks; thus, a difference was observed in the strain values at the middle of the joint and at the column face until the last cycle to R = ± 4%, while the bond stress (inclination of the lines in the figure) was lower than that in specimen J1 up to its anchorage failure because of the usage of plain rebar for specimen J2.

The crack patterns at every positive and negative peak drift ratio for each specimen are shown in **Appendix B** and the strain measurement of all reinforcing bars for each specimen are shown in **Appendix C**.

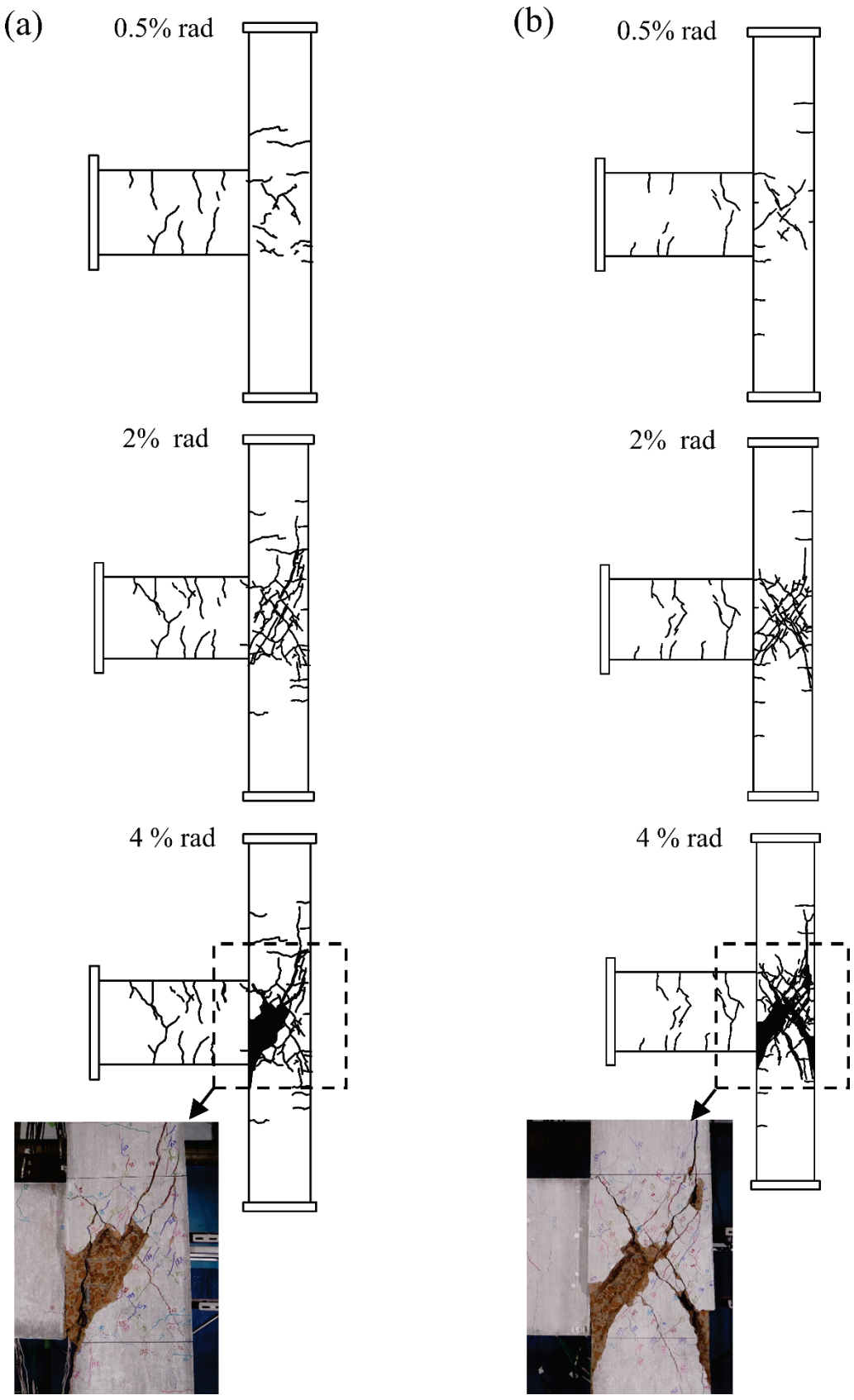

Figure 3.15 Damage to the specimens: (a) Specimen J1 (b) Specimen J2

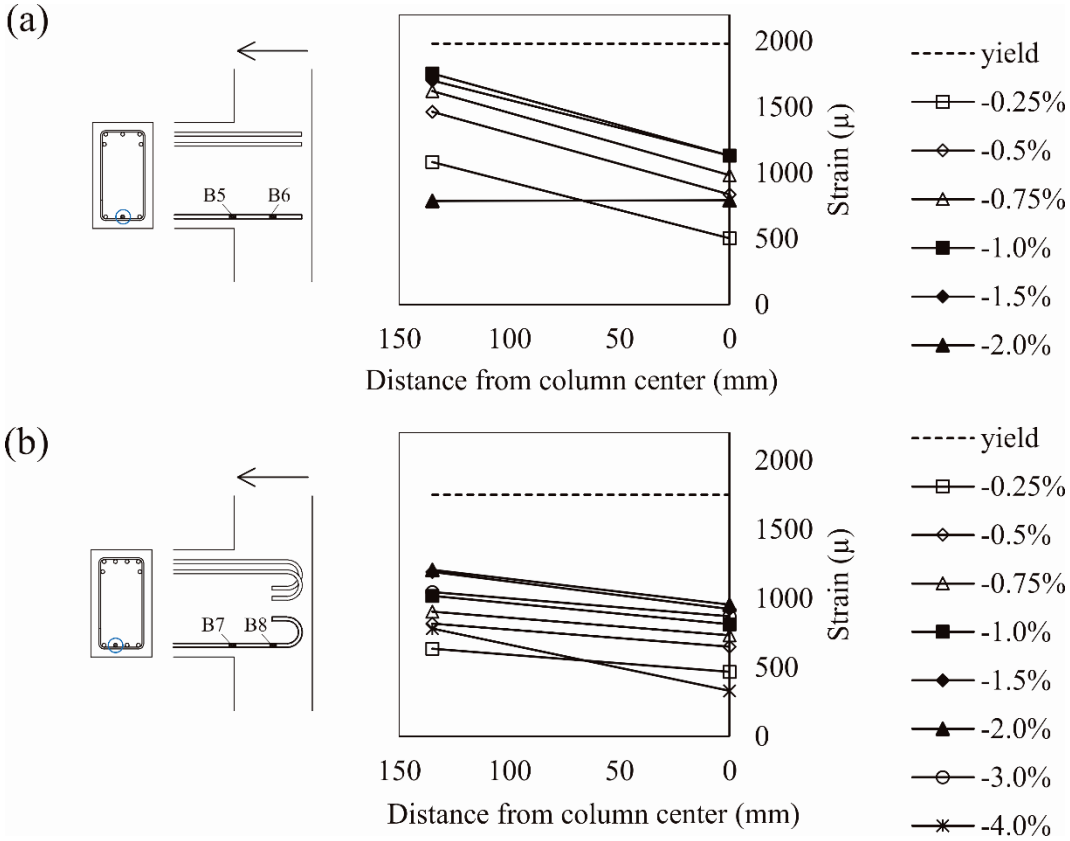

Figure 3.16 Strains along the bottom beam longitudinal bar:
(a) Specimen J1 (b) Specimen J2

3.5.2. Maximum Strength

The maximum strength of the benchmark specimen J1 in the positive loading direction was 53.7 kN·m, which agreed with the calculated ultimate strength (52.9 kN·m) determined by the moment capacity of the joint corresponding to the ultimate shear strength of the joint, M_{ju} in **Equation (3-10)**. In the negative loading direction, the maximum strength was 46.7 kN·m, greater than the calculated ultimate strength (43.7 kN·m) determined by the nodal moment at the joint when the beam yielded at the critical section, ${}_nM_{bu}$ in **Equation (3-10)**.

The maximum strengths of specimen J2 in the positive and negative loading directions were 48.4 kN·m and 45.6 kN·m, respectively. The strengths in both the positive and negative loading directions were close to the calculated ultimate strength (50.6 kN·m) determined by the

moment capacity of the joint corresponding to the ultimate shear strength of the joint, M_{ju} in **Equation (3-10)**.

3.5.3. Deformation Capacity

The deformation capacity of the specimens was evaluated by the ultimate drift ratio, which was defined as the drift ratio when the strength dropped to 80% of the maximum strength. **Figure 3.17** compares the envelopes of the hysteresis loops of both specimens shown in **Figure 3.14(a)** and **3.14(b)**. The ductility of specimen J1 in both the positive and negative loading directions was lower than that of specimen J2 because the deformability of specimen J1 decreased substantially after the loading cycle in which anchorage failure was observed.

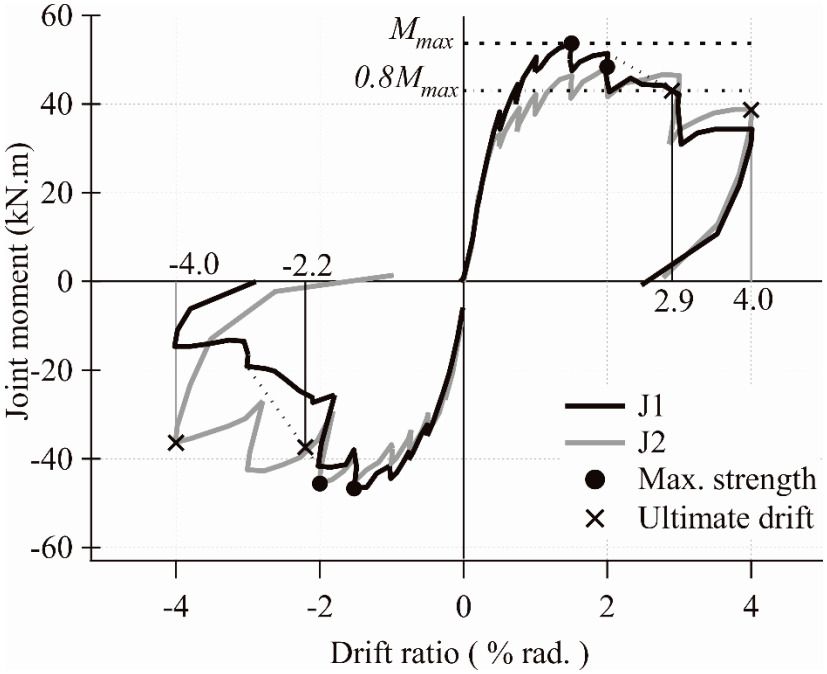

Figure 3.17 Comparison of the ultimate drift ratio of specimens J1 and J2

3.6. Summary

Two existing beam-column joint frame specimens with low-strength concrete representing typical detailing in Bangladeshi buildings were constructed and tested. Major findings are summarized as follows:

1. The specimen with deformed bar and straight anchorage at the end, J1, failed by anchorage failure (pullout of beam longitudinal bars) in the negative loading direction, while joint shear failure was observed in the positive loading direction.
2. The specimen with plain bar and 180° hooks, J2, failed by joint shear in both the positive and negative loading directions.
3. The existing Japanese design equations presented in this chapter provide a good estimate to the strength of the beam-column joint specimens.
4. The anchorage failure observed in specimen J1 showed more brittle behavior than the joint shear failure. Therefore, specimen J1 was chosen as the benchmark specimen for strengthening.

Chapter 4

Pullout Tests of Post-installed Bonded Anchors in Low Strength Concrete with Brick Chips

4.1. Introduction

In this study, a strengthening method by installing wing walls will be applied to upgrade the exterior joints with deficient beam rebar anchorage representing Bangladeshi buildings. A post-installed anchor is used to connect the existing part of the structure with the additional wing walls. Therefore, a post-installed anchor is one key element in the strengthening design. Prior to designing the details of the strengthening, a series of pullout tests was conducted to evaluate the tensile capacity of single bonded anchors in low-strength concrete with brick chip aggregate representing Bangladeshi concrete.

Several past studies [24]–[26] investigated the tensile capacity of bonded anchors in low strength concrete. However, these past studies applied the anchors to concrete with stone aggregate. No previous studies have investigated the tensile capacity of post-installed anchors for Bangladeshi concrete. The results of this test contribute to the design of the details of post-installed anchors to ensure that brittle failure of anchors does not occur in the strengthened specimen.

4.2. Experimental Program

4.2.1. Specimens and Material Properties

Five types of anchor specimens were prepared. The parameters of the specimens were anchor diameter and embedment length, as shown in **Table 4-1**. Three anchors were prepared for each type. The anchors were installed in a half-scale RC slab, as shown in **Figure 4.1**. The thickness of the slab was 75 mm and 2-D6@75 was used for slab reinforcement in both longitudinal and transverse directions. The anchors were placed at the center between slab reinforcements and the minimum distance between anchors was set to 300 mm to prevent the

concrete cone failure area from interfering with that of the neighboring anchor. **Figure 4.1** shows such arrangements of the anchors.

Table 4-1 Test parameters of the anchor specimens

No.	Specimen name	Anchor diameter d_a (mm)	Embedment length l_e (mm)
1	M6-8d_a	6	48 = 8d_a
2	M6-9.8d_a	6	59 = 9.8d_a
3	M6-12.5d_a	6	75 = 12.5d_a
4	M8-8d_a	8	64 = 8d_a
5	M8-9.4d_a	8	75 = 9.4d_a

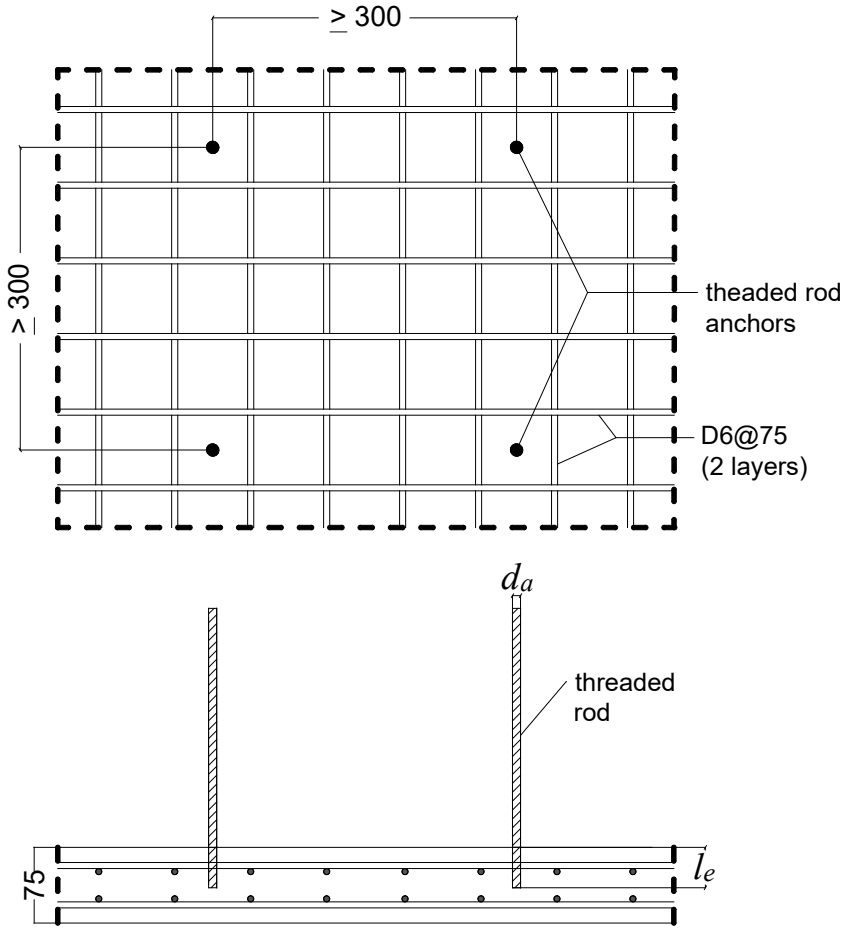

Figure 4.1 Slab reinforcement details with positions and details of anchors

The slab was made with low strength concrete using brick chips as coarse aggregate. The volumetric ratio of cement + $CaCO_3$: sand : brick chips was 1 (0.7 +0.3) : 2 : 4, where 30%

of cement was replaced by calcium carbonate ($CaCO_3$). The ratio of water to the sum of cement and $CaCO_3$ was 0.6. The mixture was designed through preliminary material tests [21]. **Table 4-2** shows the concrete mixture proportion by weight and **Table 4-3** shows the material properties of concrete.

Table 4-2 Concrete mixture in kg/m^3

W/(Cement+$CaCO_3$)	Water	Cement	$CaCO_3$	Sand	Brick chips
60%	212	248	88	596	959

Table 4-3 Material properties of concrete

Compressive strength (N/mm^2)	Elastic modulus (N/mm^2)	Split tensile strength (N/mm^2)
11.7	10,014	1.52

Threaded rods with diameters of 6 mm (M6) and 8 mm (M8) were used as anchor materials. The anchors with small diameters were applied because the test results were supposed to be used for scaled member specimens, while Japanese guidelines [22] suggest that a minimum diameter of the anchor is 13 mm. **Table 4-4** shows the material properties of threaded rod anchors.

Table 4-4 Material properties of threaded rod anchors

Type	Nominal cross-sectional area (mm^2)	Yield stress (N/mm^2)	Ultimate strength (N/mm^2)
M6	20.1	423	503
M8	36.6	398	452

Anchor holes were drilled with a diamond core drill. Dust was removed from the holes by flushing compressed air followed by brushing using a wire brush to sustain adequate bond strength. After the cleaning, the holes were filled with adhesive. Epoxy resin was used as bonding material for the anchors.

4.2.2. Design and Calculation of Tensile Capacity

The anchor specimens were designed based on Japanese guidelines [22]. The tensile capacity of single anchor, T_a is determined by three basic failure modes, as shown in **Figure 4.2**. T_a shall be the smallest value of T_{a1} which is determined by steel strength, T_{a2} which is determined by concrete cone failure, and T_{a3} which is determined by bond strength. T_{a1}, T_{a2}, and T_{a3} were evaluated by the following equations:

$$T_a = \min(T_{a1}, T_{a2}, T_{a3}) \quad (4\text{-}1)$$

$$T_{a1} = \sigma_y \cdot a_o \quad (4\text{-}2)$$

$$T_{a2} = 0.23\sqrt{\sigma_B} \cdot A_c \quad (4\text{-}3)$$

$$T_{a3} = \tau_a \cdot \pi \cdot d_a \cdot l_e \quad (4\text{-}4)$$

$$\tau_a = 10\sqrt{(\sigma_B/21)} \quad (4\text{-}5)$$

where σ_B : compressive strength of concrete (N/mm^2), σ_y : yield stress of steel (N/mm^2), a_o : nominal cross-sectional area of anchorage bar (mm^2), A_c : projected area of concrete cone failure (mm^2) $A_c = \pi \cdot l_e \cdot (l_e + d_a)$ assuming 45^o cone failure surface to the horizontal/vertical, d_a : anchor diameter (mm), l_e : effective embedment length of anchor, τ_a : bond strength of bonded anchor against pullout force.

The application range of these equations in Japanese guidelines [22] is defined for concrete compressive strength between 15 and 36 N/mm^2. Low strength concrete is originally out of scope of these equations. This study investigates the applicability of these equations in case of low strength concrete with brick chips.

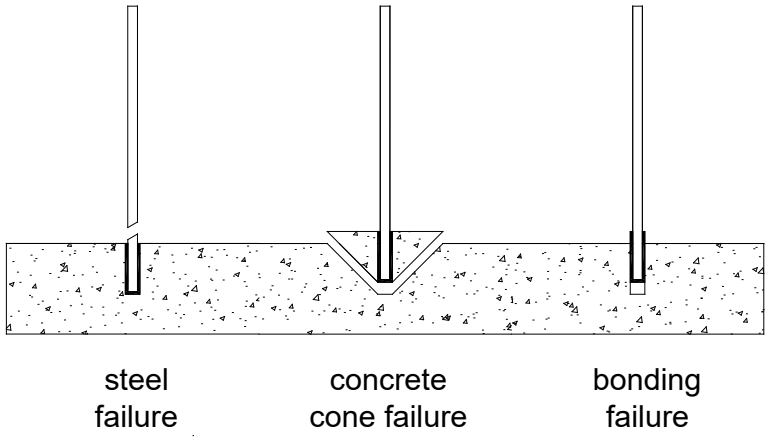

Figure 4.2 Basic failure modes of bonded anchor

The calculated tensile capacity and failure modes of anchor specimens are shown in **Table 4-5**. The specimens were designed for different failure modes to investigate the tensile strength determined by each failure mode.

Table 4-5 Calculated tensile capacity of anchor specimens

No.	T_{a1} (kN) (steel strength)	T_{a2} (kN) (cone strength)	T_{a3} (kN) (bond strength)	T_a (kN)	Failure mode
1	8.49	6.41	6.74	6.41	Cone
2	8.49	9.45	8.29	8.29	Bond
3	8.49	15.01	10.03	8.49	Steel
4	14.82	11.38	11.98	11.38	Cone
5	14.82	15.38	14.04	14.04	Bond

4.2.3. Test Setup

The loading equipment shown in **Figure 4.3** was used for the pullout test. The reaction frame consisted of a thick steel plate and supports. The distance between the supports of reaction frame and anchor rod should be at least equal to the effective embedment depth of the anchor in order to allow concrete cone failure to develop. The loading was applied through a 120 kN center hole hydraulic ram operated by a manual pump. A center hole load cell with capacity of 50 kN was placed above the hydraulic ram to measure loads during the test. An

extension rod with coupler connection was used considering the anchor rod length for applying tension using the equipment. Monotonic pullout loading was applied for each single anchor.

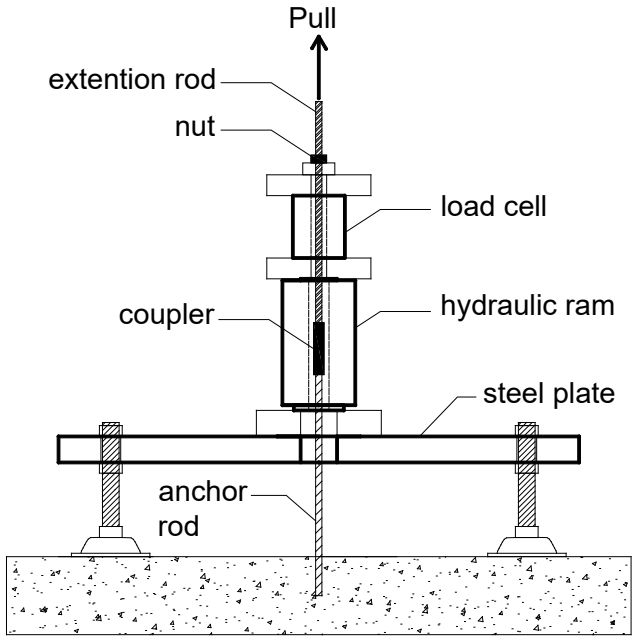

Figure 4.3 Setup of pullout test

4.3. Experimental Results and Discussions

The experimental results from the pullout tests of the anchor specimens are summarized in **Table 4-6**. The failure modes of specimen No.1 (M6-8d_a), No. 3 (M6-12.5d_a), and No.4 (M8-8d_a) matched the expected failure modes in **Table 4-5**. However, that of specimen No.2 (M6-9.8d_a) and No. 5 (M8-9.4d_a) did not agree with the expected one (bond failure). The differences for these specimens seemed to be caused by the calculated strengths of T_{a3} (bond strength) were close to T_{a1} (steel strength).

Table 4-6 Results of the pullout test and tensile capacity by observed failure mode

No.	Specimen	Tensile capacity (kN)	Average tensile capacity (kN)	Failure mode	T_{a1_cal} (kN)	T_{a1_exp} (kN)	T_{a1_exp} / T_{a1_cal}	T_{a2_cal} (kN)	T_{a2_exp} (kN)	T_{a2_exp} / T_{a2_cal}
1	M6-8d_a(1)	9.26	9.28	Cone				6.41	9.26	1.44
	M6-8d_a(2)	9.01							9.01	1.41
	M6-8d_a(3)	9.58							9.58	1.49
2	M6-9.8d_a(1)	9.76	10.01	Steel	8.49	9.76	1.15			
	M6-9.8d_a(2)	9.69				9.69	1.14			
	M6-9.8d_a(3)	10.59				10.59	1.25			
3	M6-12.5d_a(1)	10.52	10.36	Steel		10.52	1.24			
	M6-12.5d_a(2)	9.78				9.78	1.15			
	M6-12.5d_a(3)	10.79				10.79	1.27			
4	M8-8d_a(1)	15.29	15.08	Cone				11.38	15.29	1.34
	M8-8d_a(2)	14.74							14.74	1.30
	M8-8d_a(3)	15.22							15.22	1.34
5	M8-9.4d_a(1)	16.58	16.64	Steel	14.82	16.58	1.12			
	M8-9.4d_a(2)	16.67				16.67	1.12			
	M8-9.4d_a(3)	16.68				16.68	1.13			

The tensile capacity of anchor increased with the increase of embedment length. The experimental results showed that the tensile strengths of the anchors with the embedment length close to $10d_a$ (M6-$9.8d_a$, M8-$9.4d_a$) or more than $10d_a$ (M6-$12.5d_a$) were controlled by steel strength and concrete cone failure did not occur; therefore, which recommended the minimum embedment length of $10d_a$ for application in seismic retrofit to develop ductile behavior by yielding of anchor.

Figure 4.4 and **Figure 4.5** show the average tensile capacity from the experiments and design calculations of the M6 and M8 anchor specimens, respectively. The experimental tensile capacity of all specimens was higher than the calculated strengths. This indicated that the equations to estimate the tensile capacity of anchor in Japanese guidelines [22] were conservative for low strength concrete with brick chips.

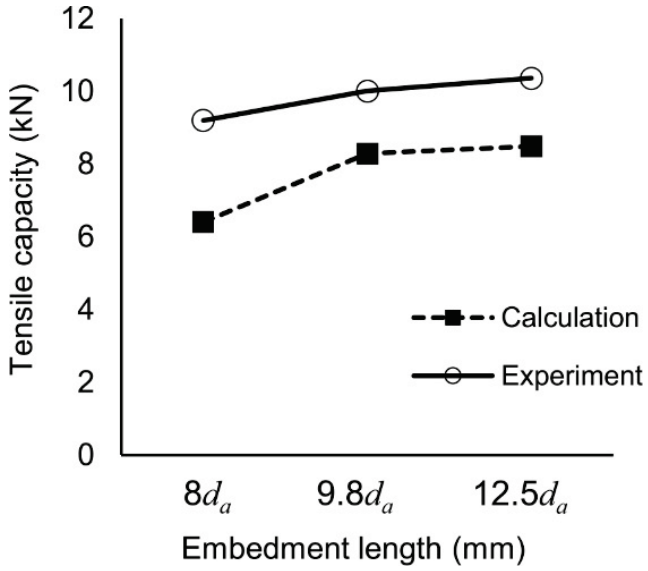

Figure 4.4 Tensile capacity of M6 specimens

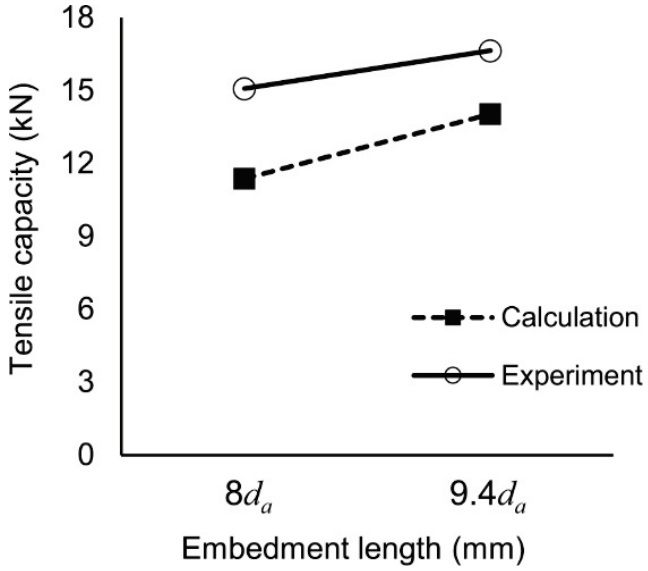

Figure 4.5 Tensile capacity of M8 specimens

4.3.1. Behavior of Concrete Cone Failure

The specimens with concrete cone failure, No.1 (M6-8d_a) and No. 4 (M8-8d_a) showed that the tensile capacity determined by concrete cone failure was much higher than the design calculations. **Table 4-6** compares the calculated tensile capacity determined by concrete cone failure (T_{a2_cal}) with the experimental results (T_{a2_exp}). The experimental tensile capacity was more than 30% higher than the design calculations. The concrete cone failure areas observed in the experiment also exceeded the design assumption in Japanese guidelines [22], as shown in **Figure 4.6** and **Figure 4.7.**

M6-8d_a(1)

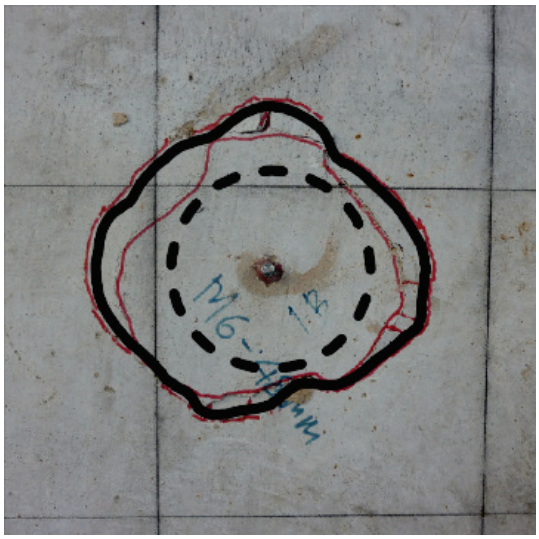

M6-8d_a(2)

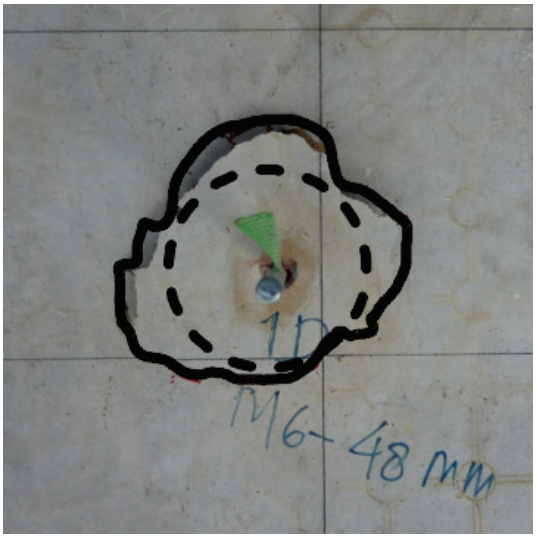

M6-8d_a(3)

Assumed failure area

Observed failure area

Figure 4.6 Concrete cone failure area of M6 specimens

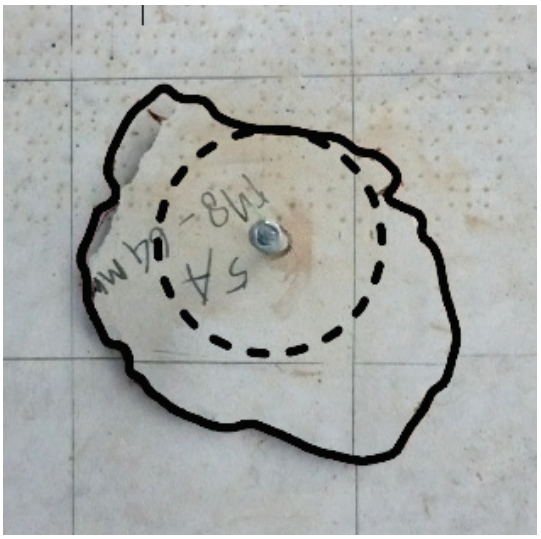

M8-8d_a(1)

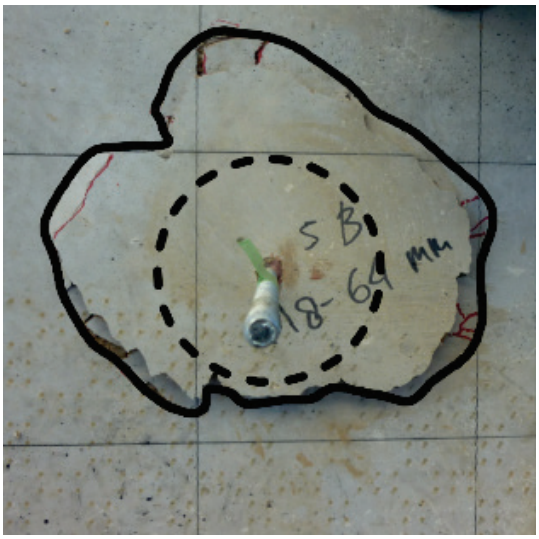

M8-8d_a(2)

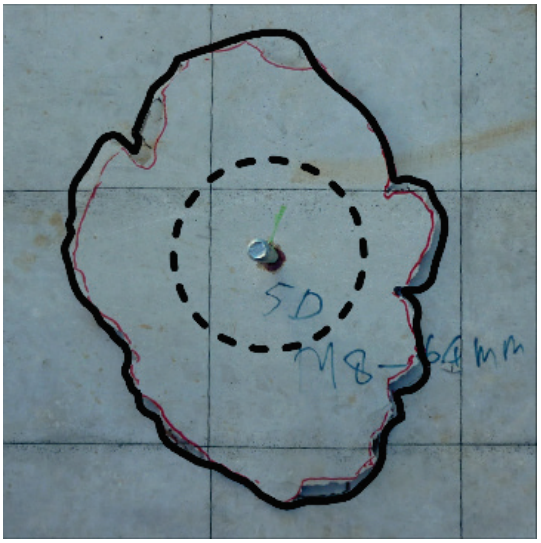

M8-8d_a(3)

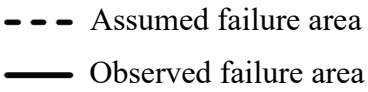

Figure 4.7 Concrete cone failure areas of M8 specimens

All specimens with concrete failure showed the formation of a shallow concrete cone at the upper part of anchor embedment with a pullout of the lower part of anchor embedment, as shown in **Figure 4.8** and **Figure 4.9**. The formation of combined failure with shallow concrete cone and anchor pullout might be affected because the anchors were not installed in pure concrete block but the concrete slab with reinforcement; however, such embedment condition is likely to be more realistic.

M6-8d_a(1)

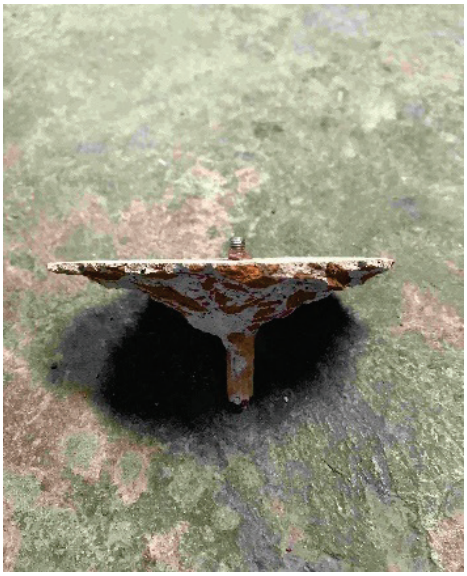

M6-8d_a(2)

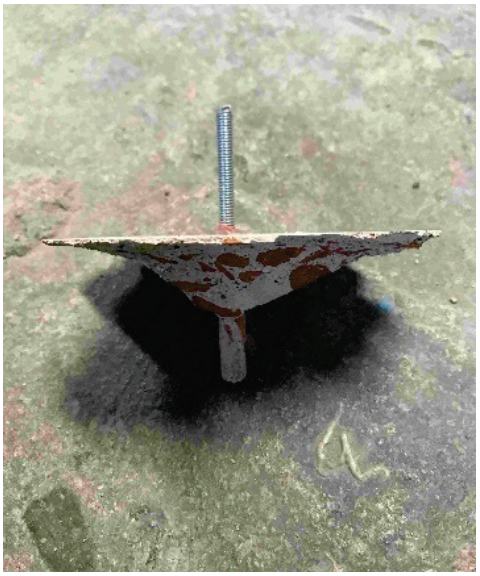

M6-8d_a(3)

Figure 4.8 Concrete cone failure with pullout of M6 specimens

M8-8d_a(1)

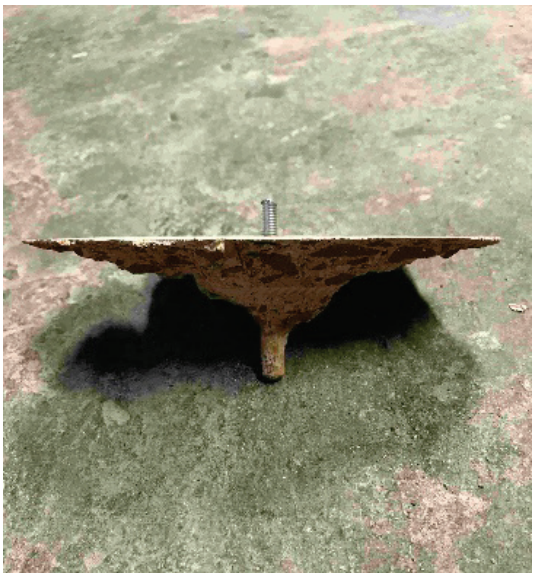

M8-8d_a(2)

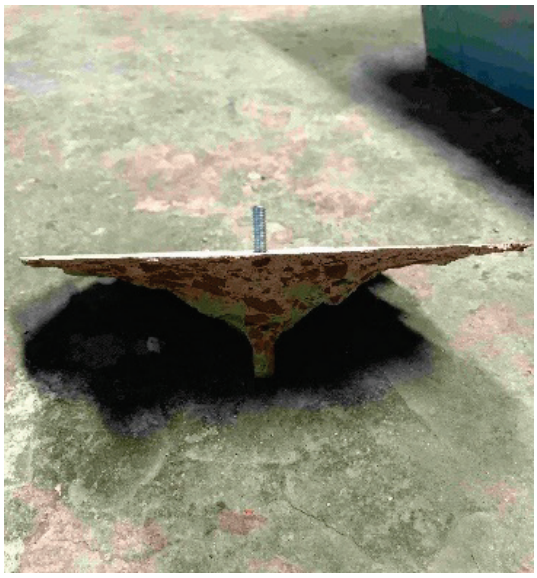

M8-8d_a(3)

Figure 4.9 Concrete cone failure with pullout of M8 specimens

4.3.2. Behavior of Steel Failure

Specimens No. 2 (M6-9.8d_a), No. 3 (M6-12.5d_a), and No. 5 (M8-9.4d_a) failed with steel tensile fracture. The tensile capacity of these anchors was also higher than the design calculations. **Table 4-6** compares the calculated tensile capacity determined by steel failure (T_{a1_cal}) with the experimental results (T_{a1_exp}), showing that the experimental capacity was more than 12% higher than the calculations. **Figure 4.10** shows an example of anchor with tensile fracture after the test.

In **Figure 4.11** and **Figure 4.12**, the experimental tensile capacity of M6 and M8 anchor specimens determined by steel failure is compared with not only T_{a1_cal} but also the ultimate tensile strength based on **Table 4-4**. The figures show that the tensile capacity of anchors agreed with the ultimate tensile strength beyond yielding. When the tensile capacity is designed assuming tensile failure to be ductile, the exceedance of tensile capacity needs to be considered.

M6-12.5d_a(1)

Figure 4.10 An anchor specimen with tensile fracture

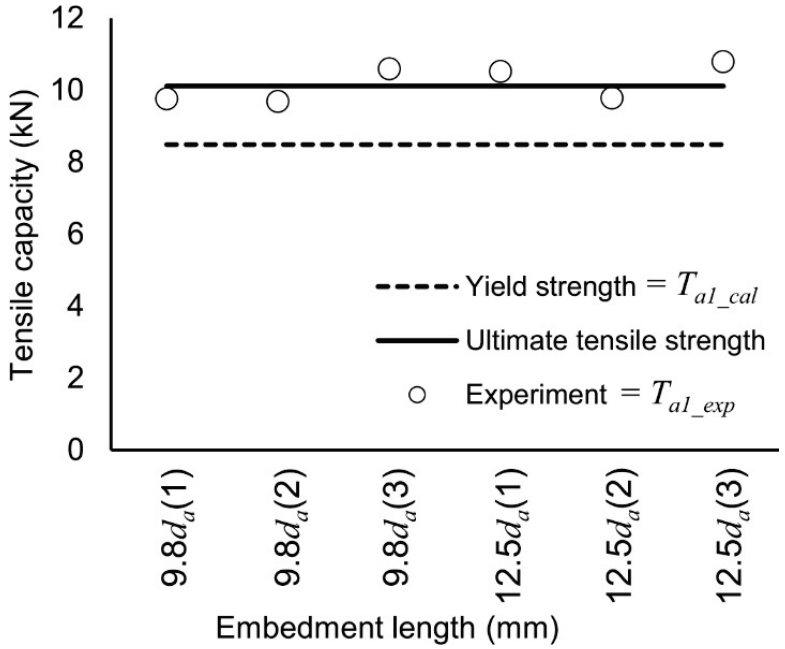

Figure 4.11 Tensile capacity determined by tensile fracture of M6 specimens

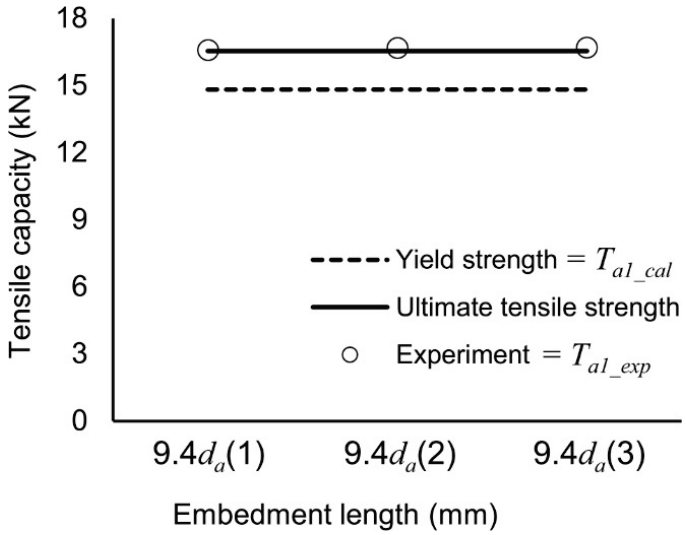

Figure 4.12 Tensile capacity determined by tensile fracture of M8 specimens

4.4. Summary

From the results of pullout loading to anchors explained in this chapter, the following findings are obtained:

1. The tensile capacity of anchors which failed in concrete cone failure was much higher than the design calculations. This might be because the anchor was not installed on pure concrete block, but on concrete slab with reinforcement.
2. The tensile capacity of anchors which failed with tensile fracture reached the ultimate tensile strength beyond the tension at yielding.
3. The design equations in Japanese guidelines conservatively estimated the tensile capacity of bonded anchors in low strength concrete with brick chips.
4. For strengthening design, the minimum anchor embedment length of $10d_a$ is recommended to develop ductile behavior by yielding of the anchor

Chapter 5

Experiment on Strengthening of an Exterior Beam-Column Joint with Deficient Anchorage by Wing Walls

5.1. Introduction

The experiments on beam-column joints with deficient anchorage in **Chapter 3** showed that specimen J1 with deformed bar and straight anchorage of beam longitudinal bars was more vulnerable to anchorage failure than specimen J2 using plain bar with standard 180° hooks as beam longitudinal bars. Therefore, specimen J1 is chosen as benchmark specimen for strengthening in this chapter.

A design concept to prevent the anchorage failure of beam-column joint was proposed and verified by an experiment of a strengthened joint. The evaluation methods to estimate the strength and the deformation capacity of the strengthened beam-column joint were also presented.

5.2. Proposed Length of Wing Walls

The present study proposes an application of the strengthening method by installing wing walls [11] to substandard exterior joints to prevent failure of the beam rebar anchorage. In the current study, length of wing walls (l_w) is proposed to extend the existing embedment length of beam longitudinal bars ($_{ex}l_d$) because the yield hinge of beam is expected to shift from the face of column to the end of wing walls, as shown in **Figure 5.1**. The development length after strengthening ($l_w + {}_{ex}l_d$) should be equal to or greater than the required development length (l_d) explained in **Section 3.1.1**, based on the Bangladeshi code [20] and the ACI code [17]. This acceptance criteria for design is defined as **Equation (5-1)**. Hence, the length of post-installed wing walls is determined by **Equation (5-2)**.

$$l_w + {}_{ex}l_d \geq l_d \quad (5\text{-}1)$$

$$l_w \geq l_d - {}_{ex}l_d \quad (5\text{-}2)$$

The proposal of consideration of l_w for the embedment length of beam longitudinal rebar is not accepted in the Japanese standard [27]; thus, the feasibility of this proposal is investigated in the current study.

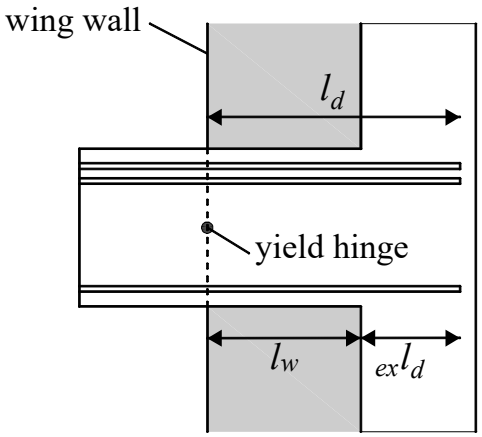

Figure 5.1 Proposal of the extension of beam rebar anchorage by considering wing walls

5.3 Specimen Design

A temporary design for details of wing walls was developed mainly according to the provisions describing wing walls for strengthening of column in the Japanese guidelines for seismic retrofit of RC buildings [22]. Procedure to confirm the sufficiency of the temporary design for strengthening of the joint will be described later in **Section 5.4**.

Strengthening by installing wing walls was applied to a specimen with the same details as specimen J1, named specimen J1-W. The wing walls were installed to the interior side along the upper and bottom columns of the specimen. The length of the wing walls was 360 mm, which was determined by **Equation (5-2)**. The thickness of the wing walls was designed according to the Japanese guidelines for seismic retrofit of RC buildings [22] (not less than 200 mm); hence, the thickness of the wing walls was set to 140 mm for the 0.7 scale.

The post-installed anchors were placed to connect the wing walls and the existing frame. The minimum spacing between the anchors and the minimum distance from the anchors to the concrete edge were designed based on Japanese guidelines [22] (not less than $7.5d_a$ and $2.5d_a$, respectively), and this design resulted in the arrangement shown in **Figure 5.2**. The embedment length of the beam and column anchors into the existing frame was 130 mm ($13d_a$), which was greater than $10d_a$, the minimum embedment length recommended to develop ductile behavior based on the pullout test results in **Chapter 4**. The anchorage length of the anchors into the wing walls was 200 mm ($20d_a$).

The vertical and horizontal reinforcements of the wing walls used double layers of D10 bars. The reinforcements of the wing walls were designed to not be less than a minimum reinforcement ratio of 0.25% according to the Japanese guidelines [22] and to be greater than the total sectional area of the beam/column anchors. For prevention of splitting failure of the concrete, ϕ6 spirals were installed at the boundaries between the wing walls and the frame.

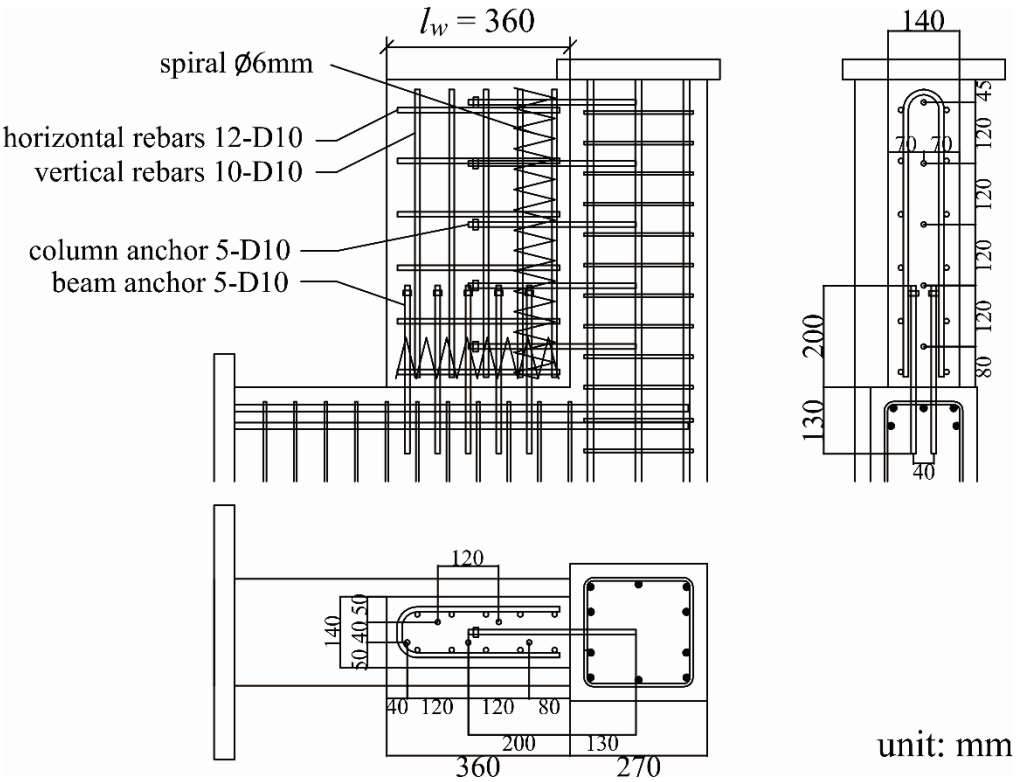

Figure 5.2 Dimensions and reinforcement details of the strengthened specimen J1-W

Strengthening work was conducted after the existing frames were cured. The existing part of the specimen was constructed with the same materials used for the benchmark specimen J1 described in **Section 3.2**, except that normal ready-mix concrete with stone as coarse aggregate was used for the wing walls. The concrete for existing frame was mixed on site using a concrete mixer and three batches of concrete mixtures were required to cast the specimen. For each concrete mixture batch, three concrete cylinder samples were prepared for the compressive tests and three concrete cylinder samples were prepared for the splitting tensile tests of concrete. **Table 5-1** gives the average mechanical properties of the concrete from the compressive tests and the split tensile tests of the concrete cylinder. The stress-strain relationship for concrete is shown in **Figure 5.3** and **5.4**. The curve with dashed line in **Figure 5.3** possibly had a problem in strain measurement; therefore, it was neglected in calculating the average Young s modulus.

The mechanical properties of reinforcement bars were obtained by the tensile tests. **Table 5-2** gives the average mechanical properties of the reinforcement bars from the tensile tests. For each type of rebar, three test samples were tested. The stress-strain relationships from the tensile test are shown in **Figure 5.5**.

Table 5-1 Mechanical properties of concrete.

Part of the specimen	Compressive strength (N/mm^2)	Young's modulus (N/mm^2)	Split tensile strength (N/mm^2)
Existing frame	11.3	8,423	0.86
Wing walls	35.0	32,614	2.32

Table 5-2 Mechanical properties of wing wall reinforcements and anchors.

Type	Grade	Yield stress (N/mm^2)	Tensile strength (N/mm^2)	Young's modulus (N/mm^2)
D10	SD 295A	338	491	172,801

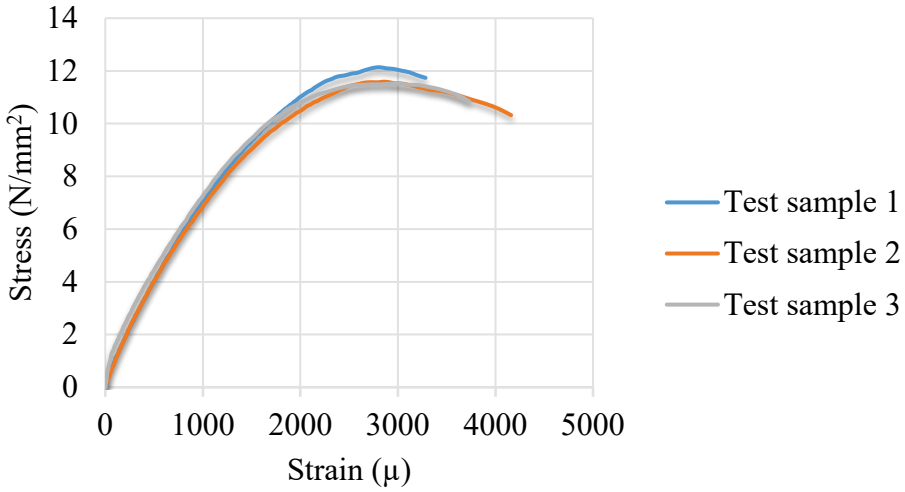

(a)

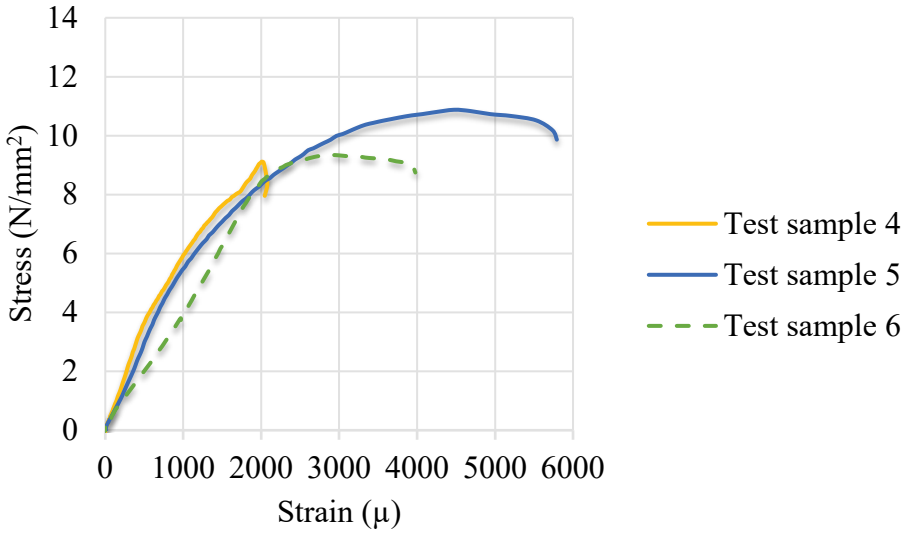

(b)

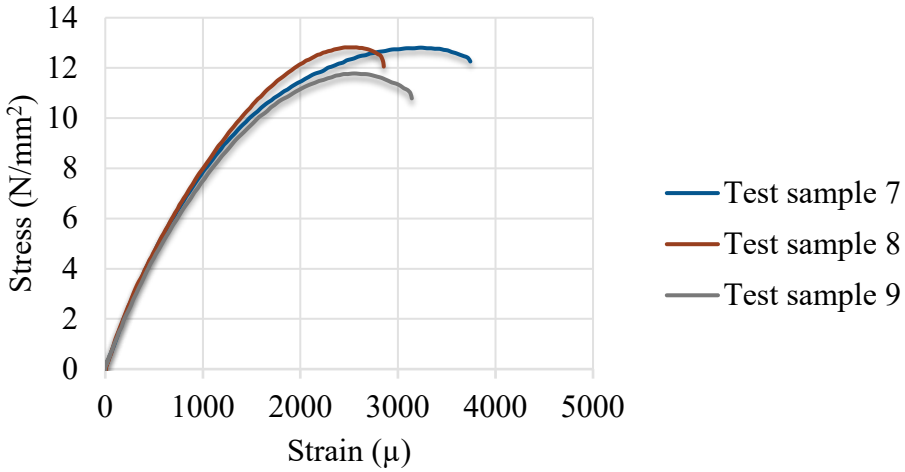

(c)

Figure 5.3 Stress-strain relationship from cylinder tests of concrete for existing frame: (a) Mixture batch 1, (b) Mixture batch 2, (c) Mixture batch 3

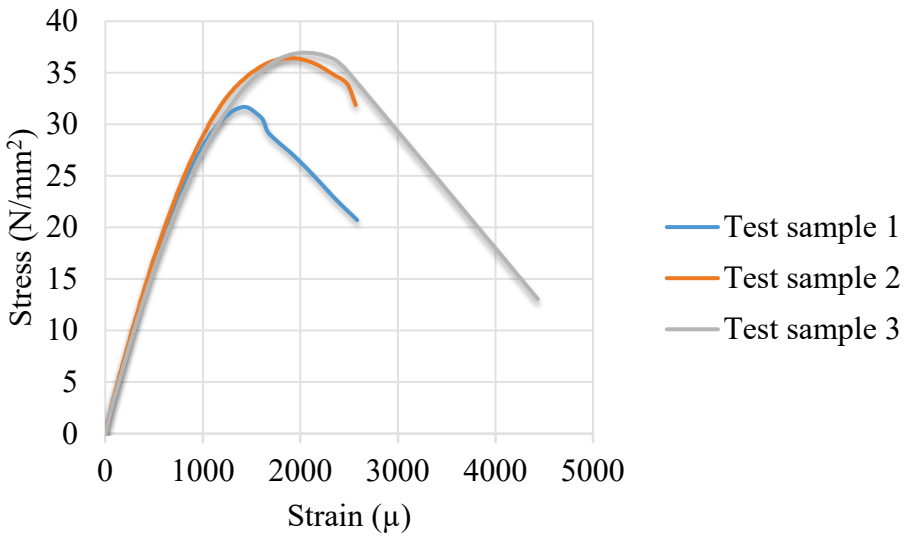

Figure 5.4 Stress-strain relationship from cylinder tests of concrete for wing walls

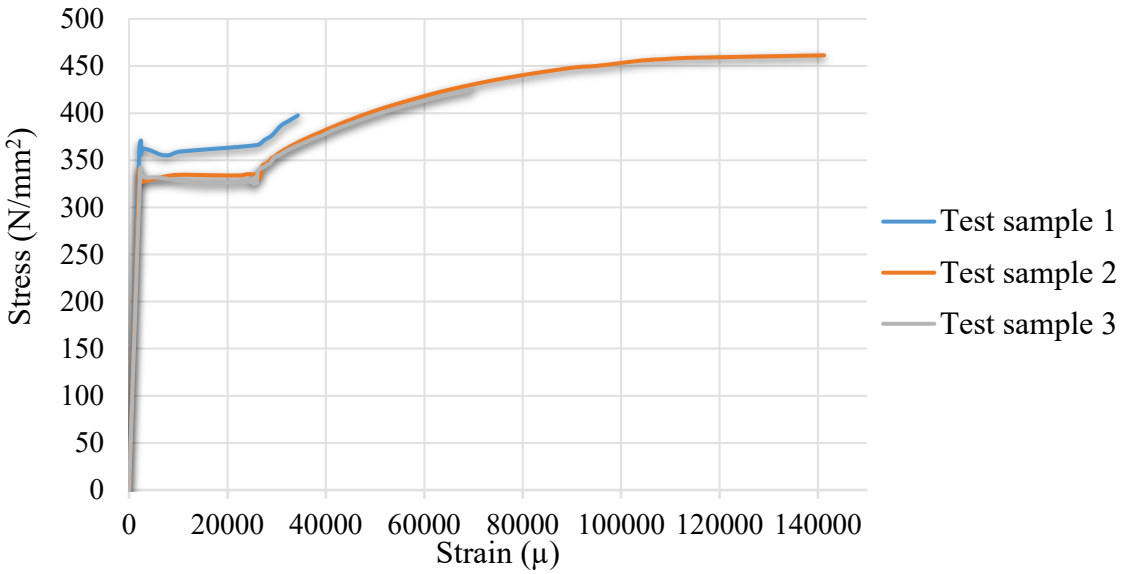

Figure 5.5 Stress-strain relationship from tensile test of rebar D10

5.4. Procedure to Ensure the Strengthening Design

Strengthening by wing walls aims to achieve a beam yielding mechanism before the joint failure. An evaluation procedure proposed in a previous study [11] was applied to confirm that the temporary design of wing walls described in **Section 5.3** is effective to achieve the beam yielding mechanism. In performing the evaluation, the design values were used for mechanical properties of the materials, which were 295 N/mm^2 for the yield stress of the

reinforcement, 10 N/mm^2 and 30 N/mm^2 for the compressive strengths of concrete for existing frame and wing walls, respectively.

Step 1: Determining the moment diagram for beam yielding mechanism

Figure 5.6 illustrates the moment diagram of an exterior when the beam yield at the wing wall end. However, the strengthened frame was idealized in the same manner as that in **Figure 3.13**, meaning that the column with a wing wall and beam was replaced by a line element along the central axis of the existing column and beam. The nodal moment at the joint when the beam yields at the wing wall end (${}_nM_{bu,r}$) is calculated by **Equation (5-3).** The moment applied to the critical section of column with wing walls is obtained by **Equation (5-4).**

$$ {}_nM_{bu,r} = M_{bu}\,\frac{L_b/2}{L_b/2 - D_c/2 - l_w} \tag{5-3}$$

$$ M_{c,cri} = \frac{1}{2}\,{}_nM_{bu,r}\,\frac{L_c - D_b}{L_c} \tag{5-4}$$

where D_b is the depth of the beam.

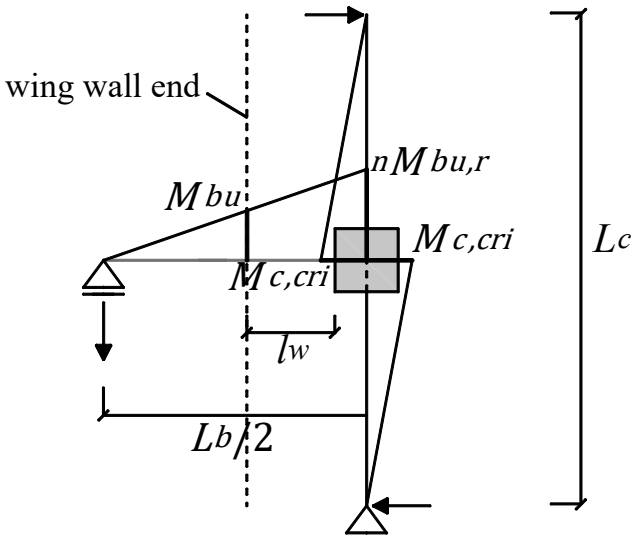

Figure 5.6 Seismic moment diagram of the strengthened specimen

Step 2: Evaluating the moment capacity of strengthened joint

The moment capacity of the strengthened joint $M_{ju,r}$ was calculated by **Equation (5-5)**, as proposed in the previous study [11]. In this equation, the moment capacity of the joint is improved by compression and tension between the wing walls and the existing beam.

$$M_{ju,r} = M_{ju} + C_c\, l_c + \sum_{i=1}^{m} C_{si}\, l_{ci} + \sum_{i=1}^{n} T_{si}\, l_{ti} \quad (5\text{-}5)$$

where C_c is the compressive force from the compressed wing wall; C_{si} is the compression from the i-th beam anchor; m is the total number of beam anchors under compression; T_{si} is the tension from the i-th beam anchor; n is the total number of beam anchors under tension; and l_c / l_{ci} / l_{ti} are the distances to the joint node from C_c / C_{si} / T_{si}.

The compressive and tensile forces were calculated by common bending analysis for the critical sections of the upper and lower columns with wing walls based on Navier's hypothesis. For example, the calculation results for specimen J1-W under the positive loading direction are shown in **Figure 5.7**. In the figure, M_{ju} and $M_{c,cri}$ were calculated based on the design value of material properties. The curvature φ and the neutral axis depth x_n are also shown in the figure. In performing the analysis, the concrete was assumed as elastic and the Young's modulus (E_c) was calculated by **Equation (5-6)** [23]. The anchor rebar was assumed as an elastoplastic material with a Young's modulus of 2.0×10^5 N/mm^2 and yield stress of 295 N/mm^2 (min. specified yield stress). The compressive and tensile forces of the anchors, C_{si} and T_{si}, were calculated from their strains, which were obtained by multiplying φ and x_n.

$$E_c = 33500 \left(\frac{\gamma}{24}\right)^2 \left(\frac{f_c'}{60}\right)^{1/3} \quad (5\text{-}6)$$

where γ is the bulk density of the concrete (=24 kN/m^3).

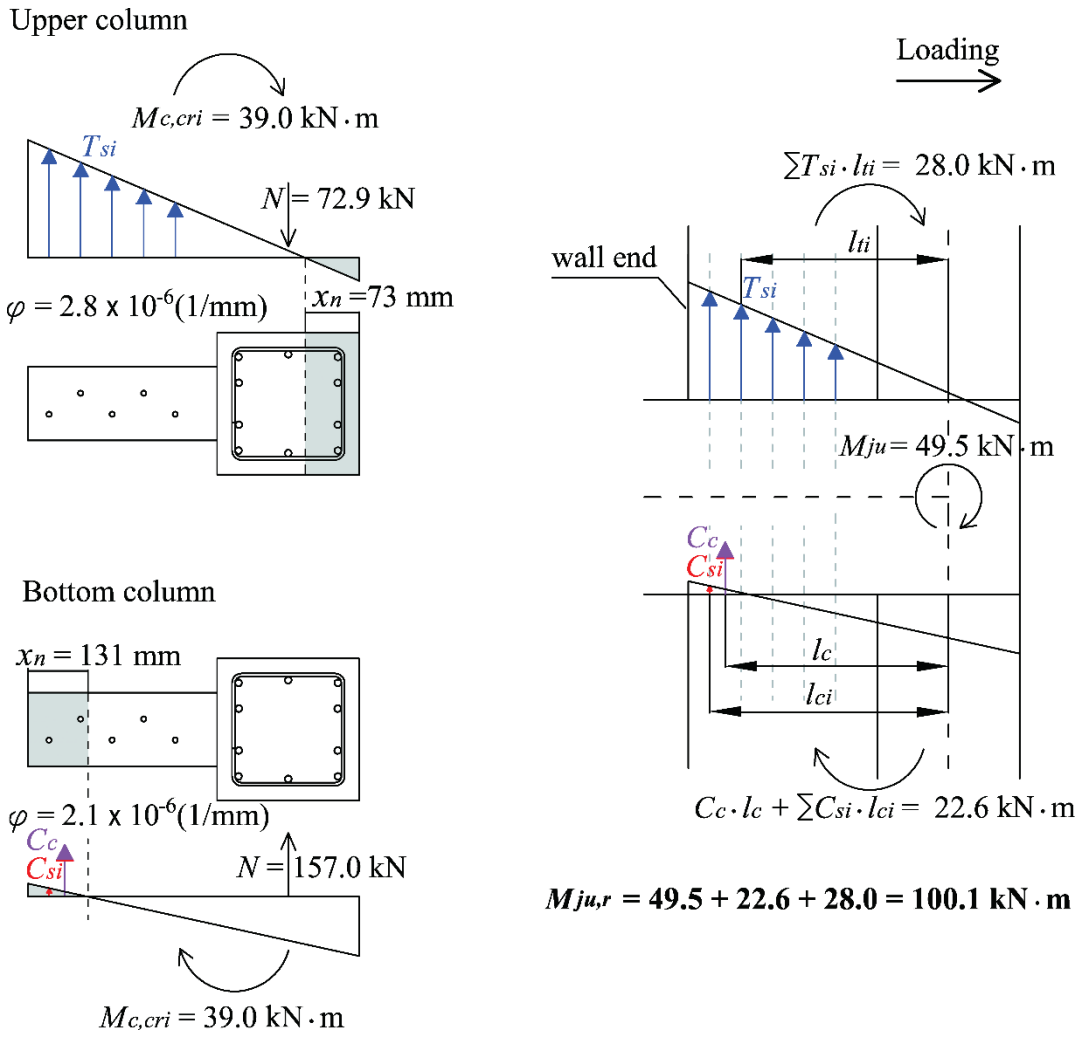

Figure 5.7 Results of the bending analysis and moment capacity of the strengthened joint.

Step 3: Evaluating the strength of column with wing wall

The flexural strength of the column with a wing wall M_{cw} was calculated by **Equations (5-7) and (5-8),** as proposed in a previous study [2]. These equations assume that all bars yield on the tensile side and that concrete reaches the ultimate strength; however, the compressive force of the bars was not counted, as illustrated in **Figure 5.8**. **Equation (5-7)** was used when wing wall is in tension, i.e. the upper column in the positive loading direction or the bottom column in the negative loading direction. **Equation (5-8)** was used when wing wall is in compressive, i.e. the bottom column in the positive loading direction or the upper column in the negative loading direction. M_{cw} was converted to the corresponding nodal moment at the joint ${}_nM_{cw}$.

$$M_{cw} = \sum a_{ti}\sigma_{yi}\left(d_i - \frac{\beta_1 x_n}{2}\right) + N\left(\frac{D_c}{2} - \frac{\beta_1 x_n}{2}\right) \quad (5\text{-}7)$$

$$M_{cw} = \sum a_{ti}\sigma_{yi}\left(d_i - \frac{\beta_1 x_n}{2}\right) + N\left(\frac{D_c}{2} + l_w - \frac{\beta_1 x_n}{2}\right) \quad (5\text{-}8)$$

where a_{ti}, σ_{yi}, and d_i are the area, yield stress, and distance to the concrete compressive edge of the *i*-th tensile bar, respectively; $\beta_1 = 0.85$ for $f_c' \leq 28$ MPa; $\beta_1 = 0.85\text{-}0.007(f_c'\text{-}28) \geq 0.65$ for $f_c' > 28$ MPa; and x_n is the depth of the neutral axis from **Equation (5-9)** based on the stress block concept by ACI [17].

$$x_n = \frac{\sum a_{ti}\sigma_{yi} + N}{0.85\,\beta_1\,f_c'\,b_w} \quad (5\text{-}9)$$

where b_w is the width of the stress block.

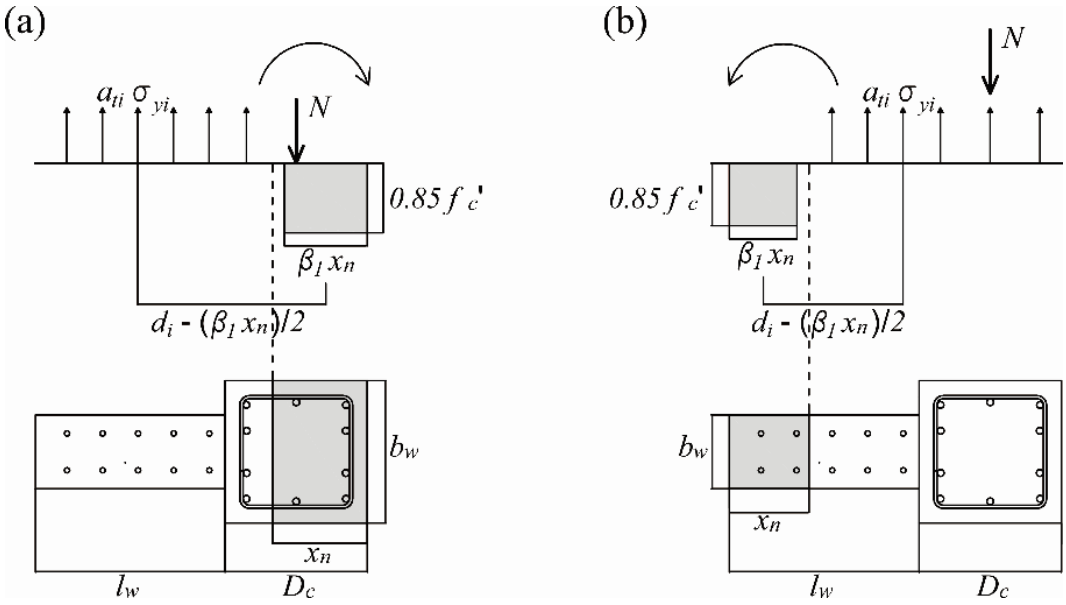

Figure 5.8 Evaluation of the ultimate strength for the column with a wing wall: (a) Wing wall in tension (b) Wing wall in compression.

Step 4: Determining the ultimate strength and failure mode of the strengthened frame

In the same manner as that in **Equation (3-10),** the ultimate strength of the strengthened specimen ($M_{u,r}$) is determined by **Equation (5-10)**. The beam yielding mechanism can be achieved if the nodal moment at the joint when the beam yields at the end of the wing wall ($_nM_{bu,r}$) is less than the summation of the nodal moment at the joint when the upper and bottom

columns with wing walls yield at the critical sections ($_nM_{cw1} + {}_nM_{cw2}$) and the moment capacity of the strengthened joint ($M_{ju,r}$), as illustrated by **Equation (5-11)**.

$$M_{u,r} = \min.[(\ {}_nM_{cw1} + {}_nM_{cw2}\ ),\ {}_nM_{bu,r},\ M_{ju,r}\ ] \quad (5\text{-}10)$$

$${}_nM_{bu,r} < \min.[(\ {}_nM_{cw1} + {}_nM_{cw2}\ ),\ M_{ju,r}\ ] \quad (5\text{-}11)$$

The equivalent joint moment at the ultimate strength of strengthened specimen J1-W are summarized in **Table 5-3**. This table shows the strengths of the specimens using the design values and tested material properties. The calculation results showed that the specimen is expected to fail in beam yielding mechanism in both the positive and negative loading directions; thus, the design of wing walls described in **Section 5.3** is effective for strengthening of the joint.

Table 5-3 Equivalent joint moment at the ultimate strength of specimen J1-W

	Loading direction	At beam flexural strength $_nM_{bu,r}$	At moment capacity of joint $M_{ju,r}$	At flexural strength of column with wing wall $_nM_{cw1} + {}_nM_{cw2}$	Expected failure mode
Based on design values	Positive	94.6 kN·m	100.1 kN·m	332.3 kN·m	Beam yielding
	Negative	59.3 kN·m	90.5 kN·m	351.3 kN·m	
Based on tested material properties	Positive	109.7 kN·m	119.4 kN·m	337.6 kN·m	Beam yielding
	Negative	68.7 kN·m	93.8 kN·m	361.6 kN·m	

5.5. Loading System, Instrumentation and Program

The test setup and the loading history were the same as those shown in **Figure 3.9** and **3.10**, respectively. The axial load applied to the strengthened specimen was also the same as that applied to the existing joint specimens described in **Section 3.3**. **Figure 5.9** shows the strain gauge arrangement for the specimen and **Figure 5.10** shows the displacement sensor arrangement.

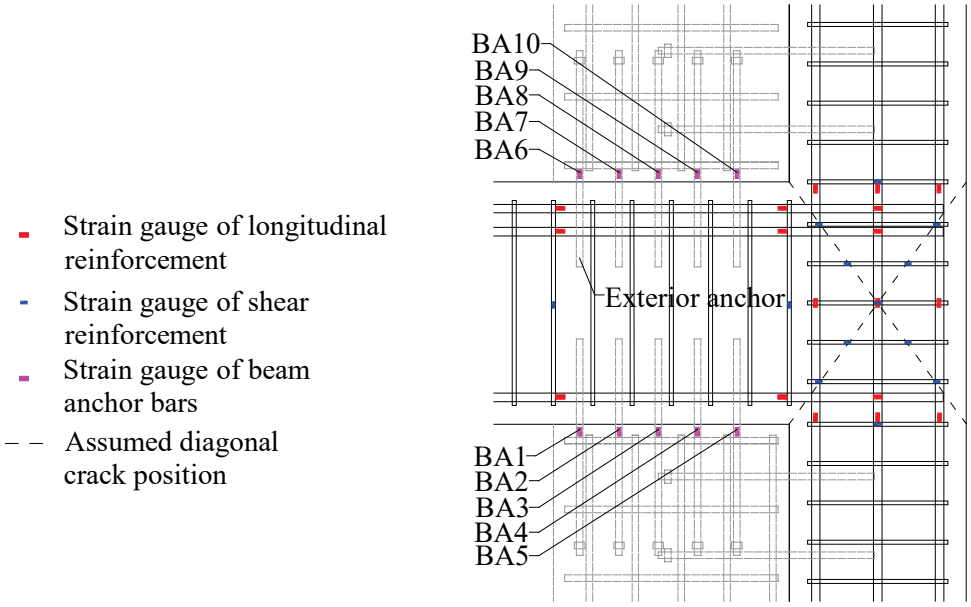

Figure 5.9 Strain gauge arrangement of specimen J1-W.

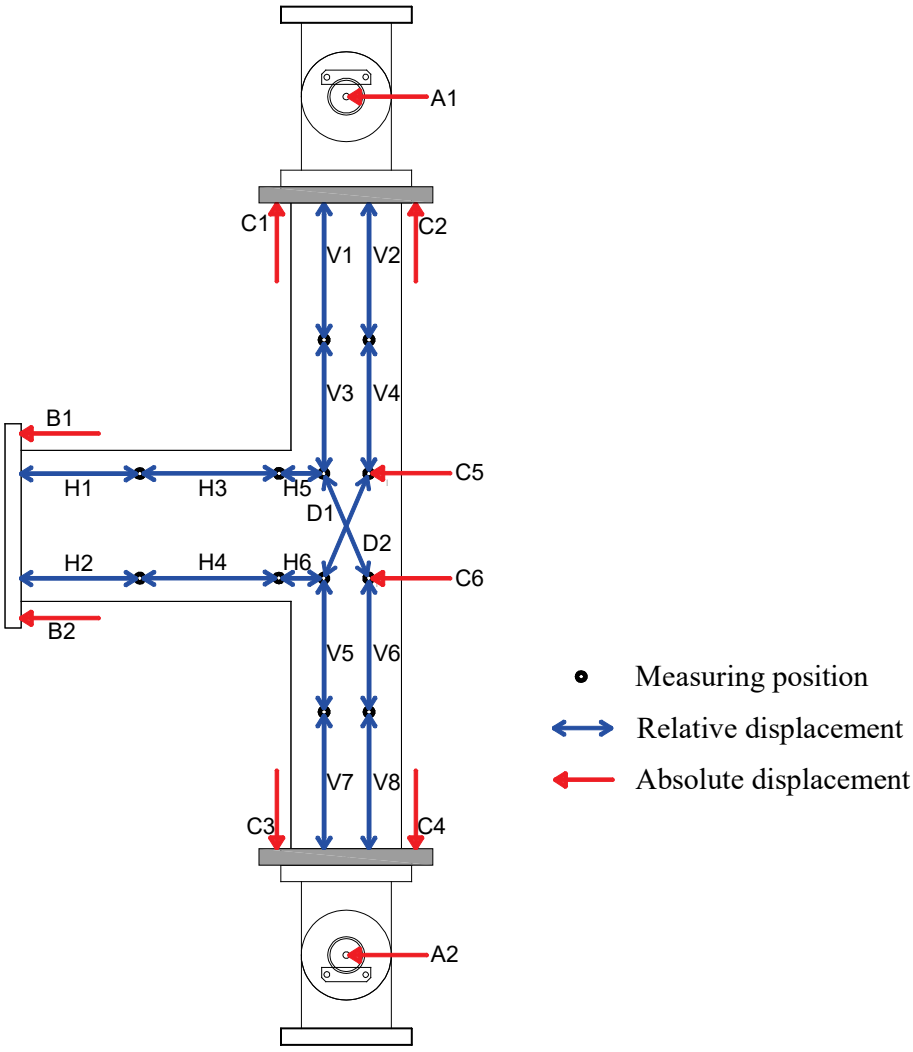

Figure 5.10 Displacement sensor arrangement

5.6. Experimental Results

Figure 5.11 shows the relationship between the experimental joint moment and drift ratio for the strengthened specimen J1-W. The observed damage to the specimen is shown in **Figure 5.12**. During the cycle to R = ± 0.5%, flexural-shear cracks appeared at the beam end attached to the wing walls, the exterior beam anchor (BA6, referring to **Figure 5.9**) yielded under the positive loading direction, and the bottom beam longitudinal bars at the wall face yielded under the negative loading direction. Diagonal cracks appeared in the existing joint panel during the cycle to R = ± 0.75%. During the cycle to R = + 1.5%, the top beam longitudinal bars at the wall face yielded, and the maximum strength under the positive loading direction was observed. The maximum strength under the negative loading direction was observed during the cycle to R = + 2%. The strength did not significantly decrease up to the cycle to R = ± 3%. Subsequently, concrete crushing of the beam was observed at the wing wall end, indicating shear failure of the beam. There was no obvious damage to the wing walls.

The crack patterns at every positive and negative peak drift ratio of the specimen are shown in **Appendix B** and the strain measurement of all reinforcing bars and anchors of the specimen are shown in **Appendix C**.

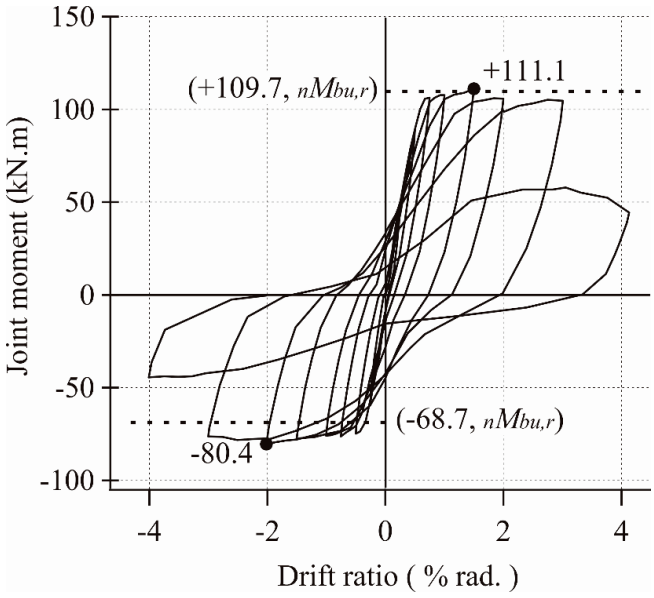

Figure 5.11 Joint moment-drift ratio relationship of specimen J1-W.

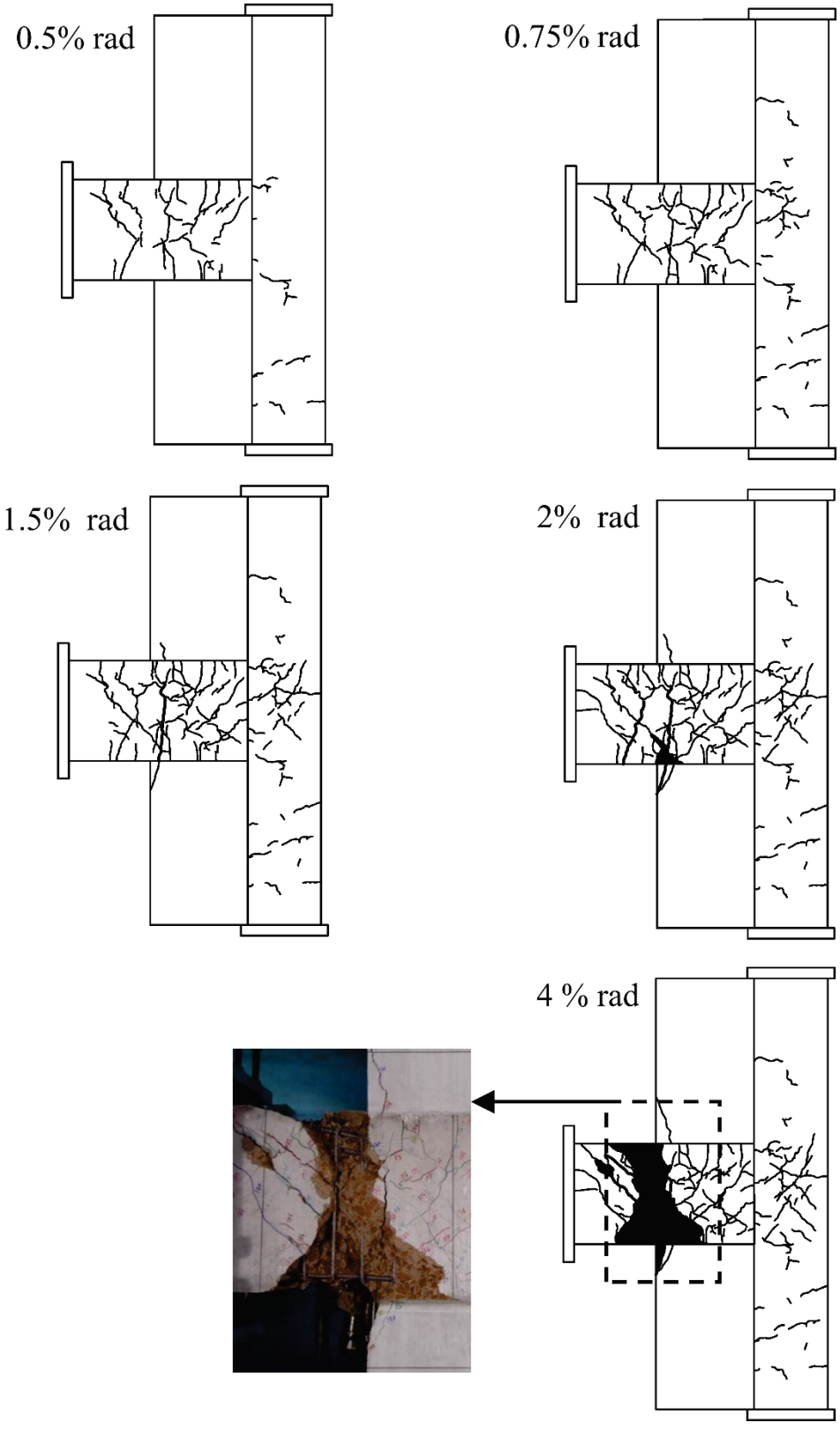

Figure 5.12 Damage to specimen J1-W.

5.7. Effectiveness of Strengthening

5.7.1. Plastic Hinge

In the retrofitted specimen, J1-W, the beam suffered damage at the wing wall end, indicating a beam yielding mechanism. The beam longitudinal bars yielded at the wall end in the positive and negative loading directions. **Figure 5.13** shows the strain measurement results along the beam bottom longitudinal bar of specimen J1-W. The lower strains at the column face indicated a significant reduction in the horizontal shear force transmitted to the joint, thus preventing joint shear failure. The high plastic strains developed at the end of the wing walls indicated that a plastic hinge formed in the beam. The anchorage (bond) was not lost until the last cycle to R = ± 4% based on clear gradients between the strain values at the middle joint and at the column face.

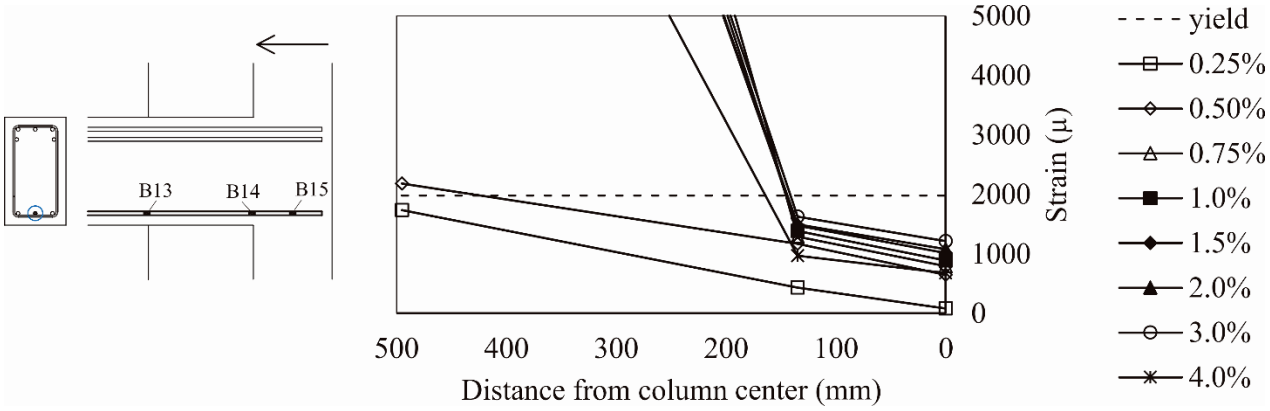

Figure 5.13 Strains along the bottom beam longitudinal bar of specimen J1-W.

5.7.2. Maximum Strength and Deformation Capacity

The maximum strengths of strengthened specimen J1-W in the positive and negative loading directions were 111.1 kN·m and 80.4 kN·m, respectively. These experimental strengths exceeded the calculated ultimate strengths based on tested material properties (109.7 kN·m and 68.7 kN·m in the positive and negative loading directions, respectively) determined by the nodal moment at the joint when the beam yielded at the end of the wing walls ($_nM_{bu,r}$). The

strengths of J1-W were improved by 2.1 and 1.7 times compared with those of J1 in the positive and negative loading directions, respectively.

Figure 5.14 compares the envelopes of the hysteresis loops shown in **Figure 3.14(a)** and **Figure 5.11**. In particular, the deformation capacity of the strengthened specimen, J1-W, was improved by 155% in the negative loading direction. It was confirmed that the deformability was improved by preventing anchorage failure. In the positive loading direction, the improvement in deformation capacity was limited; however, joint shear failure was prevented. To improve the deformation capacity beyond these results, shear strengthening should be applied to the beam end. The method to estimate the deformation capacity at the flexural-shear failure of beam will be explained later in **Section 5.8**.

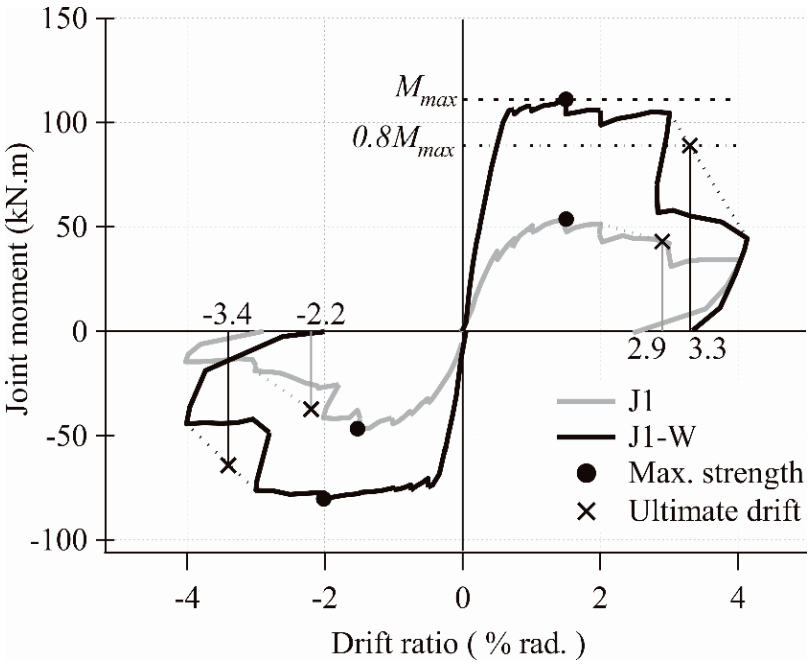

Figure 5.14 Comparison of the ultimate drift ratio of specimens J1 and J1-W.

5.8. Evaluation of Deformation Capacity of Beam

The experimental results showed that the ductility of the strengthened specimen was determined by the flexural-shear failure of the beam at the wing wall end. This kind of failure might occur due to the reduction of shear span of the beam after installation of wing wall. Therefore, evaluation of the deformation capacity of beam is important to prevent the flexural-shear failure until reaching a required deformation capacity, i.e. 2% rad based on the Japanese Guidelines [28].

Figure 5.15 shows a conceptual drawing for determining the deformation capacity of RC beams by combining the flexural performance curve with the shear strength curve. The deformation capacity at flexural-shear failure is defined as displacement at the intersection of the two curves.

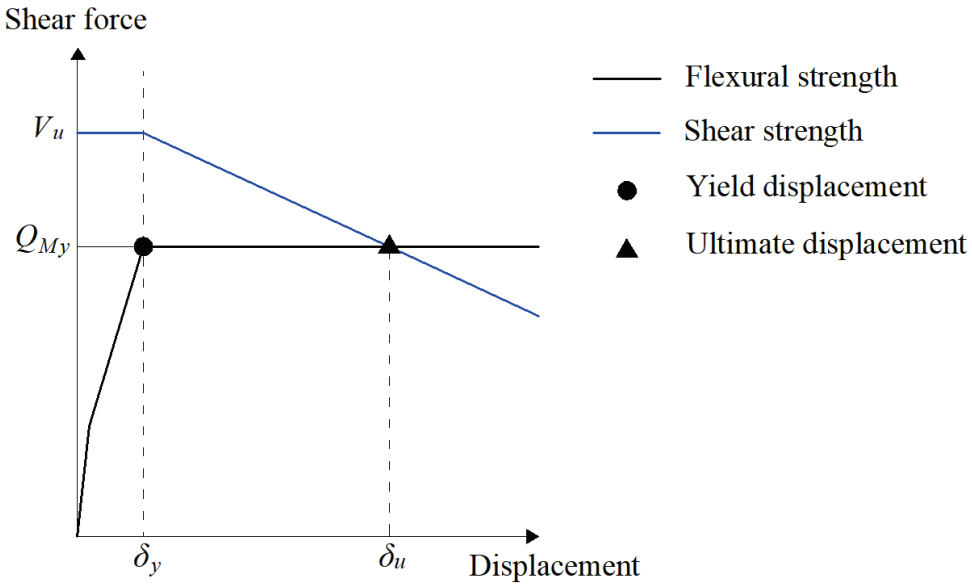

Figure 5.15 Evaluations of the deformation capacity of RC beams

5.8.1. Flexural Performance Curve

Flexural performance curve of the beam was idealized by a tri-linear function with cracking point and yielding point, as shown in **Figure 5.16**, based on **Equation (5-12)** to **(5-16)** for a practical design in Japan [27]. The cracking moment M_c and yielding moment M_y

were calculated by **Equations (5-12)** and **(5-13)**, respectively. The cracking rotation θ_c and yielding rotation θ_y were calculated by Equations **(5-14)** and **(5-15)**, respectively. **Equation (5-16)** gave the value of secant stiffness at the yielding point (α) and the post-yield stiffness was assumed to be 0.001 of the elastic flexural stiffness (k_o).

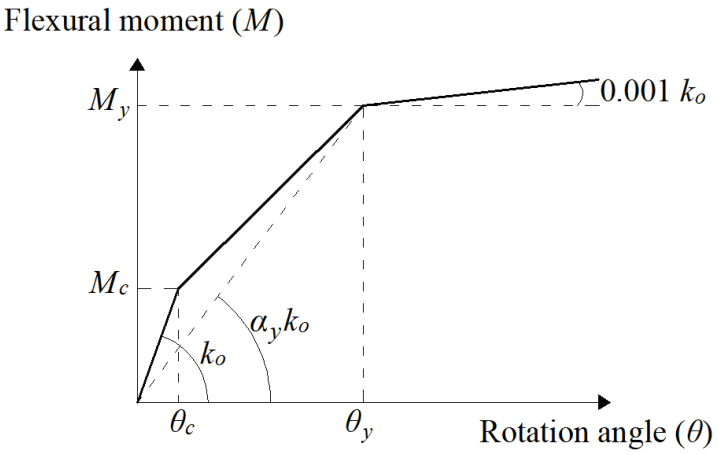

Figure 5.16 Flexural performance curve of the beam

$$M_c = 0.56\sqrt{f_c'}\ Z \tag{5-12}$$

$$M_y = 0.9\ a_t\ \sigma_y\ d \tag{5-13}$$

$$\theta_c = M_c\ /\ k_o \tag{5-14}$$

$$\theta_y = M_y\ /\ (\alpha_y\ k_o) \tag{5-15}$$

$$\alpha_y = \left(0.043 + 1.64\,\eta\,p_t + 0.043\,\frac{a}{d}\right)\left(\frac{d}{D}\right)^2 \tag{5-16}$$

where f_c' is the compressive strength of concrete; Z is the section modulus; a_t is the area of tensile reinforcement; σ_y is the yield stress of the longitudinal reinforcement; d is the effective depth of beam; η is the ratio of Young's modulus of the reinforcement to that of the concrete; p_t is tensile reinforcement ratio; a is the shear span; D is the depth of beam.

5.8.2. Shear Strength Evaluation Models

Two existing shear strength models were evaluated to investigate the applicability of the models to estimate the deformation capacity of the beam. These models consider the shear strength degradation related to plastic hinge rotation.

5.8.2.1. AIJ 1990

Based on the Japanese Design Guidelines AIJ 1990 [28], the shear strength of an RC member was evaluated by the sum of the contributions of the truss action V_t and strut action V_s, as shown in the following equations. The equations were adopted from a shear strength model described by Ichinose [29].

$$V_u = V_t + V_s \tag{5-17}$$

$$V_u = b\, j_t\, p_w\, \sigma_{wy}\, cot\, \phi + \frac{tan\, \theta\, (1-\beta)\, b\, D\, \nu\, \sigma_B}{2} \tag{5-18}$$

$$\text{use } p_w\, \sigma_{wy} = \frac{\nu\, \sigma_B}{2} \text{ when } p_w\, \sigma_{wy} \geq \frac{\nu\, \sigma_B}{2} \tag{5-19}$$

where b is the width of the member, j_t is the distance between the top and bottom flexural reinforcements; p_w is the shear reinforcement ratio; σ_{wy} is the yield stress of shear reinforcement; ϕ is the angle of truss action; θ is the angle of concrete compressive stress of the arch action to the member axis; $tan\, \theta = \sqrt{\left(\frac{h}{D}\right)^2 + 1} - \frac{h}{D}$; $\beta = \frac{(1+cot^2\, \phi)\, p_w\, \sigma_{wy}}{\nu\, \sigma_B}$; $\sigma_B = f_c'$; D is the depth of the member; and ν is the effectiveness factor on the compressive strength.

Two coefficients, ν and $cot\, \phi$ in this model, were related to plastic hinge rotation (R_p). The coefficient ν was determined by the following equations or **Figure 5.17**.

$$\nu = v_0 = 0.7 - \frac{\sigma_B}{200} \quad (\sigma_B \text{ is in MPa}) \quad \text{for } R_p = 0 \tag{5-20}$$

$$\nu = (1.0 - 15)v_0 \qquad \text{for } 0 < R_p < 0.05 \tag{5-21}$$

$$\nu = 0.25\, v_0 \qquad \text{for } R_p \geq 0.05 \tag{5-22}$$

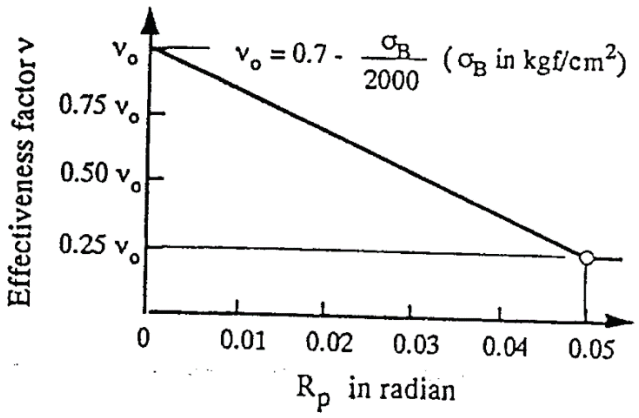

Figure 5.17 Relationship between R_p and ν [28]

The coefficient $cot\ \phi$ was determined by the minimum value of the following equations. The first three equations are shown in **Figure 5.18**.

$$cot\ \phi = 2.0 \qquad \text{for } R_p = 0 \tag{5-23}$$

$$cot\ \phi = 2.0 - 50R_p \qquad \text{for } 0 < R_p < 0.02 \tag{5-24}$$

$$cot\ \phi = 1.0 \qquad \text{for } R_p \geq 0.02 \tag{5-25}$$

$$cot\ \phi = \frac{j_t}{D \tan\theta} \tag{5-26}$$

$$cot\ \phi = \sqrt{\frac{\nu\ \sigma_B}{p_w\ \sigma_{wy}} - 1} \tag{5-27}$$

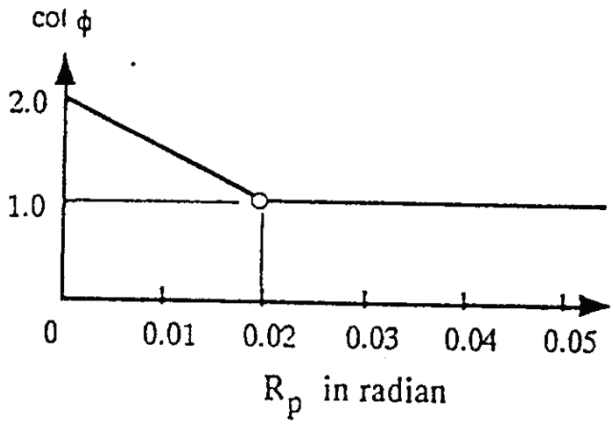

Figure 5.18 Relationship between R_p and $cot\ \phi$ [28]

5.8.2.2. AIJ 1997

In the Japanese Design Guidelines AIJ 1997 [23], the shear strength of RC member was expressed as the minimum of the following three equations.

$$V_{u1} = \mu\, p_{we}\, \sigma_{wy}\, b_e\, j_e + \left(\nu\, \sigma_B - \frac{5\, p_{we}\, \sigma_{wy}}{\lambda}\right)\frac{b\, D}{2}\, tan\, \theta \quad (5\text{-}28)$$

$$V_{u2} = \frac{\lambda\, \nu\, \sigma_B + p_{we}\, \sigma_{wy}}{3}\, b_e\, j_e \quad (5\text{-}29)$$

$$V_{u3} = \frac{\lambda\, \nu\, \sigma_B}{2}\, b_e\, j_e \quad (5\text{-}30)$$

where μ is the coefficient concerning the angle of concrete truss action; μ = 2-20R_p (or **Figure 5.19**); p_{we} is the effective shear reinforcement ratio; $p_{we} = a_w/(b_e\, s)$; a_w is the cross-sectional area of the shear reinforcement; b_e is the effective width of the member; s is the spacing of the shear reinforcement, j_e is the effective depth of the member; $\nu = (1 - 20R_p)\nu_0$ (or **Figure 5.20**); $\nu_0 = 0.7 - \sigma_B/200$; λ is the effective depth coefficient for truss action; $\lambda = 1 - \frac{s}{2j_e} - \frac{b_s}{4j_e}$; b_s is the largest distance between ties; θ is the angle of compression strut of arch mechanism; $tan\,\theta = 0.9\,\frac{D}{2L}$ when $\frac{L}{D} \geq 1.5$; $tan\,\theta = 0.9\,\frac{D}{2L}$ when $\frac{L}{D} < 1.5$; and L is the clear length of the member.

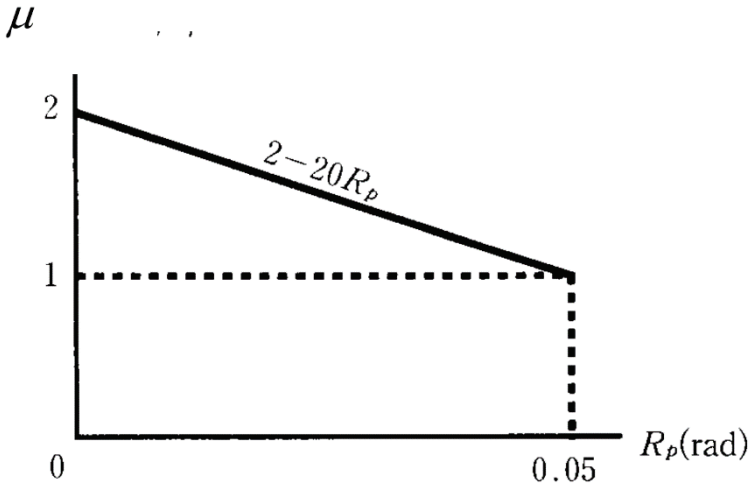

Figure 5.19 Relationship between R_p and μ [23]

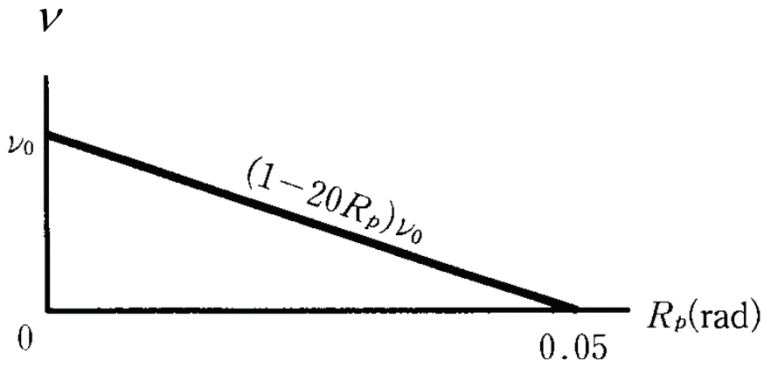

Figure 5.20 Relationship between R_p and ν [23]

5.8.3. Evaluation Results

In the experiment, inter story-drift angle (θ) was defined as the ratio of column-relative displacement (δ_h) to the column height (L_c), as shown in **Figure 5.21**. However, for the evaluation of deformation capacity of beam, beam displacement (δ) need to be defined. Assuming rigid column, the drift angle (θ) is assumed equal to the ratio of beam displacement (δ) to the beam length (L_b). The conversion of joint moment – drift ratio relationship of specimen J1-W in **Figure 5.11** into beam shear force (Q) – beam displacement (δ) relationship is shown as experimental hysteresis curve in **Figure 5.22** or **Figure 5.23**.

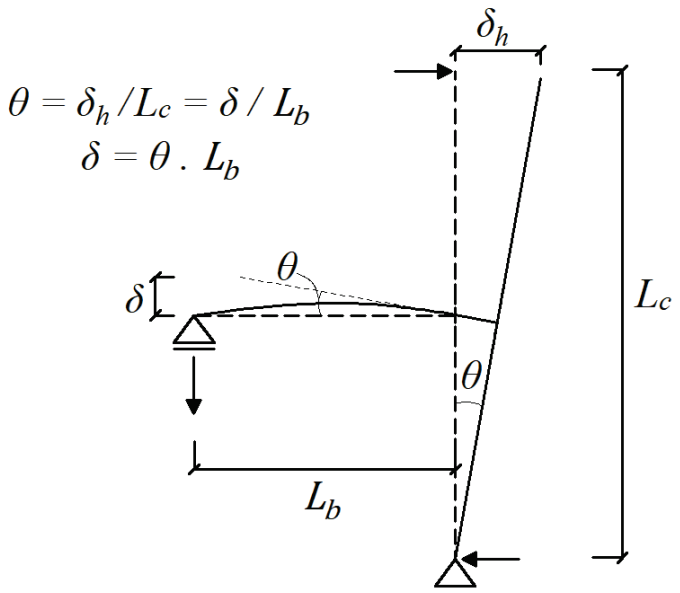

Figure 5.21 Converting drift angle to beam displacement

Evaluation results of deformation capacity of beam using the AIJ 1990 shear strength model [28] combined with the flexural performance curve are described in **Figure 5.22**. The tested material properties, explained in **Section 5.3,** were used for calculations. The flexural performance curve obtained using the method explained in **Section 5.8.1** well predicted the flexural behavior of the specimen before the flexural-shear failure occurred. However, the application of the AIJ1990 shear strength model quantitatively overestimated the ultimate displacement of beam at flexural-shear failure in both positive and negative loading direction. Therefore, this model is not recommended for estimating the deformation capacity of beam within the present investigation.

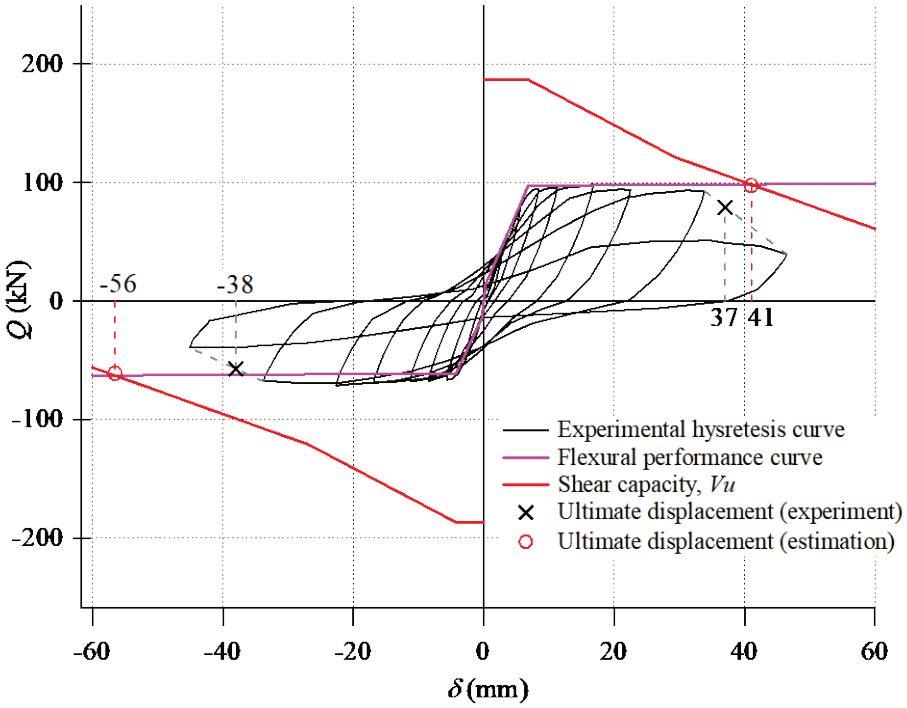

Figure 5.22 Estimated deformation capacity of beam using AIJ 1990 shear strength model [28]

Figure 5.23 shows evaluation results of deformation capacity of beam using the AIJ 1997 shear strength model [23] combined with the flexural performance curve. The results show that the application of this model well estimated the ultimate displacement of beam in the negative loading direction (38 mm), which is equal to the experimental value. The estimated

ultimate displacement of beam in the positive loading direction (30 mm) also give reasonable value, because it was less than the experimental value (37 mm). This model is recommended for application to estimate the deformation capacity of beam.

The minimum value of the estimated ultimate displacement of beam was 30 mm, equal to beam drift angle 2.67% rad. If a larger deformation capacity is expected in design, shear strengthening of beam should be applied.

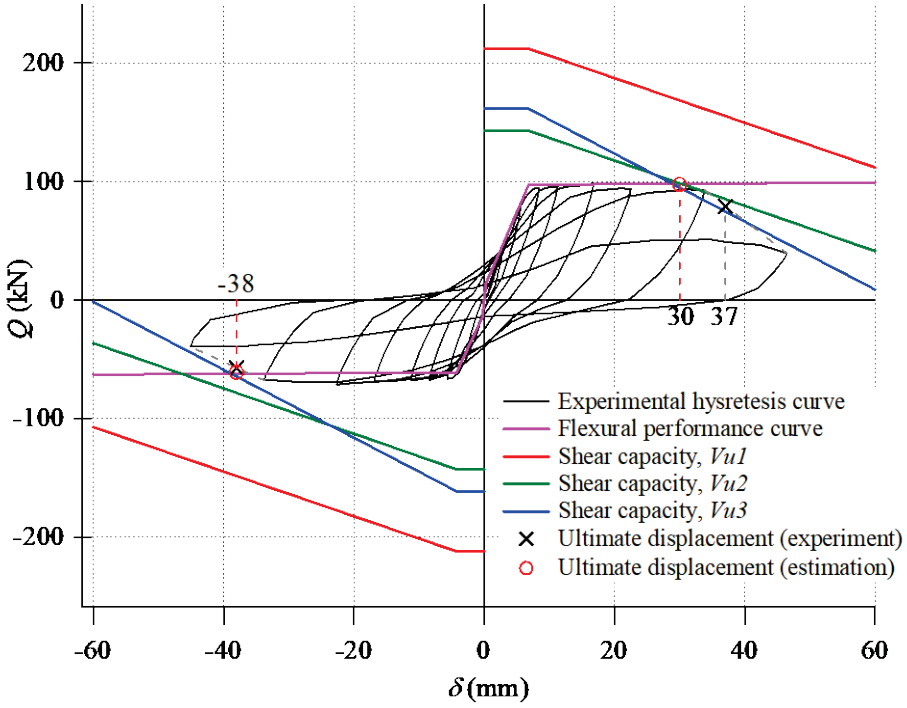

Figure 5.23 Estimated deformation capacity of beam using AIJ 1997 shear strength model [23]

5.9. Summary

A strengthening method by installing wing walls was proposed and applied to a beam-column specimen with deficient beam rebar anchorage. Major findings are summarized as follows:

(1) Experimental results showed that the failure mode of the specimen strengthened by installing wing walls was successfully changed from brittle anchorage failure and joint shear failure to ductile beam yielding.

(2) The proposed design concept considering the length of wing walls to extend the development length of beam longitudinal bars was effective to prevent the pullout of beam longitudinal bars from the joint.

(3) It was experimentally verified that installing RC wing walls was effective for strengthening exterior beam-column joints with substandard straight anchorage of beam longitudinal rebar.

(4) The applied procedure to evaluate the strengthening design was effective to confirm that the beam yielding mechanism can be achieved and to estimate the strength of the strengthened frame.

(5) The presented method on evaluation of deformation capacity of beam was effective to evaluate the deformation capacity of strengthened frame controlled by the flexural-shear failure of beam.

Chapter 6

Analytical Evaluation on Seismic Performance of an RC Building Strengthened with Wing Walls

6.1. Introduction

The proposed strengthening method by installing wing walls was effective for strengthening the exterior beam-column joint with deficient anchorage, as verified in **Chapter 5**. This strengthening method is expected to increase the global seismic performance of the building. Therefore, the static nonlinear pushover analysis was conducted to identify the strength and deformation capacity of an RC building under static lateral loads before and after strengthening by wing walls.

6.2. Focused Building

The strengthening by installing wing walls was applied to the building which was focused on the previous experimental study described in **Chapter 3**, as shown in **Figure 6.1**. The wing walls were assumed to be applied to the interior side of exterior columns in all stories of the building, as shown in the figure. Low strength materials used in the previous experimental study was applied to the existing frame in which the design strength of concrete f_c' was 10 MPa and the grade of rebar was SD295 (f_y = 295 MPa). However, normal strength concrete (f_c' = 30 MPa) was used for the wing walls

The prototype building was assumed to have deficient straight anchorage of beam reinforcement to the exterior joints. Therefore, the length of wing walls was determined by **Equation (5-2)**, resulting the length of wing walls of 590 mm, as shown in **Figure 6.2(a)**. The cross-section of wing walls is shown in **Figure 6.2(b)**, which were designed with the same ratio of wall reinforcement and anchors with the specimen described in **Section 5.3**.

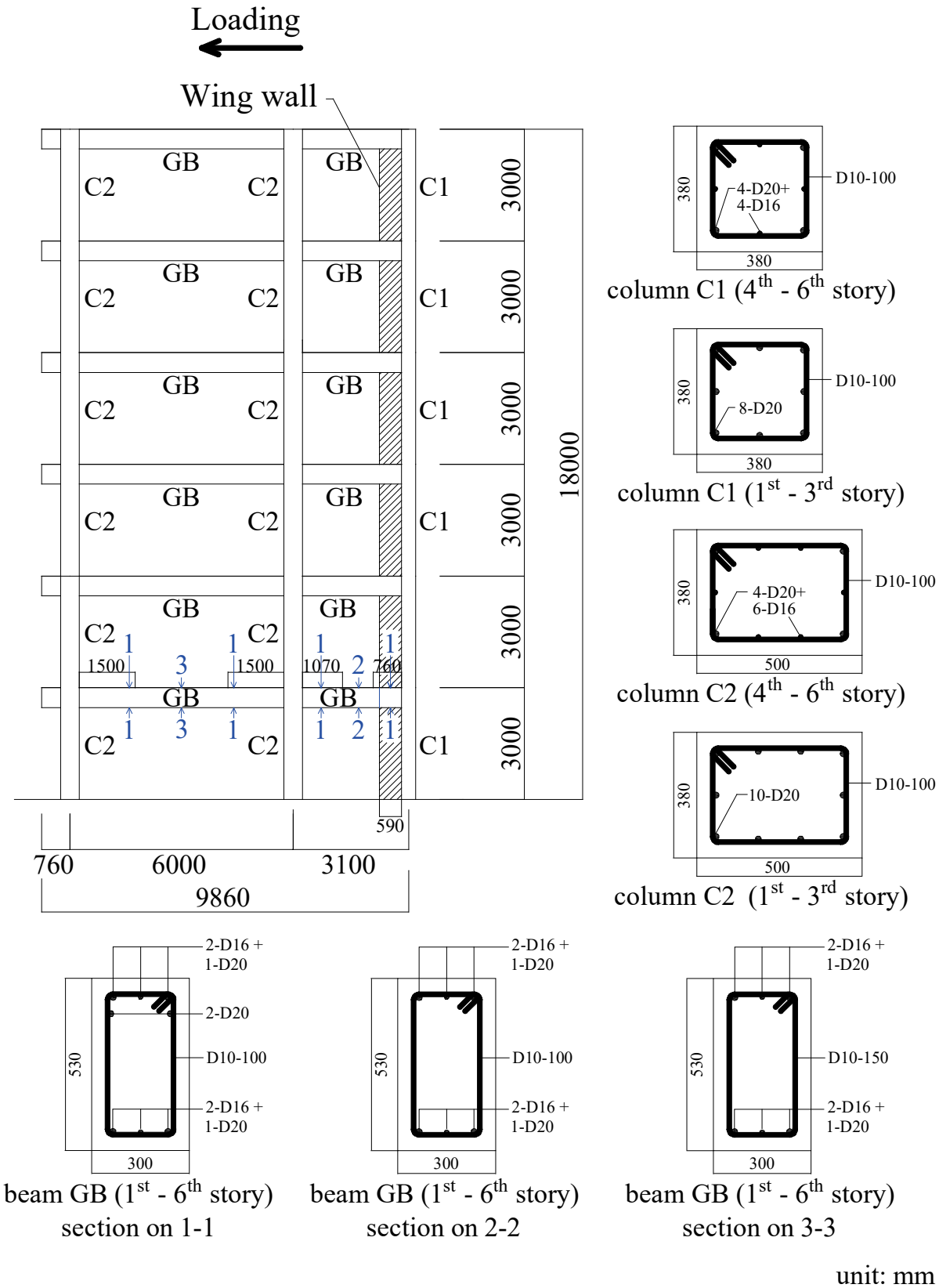

Figure 6.1 The focused building and reinforcement details of the structural members

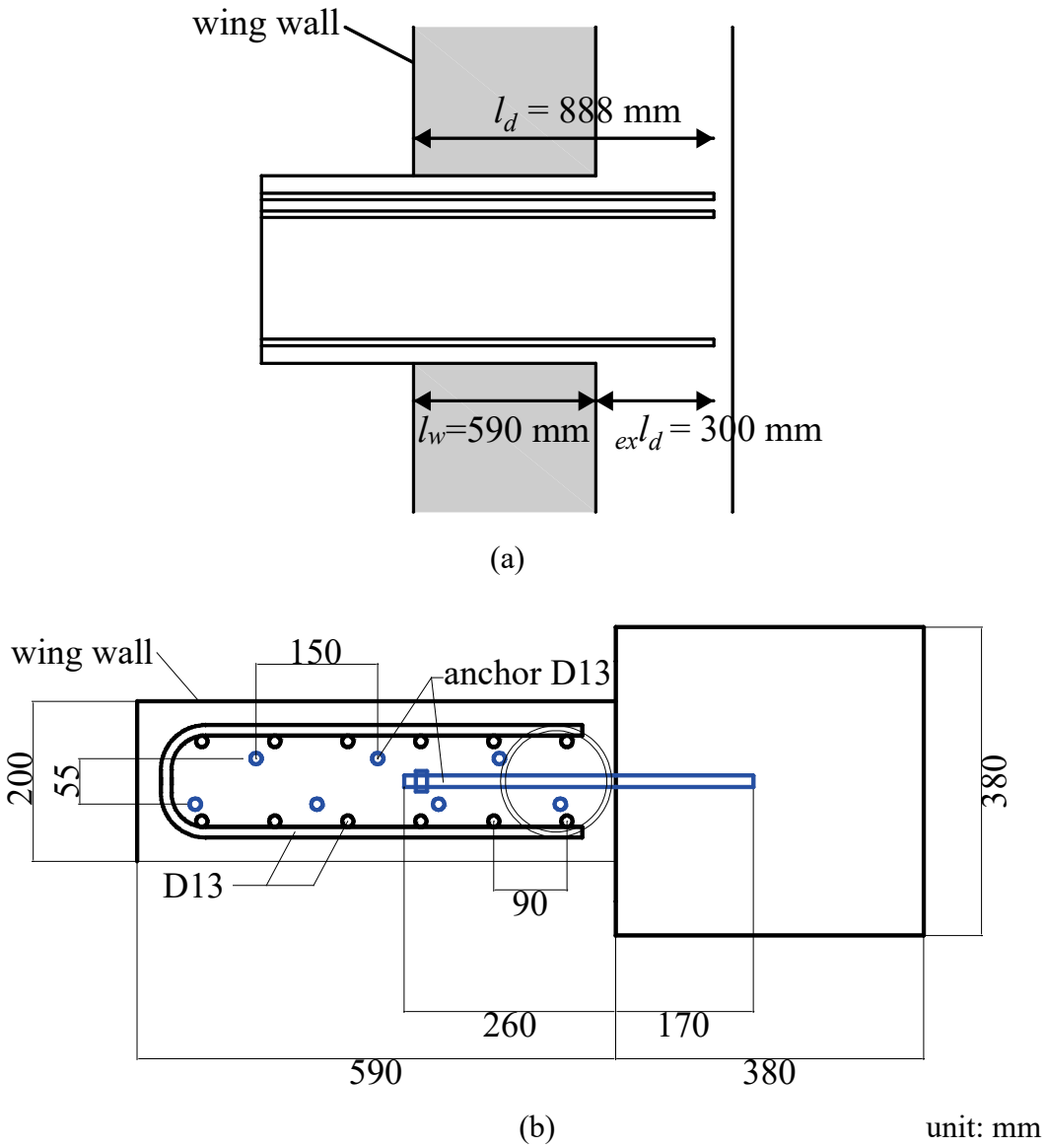

Figure 6.2 (a) Length of wing wall (b) Details of wing wall

6.3. Analytical Assumptions

Pushover analysis was conducted for two models, the frame without wing walls and the frame with wing walls. The beams and columns were replaced by line elements with rigid zones at beam-column joints, as shown in **Figure 6.3(a)**. The columns with wing walls were also replaced by line element along the central axis of the existing columns, and the beam above/below the wing walls are assumed as rigid zones, as shown in **Figure 6.3(b)**.

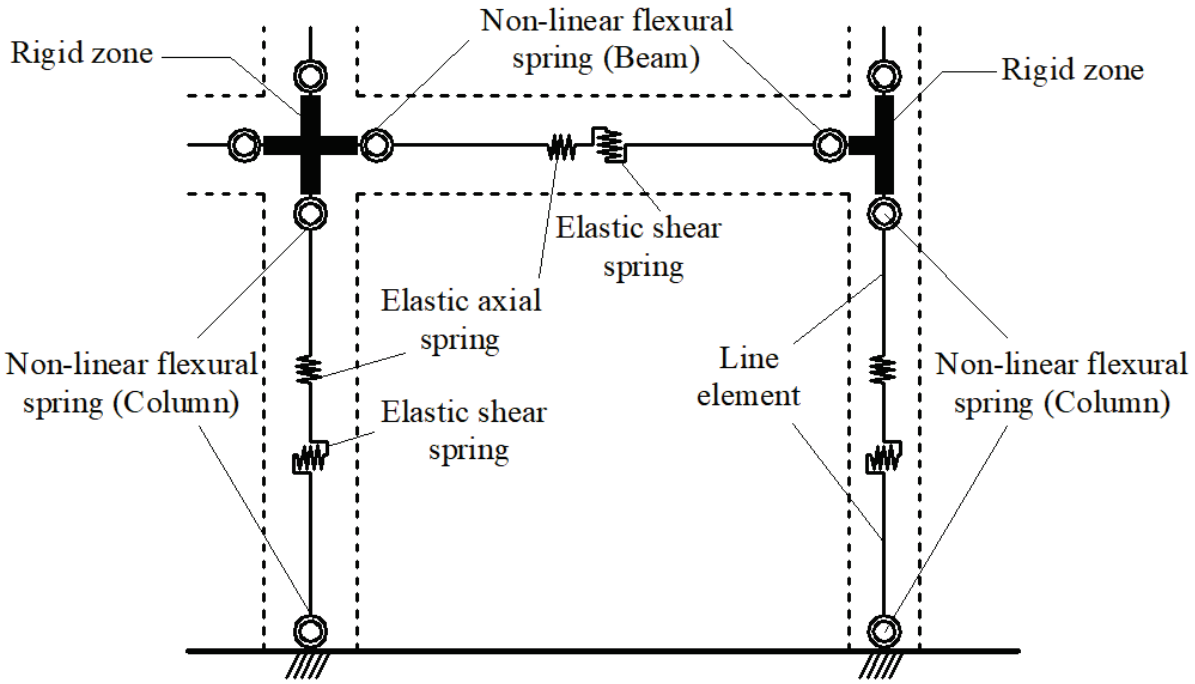

(a)

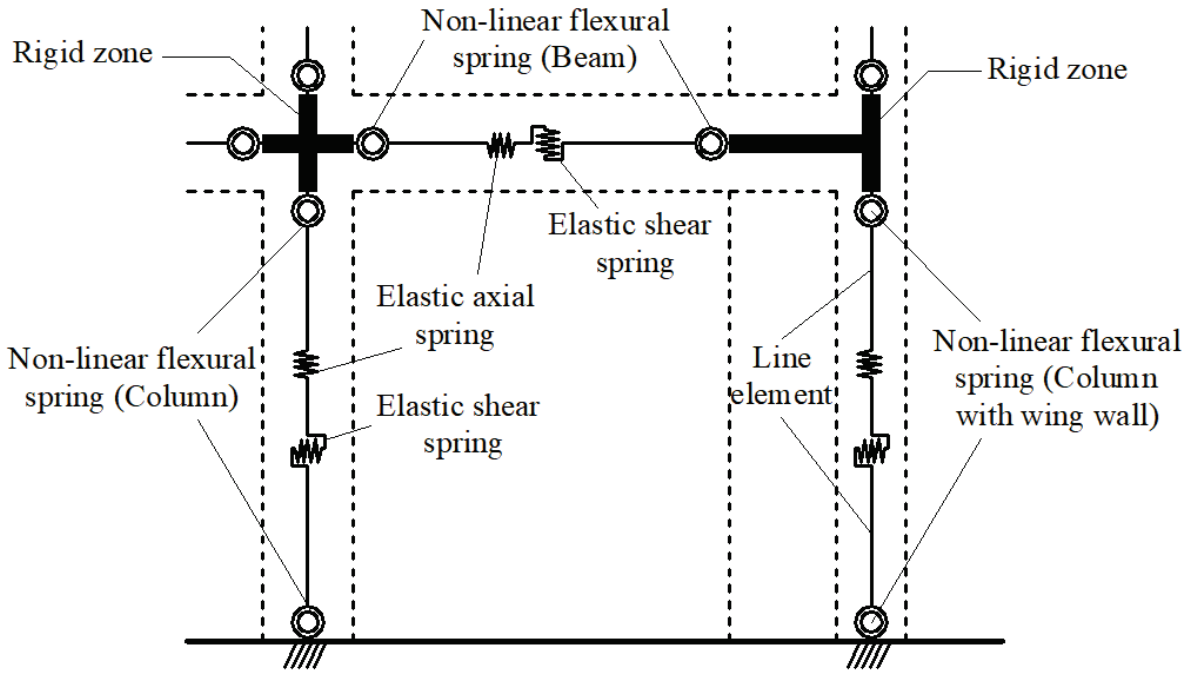

(b)

Figure 6.3 Modeling of the structural components: (a) Without wing walls (b) With wing walls

The RC beams considered nonlinear flexural characteristics, elastic shear and axial deformation. Flexural performance curve of the beam was idealized by a trilinear function, as explained in **Section 5.8.1.** The shear spring is defined as the elastic shear force-shear rotation relationship. The elastic shear stiffness k_s is defined by **Equation (6-1).**

$$k_s = G \cdot A \tag{6-1}$$

where G is the shear modulus and A is the effective shear area.

The RC columns considered nonlinear flexural characteristics, elastic shear and axial deformation. Flexural performance curve of the column was idealized by a trilinear function, as shown in **Figure 6.4**, based on **Equation (6-2)** to **(6-6)** for a practical design in Japan [27]. The cracking moment M_c and yielding moment M_y were calculated by **Equation (6-2)** and **(6-3)**, respectively. The cracking rotation θ_c and yielding rotation θ_y were calculated by **Equation (6-4)** and **(6-5)**, respectively. **Equation (6-6)** gave the value of secant stiffness at the yielding point (α) and the post-yield stiffness was assumed to be 0.001 of the elastic flexural stiffness (k_o).

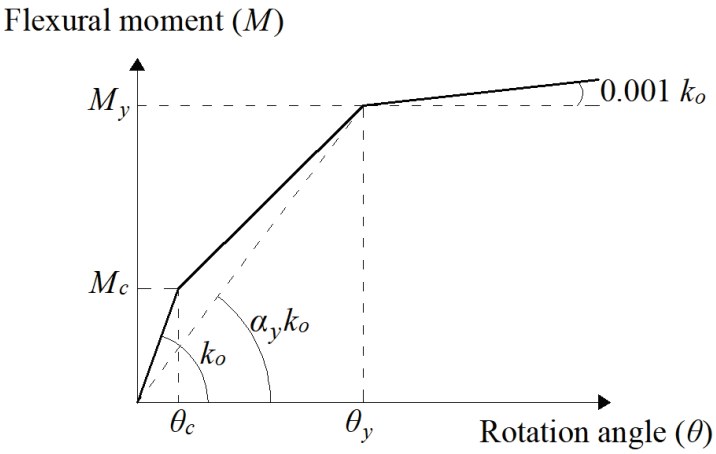

Figure 6.4 Trilinear moment-rotation relationship of flexural spring

$$M_c = 0.56\sqrt{f_c'}\ Z + \frac{N\,D}{6} \tag{6-2}$$

$$M_y = 0.8\,a_t\,\sigma_y\,D + 0.5\,N\,D\left(1 - \frac{N}{b\,D\,f_c'}\right) \qquad for\ 0 < N \le 0.4\,b\,D\,f_c' \qquad \text{or}$$

$$M_y = \{0.8\, a_t\, \sigma_y\, D + 0.12\, b\, D^2\, f_c'\} \left(\frac{N_{max} - N}{N_{max} - 0.4\, b\, D\, f_c'}\right) \quad \text{for} \quad 0.4\, b\, D\, f_c' < N \leq N_{max} \quad (6\text{-}3)$$

$$\theta_c = M_c \,/\, k_o \quad (6\text{-}4)$$

$$\theta_y = M_y \,/\, (\alpha_y\, k_o) \quad (6\text{-}5)$$

$$\alpha_y = \left(0.043 + 1.64\, \eta\, p_t + 0.043\, \frac{a}{d}\right) \left(\frac{d}{D}\right)^2 \quad (6\text{-}6)$$

where D is the depth of column; b is the width of column; $N_{max} = b\, D\, f_c' + a_g\, \sigma_y$; a_g is the total cross-sectional area of reinforcing bars; k_o is the elastic stiffness; $k_o = 6EI/L$; is E is the Young's modulus; I is the moment of inertia of the cross section; L is the clear height of the column; η is the ratio of the Young's modulus of the reinforcement to the Young's modulus of the concrete; p_t is tensile reinforcement ratio; a is the shear span; and d is the effective depth of beam.

The columns with wing wall considered nonlinear flexural characteristics, elastic shear and axial deformation. Flexural performance curve of the columns with wing wall was idealized similar as that of columns, as illustrated in **Figure 6.4**. However, the cracking moment M_c was calculated by **Equation (6-7)** [27] and the yielding moment M_y was calculated as the fully plastic moment by **Equation (5-7)** and **(5-8)**, explained in **Section 5.4**. The yielding rotation θ_y is assumed to be a constant value of 0.67%, based on the Japanese standard [22].

$$M_c = \left(0.56\, \sqrt{f_c'} + \frac{N}{A}\right) Z + N \cdot e \quad (6\text{-}7)$$

where A is the cross sectional area of column with wing wall, and e is the distance from the centroid of the cross section to the center of the column (assuming axial load acts at the center of the column).

In the modeling, the foundations and slabs of the focused building were regarded as rigid. The gravity loads (dead loads and live loads) were estimated according to the Bangladeshi code [20] and distributed to each node considering the tributary area. The lateral load force distribution for the static analysis was assumed to be a triangular distribution, determined by

the following equations based on the Bangladeshi code [20], which are similar to that of ASCE code [30]. The distribution of lateral force C_{vx} for each story is shown in **Figure 6.5**.

$$F_x = C_{vx} V \tag{6-8}$$

$$C_{vx} = \frac{w_x h_x^k}{\sum_{i=1}^{n} w_i h_i^k} \tag{6-9}$$

where C_{vx} is the vertical distribution factor; V is the total design force or shear at the base of structure; w_i and w_x are the portion of the total gravity load assigned to level i or x; h_i and h_x are the height from the base to level i or x; n is the number of stories; k is an exponent related to the structure period; k = 1 for structure period $\leq$ 0.5s; k = 2 for structure period $\geq$ 2.5s; and k = linear interpolation between 1 and 2 for other periods. The structure period T was approximated by the following equation [20], [30]:

$$T = C_t (h_n)^m \tag{6-10}$$

where h_n is the height of buildings in meters from foundation or from top of rigid basement; C_t = 0.0466 and m = 0.9 for concrete moment-resisting frames.

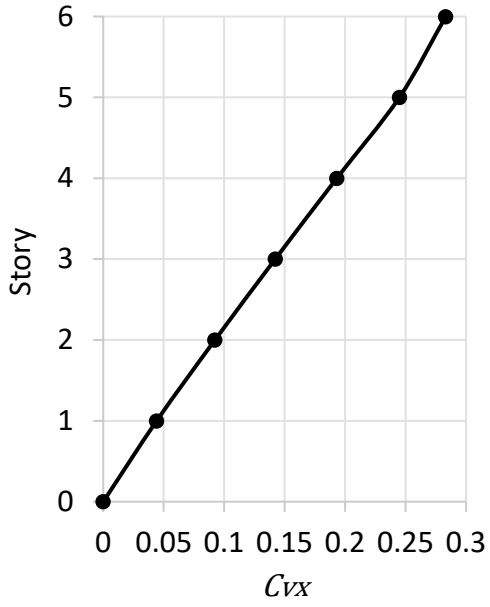

Figure 6.5 Lateral force distribution

6.4. Analytical Results

Pushover analysis was conducted using the commercial software SNAP Ver.7. The analysis was conducted for one loading direction, as shown in **Figure 6.1**, because the existing frame without wing wall is expected to fail by anchorage failure of joint which leads to more brittle behavior than the shear failure of joint in the opposite loading direction, as confirmed by the experimental results of specimen J1 explained in **Chapter 3**.

Figure 6.6 shows the base shear force - roof drift angle relationship for the frame without wing walls. The performance limit of the curve was assumed as the point at which strength degradation start, obtained from the experimental results in **Chapter 3**. The exterior beam-column joint specimen J1 reached the maximum strength in the negative loading direction at a drift ratio of 1.5%, as shown in **Figure 3.14(a),** followed by strength degradation due to anchorage failure of the joint. Therefore, the performance limit of the frame was defined when the rotation of beam end at an exterior joint reached this drift angle, based on the assumption described in **Figure 5.21**. The performance limit of the frame was obtained at roof drift angle of 0.87% and base shear force of 1030 kN.

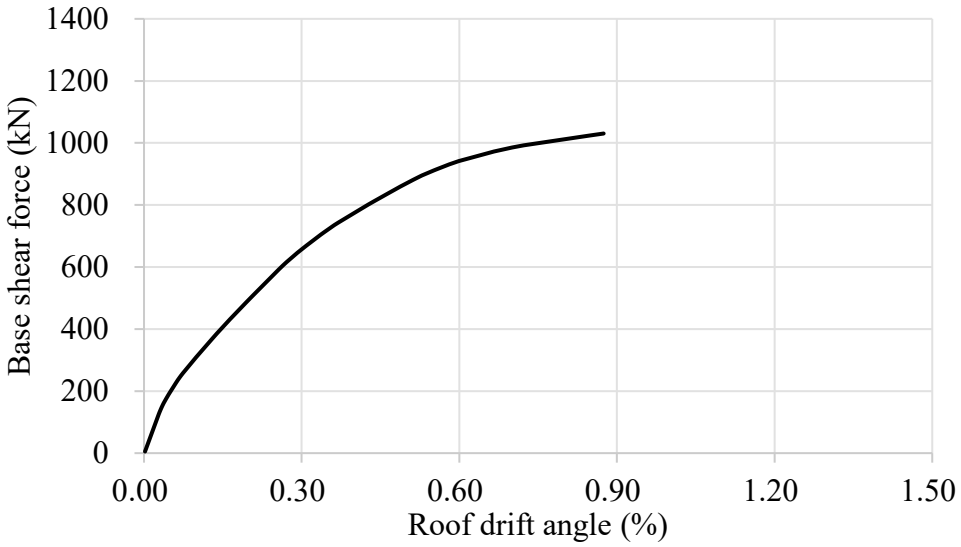

Figure 6.6 Base shear force – roof drift relationship for frame without wing walls

In the case of the frame with wing walls, the performance limit was controlled by the flexural-shear failure of beam due to shortening of beam span after installation of wing walls. **Figure 6.7** shows the evaluation results of deformation capacity of a beam connected to the exterior joint with wing walls which reach the yield rotation at the earliest step in the pushover analysis. The shear capacity of beam was calculated by the AIJ 1997 [23] shear strength model, as explained in **Section 5.8.2.2**. In the figure, the shear force act on beam (Q) was calculated by **Equation (6-10)**, and the total deformation of beam (δ) was calculated by **Equation (6-11)**, using the results from pushover analysis. The estimated ultimate displacement of beam was 61 mm, equal to beam drift angle 2.95% rad. If a larger deformation capacity is expected in design of the strengthened building, shear strengthening of beam should be applied.

$$Q = \frac{M_A + M_B}{L} \tag{6-11}$$

$$\delta = \delta_f + \delta_s \tag{6-12}$$

where, M_A , M_B is the moment at both end of beam, obtained from flexural spring; L is the clear span of beam; δ_f is the flexural deformation, obtained from the rotation (θ) of the flexural spring, assuming a fixed point of contra flexure at the middle length of the beam, as described in **Figure 6.8**; and δ_s is the shear deformation, obtained as deformation of the shear spring.

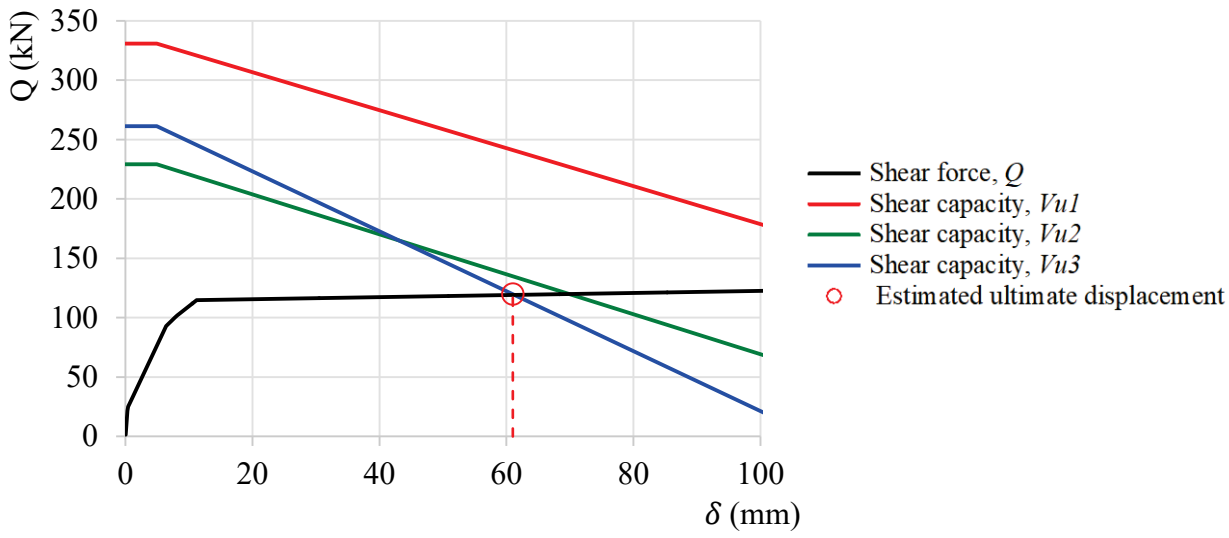

Figure 6.7 Estimated deformation capacity of beam

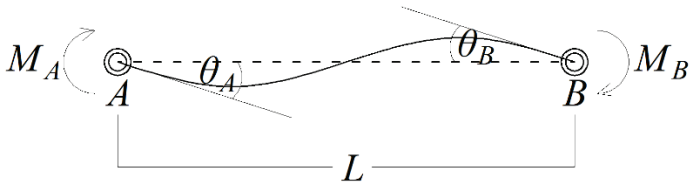

$$\delta_f = \theta_A \,.\, L/2 + \theta_B \,.\, L/2$$

Figure 6.8 Flexural deformation from the flexural spring

Figure 6.9 shows the base shear force - roof drift angle relationship for the frame strengthened with wing walls. The performance limit of the frame with wing walls was obtained at roof drift angle of 1.32% and base shear force of 1278 kN.

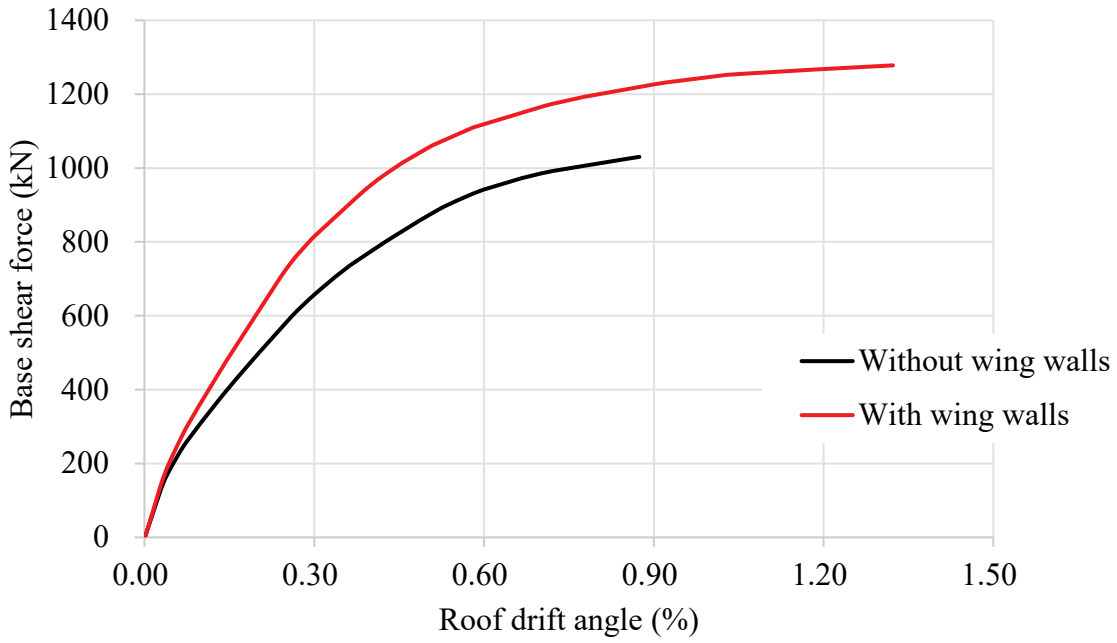

Figure 6.9 Base shear force – roof drift relationship for frame with and without wing walls

Figure 6.9 also compares the base shear force - roof drift angle relationship for the frame without and without wing walls. The strengthening of the frame with wing walls increased the lateral strength of the building by 24% and the improved deformation capacity of the building by 52% compared with those of frame without wing walls.

6.5. Summary

The pushover analysis has been conducted for an RC building with and without wing walls. Major findings are summarized as follows:

1. The presented analytical procedure can be used to estimate the performance limit of the building with wing walls controlled by the flexural-shear failure of the beam. However, further study is needed to analytically estimate the performance limit of the building without wing wall controlled by anchorage failure of the exterior joint.
2. The strengthening by installing wing walls is not only effective for strengthening of the joint, but also contribute to increase the strength and the deformation capacity of the building.

Chapter 7

Summary and Conclusions

7.1 Summary

RC buildings with deficient details of beam-column joint, where the joints contain little/no shear reinforcement and/or insufficient anchorage of beam longitudinal rebar, exist in developing countries in earthquake-prone areas. Aggressive research works focusing on strengthening of beam-column joints have been conducted by a number of researchers; however, they are not easily implemented in developing countries.

A strengthening method by installing wing was has been developed for strengthening of the exterior joints with deficient shear reinforcements. This study proposed this strengthening method for the exterior joints with deficient anchorage. This strengthening method can be a practical solution for strengthening the substandard joints in developing countries because of the use of inexpensive materials and simple construction techniques.

The study was prefaced by a field investigation in West Sumatra, Indonesia, which was affected by the 2009 Sumatra Earthquake. The investigation was conducted on newly constructed buildings, showing that the deficiencies of material specification and detailing of beam-column joints were exist many buildings, regardless of the experience of damage by the past earthquake.

An experiment was conducted to evaluate the seismic performance of the existing exterior joints with deficient anchorage. However, the specimens were constructed to represent the Bangladeshi buildings with low strength concrete, which gives the worst scenario on vulnerability of existing beam-column joints. Two specimens (J1 and J2) with deficient anchorage details were tested. One of the specimens with straight anchorage of beam

longitudinal bar (J1) failed in anchorage failure was chosen for the benchmark specimen for strengthening.

Prior to design of the strengthening by wing walls, a series of pullout test was conducted evaluate the performance of post-installed anchors in low-strength concrete with brick chip aggregate representing Bangladeshi concrete. From the test results, minimum embedment length of anchors to prevent brittle failure of anchors was concluded, then applied for the details of post-installed anchors for in the strengthening.

The strengthening by installing wing walls was applied to a specimen (J1-W) with the benchmark specimen (J1) from the previous experiment of existing joints. A design concept was proposed to prevent the anchorage failure by considering the length of wing walls to extend the development length of beam longitudinal bars. The proposed strengthening method was verified to upgrade joints with deficient anchorage.

Moreover, a pushover analysis was conducted to evaluate the seismic performance of an RC building before and after strengthening by wing walls. It confirmed that the strengthening by wing walls not only effective for the local strengthening of joints, but also to increase the global seismic performance of the buildings.

7.2 Conclusions

The major conclusions of this research are summarized as follows.

1. The field investigation in West Sumatra, Indonesia, revealed that the deficiencies of seismic detailing, particularly in beam-column joint details exist in current construction practice. The worst detail observed on exterior beam-column joints was straight anchorage of beam reinforcement to the exterior joint. (Chapter 2)
2. The experiments on existing beam-column joints representing Bangladeshi buildings showed that the specimen with deformed bar and straight anchorage at the end, J1, failed

by anchorage failure (pullout of beam longitudinal bars) in the negative loading direction, while joint shear failure was observed in the positive loading direction. The specimen with plain bar and 180° hooks, J2, failed by joint shear in both the positive and negative loading directions. The anchorage failure observed in specimen J1 showed more brittle behavior than the joint shear failure. Therefore, specimen J1 was chosen as the benchmark specimen for strengthening by installing wing walls. (Chapter 3)

3. Pullout test results confirmed that for strengthening design of bonded anchors in low-strength concrete, the minimum anchor embedment length of $10d_a$ is recommended to develop ductile behavior by yielding of the anchor. (Chapter 4)

4. The experiment on a specimen strengthened by installing wing walls, J1-W, confirmed that the failure mode was successfully changed from brittle anchorage failure and joint shear failure to ductile beam yielding. The proposed design concept considering the length of wing walls to extend the development length of beam longitudinal bars was effective to prevent the pullout of beam longitudinal bars from the joint. (Chapter 5)

5. The pushover analysis on an RC building confirmed that the strengthening by wing walls was also effective to increase the global performance of the building, in term of strength and deformation capacity of the building. (Chapter 6)

7.3 Suggestions for Future Research

The following are some suggestions for future research of strengthening of beam-column joint with wing walls.

1. To conduct the field investigation on seismic detailing of beam-column joint in other areas, especially developing countries in high seismic risk area. The investigation is expected to provide more information on the typical details on deficiencies of beam-column joint detail.

2. To evaluate the behavior of exterior beam-column joints with deficient anchorage experimentally considering more variables of embedment length and concrete strength.
3. To develop an analytical model to estimate the failure of beam rebar anchorage with variable anchorage details which is calibrated by the experimental tests.
4. To investigate the applicability of the strengthening by installing wing walls for the anchorage-shear deficient exterior beam-column joints.

References

[1] Architectural Institute of Japan, "Reconnaissance Report on the 2015 Nepal Gorkha Earthquake," 2016.

[2] Y. Li, Y. Sanada, S. Takahashi, K. Maekawa, H. Choi, and K. Matsukawa, "Seismic Performance Evaluation and Strengthening of RC Frames with Substandard Beam-Column Joint: Lessons Learned from the 2013 Bohol Earthquake," *J. Earthq. Tsunami*, vol. 10, no. 03, p. 1640007, 2016.

[3] Earthquake Engineering Research Institute, "Learning from earthquakes the Mw 7.6 Western Sumatra Earthquake of September 30, 2009," 2009.

[4] A. Ghobarah, T. S. Aziz, and A. Biddah, "Seismic rehabilitation of reinforced concrete beam-column connections," *Earthq. Spectra*, vol. 12, no. 4, pp. 761–780, 1996.

[5] C. P. Pantelides, C. Clyde, and L. D. Reaveley, "Rehabilitation of R/C Building Joints With FRP Composites," in *12th World Conference on Earthquake Engineering*, 2000, Paper No. 2306.

[6] A. Ghobarah and A. Said, "Shear Strengthening of Beam-Column Joints," *Eng. Struct.*, vol. 24, pp. 881–888, 2002.

[7] C. P. Antonopoulos and T. C. Triantafillou, "Experimental Investigation of FRP-Strengthened RC Beam-Column Joints," *J. Compos. Constr.*, vol. 7, no. 1, pp. 39–49, 2003.

[8] M. K. Sharbatdar, A. Kheyroddin, and E. Emami, "Cyclic performance of retrofitted reinforced concrete beam-column joints using steel prop," *Constr. Build. Mater.*, vol. 36, pp. 287–294, 2012.

[9] I. S. Misir and S. Kahraman, "Strengthening of non-seismically detailed reinforced concrete beam-column joints using SIFCON blocks," *Sadhana - Acad. Proc. Eng. Sci.*,

vol. 38, no. 1, pp. 69–88, 2013.

[10] Y. Sanada, “Experience on earthquake damage investigation of buildings in foreign country: 2003 Bam-Iran Earthquake, 2005 Kashmir Pakistan Earthquake (in Japanese),” *Bull. Japan Assoc. Earthq. Eng.*, vol. 13, pp. 31–35, 2011.

[11] Y. Li and Y. Sanada, “Seismic strengthening of existing RC beam-column joints by wing walls,” *Earthq. Eng. Struct. Dyn.*, vol. 41, no. 11, pp. 1549–1568, 2017.

[12] A. M. S. Biddah, “Seismic behavior of existing and rehabilitated reinforced concrete frame connections,” McMaster Univ. Hamilton, Ont., Canada, 1997.

[13] A. Ghobarah and T. El-Amoury, “Seismic Rehabilitation of Deficient Exterior Concrete Frame Joints,” *J. Compos. Constr.*, vol. 9, no. 5, pp. 408–416, 2005.

[14] A. Parvin, S. Altay, C. Yalcin, and O. Kaya, “CFRP Rehabilitation of Concrete Frame Joints with Inadequate Shear and Anchorage Details,” *J. Compos. Constr.*, vol. 14, no. 1, pp. 72–82, 2010.

[15] G. I. Kalogeropoulos, A. D. G. Tsonos, D. Konstandinidis, and S. Tsetines, “Pre-earthquake and post-earthquake retrofitting of poorly detailed exterior RC beam-to-column joints,” *Eng. Struct.*, vol. 109, pp. 1–15, 2016.

[16] National Standardization Agency of Indonesia, “Requirements for Structural Concrete for Buildings, SNI 2847:2013,” 2013.

[17] American Concrete Institute (ACI), “Building code requirements for structural concrete (ACI 318M-11),” 2011.

[18] “West Sumatra Province,” *Maps Online ANU College of Asia & the Pacific*. [Online]. Available: http://asiapacific.anu.edu.au/mapsonline/base-maps/west-sumatra-province.

[19] National Standardization Agency of Indonesia, “Design Procedure of Earthquake Resistance for Buildings and Other Structures, SNI 1726:2012, 2012,” 2012.

[20] Housing and Building Research Institute, “Bangladesh National Building Code (BNBC)

2015 Final Draft," 2015.

[21] K. Esaki, S. Kim, T. Suzuki, S. Takahashi, and Y. Sanada, "Compressive Test on Concrete Considering of Brick Chip as Coarse Aggregate," in *Proceedings of Tokai Chapter Architectural Research Meeting*, 2018, pp. 49–52.

[22] JBDPA (The Japan Building Disaster Prevention Association), "Standard for Seismic Evaluation of Existing Reinforced Concrete Buildings, 2001, Guidelines for Seismic Retrofit of Existing Reinforced Concrete Buildings, 2001 and Technical Manual for Seismic Evaluation and Seismic Retrofit of Existing Reinforced Concrete," 2005.

[23] Architectural Institute of Japan (AIJ), "Design guideline for earthquake resistant reinforced concrete buildings based on inelastic displacement concept," 1997.

[24] T. Akiyama, Y. Yamamoto, S. Ichihashi, and K. Ariki, "Experimental Study on Performance of Bonded Anchors in the Low Strength Reinforced Concrete," in *Proceedings of 13th World Conference on Earthquake Engineering*, 2004, no. 748.

[25] T. Gurbuz and A. Ilki, "Pullout performance of fully and partially bonded retrofit anchors in low-strength concrete," *ACI Struct. J.*, vol. 108, no. 1, pp. 61–70, 2011.

[26] S. Yilmaz, M. A. Özen, and Y. Yardim, "Tensile behavior of post-installed chemical anchors embedded to low strength concrete," *Constr. Build. Mater.*, vol. 47, no. January 2018, pp. 861–866, 2013.

[27] Architectural Institute of Japan (AIJ), "AIJ Standard for Structural Calculation of Reinforced Concrete Structures revised 2018 (in Japanese)," 2018.

[28] Architectural Institute of Japan (AIJ), "Design Guidelines for Earthquake Resistant Reinforced Concrete Buildings Based on Ultimate Strength Concept (in Japanese)," 1990.

[29] T. Ichinose, "A shear design equation for ductile R/C members," *Earthq. Eng. Struct. Dyn.*, vol. 21, no. 3, pp. 197–214, 1992.

[30] American Society of Civil Engineers (ASCE), “Minimum Design Loads for Buildings and Other Structures (ASCE/SEI 7-10),” 2010.

Appendix A

Results of Field Investigation in West Sumatra Indonesia

This appendix described the investigation results on items which are not explained in **Chapter 2**. The investigation results on detailing of column and beam are described in this section.

A.1. Detailing of Column

A.1.1. Dimensions of Column

The Indonesian code [16] regulates that the shortest cross-sectional dimensions of column shall be not less than 300 mm. Approximately 80% of the investigated buildings in all five cities satisfied this requirement, as shown in **Figure A.1(a)**. The code also regulates that ratio of the shortest cross-sectional dimension (b) to perpendicular dimension (h) shall be not less than 0.4. Most of the investigated buildings in all five cities satisfied this requirement, as shown in **Figure A.1(b)**.

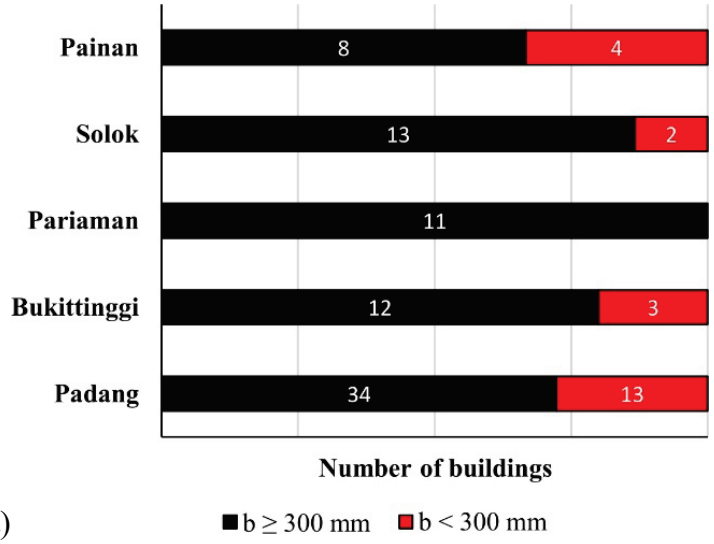

(a)

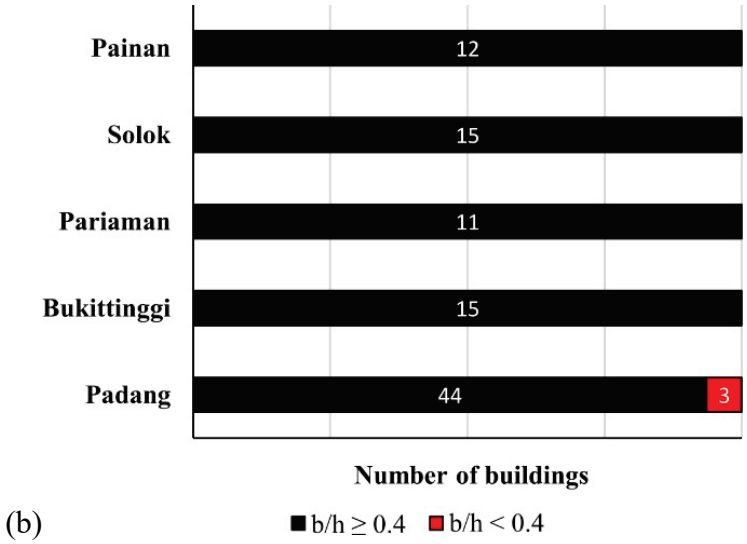

Figure A.1 Field investigation results on cross-sectional dimensions of column; (a) Minimum cross-sectional dimension; (b) Ratio of cross-sectional dimensions

A.1.2. Longitudinal Reinforcement in Column

The Indonesian code [16] regulates that the volumetric ratio of longitudinal reinforcement (ρ) shall not be less than 0.01 and shall not exceed 0.06. The minimum ratio of longitudinal reinforcement is to have the yield moment exceeding the cracking moment. The investigation results in **Figure A.2** show that more than 80% of the investigated buildings in all five cities satisfied this requirement.

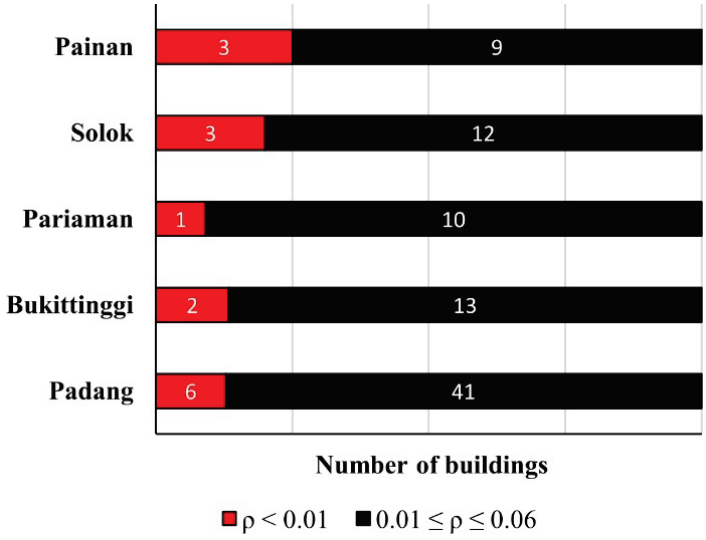

Figure A.2 Field investigation results on ratio of flexural reinforcement in column

A.1.3. Transverse Reinforcement in Column

Requirement of transverse reinforcement in column is intended not only for shear resistant, but also for confinement of the concrete. Based on the Indonesian code [16], the area of transverse reinforcement (A_v) in the potential plastic hinge region shall not be less than values of A_{sh} given by the following two equations:

$$A_{sh} = 0.3\ (s\ b_c\ fc'\ /\ f_{yt})\ [(A_g\ /\ A_{ch})-1] \quad \text{(A-1)}$$

$$A_{sh} = 0.09\ (s\ b_c\ fc'\ /\ f_{yt}) \quad \text{(A-2)}$$

where A_{sh} is the total cross-sectional area of hoops in each cross-sectional direction; s is the spacing of transverse reinforcement; b_c is the core width of column measured between outside edges of the transverse reinforcement in the direction concerned; f_{yt} is the yield stress of transverse reinforcement; A_g is the gross area of concrete section; A_{ch} is the cross-sectional area of a structural member measured to the outside edges of transverse reinforcement. **Figure A.3** shows that most of the investigated buildings in all five cities did not satisfy the requirement for the area of transverse reinforcement in column. Many of them lacked inner hoops (cross-ties) for confinement of column.

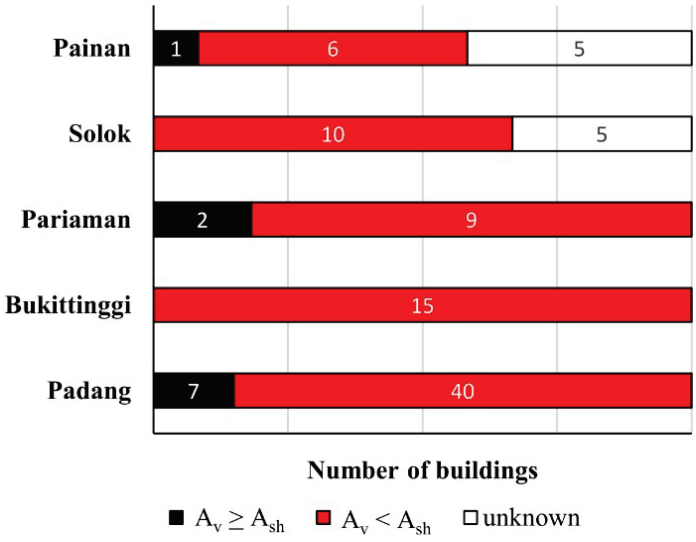

Figure A.3 Field investigation results on area of transverse reinforcement in column

Figure A.4 describes the requirements for the maximum spacing of transverse reinforcement in accordance with the Indonesian code [16]. The field investigation results in **Figures A.5(a)** and **A.5(b)** show that more than half of the investigated buildings in Padang and all buildings in other four cities did not satisfy the requirements for spacing of hoops in hinge region (s*) and non-hinge region (s**), respectively.

In the rebar works observed in the workshops with local workers, most of the workers did rough measurement for spacing of transverse reinforcement which leads to wider spacing than those on design drawing (s), as shown in the workshop results in **Figure A.6**

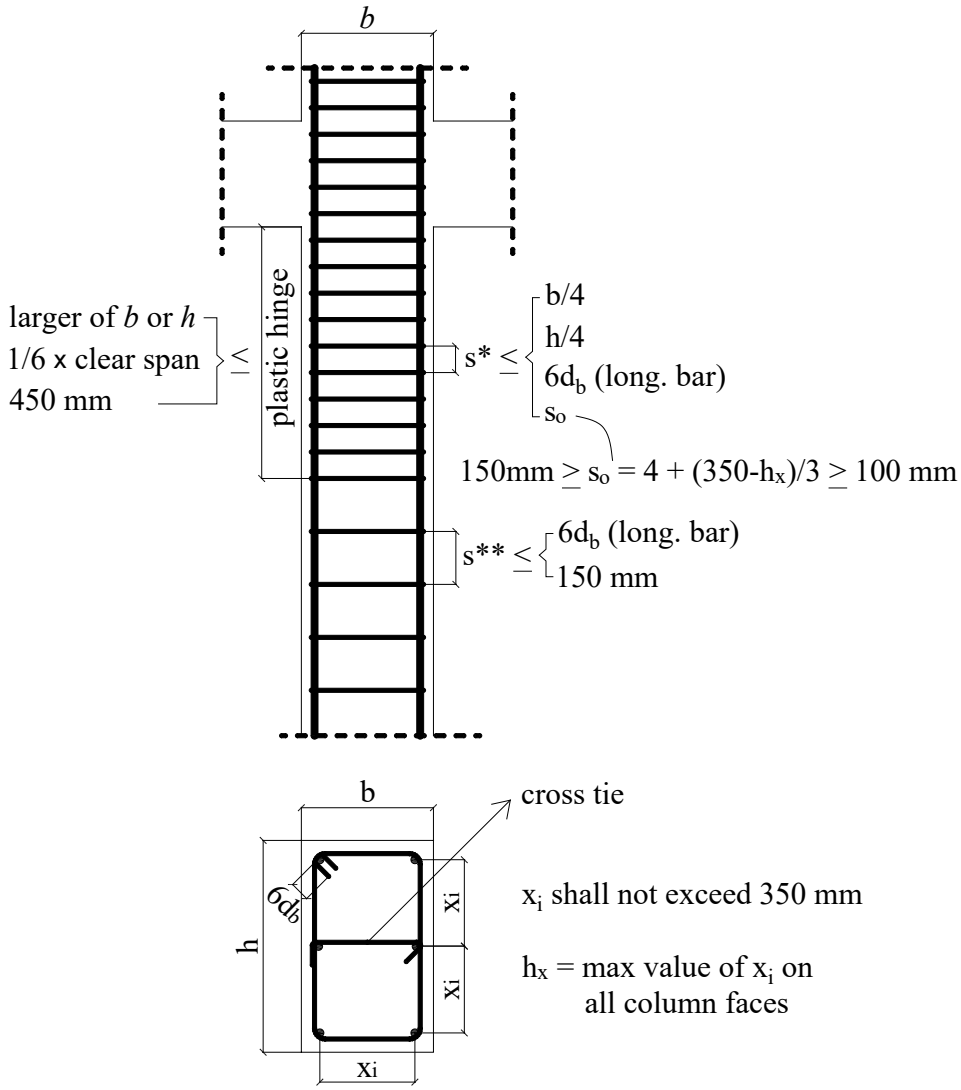

Figure A.4 Requirements for transverse reinforcement of column

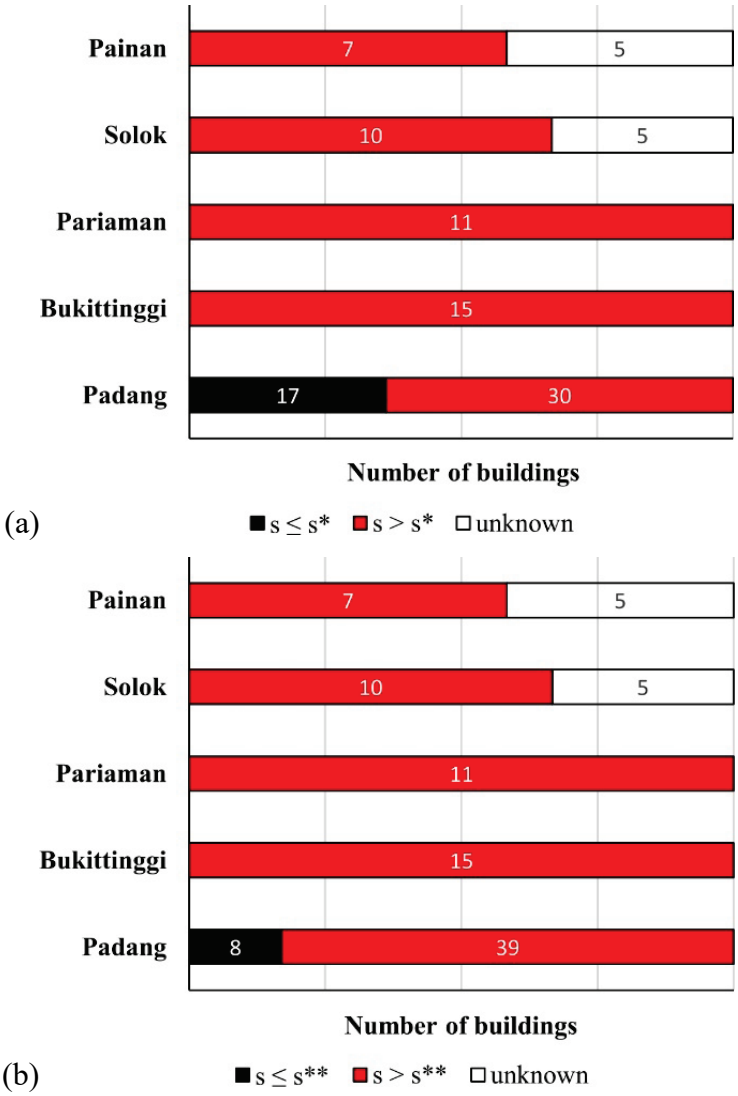

Figure A.5 Field investigation results on spacing of transverse reinforcement in column; (a) Hinge region; (b) Non-hinge region

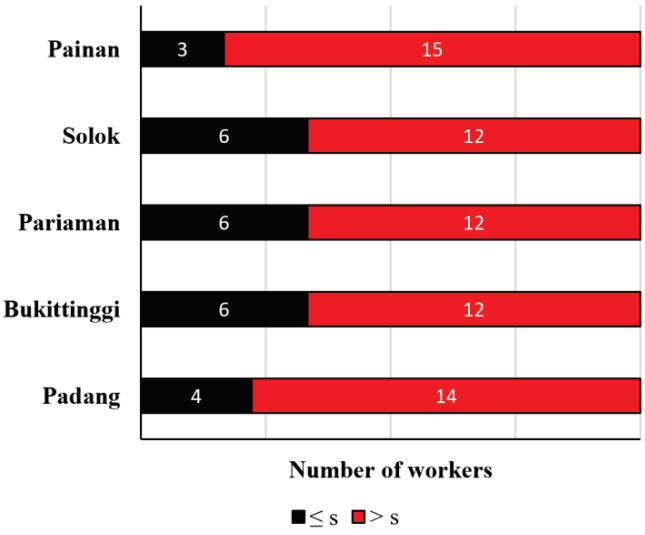

Figure A.6 Workshop results on spacing of transverse reinforcement in column

Seismic hooks with 135° or more and the length not less than $6d_b$ (diameter of transverse bar) shall be applied to column stirrups, as regulated in the Indonesian code [16]. However, the field investigation results showed that many of the investigated buildings were applied 90° hooks for column stirrups and the length of hooks less than $6d_b$, as shown in **Figure A.7(a)** and **Figure A.7(b)**, respectively.

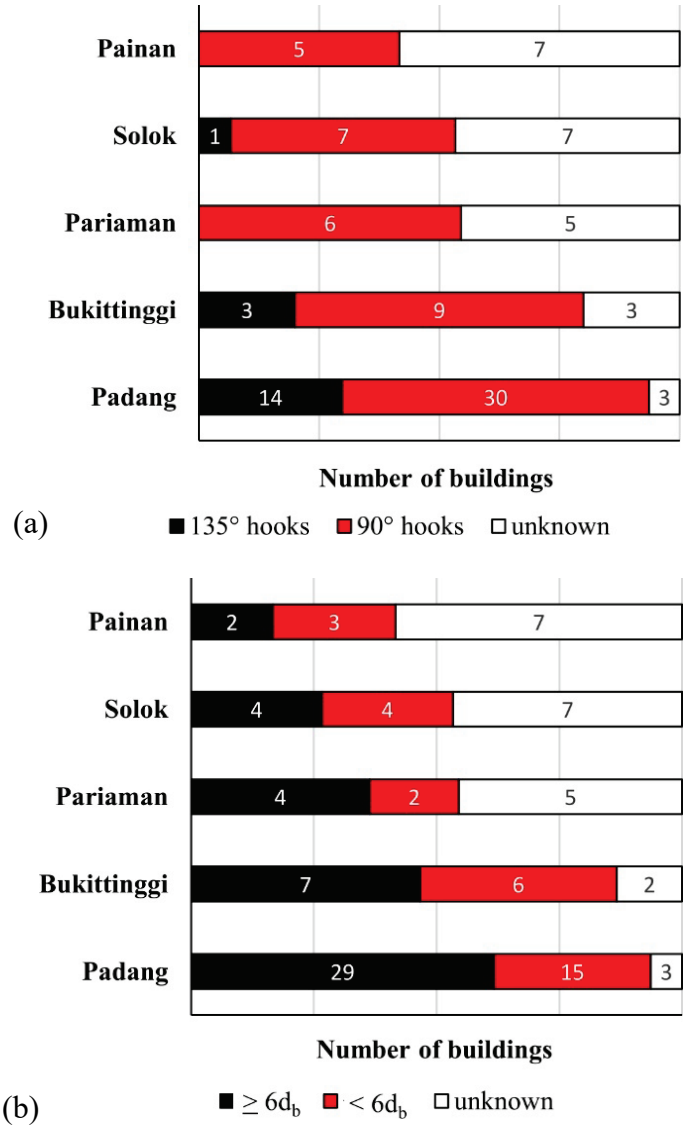

(a)

(b)

Figure A.7 Investigation results on details of seismic hooks of column stirrups; (a) Angle of hooks; (b) Length of hooks

Evaluation of the rebar works in the workshops with local workers also showed that most of the workers made the 90° hooks with the length less than $6d_b$, as shown in **Figure**

A.8(a) and **Figure A.8(b)**, respectively. These results indicated that the poor details of hooks in real construction were likely to result from poor quality of rebar works by the workers.

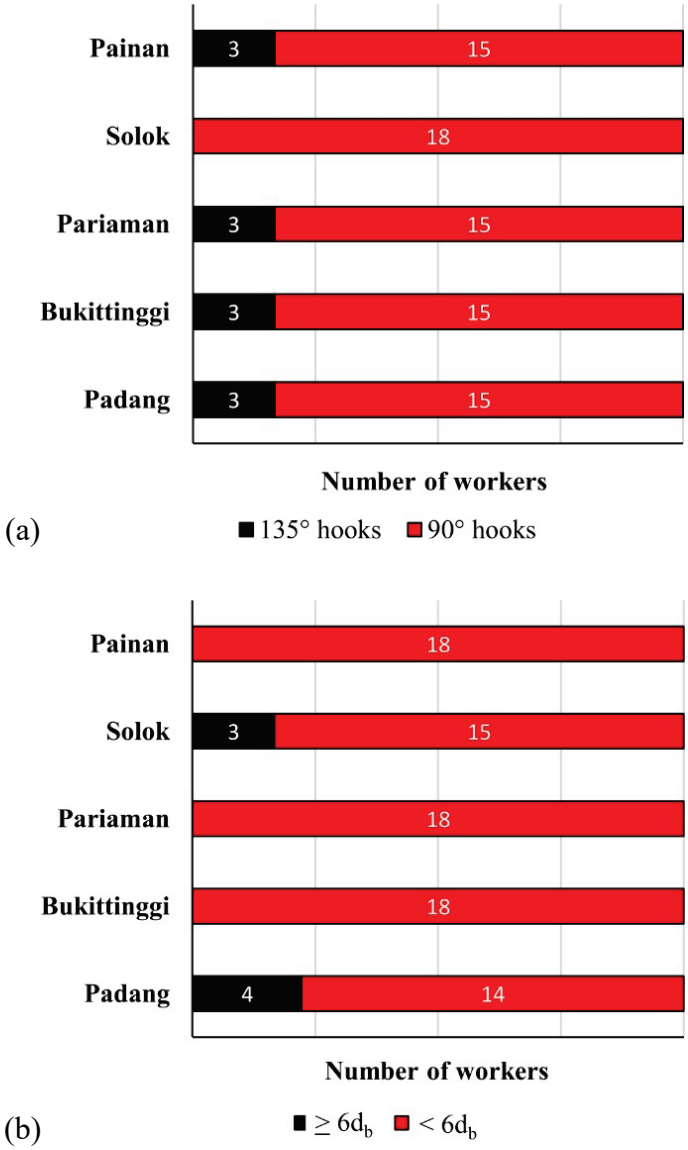

Figure A.8 Workshop results on details of seismic hooks of column stirrups; (a) Angle of hooks; (b) Length of hooks

A.1.4. Lap Splice in Column

The lap splice shall not be applied in area within joint or within a distance of twice member depth from the face of joint (hinge area), as regulated in the Indonesian code [16]. However, most of the investigated buildings in Padang city and all buildings in the other four cities were applied the lap splice in hinge area, as shown in **Figure A.9(a)**. Based on interview in the workshops with local workers, all the workers from five cities informed that lap splice in column was usually located immediately above the floor level (hinge area) for easy work. This construction method has been a "common mistake".

The lap splice of column shall be designed as a tension splice and the length of lap splice (l_d) should not be less than:

$$l_d = \frac{f_y \psi_t \psi_e d_b}{1.7\lambda\sqrt{f_c'}} \quad \text{for } d_b \geq 22 \text{ mm} \qquad \text{(A-3)}$$

$$l_d = \frac{f_y \psi_t \psi_e d_b}{2.1\lambda\sqrt{f_c'}} \quad \text{for } d_b < 22 \text{ mm} \qquad \text{(A-4)}$$

where f_y is yield stress of longitudinal reinforcement, ψ_t is a rebar location factor that accounts for the position of rebar in freshly placed concrete (where horizontal reinforcement is placed such that more than 300 mm height of fresh concrete is cast below the development length, use $\psi_t = 1.3$; for other reinforcement, use $\psi_t = 1.0$), in this study, $\psi_t = 1.0$ is used for all longitudinal bars, $\psi_e = 1.0$ for uncoated reinforcement, $\lambda = 1.0$ for normal-weight concrete, and d_b is diameter of longitudinal reinforcement.

The field investigation results in **Figure A.9(b)** shows that more than half of the buildings in all cities where the data could be obtained were applied less length of splice than the requirement. Based on interview in the workshops with local workers, all the workers responded that the length of lap splice was determined based on their experience with the splice length between 500 mm to 1000 mm, which often to be smaller length than **Equation (A-3)** or **(A-4)**.

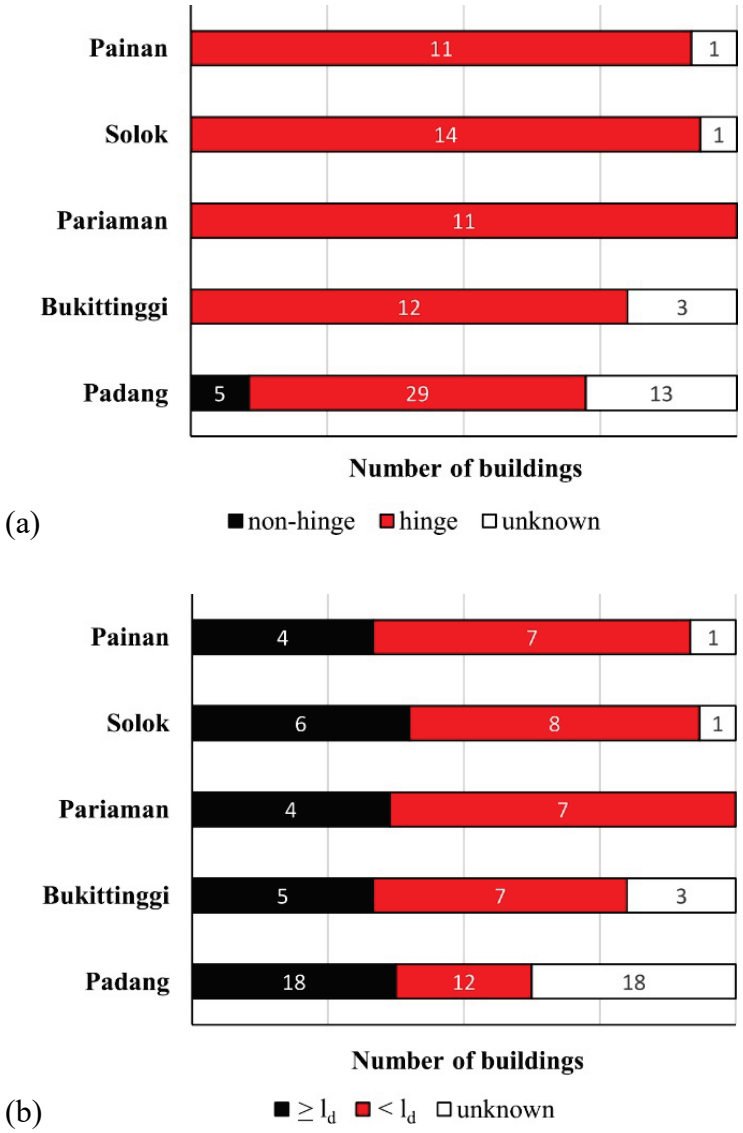

Figure A.9 Field Investigation results on lap splice in column; (a) Location of splice; (b) Length of splice

A.2 Detailing of Beam

A.2.1. Dimensions of Beam

Beam must be sufficient to provide efficient moment transfer to supporting columns. The Indonesian code [16] regulates that the width of beam shall be > 250 mm and ratio of width (b) to depth (h) shall be > 0.3. The field investigation results showed that approximately 80% of the observed beam dimensions satisfied the requirement on the minimum width of beam, as shown in **Figure A.10(a)**. The requirement on the ratio of width to depth was satisfied in almost all of the observed beams, as shown in **Figure A.10(b)**.

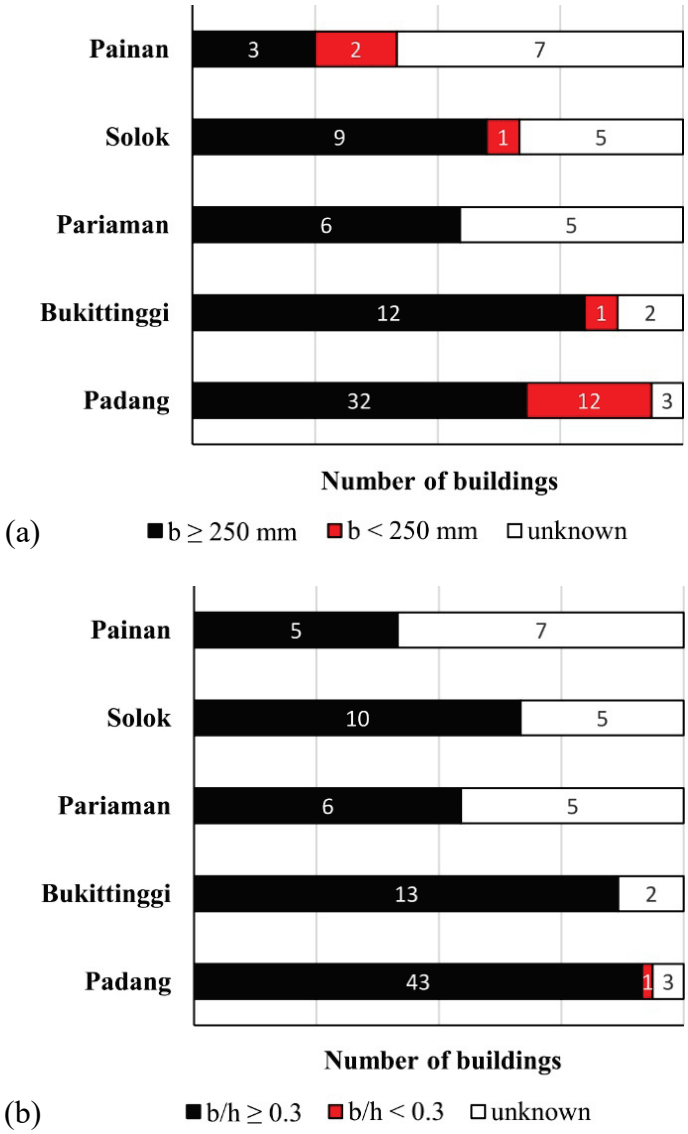

Figure A.10 Field investigation results on cross-sectional dimensions of beam; (a) Minimum width; (b) Ratio of width to depth

A.2.2. Longitudinal Reinforcement in Beam

Referring to the Indonesian code [16], the minimum ratio (ρ_{min}) of tensile or compressive reinforcement in beam shall not be less than the maximum value obtained by **Equation (A-5)** and **(A-6)**, and the reinforcement ratio (ρ) shall not exceed 0.025. The field investigation results in **Figure A.11** show that in more than half of the observed beams, the ratio of longitudinal reinforcement satisfied this requirement, except for Solok city and Painan city.

$$\rho_{min} = \frac{1.4\, b\, d}{f_y} \quad \text{(A–5)}$$

$$\rho_{min} = \frac{0.25\sqrt{f_c'}}{f_y} b\, d \quad \text{(A–6)}$$

where d is the effective depth of beam.

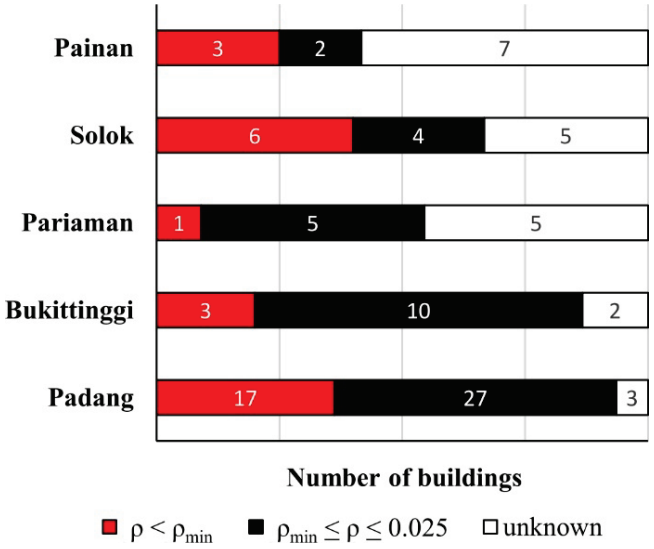

Figure A.11 Field investigation results on ratio of longitudinal reinforcement in beam.

A.2.3. Transverse Reinforcement in Beam

Adequate confinement is required to ensure sufficient ductility of the beam under seismic load. The maximum spacing of transverse reinforcement in beam based on the Indonesian code [16] is described in **Figure A.12**.

The field investigation results in **Figure A.13(a)** shows that more than half of the investigated buildings in Padang and most of the buildings in the other four cities did not satisfy the requirement for spacing of transverse reinforcement in hinge region. The situation was relatively better in non-hinge region, as shown in **Figure A.13(b)**, because several buildings were applied uniform spacing throughout the length of beam. The observation of the rebar works in the workshops with local workers showed that most of the workers did rough measurement for spacing of transverse reinforcement which leads to wider spacing than those on design drawing, as shown in the workshop results in **Figure A.14**

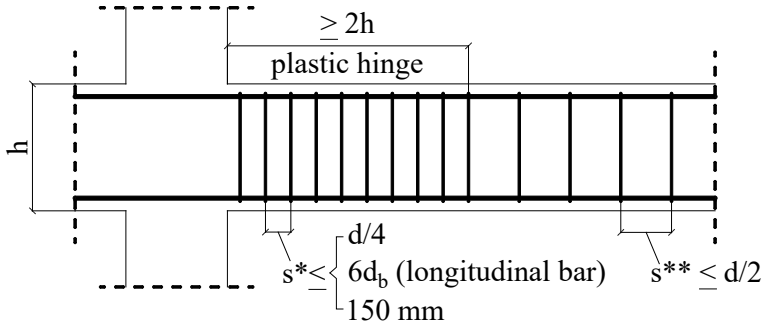

Figure A.12 Requirements for spacing of transverse reinforcement in beam

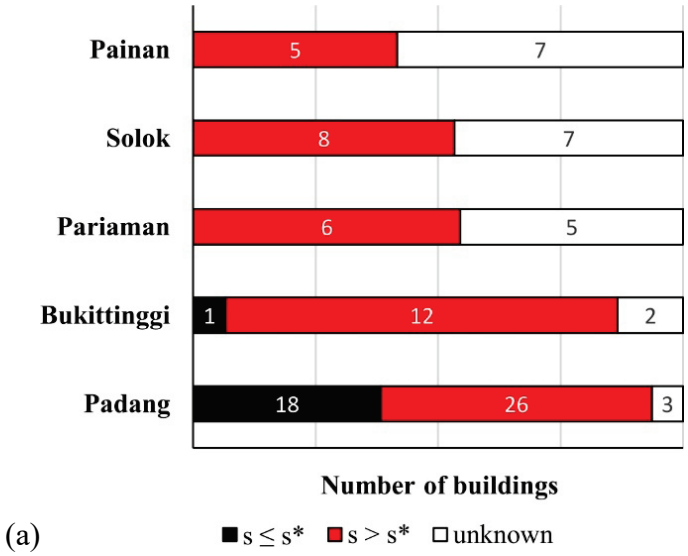

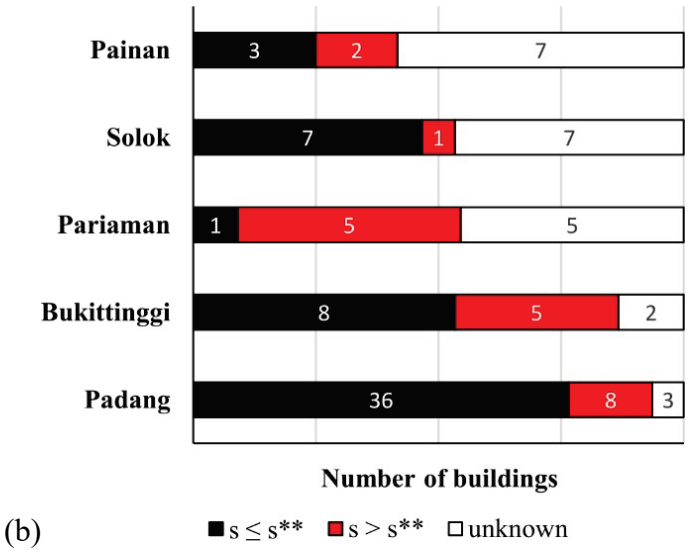

Figure A.13 Field investigation results on spacing of transverse reinforcement in beam; (a) Hinge region; (b) Non-hinge region

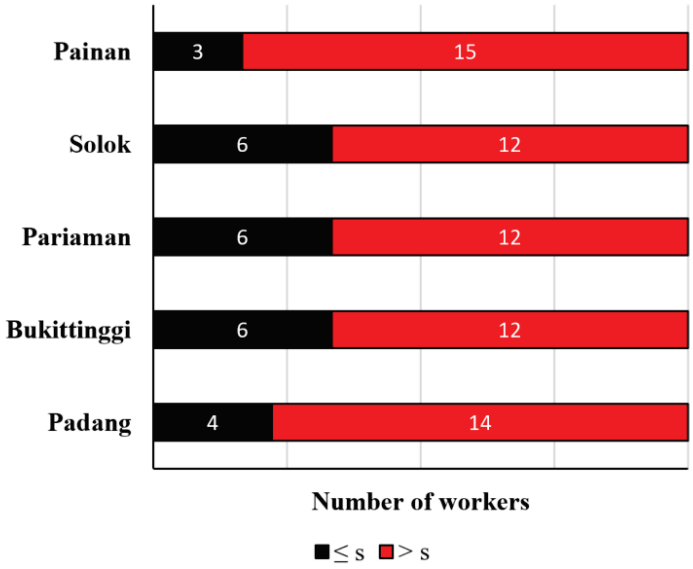

Figure A.14 Workshop results on spacing of transverse reinforcement in beam

Seismic hooks with 135° or more and the length not less than $6d_b$ (diameter of transverse bar) should also be applied to beam stirrups. However, the field investigation results showed that approximately 80% of the observed beams were applied 90° hooks for the stirrups, as shown in **Figure A.15(a)**. Beam stirrups with the length of the hooks less than $6d_b$ were also observed in many buildings, as shown in **Figure A.15(b)**.

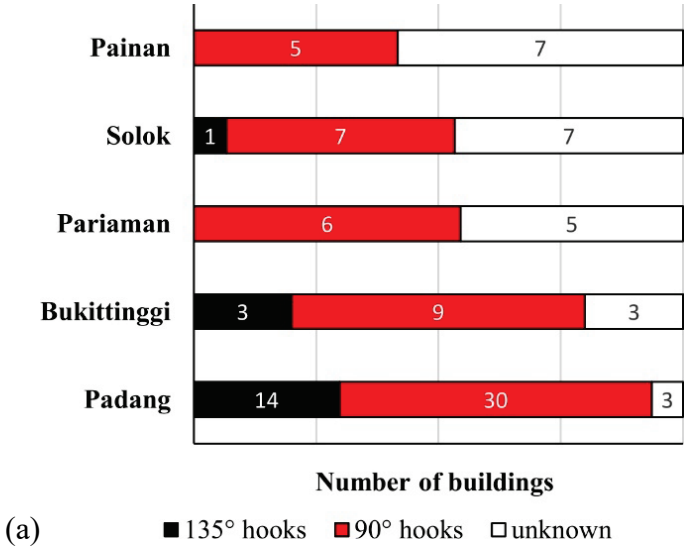

(a)

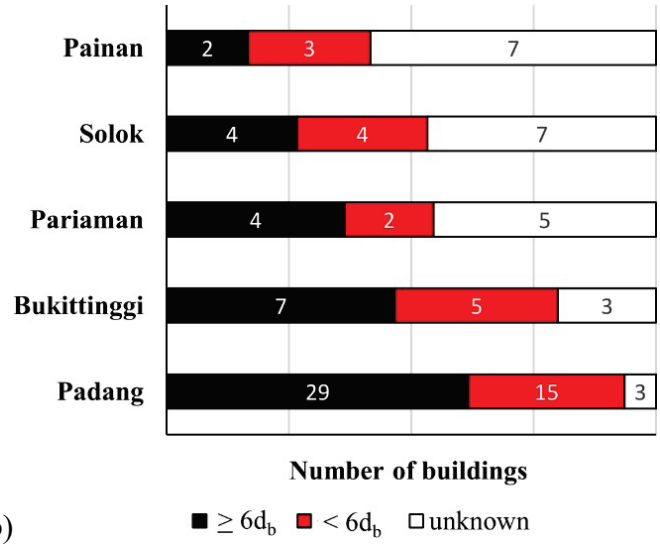

Figure A.15 Field investigation results on details of seismic hooks of beam stirrups: (a) Angle of hooks; (b) Length of hooks

The observation of the rebar works in the workshops with local workers also showed that most of the workers made the 90º hooks with the length less than $6d_b$ for beam stirrups, as shown in **Figures A.16(a)** and **A.16(b)**, respectively. This tendency was similar to the results on column shown in **Figure (a)** and **Figure A.8(b)**.

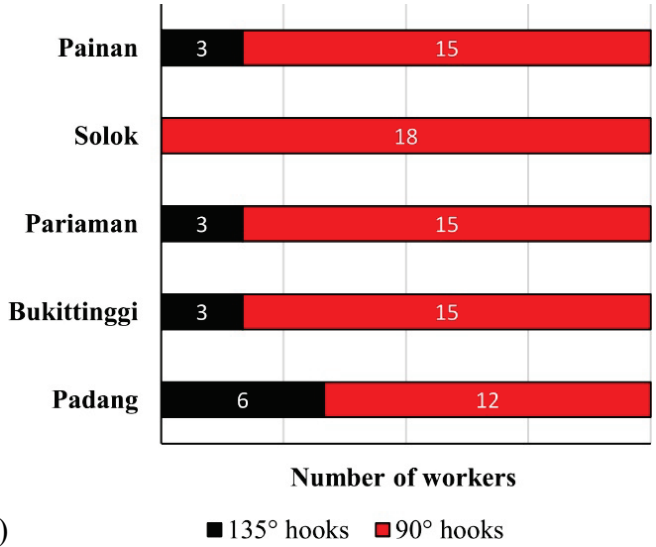

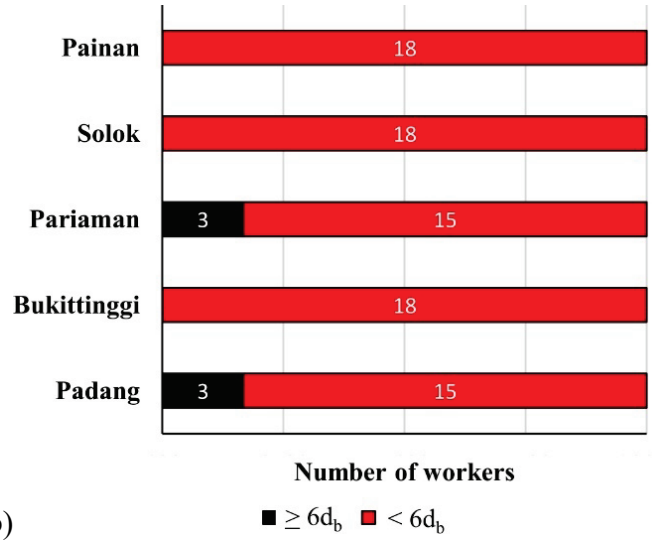

(b)

Figure A.16 Workshop results on details of seismic hooks of beam stirrups: (a) Angle of hooks; (b) Length of hooks

A.2.4. Lap Splice in Beam

The provisions for lap splices in beam are similar to those on column as explained in Section A.1.4. Lap splice of reinforcement is prohibited at hinge area because it is not reliable under seismic load. However, many of the investigated buildings in all five cities were applied lap splice in hinge area, as shown in **Figure A.17(a)**. Based on interview in the workshops with local workers, all the workers from five cities answered that lap splice in beam was usually determined based on the length of available rebar without considering the location.

The field investigation results in **Figure A.17(b)** shows more than half of the buildings in Padang city/other four cities where the data on length of splice could be obtained satisfied/disturbed the requirement. Based on interview in the workshops with local workers, all the workers determined the length of lap splice based on their experience with the splice length between 500 mm to 1000 mm, similarly to the column rebar works as mentioned in Section A.1.4.

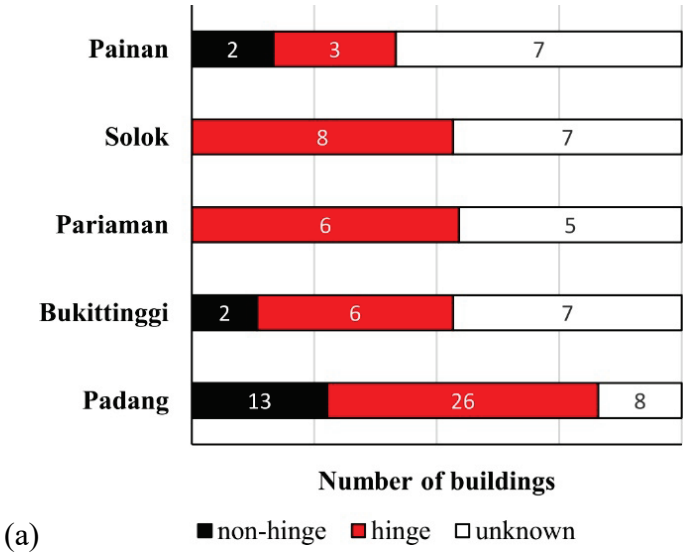

(a)

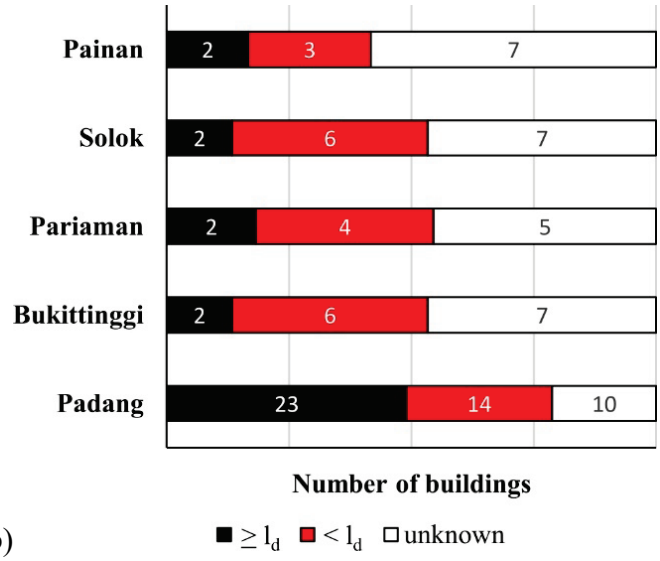

(b)

Figure A.17 Field investigation results on lap splice in beam; (a) Location of splice; (b) Length of splice

A.3 Summary

From the field investigation, common deficiencies of seismic detailing of column and beam found on the investigated buildings were as follows:

1. Poor details of transverse reinforcement: lack of hoops for confinement of column, large spacing of transverse reinforcement and transverse reinforcement with a 90^{o} hook in column and beam.

2. Improper splicing of longitudinal reinforcement of column and beam: lap splice in hinge region with insufficient lap splice.

The results of the workshops with local construction workers showed that the mistakes by the local workers in the rebar works were almost similar to the deficiencies found in the field investigation. These indicated that lack of knowledge and skill by the workers lead such deficiencies.

Appendix B
Crack Pattern of the Beam-Column Joint Specimens

The propagation of cracks of each specimen was marked and the crack widths were measured using crack scales at each peak loading and unloading of the loading program. This section shows the figures of crack patterns of the specimens at peak loading. In figures, the solid lines represent the cracks that appeared during the positive loading direction and the dotted lines represent the cracks that appeared during the negative loading direction.

B.1. Crack Pattern of Specimen J1

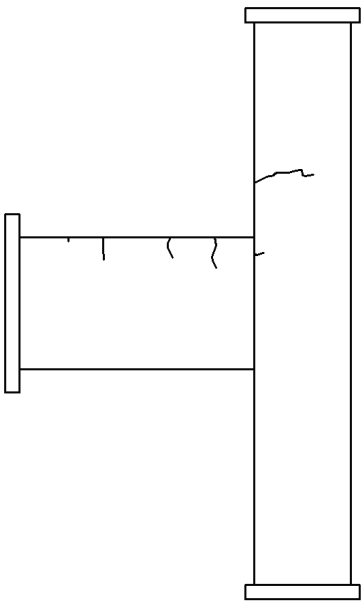

R = 0.25% rad

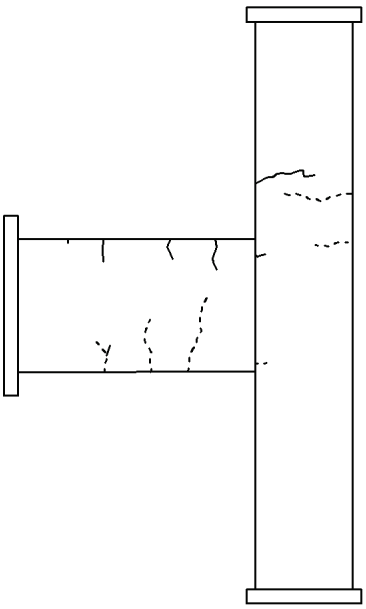

R = -0.25% rad

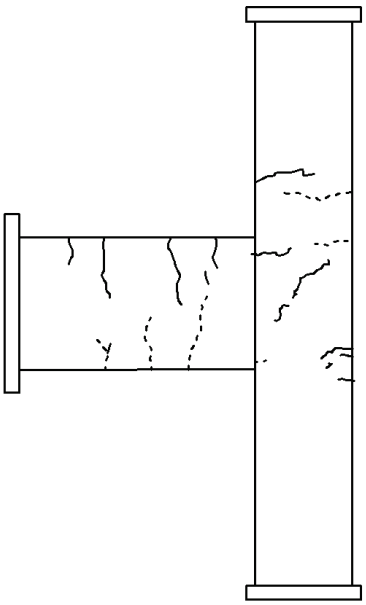

R = 0.50% rad

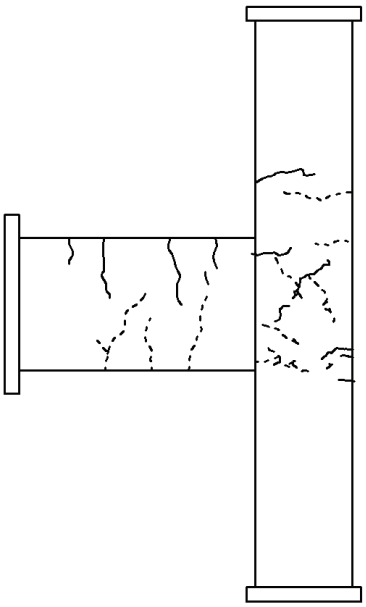

R = -0.50% rad

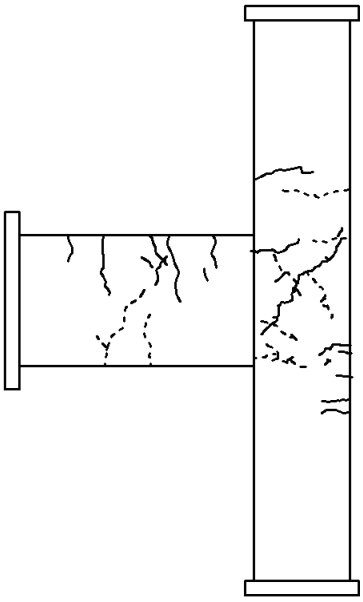

R = 0.75% rad

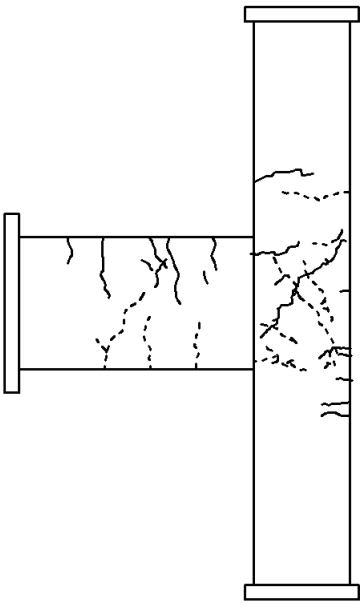

R = -0.75% rad

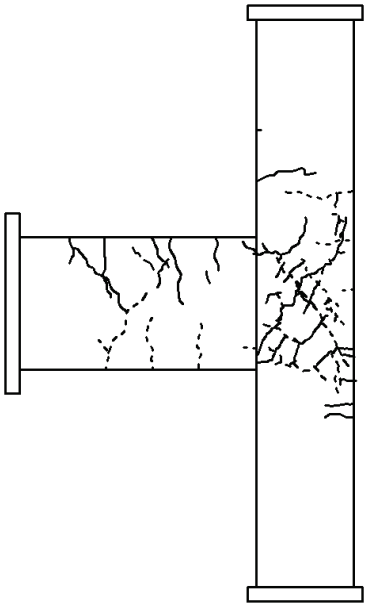

R = 1.00% rad

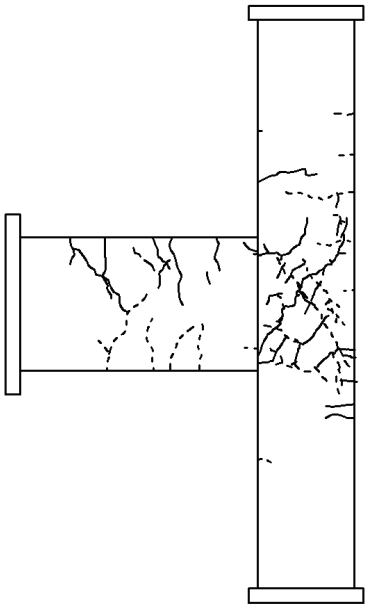

R = -1.00% rad

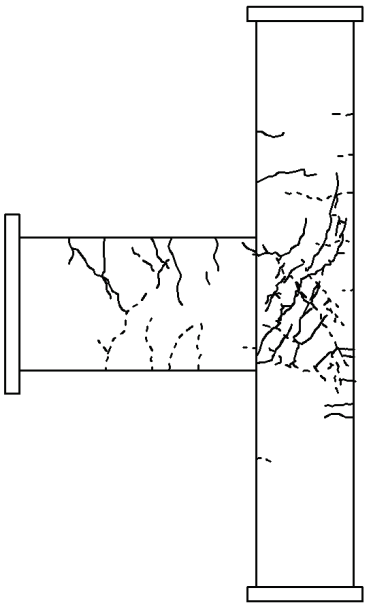

R = 1.50% rad

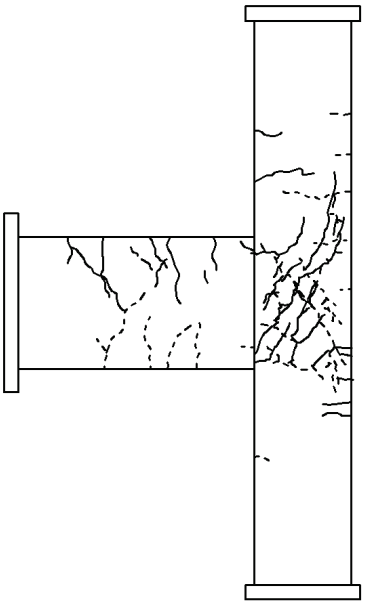

R = -1.50% rad

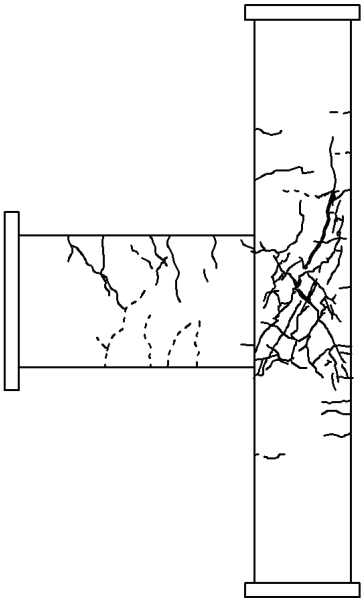

R = 2.00% rad

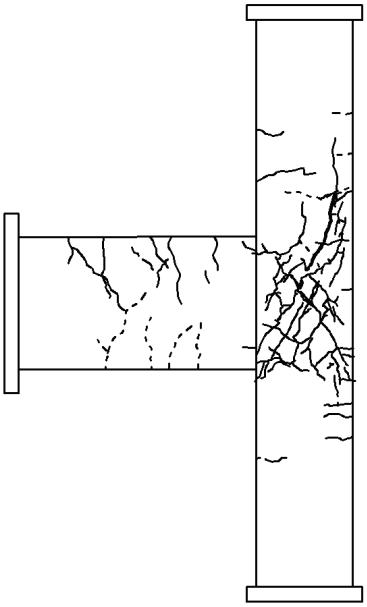

R = -2.00% rad

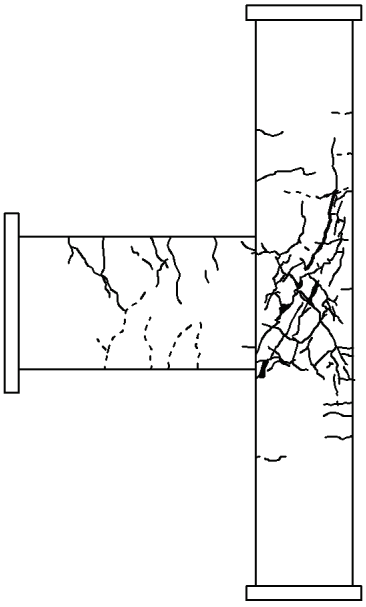

R = 3.00% rad

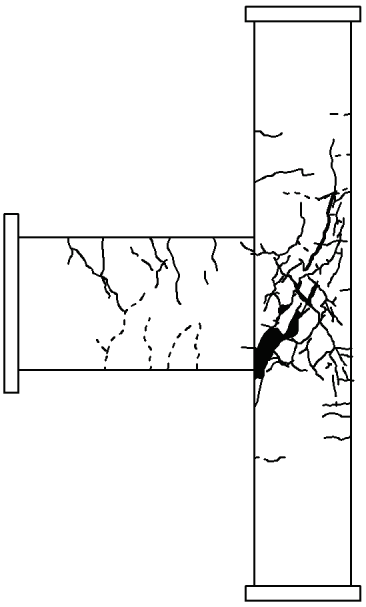

R = -3.00% rad

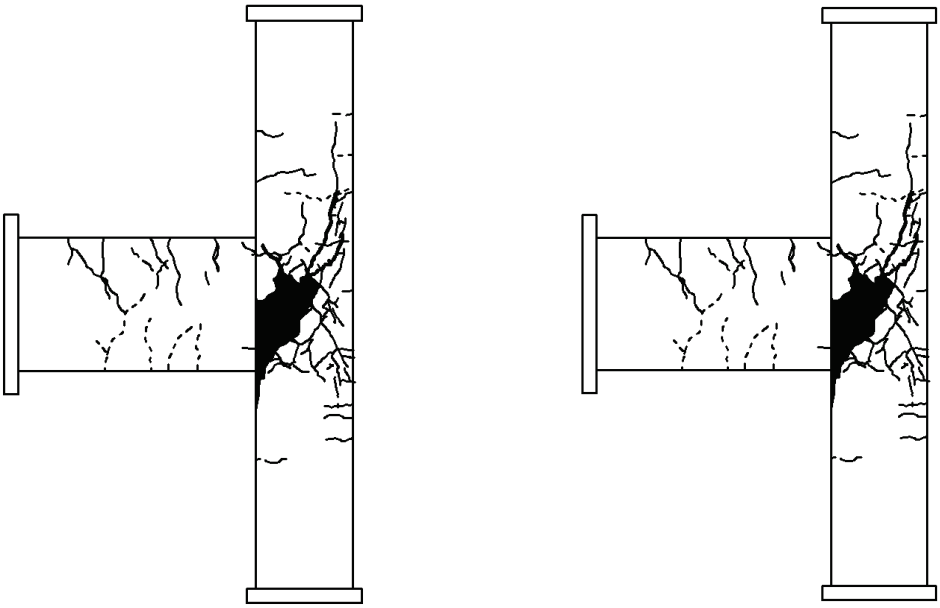

R = 4.00% rad

R = -4.00% rad

Final crack pattern

Figure B.1 Crack pattern of specimen J1

B.2. Crack Pattern of Specimen J2

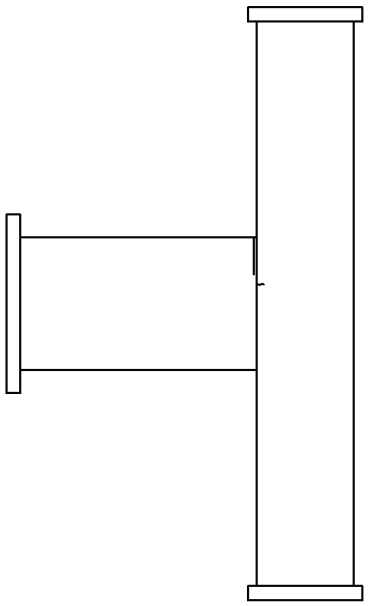

R = 0.25% rad

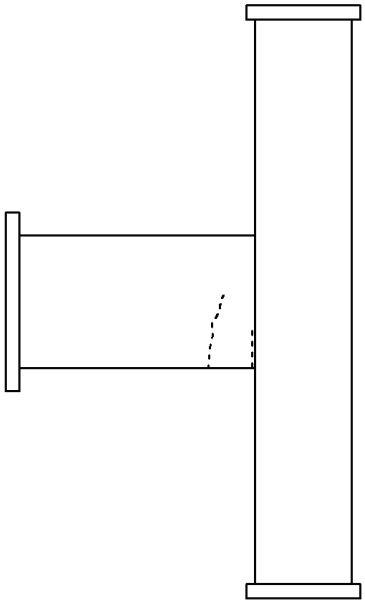

R = -0.25% rad

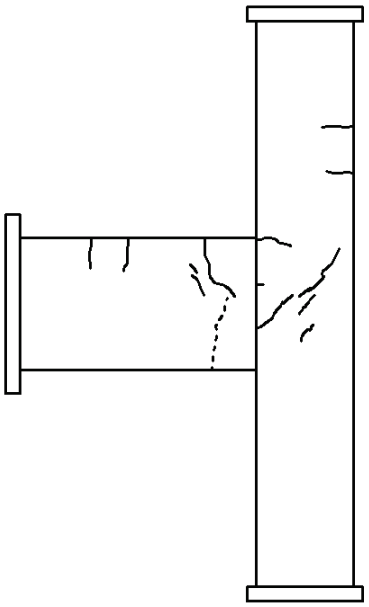

R = 0.50% rad

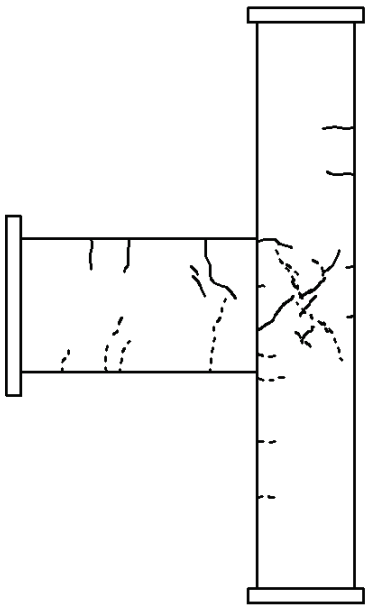

R = -0.50% rad

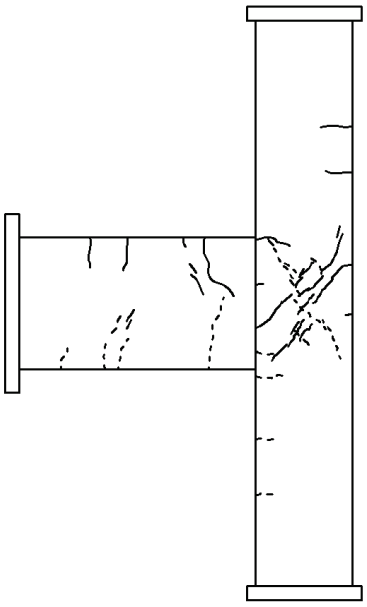

R = 0.75% rad

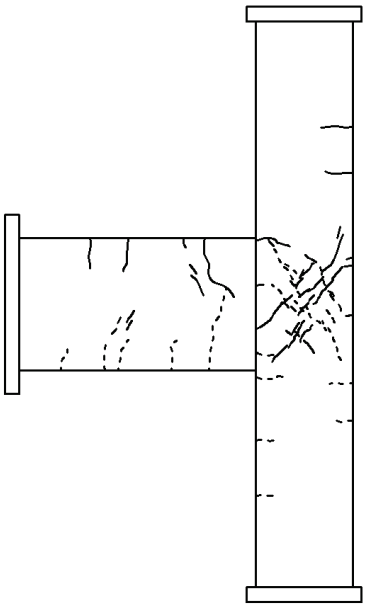

R = -0.75% rad

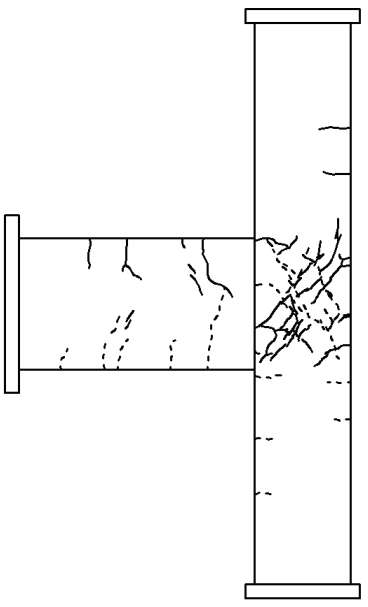

R = 1.00% rad

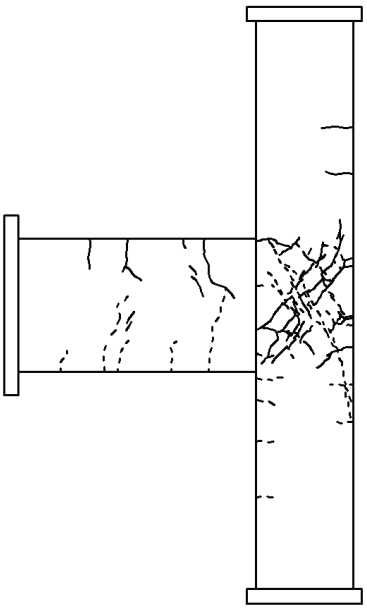

R = -1.00% rad

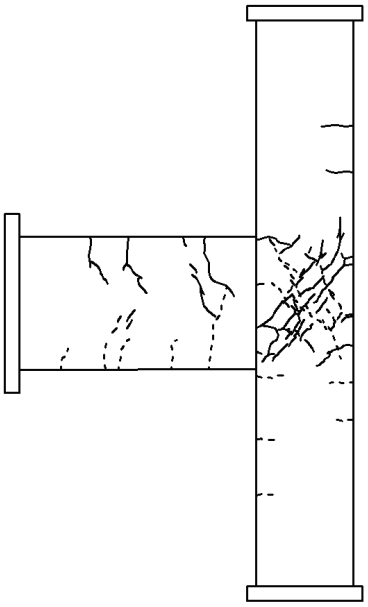

R = 1.50% rad

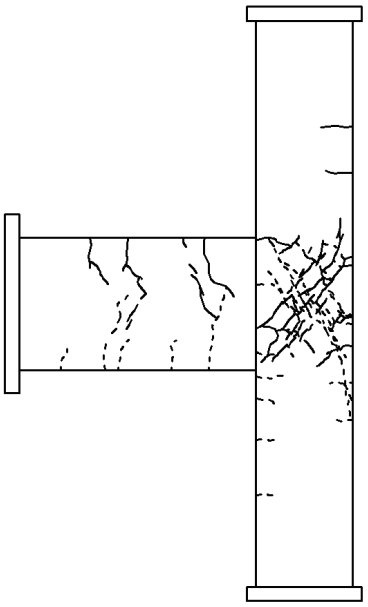

R = -1.50% rad

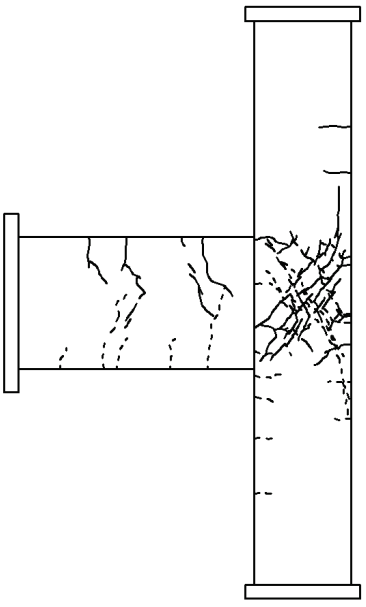

R = 2.00% rad

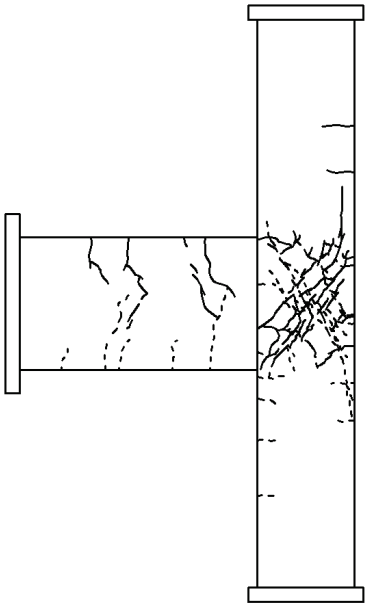

R = -2.00% rad

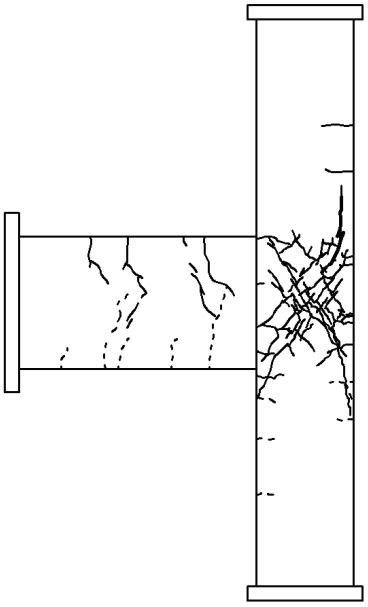

R = 3.00% rad

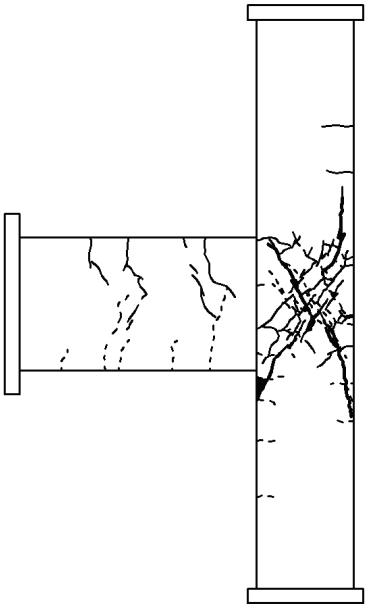

R = -3.00% rad

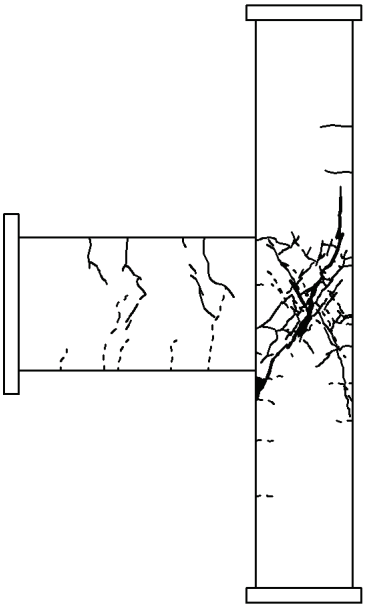

R = 4.00% rad

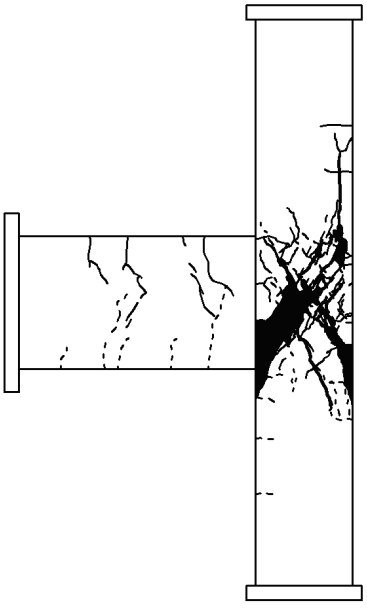

R = -4.00% rad

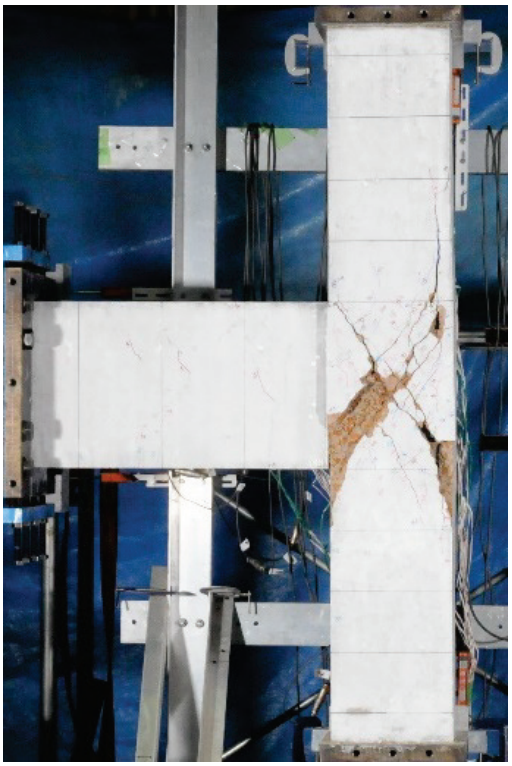

Final crack pattern

Figure B.2 Crack pattern of specimen J2

B.3. Crack Pattern of Specimen J1-W

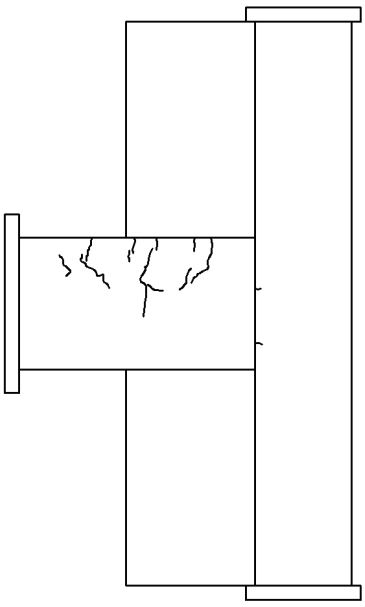

R = 0.25% rad

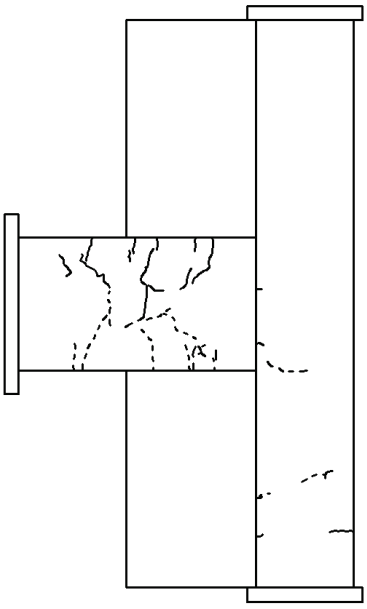

R = -0.25% rad

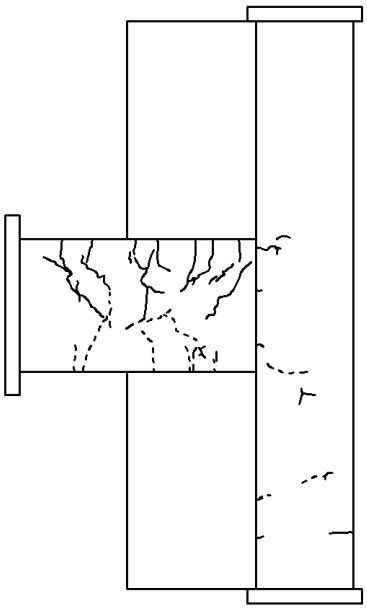

R = 0.50% rad

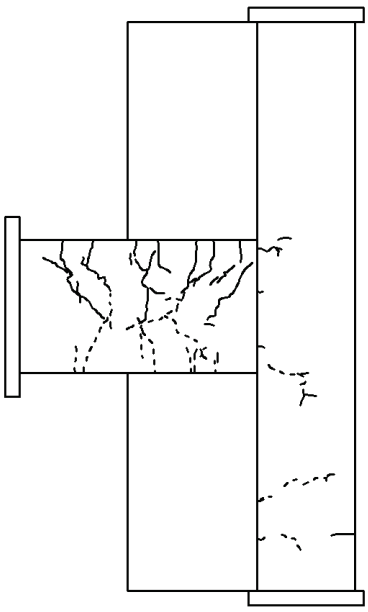

R = -0.50% rad

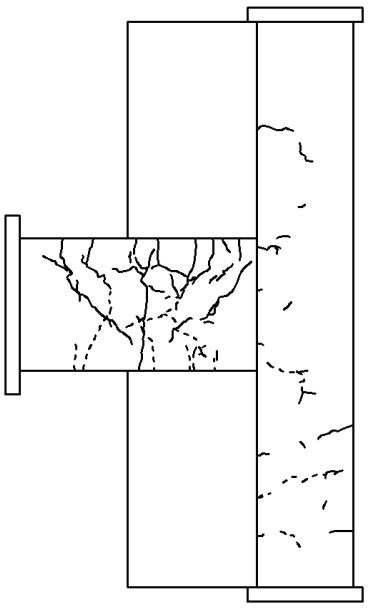

R = 0.75% rad

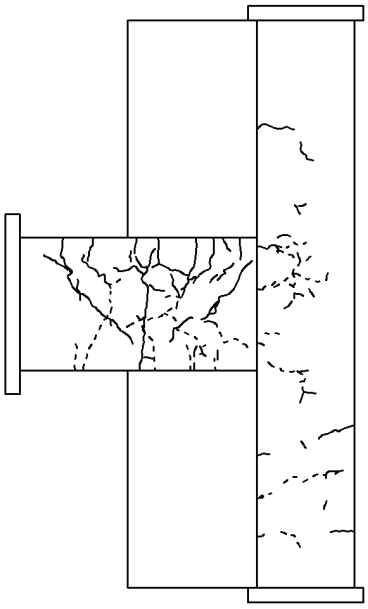

R = -0.75% rad

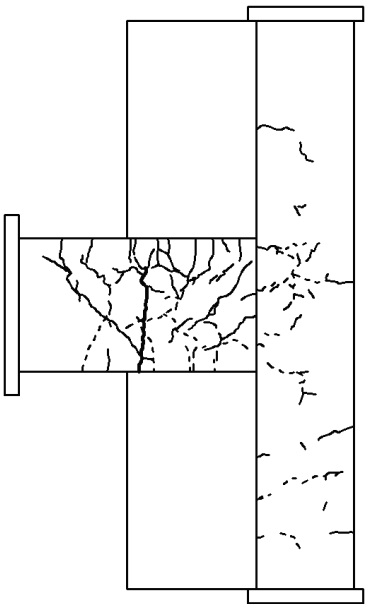

R = 1.00% rad

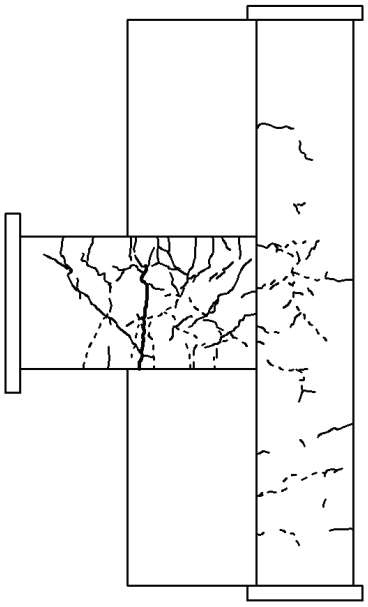

R = -1.00% rad

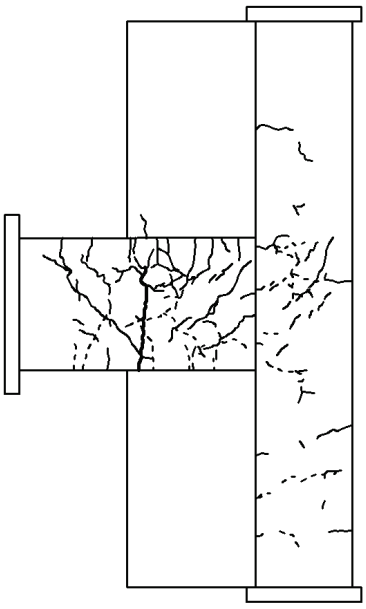

R = 1.50% rad

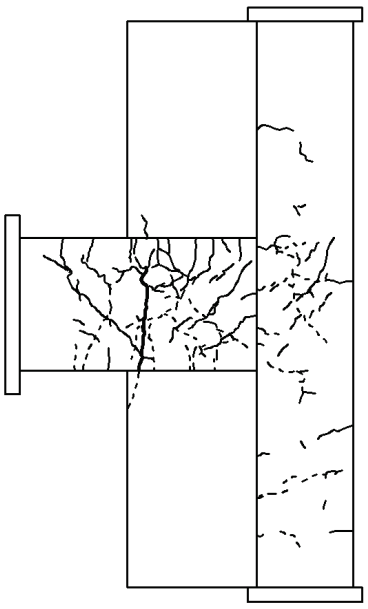

R = -1.50% rad

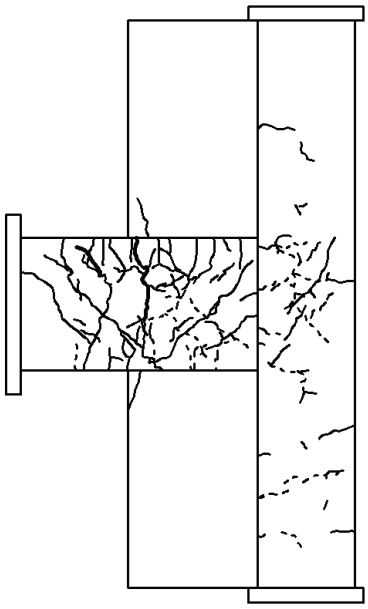

R = 2.00% rad

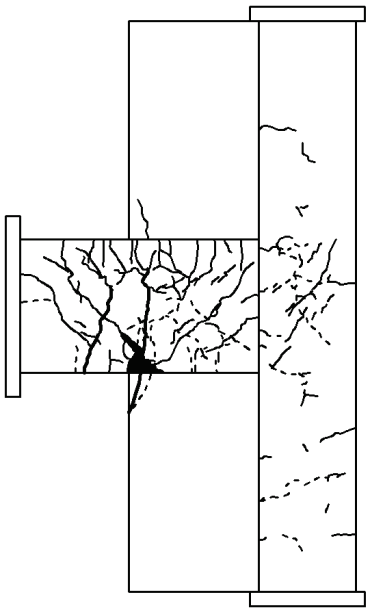

R = -2.00% rad

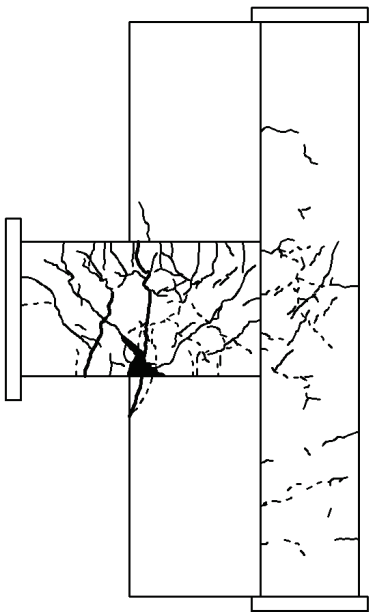

R = 3.00% rad

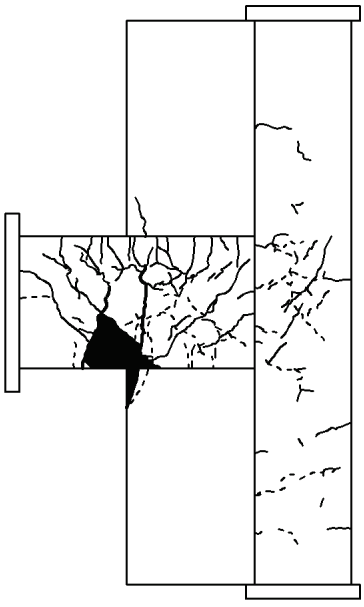

R = -3.00% rad

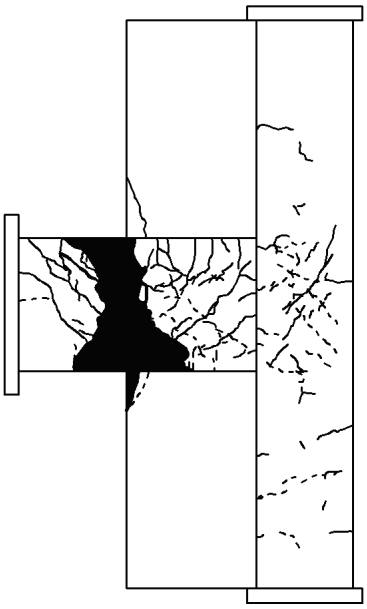

R = 4.00% rad

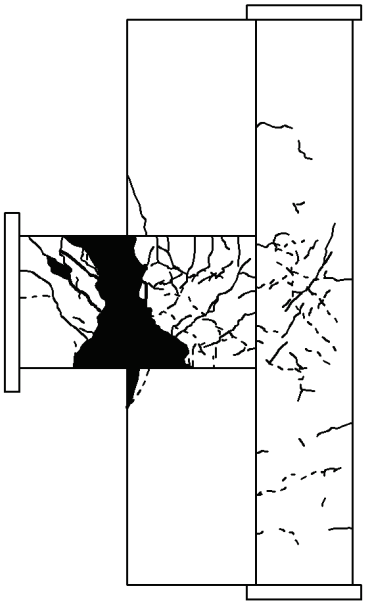

R = -4.00% rad

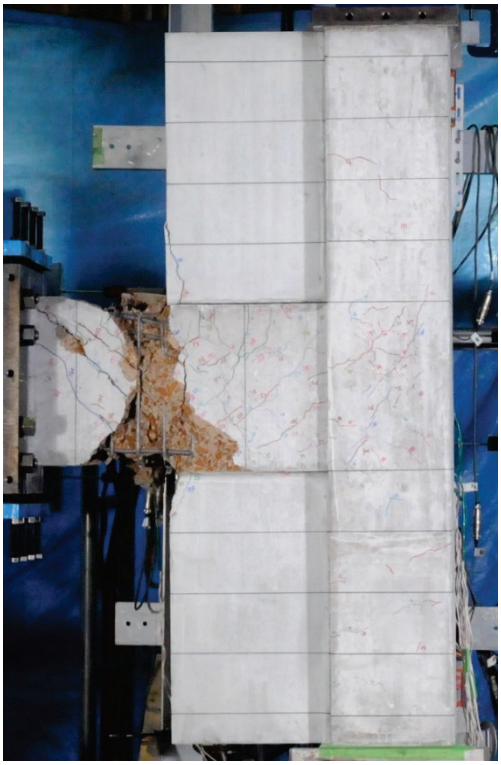

Final crack pattern

Figure B.3 Crack pattern of specimen J1-W

Appendix C

Strain of Reinforcing Bars of Beam-Column Joint Specimens

Several strain gauges were placed on the reinforcement of the beam-column joint specimens. The arrangements of those gauges and the measured strain during the loading cycle are shown in the following figures.

C.1. Strain of Reinforcing Bars of Specimen J1

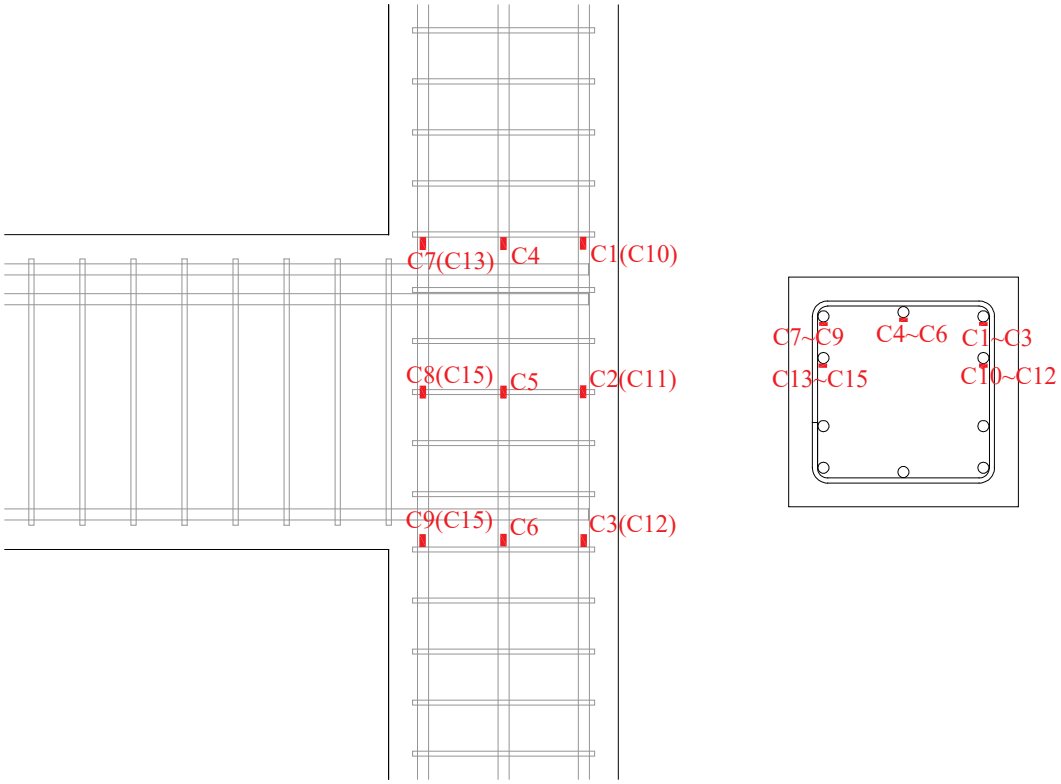

Figure C.1 Position of strain gauges of column main bars of specimen J1

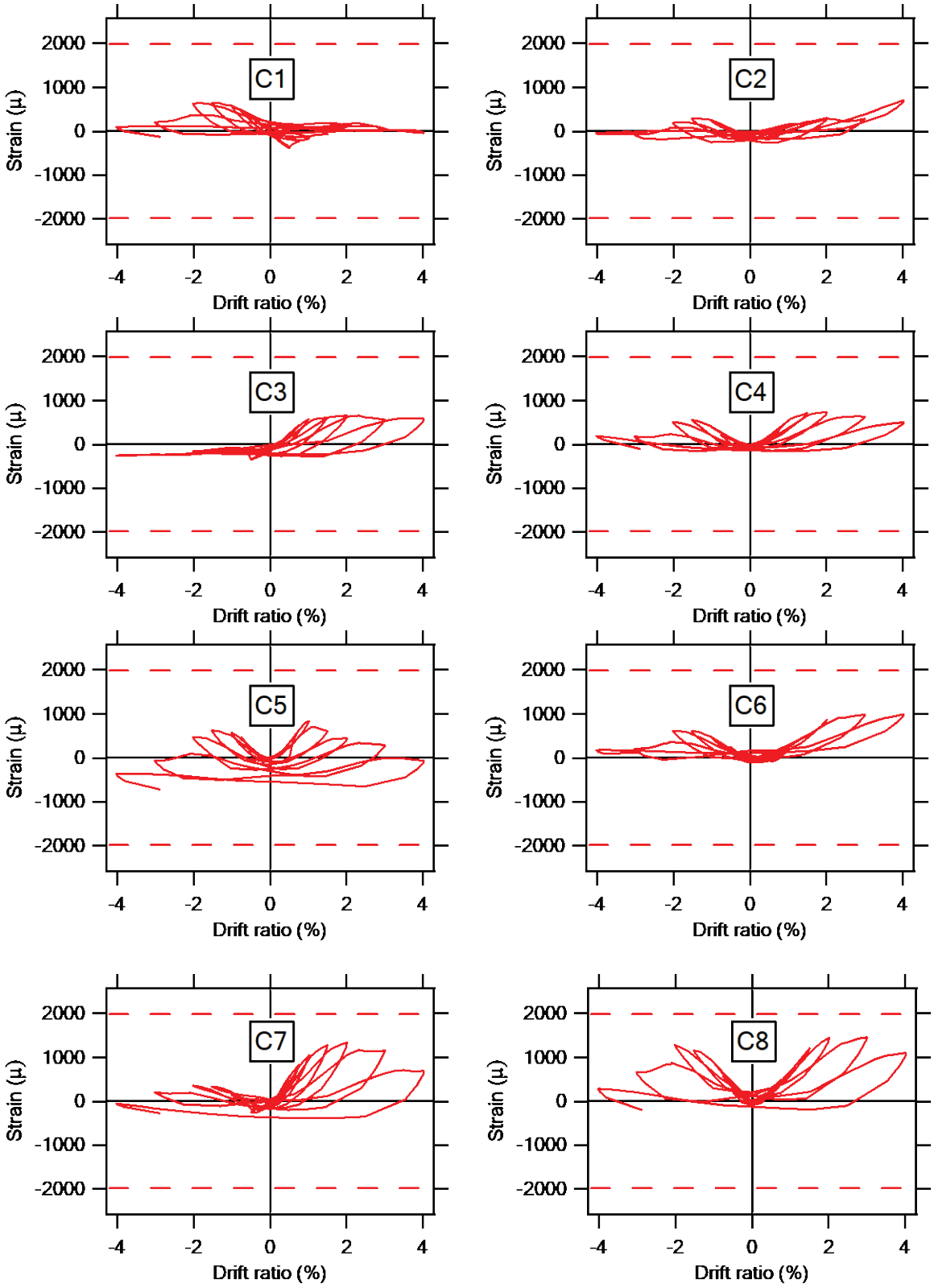
C1
C2
C3
C4
C5
C6
C7
C8
Strain (μ)
2000
1000
0
-1000
-2000
-4
-2
0
2
4
Drift ratio (%)

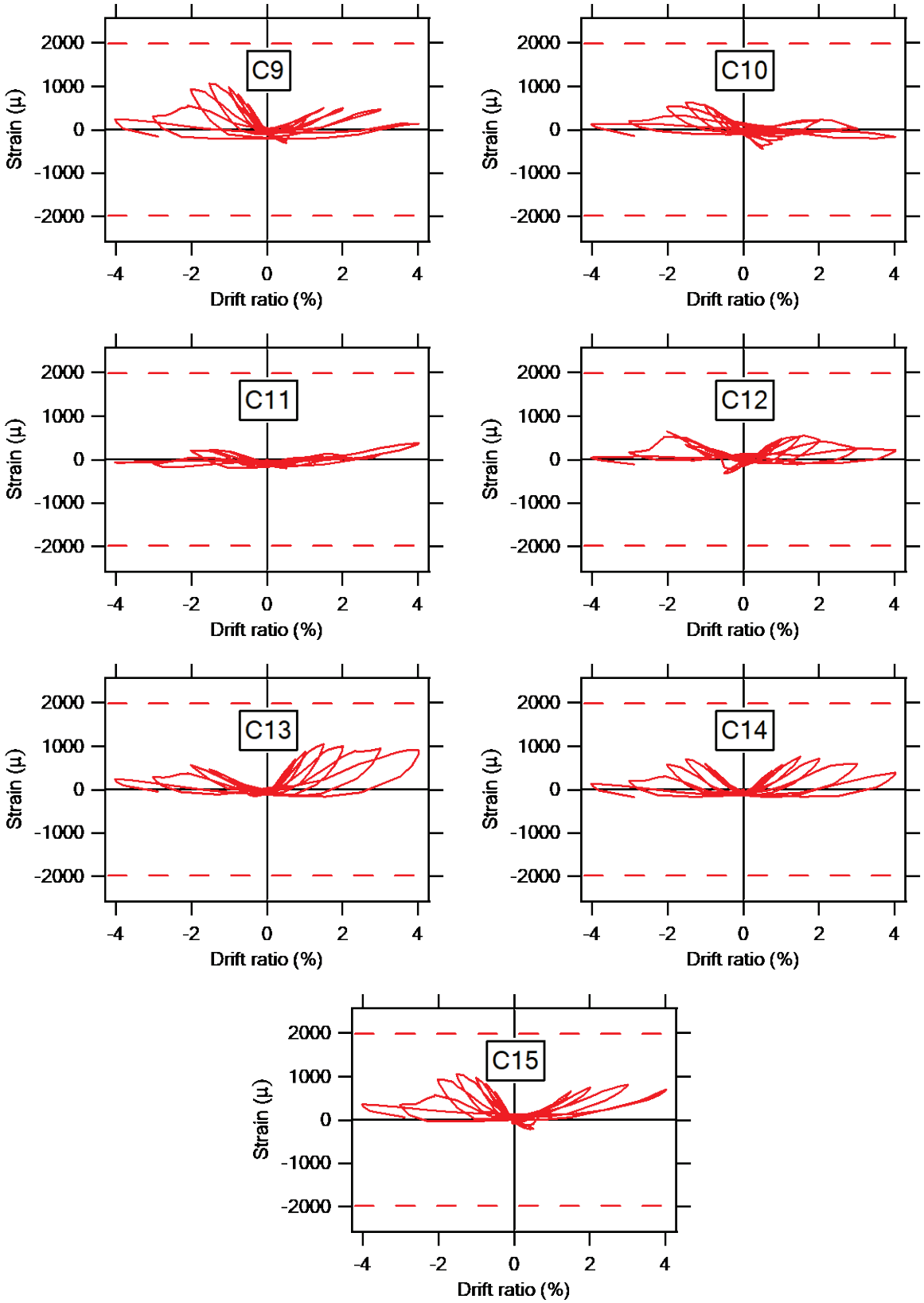

Figure C.2 Strain of column main bars of specimen J1

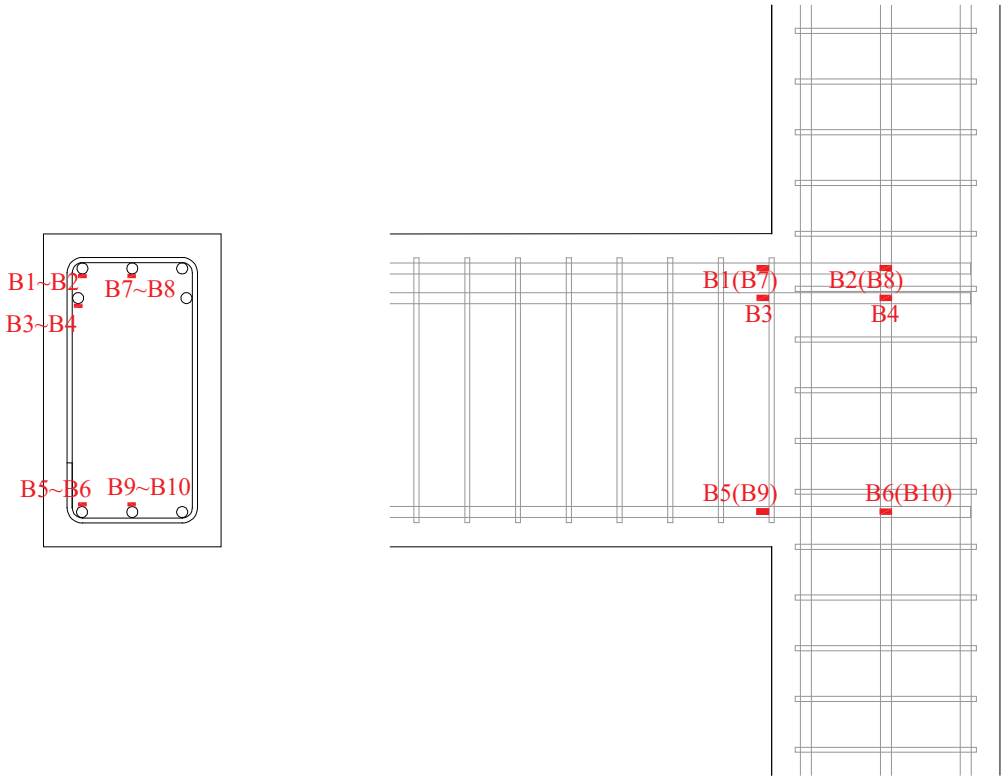

Figure C.3 Position of strain gauges of beam main bars of specimen J1

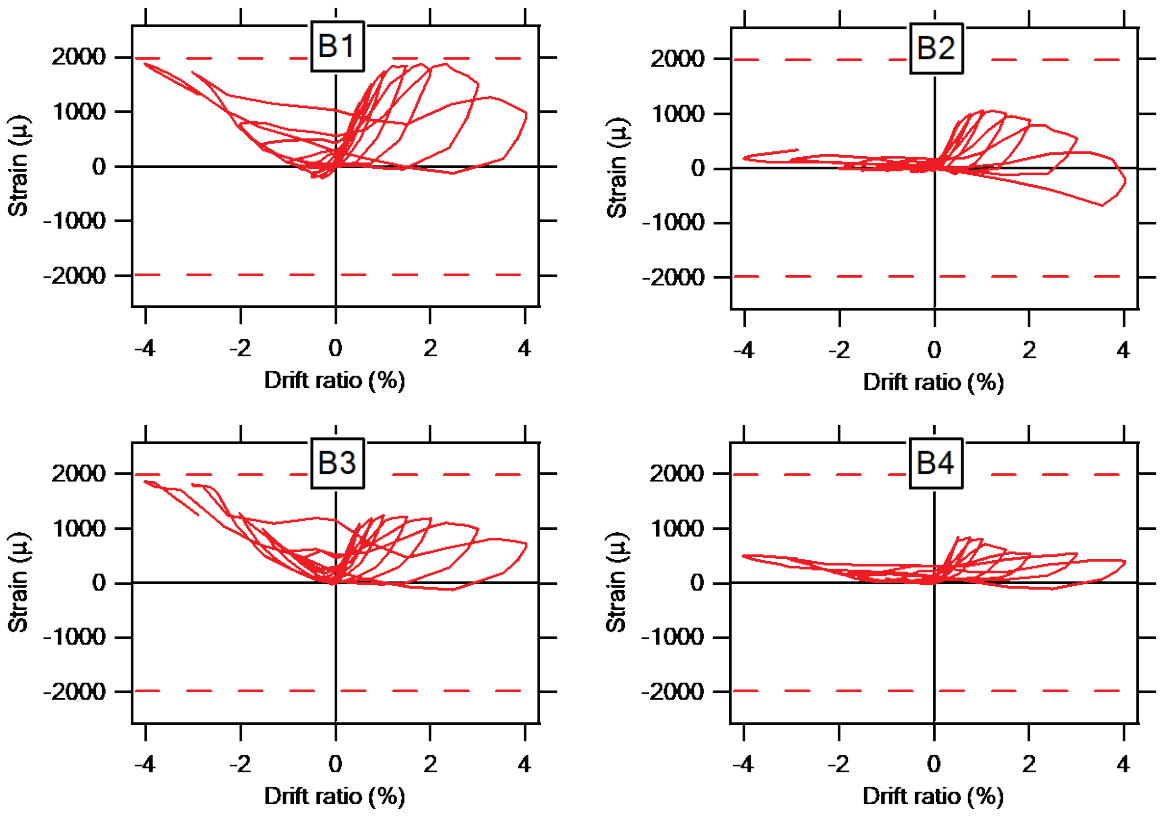

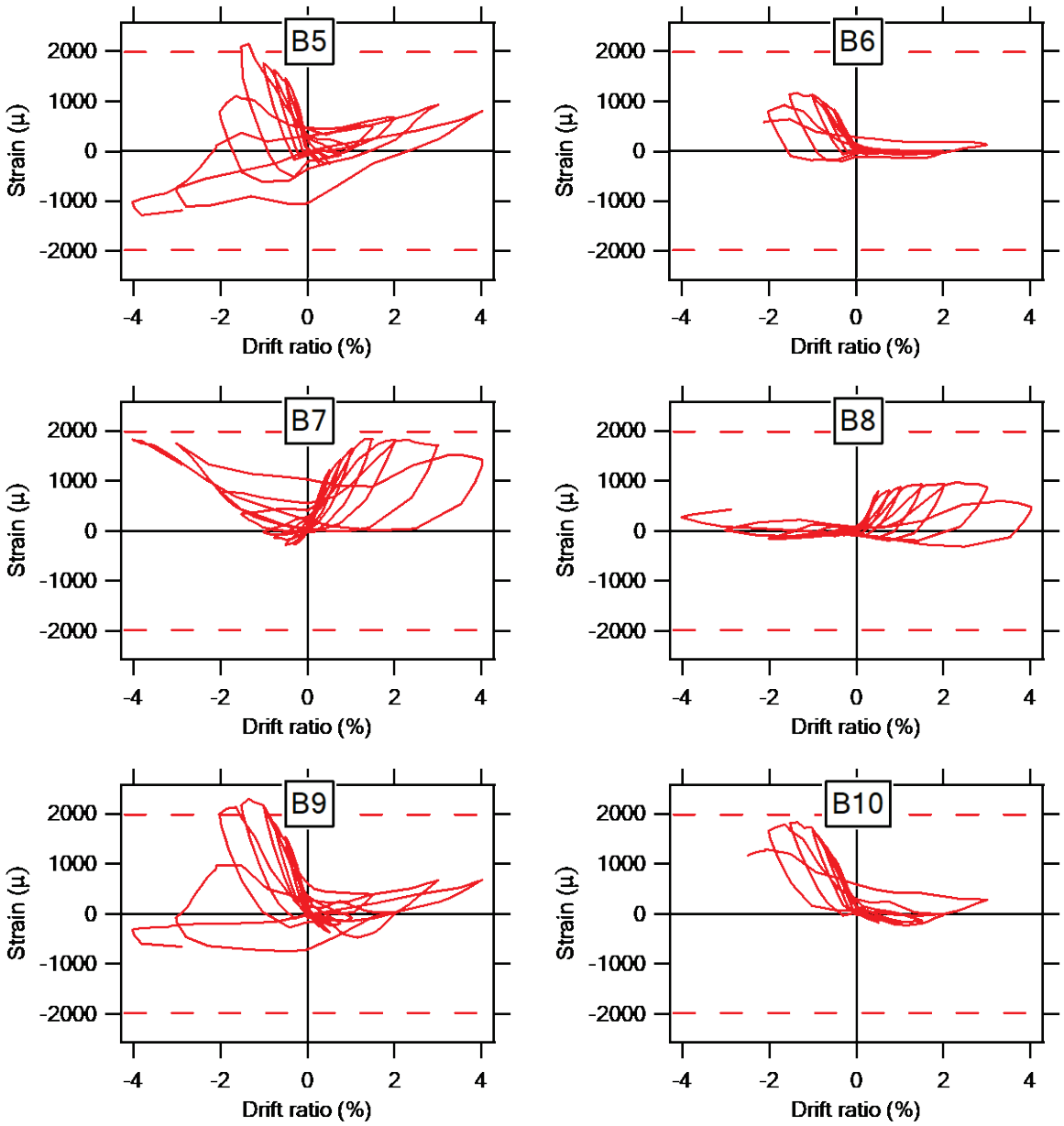

Figure C.4 Strain of beam main bars of specimen J1

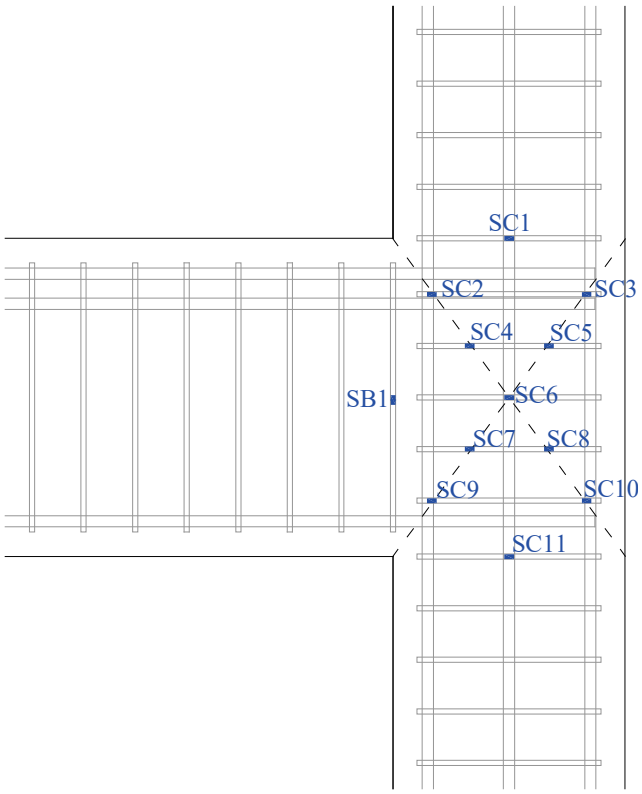

Figure C.5 Position of strain gauges of shear reinforcement of specimen J1

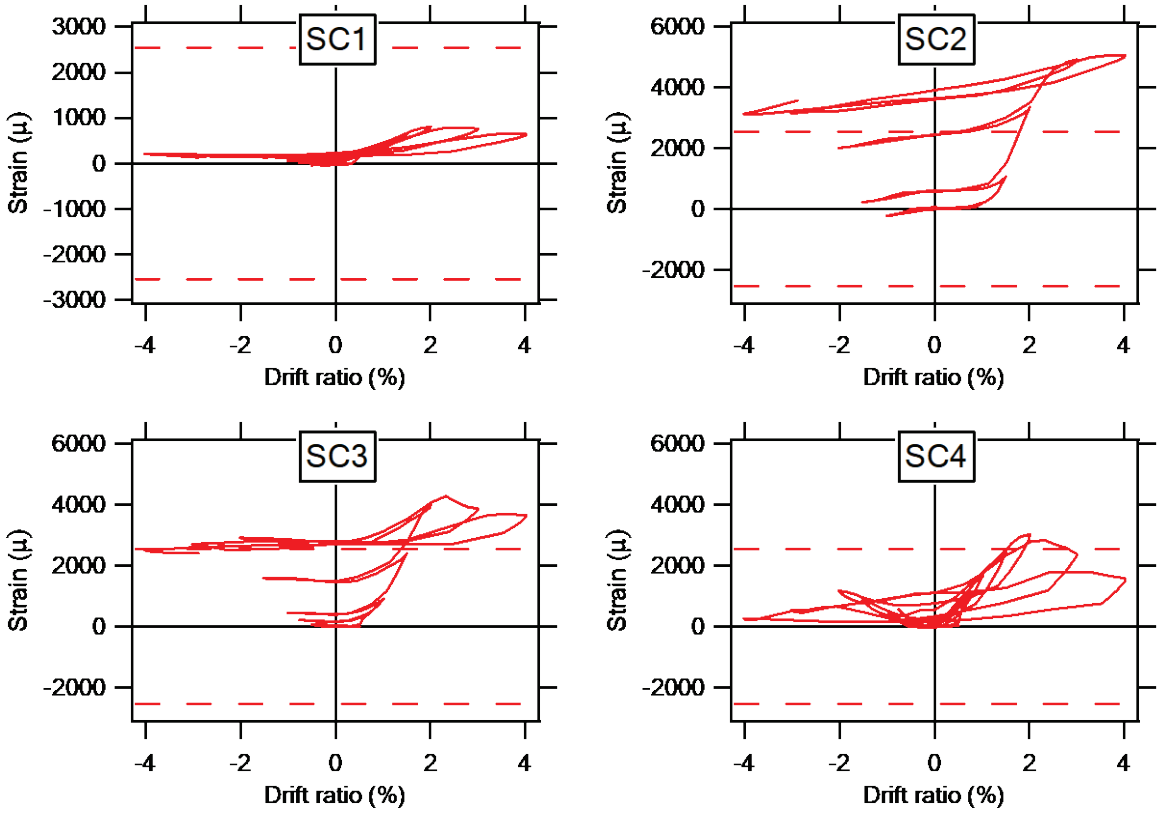

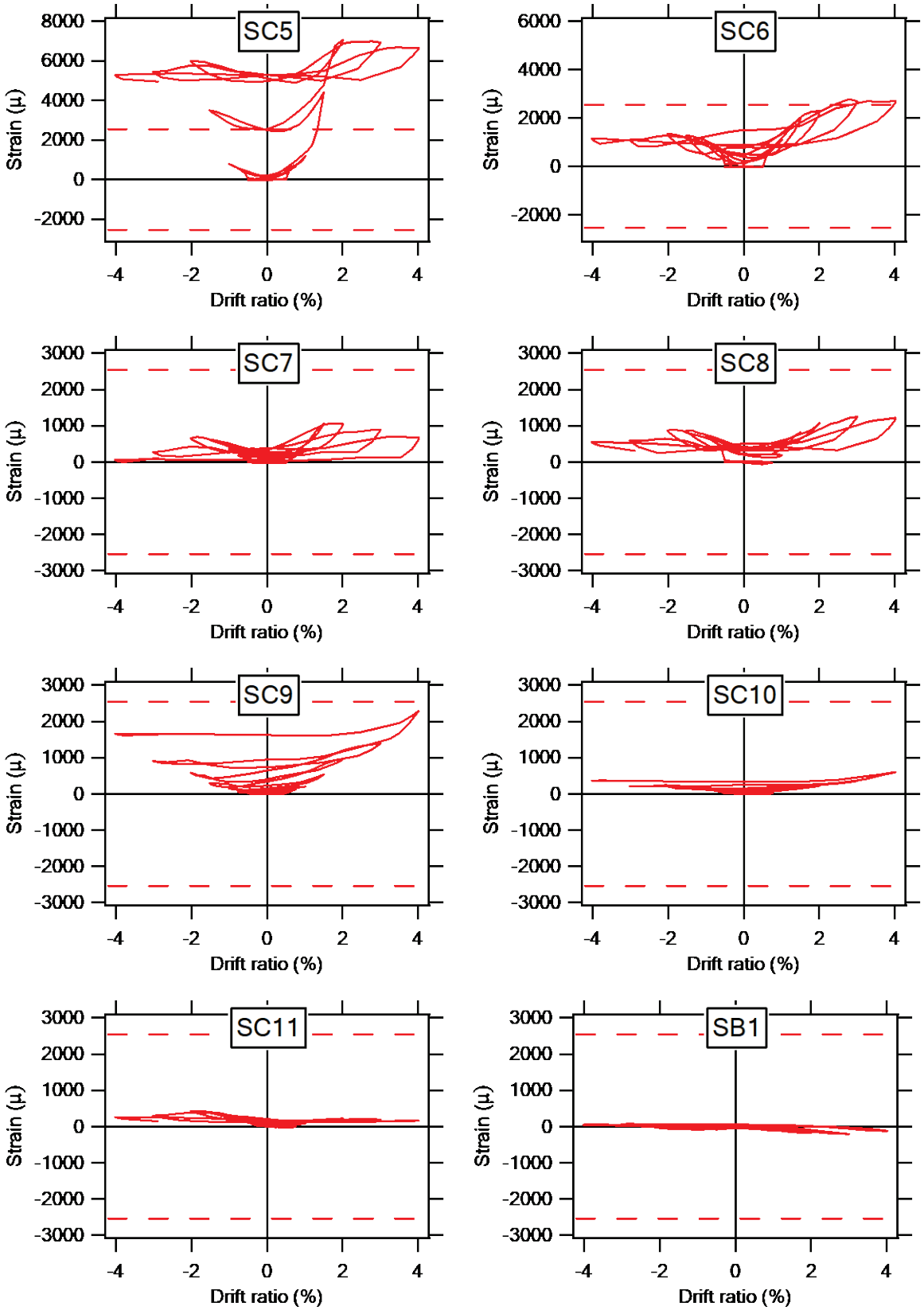

Figure C.6 Strain of shear reinforcement of specimen J1

C.2. Strain of Reinforcing Bars of Specimen J2

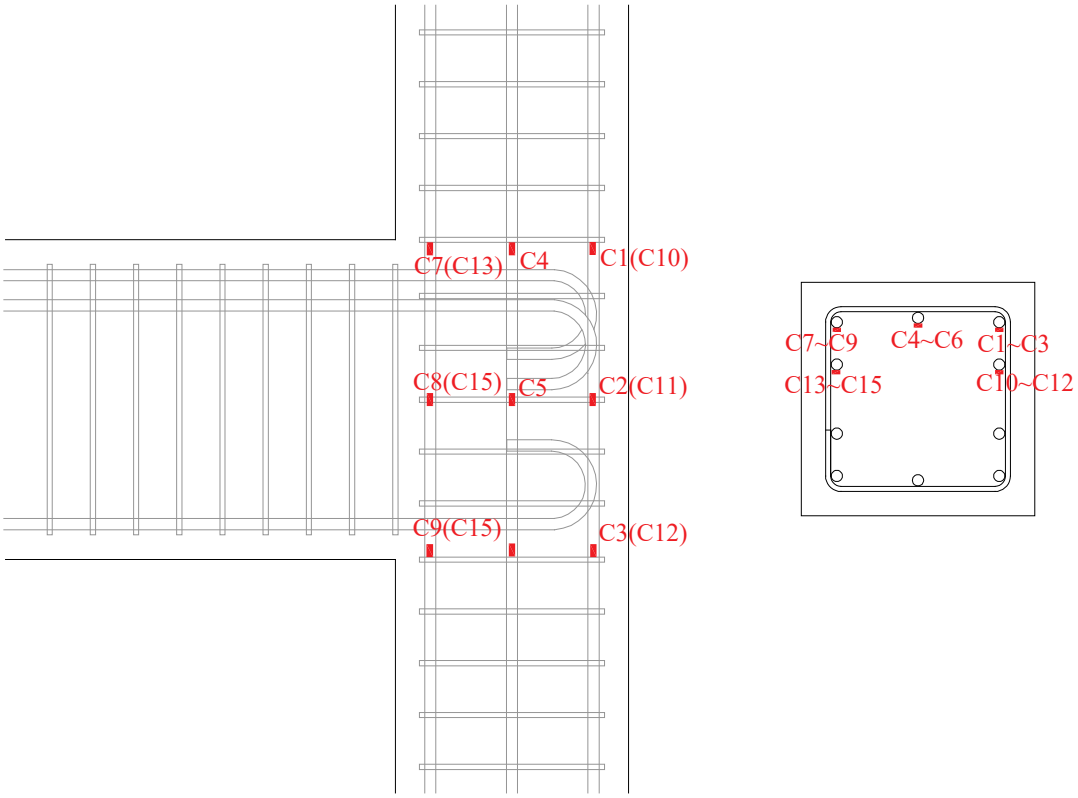

Figure C.7 Position of strain gauges of column main bars of specimen J2

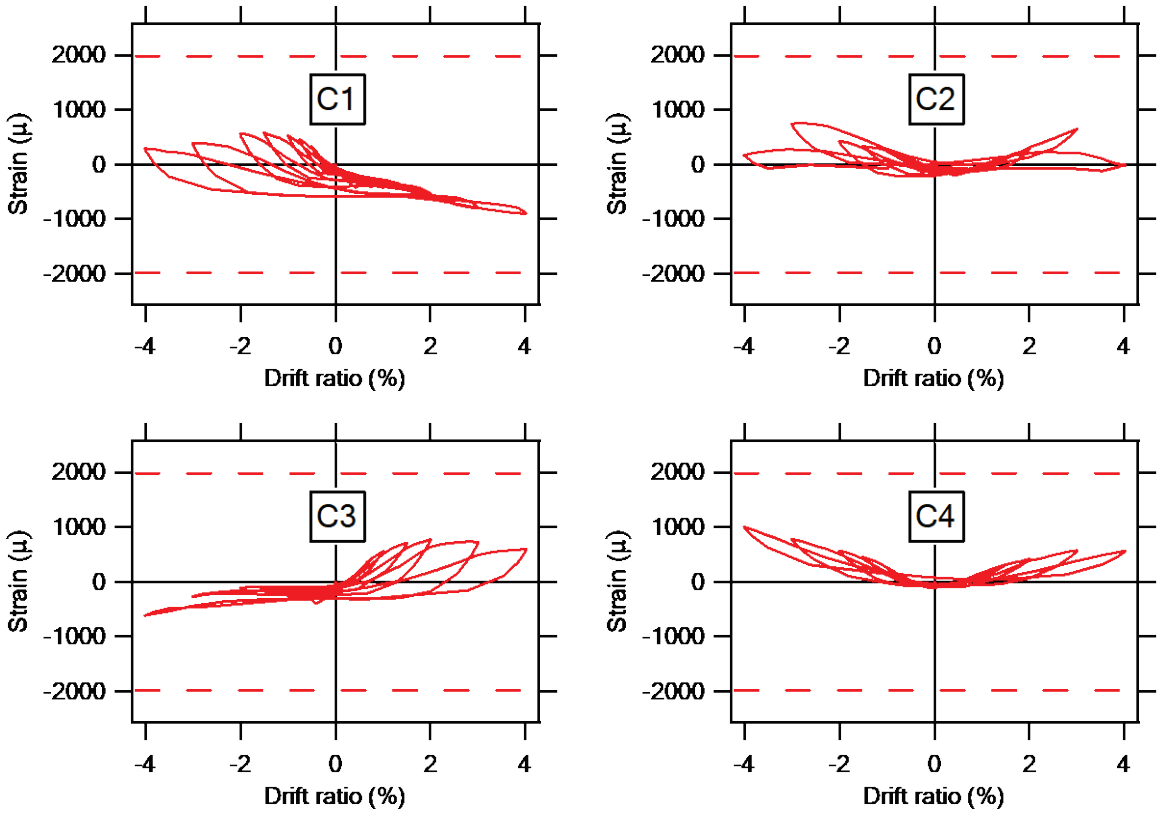

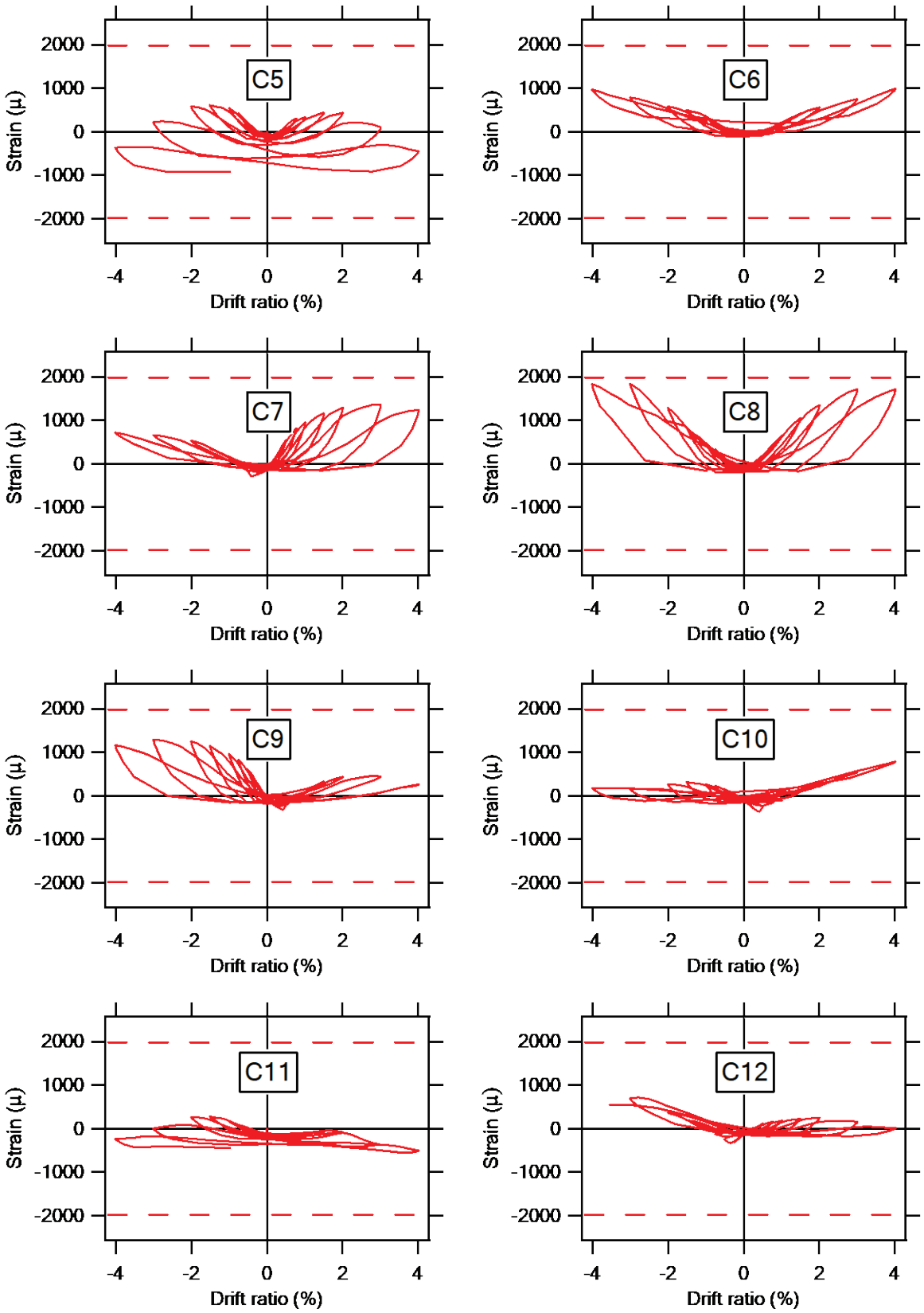
C5
C6
C7
C8
C9
C10
C11
C12
Strain (μ)
2000
1000
0
-1000
-2000
-4
-2
0
2
4
Drift ratio (%)

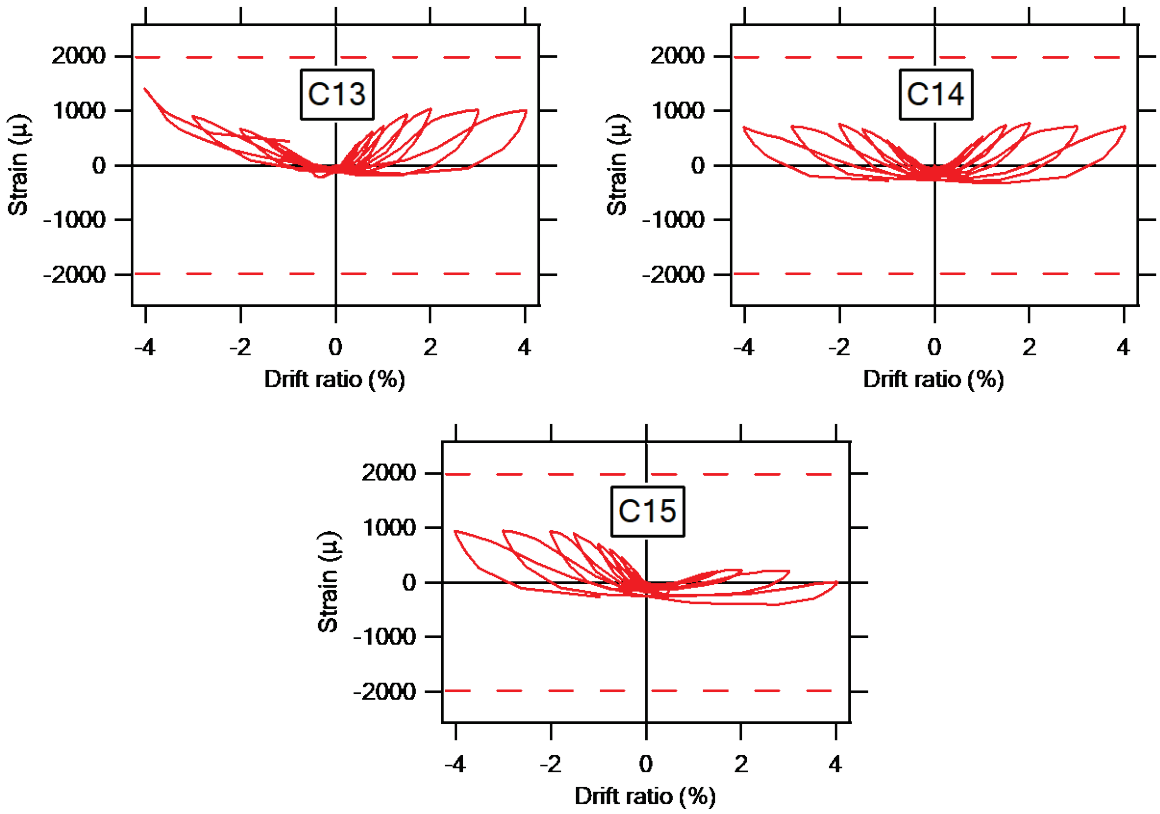

Figure C.8 Strain of column main bars of specimen J2

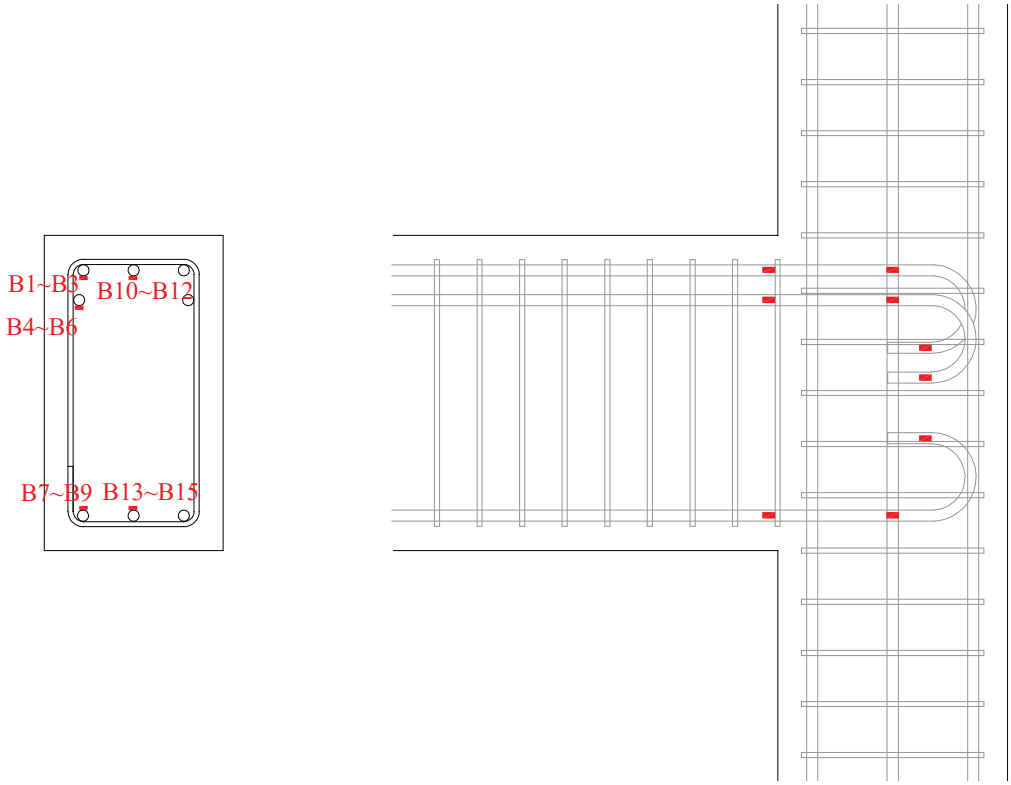

Figure C.9 Position of strain gauges of beam main bars of specimen J2

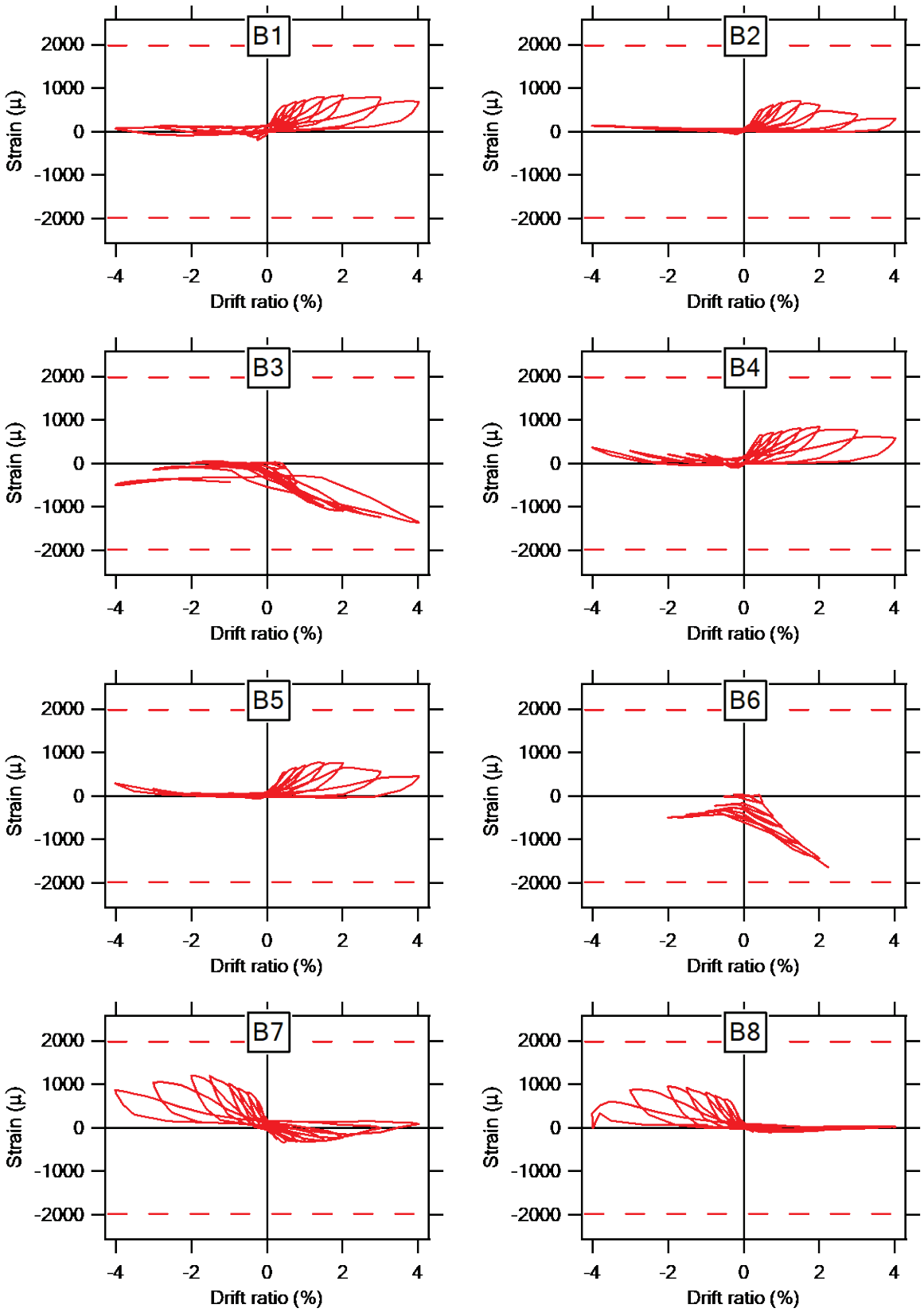
B1
B2
B3
B4
B5
B6
B7
B8
Strain (μ)
2000
1000
0
-1000
-2000
-4
-2
0
2
4
Drift ratio (%)

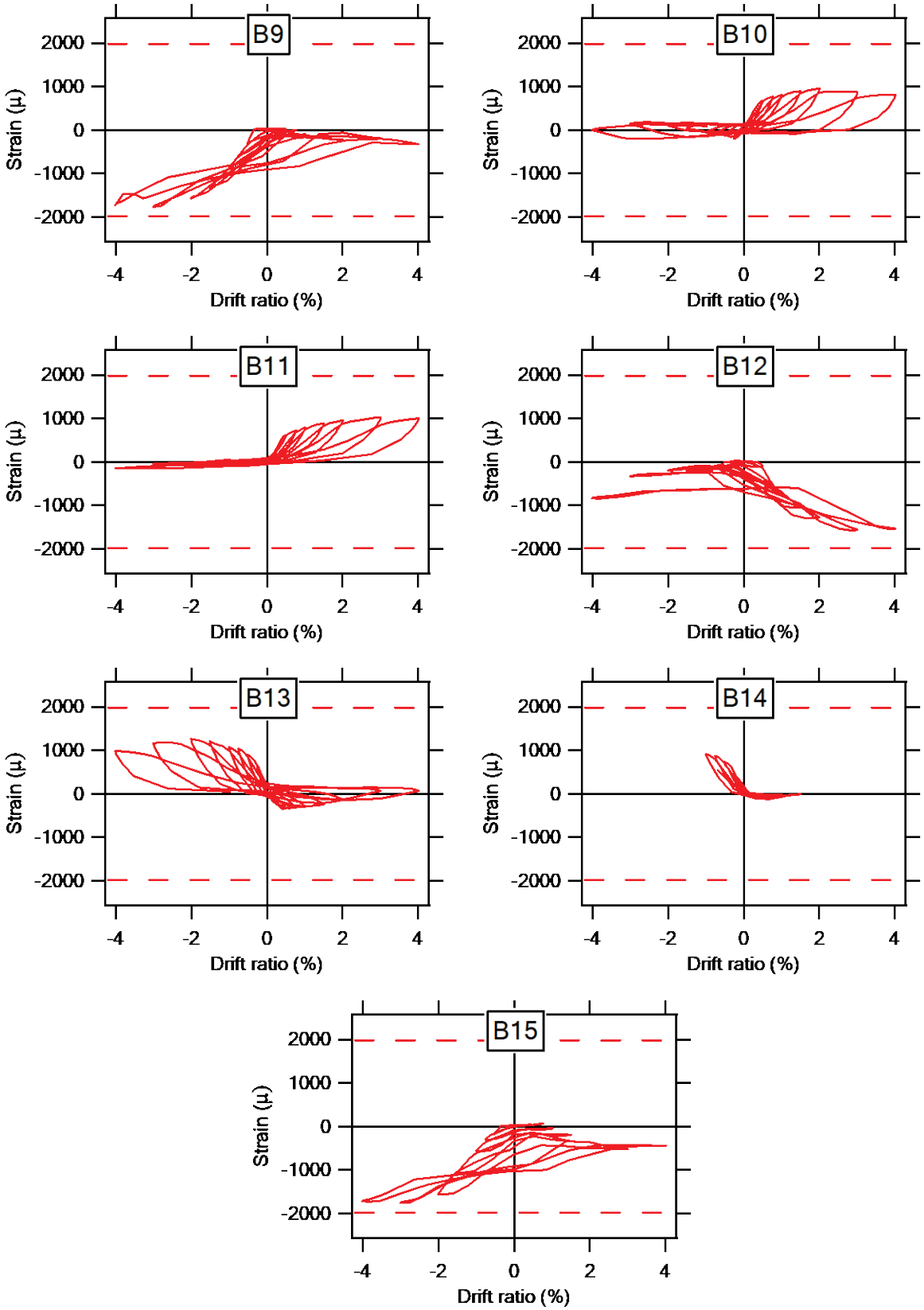

Figure C.10 Strain of beam main bars of specimen J2

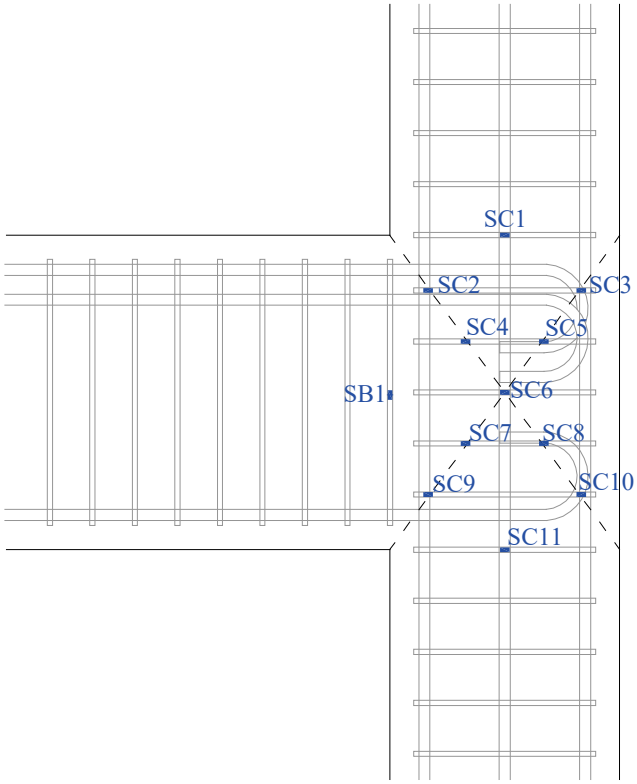

Figure C.11 Position of strain gauges of shear reinforcement of specimen J2

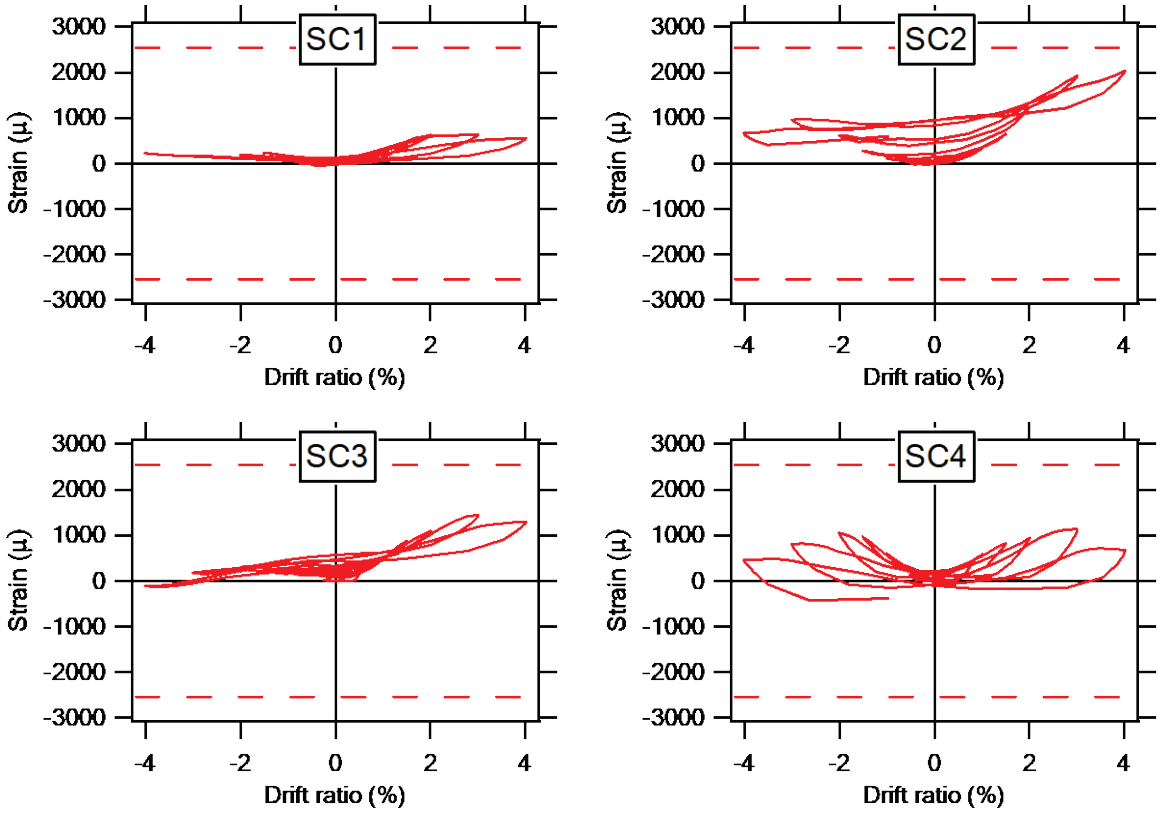

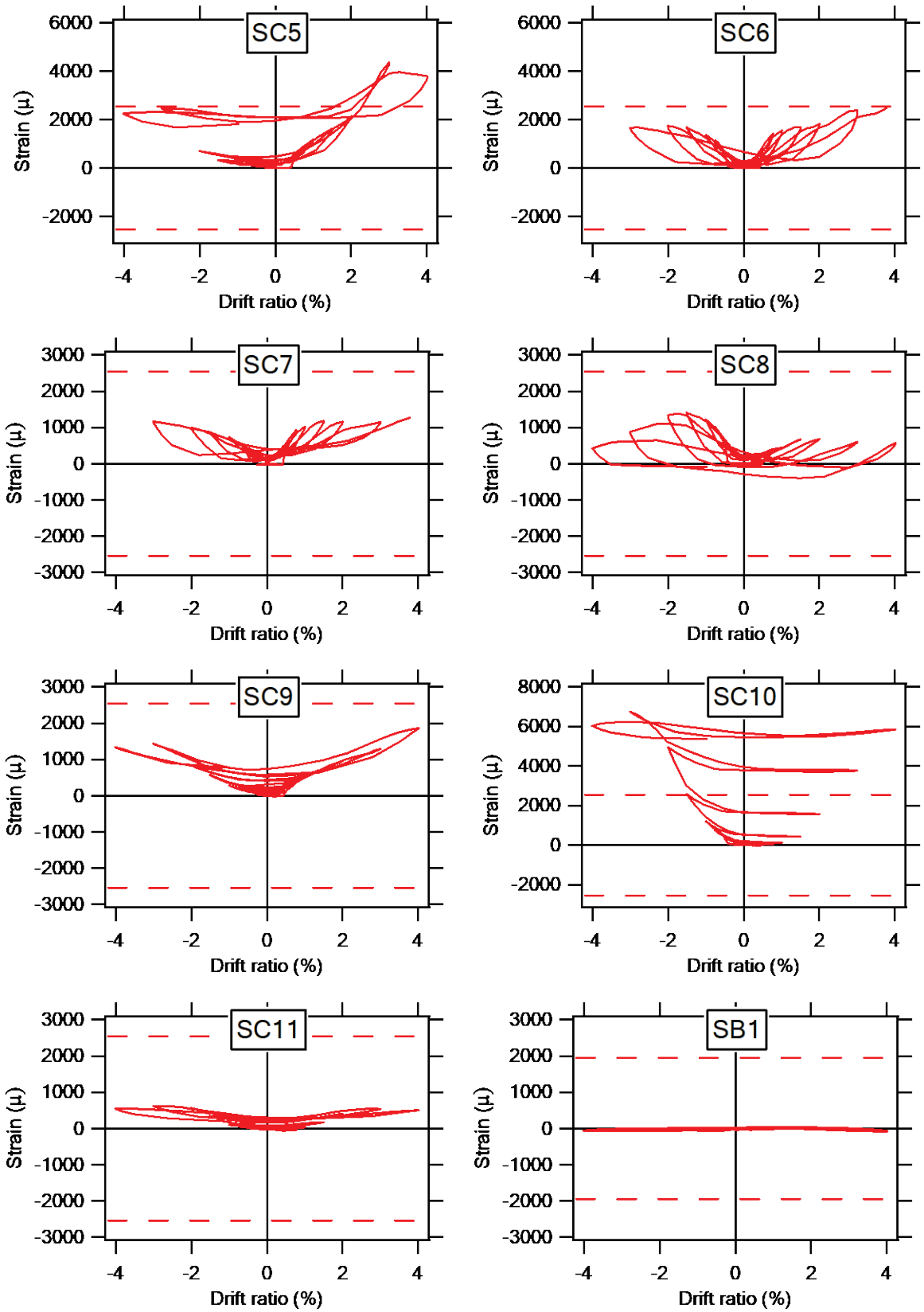

Figure C.12 Position of strain gauges of shear reinforcement of specimen J2

C.3. Strain of Reinforcing Bars of Specimen J1-W

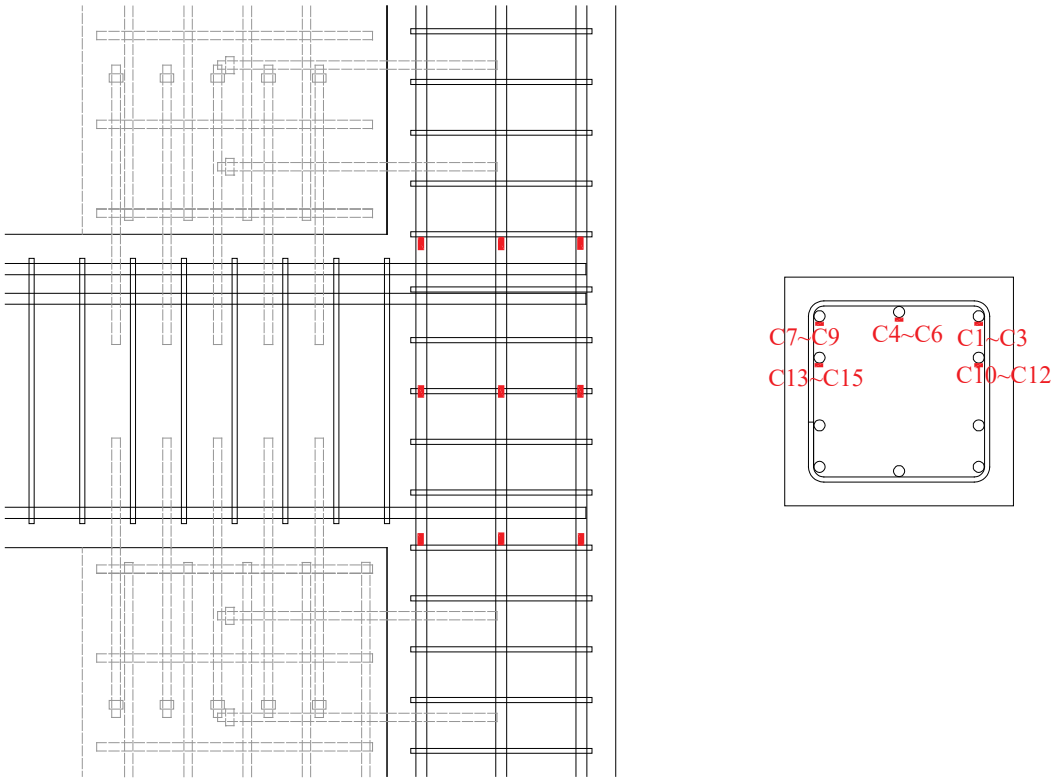

Figure C.13 Position of strain gauges of column main bars of specimen J1-W

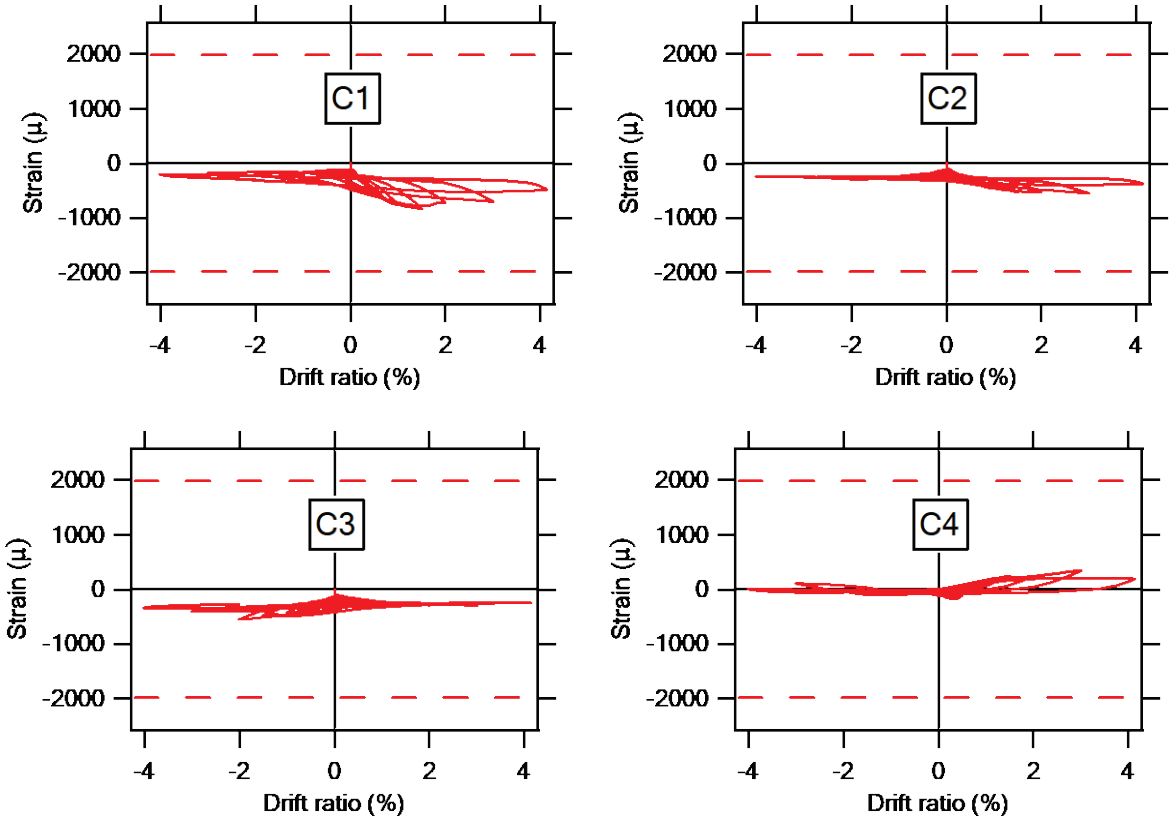

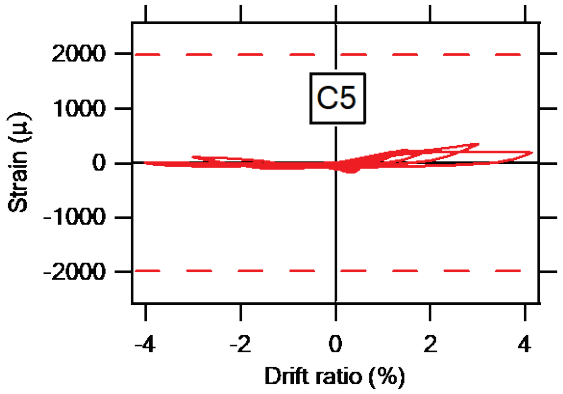
C5
Strain (μ)
2000
1000
0
-1000
-2000
-4
-2
0
2
4
Drift ratio (%)

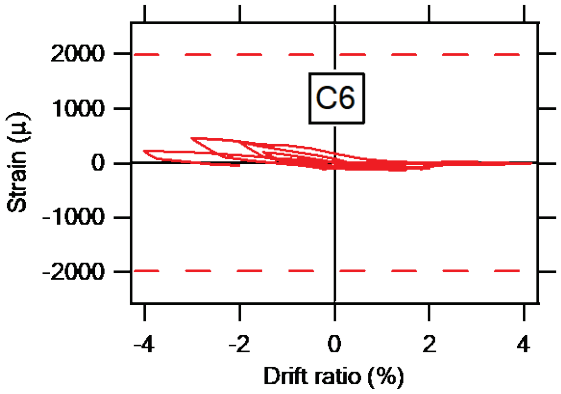
C6
Strain (μ)
2000
1000
0
-1000
-2000
-4
-2
0
2
4
Drift ratio (%)

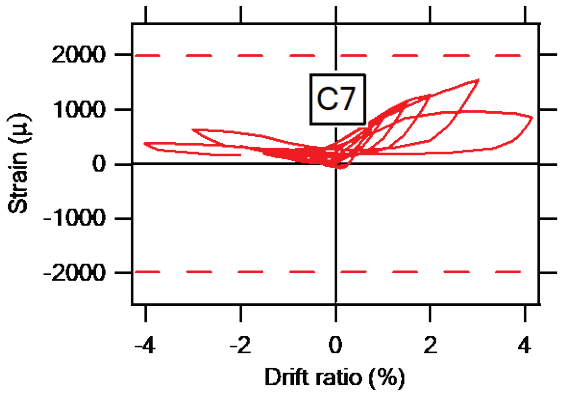
C7
Strain (μ)
2000
1000
0
-1000
-2000
-4
-2
0
2
4
Drift ratio (%)

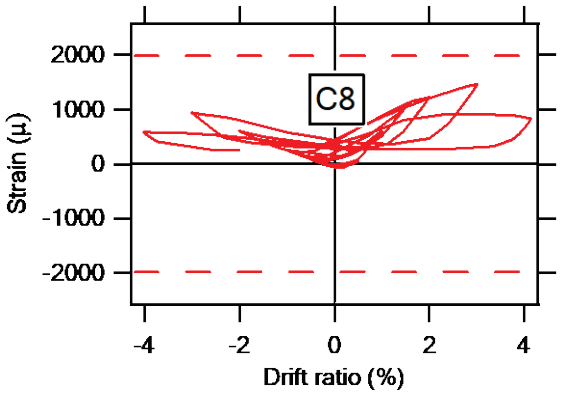
C8
Strain (μ)
2000
1000
0
-1000
-2000
-4
-2
0
2
4
Drift ratio (%)

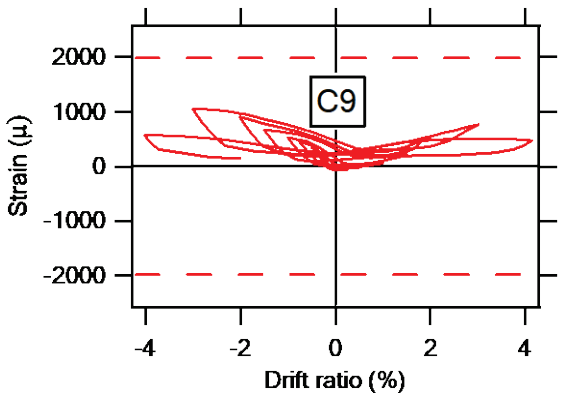
C9
Strain (μ)
2000
1000
0
-1000
-2000
-4
-2
0
2
4
Drift ratio (%)

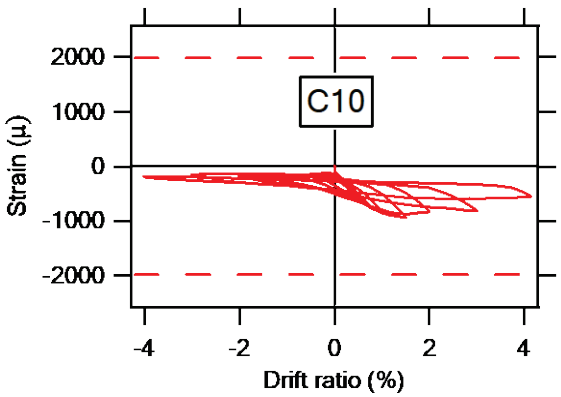
C10
Strain (μ)
2000
1000
0
-1000
-2000
-4
-2
0
2
4
Drift ratio (%)

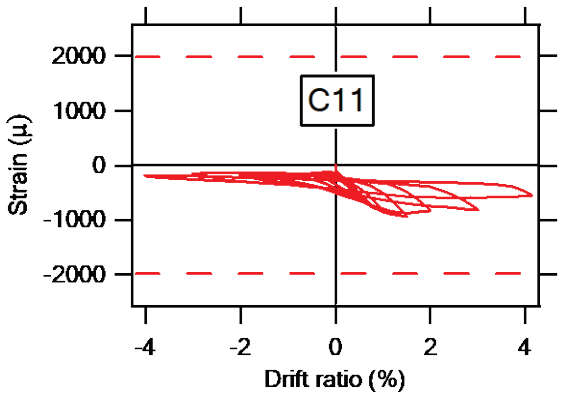
C11
Strain (μ)
2000
1000
0
-1000
-2000
-4
-2
0
2
4
Drift ratio (%)

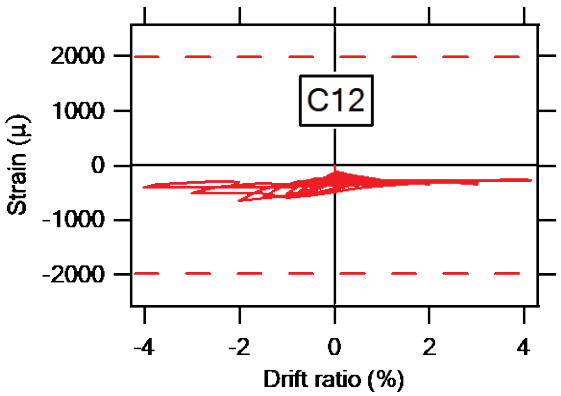
C12
Strain (μ)
2000
1000
0
-1000
-2000
-4
-2
0
2
4
Drift ratio (%)

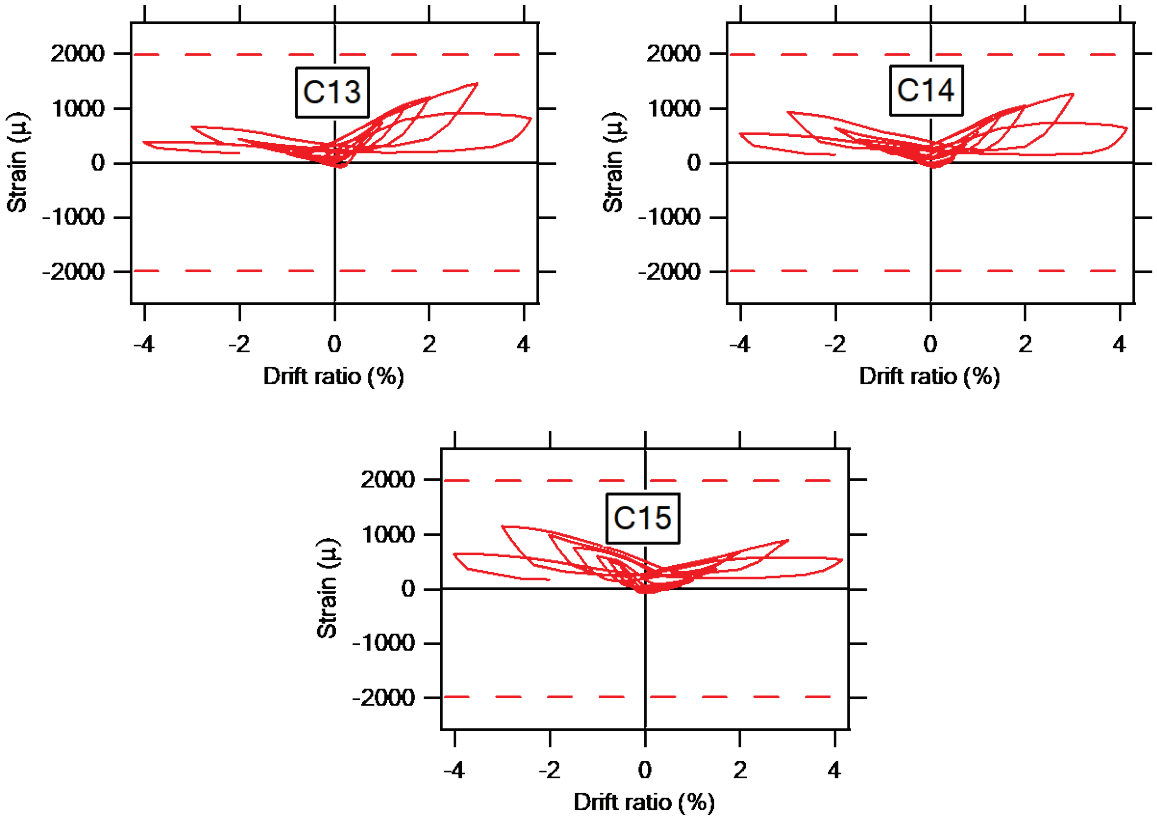

Figure C.14 Strain of column main bars of specimen J1-W

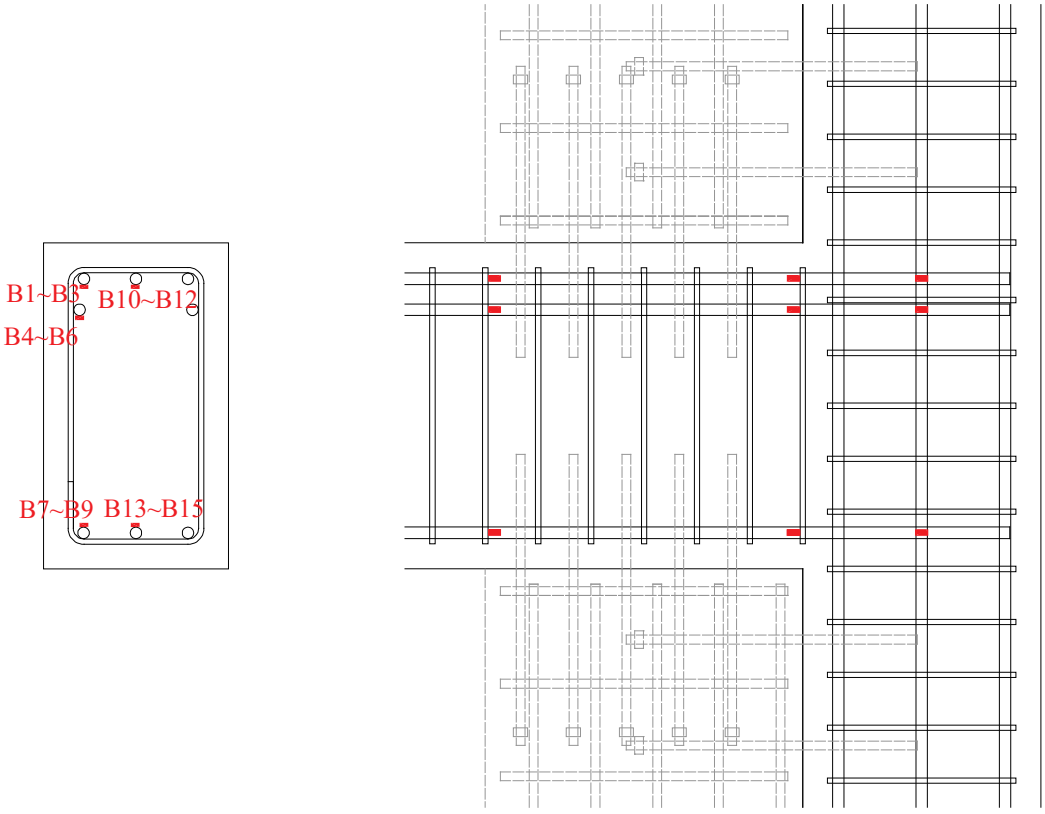

Figure C.15 Position of strain gauges of beam main bars of specimen J1-W

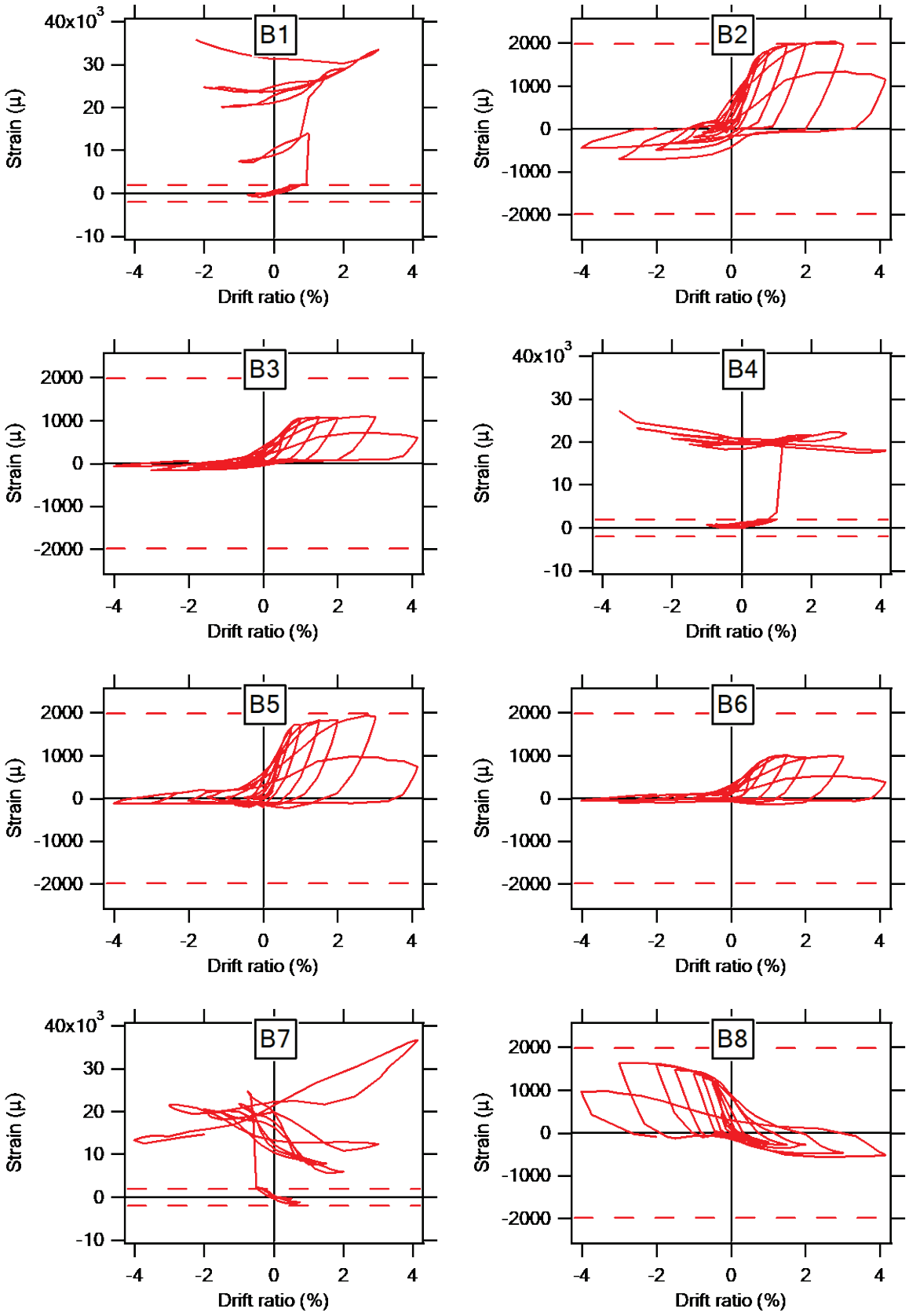
B1
B2
B3
B4
B5
B6
B7
B8
Strain (μ)
Drift ratio (%)
40x10^3
2000
1000
0
-1000
-2000
30
20
10
-10
-4
-2
2
4

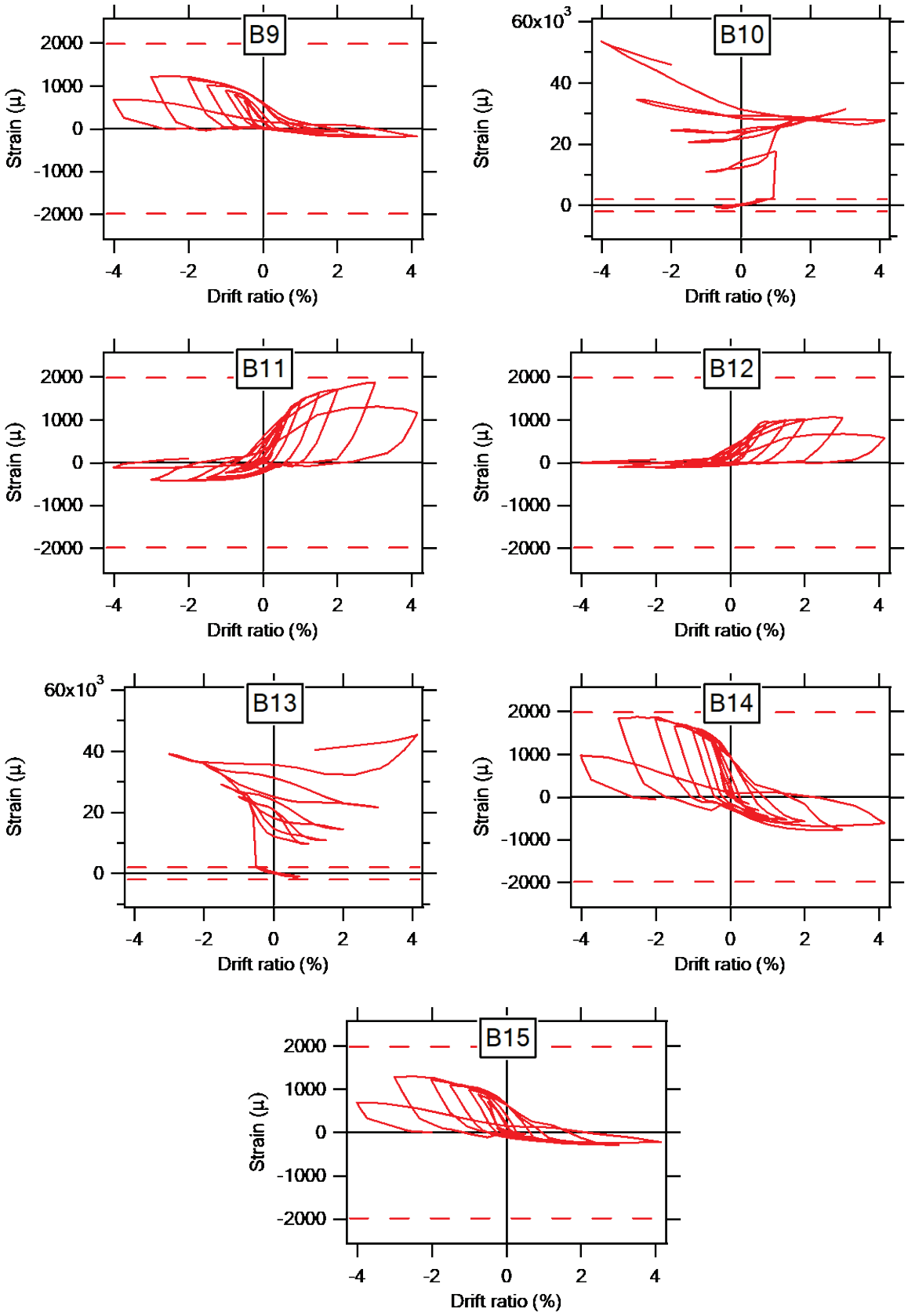

Figure C.16 Strain of beam main bars of specimen J1-W

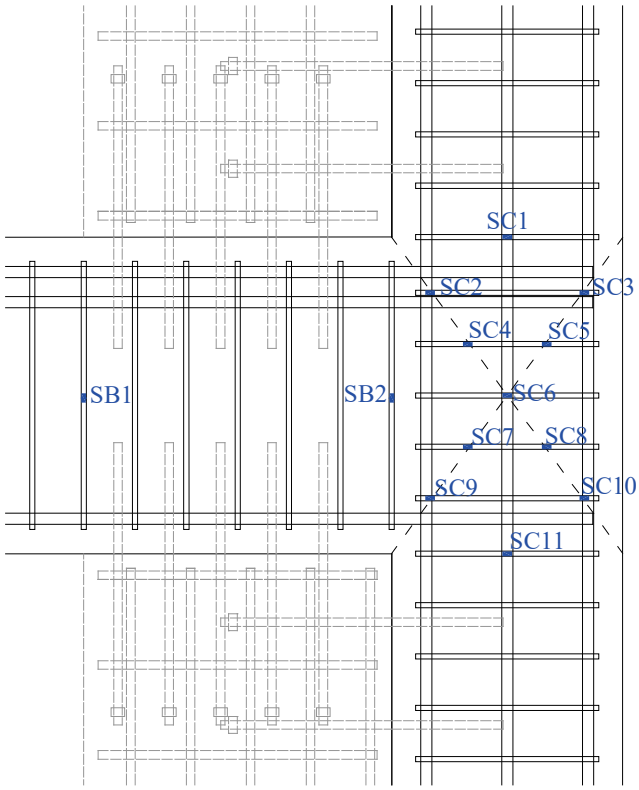

Figure C.17 Position of strain gauges of shear reinforcement of specimen J1-W

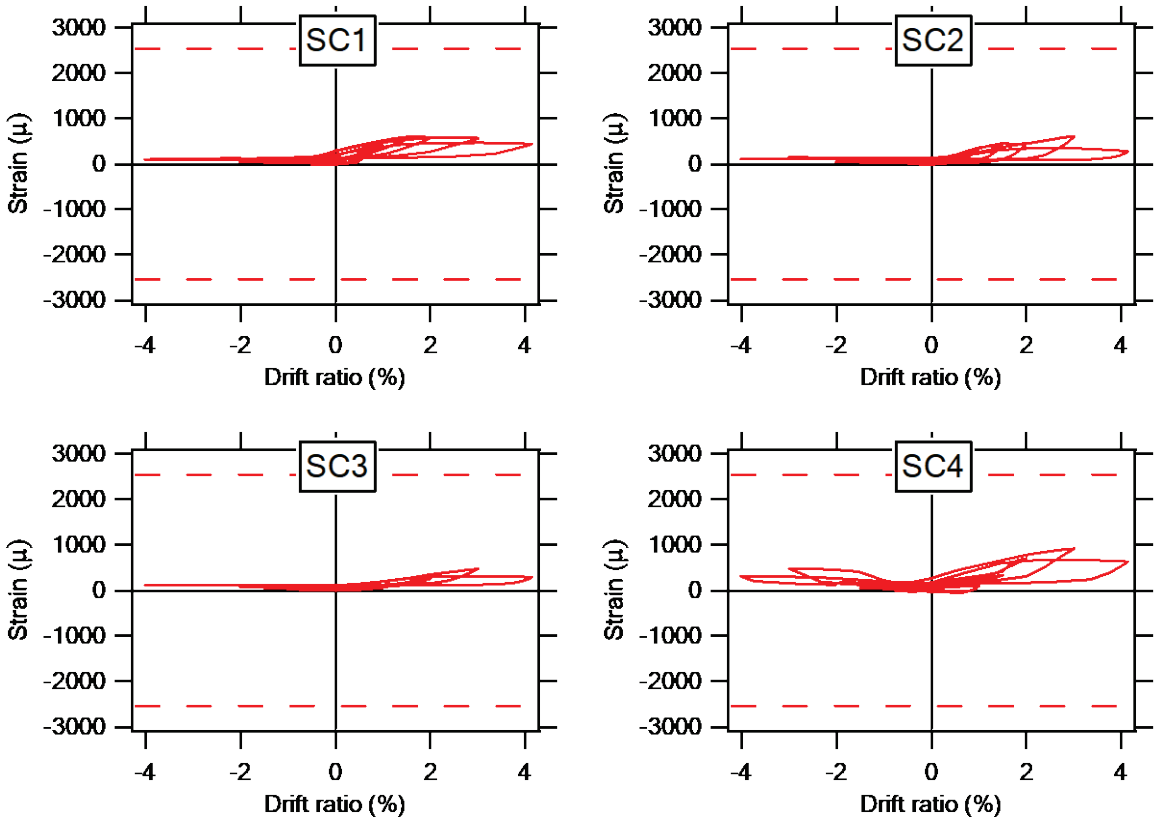

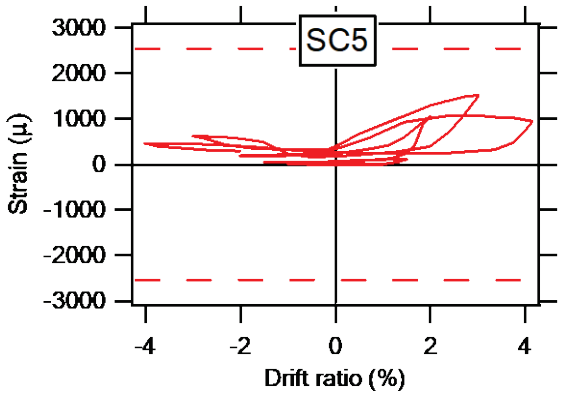
SC5
Strain (μ)
3000
2000
1000
0
-1000
-2000
-3000
-4
-2
0
2
4
Drift ratio (%)

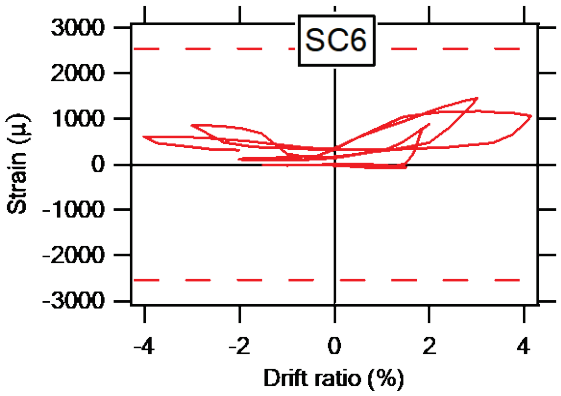
SC6
Strain (μ)
3000
2000
1000
0
-1000
-2000
-3000
-4
-2
0
2
4
Drift ratio (%)

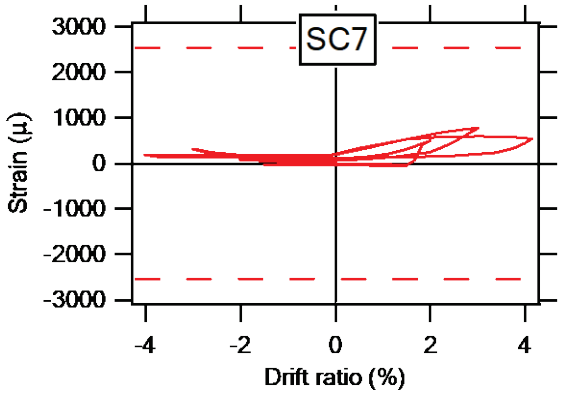
SC7
Strain (μ)
3000
2000
1000
0
-1000
-2000
-3000
-4
-2
0
2
4
Drift ratio (%)

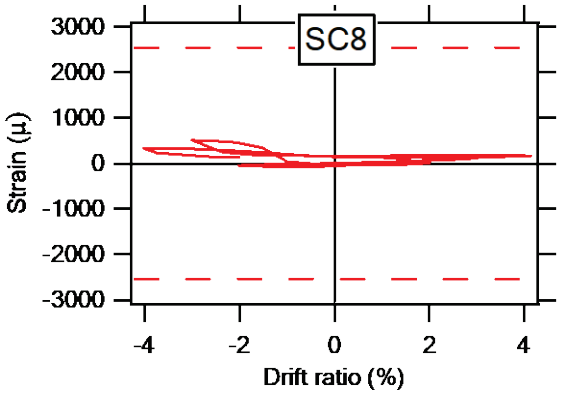
SC8
Strain (μ)
3000
2000
1000
0
-1000
-2000
-3000
-4
-2
0
2
4
Drift ratio (%)

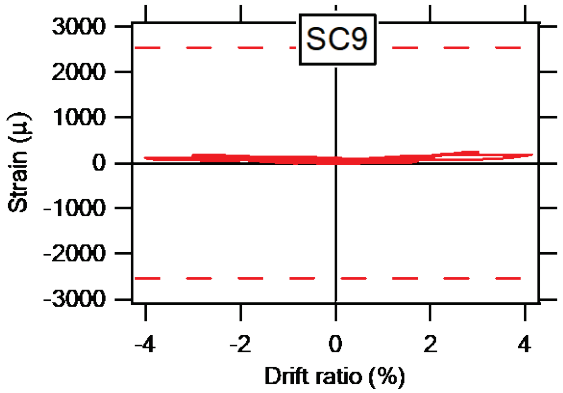
SC9
Strain (μ)
3000
2000
1000
0
-1000
-2000
-3000
-4
-2
0
2
4
Drift ratio (%)

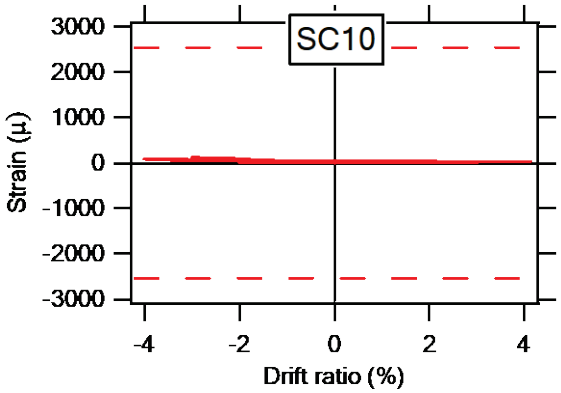
SC10
Strain (μ)
3000
2000
1000
0
-1000
-2000
-3000
-4
-2
0
2
4
Drift ratio (%)

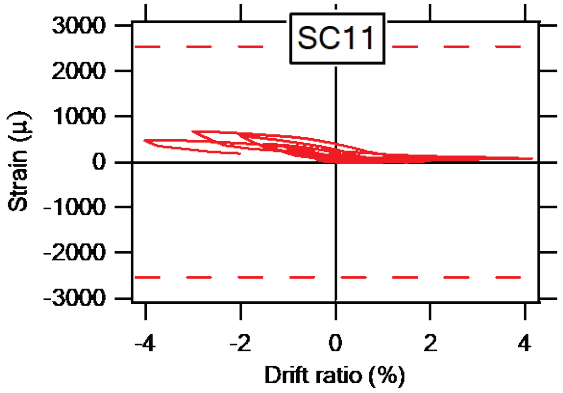
SC11
Strain (μ)
3000
2000
1000
0
-1000
-2000
-3000
-4
-2
0
2
4
Drift ratio (%)

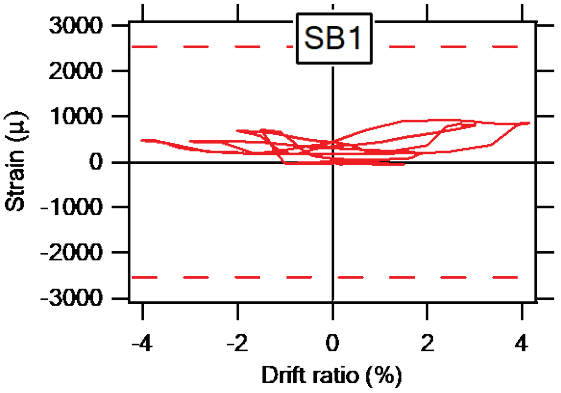
SB1
Strain (μ)
3000
2000
1000
0
-1000
-2000
-3000
-4
-2
0
2
4
Drift ratio (%)

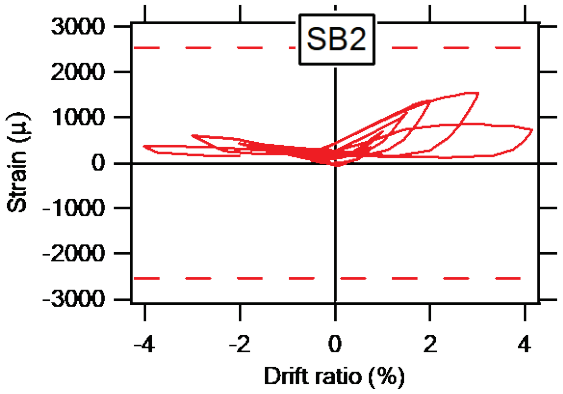

Figure C.18 Strain of shear reinforcement of specimen J1-W

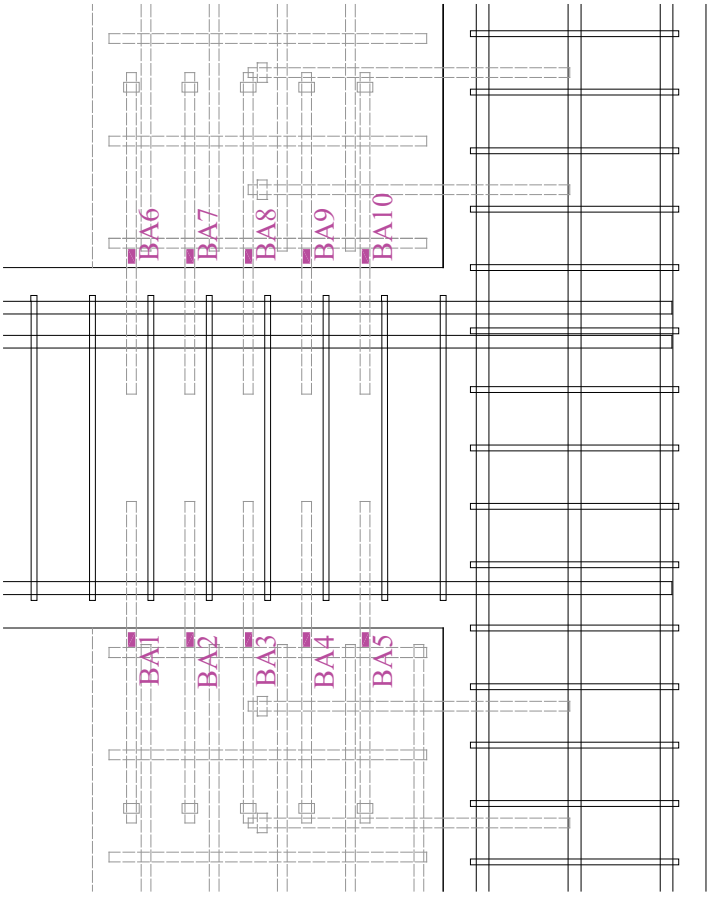

Figure C.19 Position of strain gauges of beam anchors of specimen J1-W

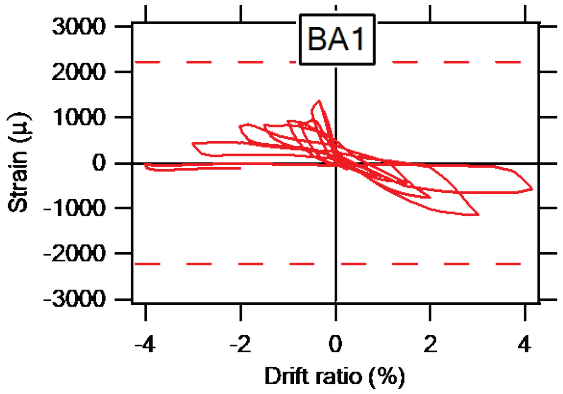
BA1
Strain (μ)
3000
2000
1000
0
-1000
-2000
-3000
-4
-2
0
2
4
Drift ratio (%)

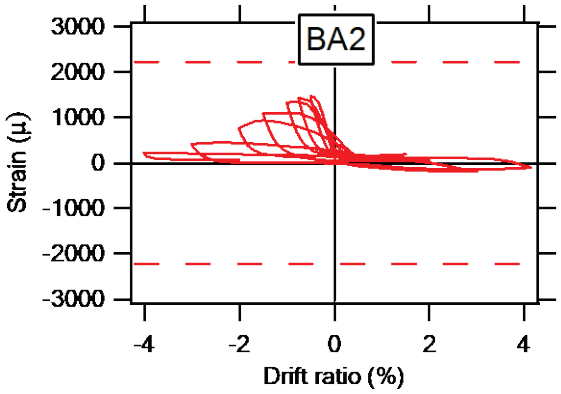
BA2
Strain (μ)
3000
2000
1000
0
-1000
-2000
-3000
-4
-2
0
2
4
Drift ratio (%)

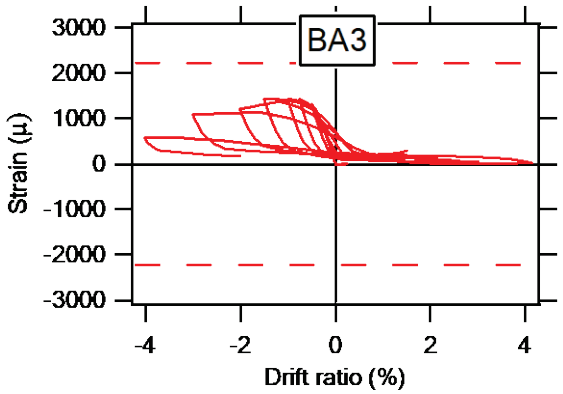
BA3
Strain (μ)
3000
2000
1000
0
-1000
-2000
-3000
-4
-2
0
2
4
Drift ratio (%)

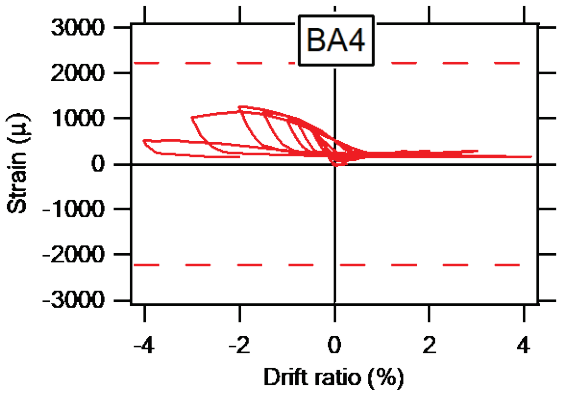
BA4
Strain (μ)
3000
2000
1000
0
-1000
-2000
-3000
-4
-2
0
2
4
Drift ratio (%)

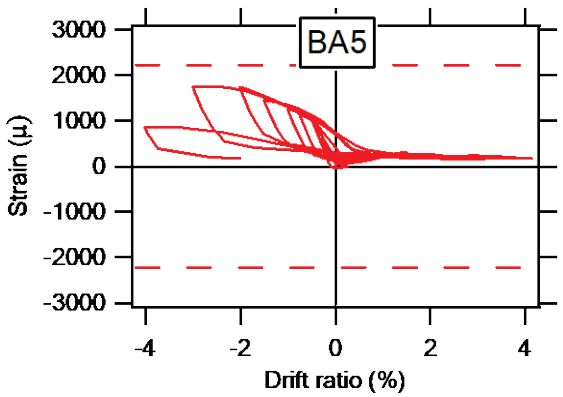
BA5
Strain (μ)
3000
2000
1000
0
-1000
-2000
-3000
-4
-2
0
2
4
Drift ratio (%)

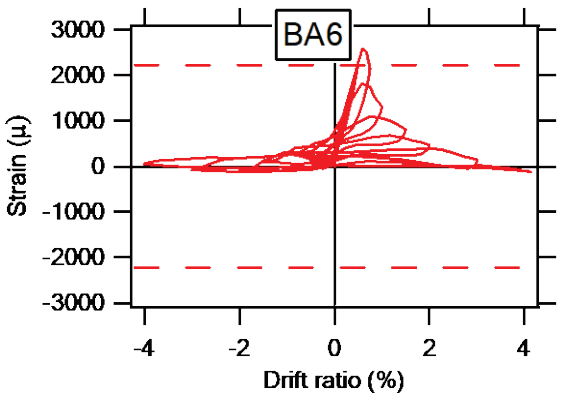
BA6
Strain (μ)
3000
2000
1000
0
-1000
-2000
-3000
-4
-2
0
2
4
Drift ratio (%)

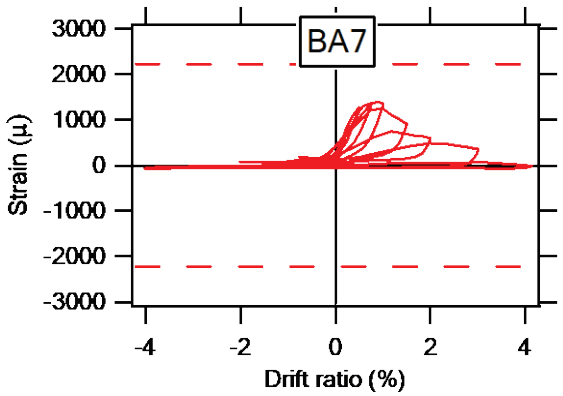
BA7
Strain (μ)
3000
2000
1000
0
-1000
-2000
-3000
-4
-2
0
2
4
Drift ratio (%)

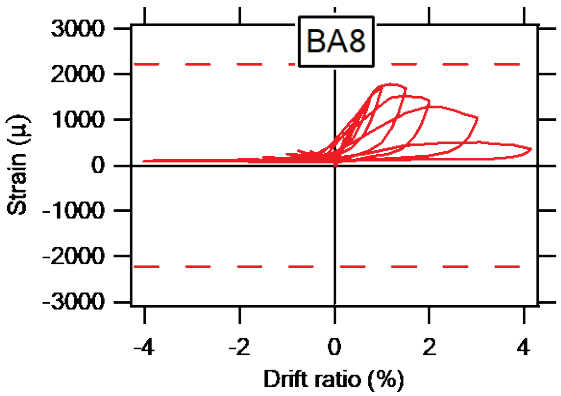
BA8
Strain (μ)
3000
2000
1000
0
-1000
-2000
-3000
-4
-2
0
2
4
Drift ratio (%)

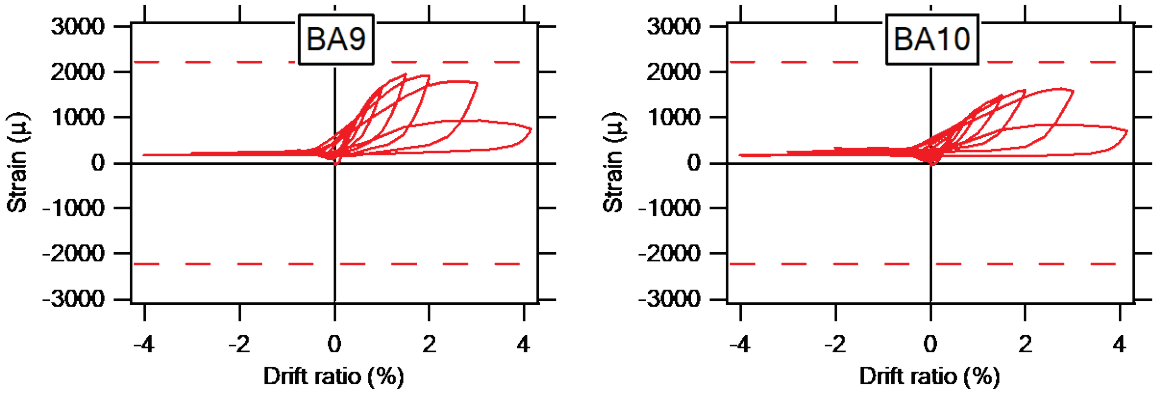

Figure C.20 Strain of beam anchors of specimen J1-W